NASA Conference Publication 2337

Fundamentals of Alloy Solidification Applied to Industrial Processes

Proceedings of a symposium sponsored by
NASA Office of Science and Applications,
NASA Lewis Research Center,
and Case Western Reserve University Department
of Metallurgy and Materials Science
held at NASA Lewis Research Center
Cleveland, Ohio
September 12 and 13, 1984

NASA
National Aeronautics
and Space Administration

Scientific and Technical
Information Branch

1984

FOREWORD

The NASA microgravity science and applications program has recently augmented its in-house and sponsored research program with a new thrust at Lewis Research Center focused on solidification fundamentals. Access to the unique microgravity environment of space is now routinely available via the space shuttle. NASA expects shuttle-based research on containerless processing and the role of gravity on fluid flow to greatly improve our understanding of solidification theory.

This two-day symposium at the Lewis Research Center is intended to foster increased communication and to establish new interactions among all researchers studying solidification fundamentals and processing problems, whether the researcher be in industry, government, or academia. Improved communications and understanding of the phenomena in a microgravity environment cannot help but lead to improvements on ground-based solidification processes. This publication contains papers or abstracts of papers presented at the symposium.

The cochairmen wish to acknowledge the support and encouragement by NASA Headquarters and the management of the Lewis Research Center for holding this symposium. The members of the program arrangements committee were Joanne M. Flowers, Dr. Fred J. Kohl, Dr. V. Laxmanan, and Gloria J. O'Donnell. This publication was compiled and edited by Fredric H. Harf.

Hugh R. Gray
Chief, Metallic Materials Branch
NASA Lewis Research Center

John F. Wallace
Republic Steel Professor of Metallurgy
Case Western Reserve University

CONTENTS

OMIT TO P.11

OVERVIEW OF NASA'S MICROGRAVITY SCIENCE AND APPLICATIONS PROGRAM

Richard E. Halpern
Director, Microgravity Science and Applications Division
National Aeronautics and Space Administration
Washington, D.C.

From the beginning of recorded history, processing materials has been an essential part of organized society. The art was practiced by skilled craftsmen who worked with simple materials to advance their utility and aesthetic appeal. Many illustrious exist. We need only to recall the pottery, textiles, and gold jewelry of the middle east and Egypt of 5000 years ago, the beautiful and functional Toledo steel swords of Spain, and the legendary scimitars of Arabia.

The knowledge of these early artisans was empirical, and their processing can best be described as craftsmanship rather than science as we currently define that term. They achieved properties and performance through repeated attempts at processing, but without basic knowledge or understanding as we know it today. Beginning about 1000 years ago, materials science and processing came into being along with elements of the Industrial Revolution. Not only did a producer want a process to work, he wanted to know why it worked, so that it might be improved. The essential modern concept concerning materials is that properties and performance can be regulated through the control of the material structure. The crucial role of microstructural control at all levels must be understood, as this is the essential linkage of materials processing to the materials scientific base and to the needs of the manufacturer. Thus, materials processing became central to the development and economic productions of sophisticated new materials concerned with energy, transportation, electronics, and aerospace technologies. As with all practitioners of materials science on Earth, these scientists had to deal with the effects of gravity, which include convection and sedimentation, in their processes. The advent of the space era therefore opens up an entirely new and potentially revolutionary arena where these factors no longer play a significant or controlling part.

NASA is cautiously optimistic about the potential for research leading to applied technology in the materials area in space. Microgravity research is a relatively new field and many areas are, therefore, still unknown. However, the processing of materials without the effects of gravity or convection can lead to speculation about a multitude of new materials, so that it is almost impossible to recite the entire list currently open to us. NASA is engaged in a program of research in solidification which may lead to the development of hitherto unobtainable combinations of materials with homogeneous structure and properties not currently available on Earth, a program in bioseparation where new pharmaceutical drugs may be produced in quantity, a program in the development of semiconductor crystals which may allow production of a size and purity unobtainable in a gravity field, and, most importantly, in a program of containerless processing.

The gravity field of the Earth requires that anything which is to be processed, all the way from the familiar glass of water to the production of

steel and other valuable metals, be held in a container, otherwise the material would, of course, run over the ground. In the laboratory of space, such a container is not necessary. Water and molten metal, alike, will form into spheroids, which, if properly manipulated can be processed in many forms. The potential for levitating materials and processing them at elevated temperatures, therefore, opens an entirely new domain in the area of materials purification and manufacturing. This is truly a process which is on the verge of exploration and is available no where else but in the micropgravity environment of space.

NASA, as has been pointed out, is actively involved on a program of basic research in the materials science on space discipline and has embarked on an effort to more tightly involve United States industry in a program of applied research.

The cost of access to space is currently high. Therefore, we are today in an era where commercial benefits from space may typically result from relatively small experimentation in the microgravity environment which lead to a change in the "on-Earth processes" rather than in a large scale manufacturing in space environment. The space shuttle, or space transportation system as it is more properly designated, has just become operational; and a great, new, tool is mow available on a regular basis to the materials scientists. Plans have been made at NASA to use this tool on a regular basis, and it is expected that flights that carry materials science experiments will routinely be launched from the Kennedy Space Center.

We are actively working with several corporations by means of an arrangement known as a Joint Endeavor Agreement (JEA). These agreements seek industrial capital investment in equipment, in return for which NASA participates in the research program, and offsets the cost of access to space during the period necessary to demonstrate that the process may become commercially viable. The McDonnell-Douglas Corporation is the first NASA-industry partner participating under a JEA working on a program of electrophoretic separation for pharmaceuticals production. NASA is also involved in a program which allows United States industrial firms to cooperate in more basic research, thereby exchanging intellectual information as well as allowing the use of facilities which were originally built to support the NASA program. A third program which NASA has evolved is one in which a guest researcher from an industrial organization may work in a NASA facility on a program of mutual interest. In all of these programs, it should be understood that costs are shared between the industrial partner and NASA.

As the title of this article implies, the science of materials in microgravity is in its embryonic stage. It can be reasonably expected that materials science as well as fundamental physics and chemical science in the zero-g environment will rapidly expand as more frequent and longer experiments occur. Experiments that are now planned will lead to other experiments. Results that are totally unexpected will almost certainly surprise and excite us, and the way is already being paved for the future.

At some point in time, hopefully, not far away, the United States will decide that it is necessary to remain in space on a more or less permanent basis. When that occurs, the decision to build a space station will be a concomitant decision. A space station will inaugurate a second and mature phase in the field of microgravity science and applications.

The space station is expected to accomplish a number of things currently unavailable to the materials scientist. First of all (and the most obvious) is that long time processing in the microgravity environment will become available. Secondly, the high power levels, so necessary to this particular endeavor, will also, for the first time, be available. An inherent part of the processing of materials, particularly in the areas of metals and crystal growth, is the requirement for high power consumption. A third and perhaps not as obvious an advantage when a space station becomes a reality, will be the continued manned interaction in the evolution of a particular process. The ability to have the observation and acumen of the manned presence and to be able to make needed changes during studies is almost certain to affect the outcome of the experiment that will be conducted on the space station. Furthermore, the ability of the human brain in the control of processes should lead to an enhancement of commercial activities that are certain to be accomplished there. Plans are already being considered to produce pharmaceuticals on the space station, and it is expected that other commercial ventures will take advantage of what may become known as the Second Industrial Revolution.

MICROGRAVITY SCIENCE AND APPLICATIONS GOALS

- Investigate behavior of materials and fluids and effects on processes performed in microgravity.
  - — Provide better understanding of effects and limitations imposed by gravity on processes performed on earth.
  - — Evolve processes that exploit microgravity environment of space.
  - — Accomplish results that cannot be obtained on earth.
- Expand, centralize, and disseminate the scientific research base and experimental results.
- Explore and determine potential applications for commercialization in space.
- Utilize manned laboratory module(s) of Space Station to provide a facility.
  - — Scientific and commercial research
  - — Technology development
  - — Commercial process verification
  - — Commercial manufacturing

MICROGRAVITY SCIENCE BASE

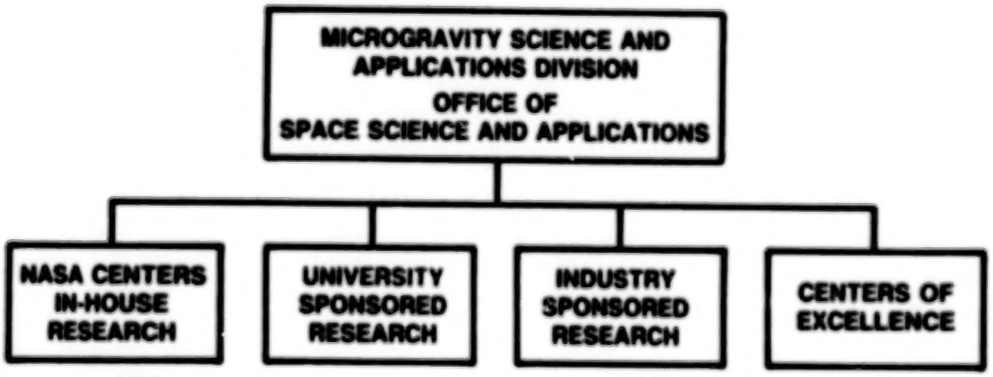

- — LARC
- — LERC
- — MSFC
- — JPL
- — JSC

THE APPROACH

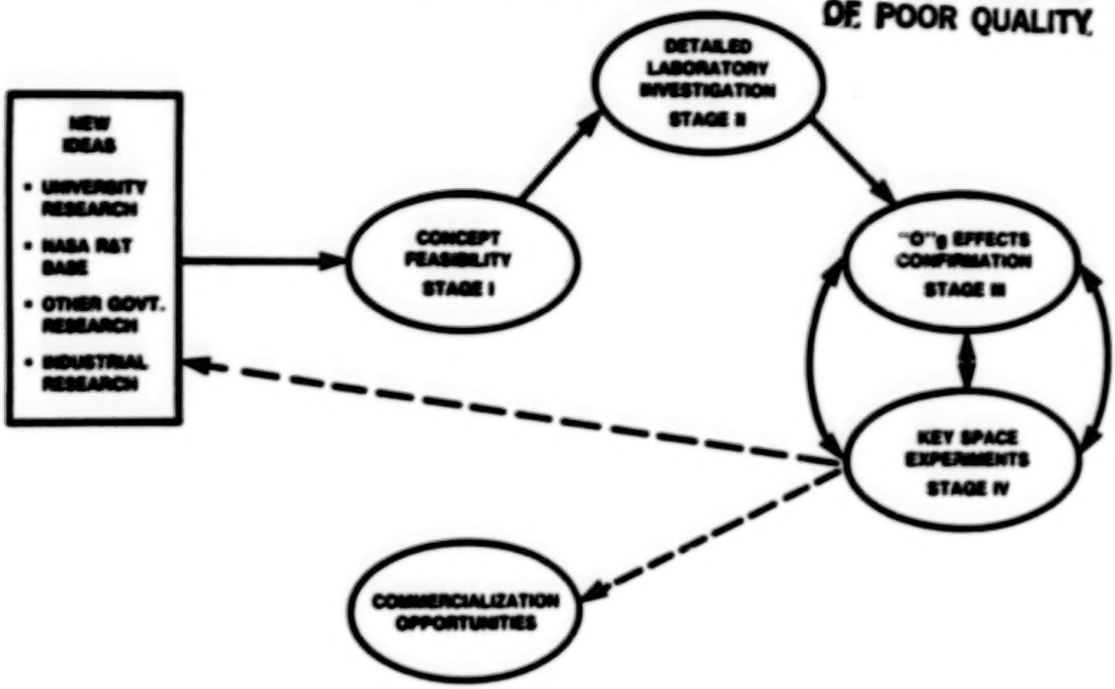

MICROGRAVITY SCIENCE AND APPLICATIONS PROGRAM UNIVERSITIES

COMBUSTION SCIENCE

FLUID DYNAMICS AND TRANSPORT PHENOMENA

BIOTECHNOLOGY

GLASSES AND CERAMICS

ELECTRONIC MATERIALS
METALS AND ALLOYS

OVERVIEW OF THE LEWIS RESEARCH CENTER'S MATERIAL SCIENCE IN SPACE PROGRAM

Fred J. Kohl
NASA Lewis Research Center
Cleveland, Ohio

The Materials Science in Space Project at the Lewis Research Center is part of the NASA Microgravity Science and Applications Program. The project is focused on the areas of materials science, combustion science, and fluid physics. The objectives of the project are (1) to improve the understanding of the role of gravity in the fundamentals of materials science and processing, (2) to define potential applications for low-gravity processing and to conduct experiments using Earth-based or space-based facilities, and (3) to develop the joint involvement of industry, university, and NASA in cooperative efforts.

The major thrusts of the project are to study materials phenomena in the areas of solidification fundamentals, ceramics processing, vapor crystal growth and to study the complementary fundamental fluid physics concepts in transport phenomena, thermo/diffusocapillary flow, and interfacial fluid dynamics.

One of the important elements of the Lewis Research Center project is the establishment of the microgravity materials science laboratory. The goal of this facility is to provide easy access to industry, university, and government researchers to conduct materials research on shuttle flight-type experimental equipment.

SOLIDIFICATION FUNDAMENTALS

WHY μ-g ?

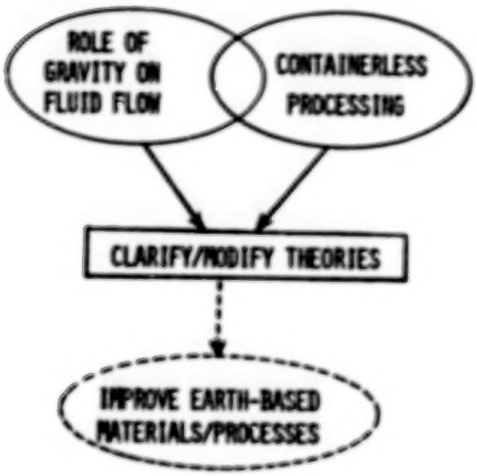

SOLIDIFICATION FUNDAMENTALS

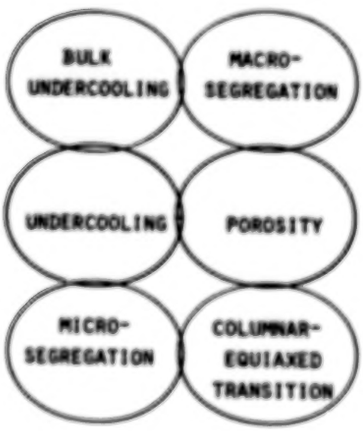

MICROGRAVITY MATERIALS SCIENCE LABORATORY

GOAL - Easy Access For University, Industry and NASA Researchers To Conduct Materials Research On Shuttle Flight-Type Experimental Equipment

- Test Bed For Space Station Microgravity and Materials Processing Facility (MMPF)

ORIGINAL PAGE IS
OF POOR QUALITY

MICROGRAVITY MATERIALS SCIENCE LABORATORY

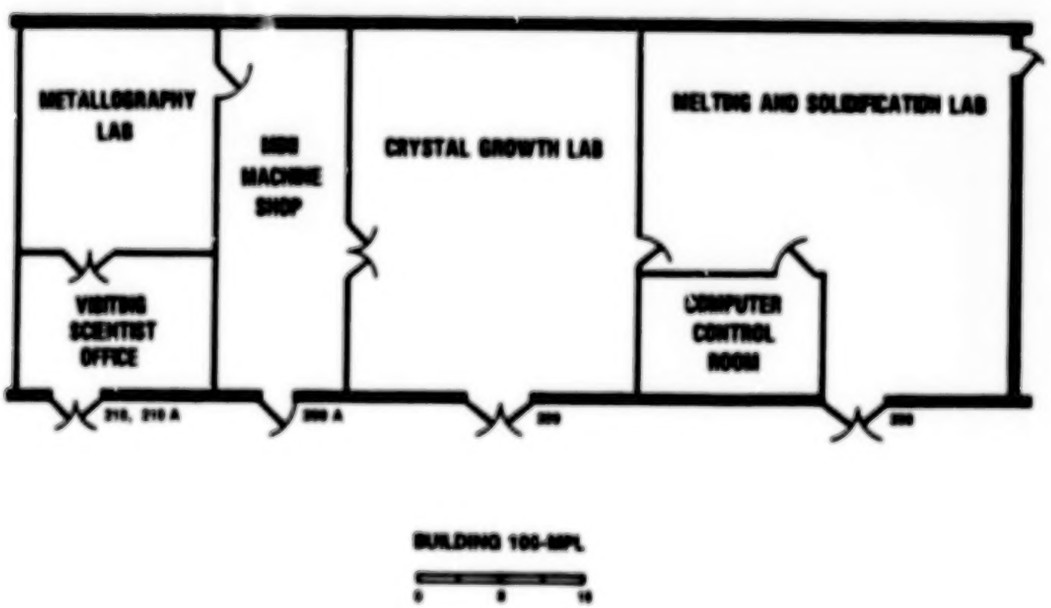

MICROGRAVITY & MATERIALS PROCESSING FACILITY (MMPF)

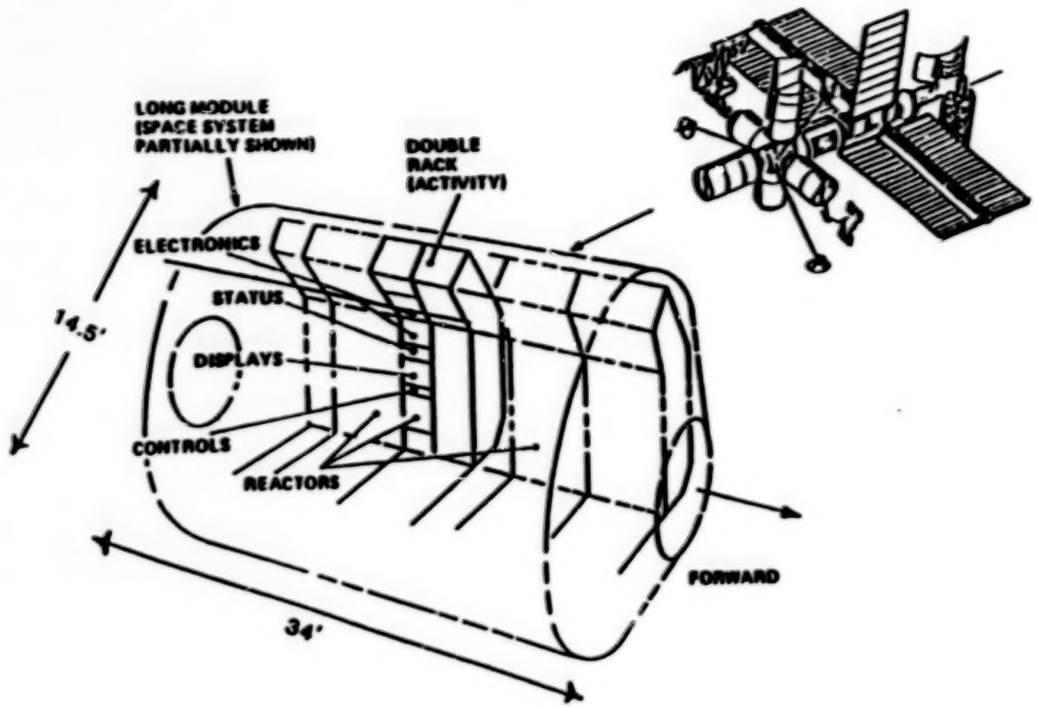

THE UNDERCOOLING OF LIQUIDS

David Turnbull
Harvard University
Cambridge, Massachusetts

The formation by melt quenching of such metastable structures as glassy or microcrystalline solids and highly supersaturated solutions is made possible by the extreme resistance of most melts to homophase crystal nucleation at deep undercooling. This nucleation resistance contrasts sharply with the very low kinetic resistance to the movement of crystal-melt interfaces, once formed, in metals and other fluid systems at even minute undercooling. The methods of nucleation study which have proven especially effective in bypassing nucleation by heterophase impurities thereby exposing the high resistance of melts to homophase nucleation may be summarized as follows:

(1) Observation of the crystallization behavior of dispersed small droplets

(2) Drop tube experiments in which liquid drops solidify, under "containerless" conditions, during their fall in the tube

(3) Observation of the crystallization of bulk specimens immersed in fluxes chosen to dissolve or otherwise deactivate (e.g., by "wetting") heterophase nucleants. This method has proven to be remarkably effective in deactivating such nucleants in certain pure metals, e.g., Ag, Fe, Co, and Ni, and some alloys, e.g., $Ni_{40}Pd_{40}P_{20}$.

By applying these techniques it has been learned that in finite systems of metals and most nonmetals the frequency, I, of crystal nucleation reaches measurable levels only when the undercooling exceeds some virtual threshold value which for metals and alloys is 20 to 30 percent of the liquidus temperature. However, careful measurements have indicated that, at this threshold, nucleation occurs stochastically in time with frequencies which, in general, increase sharply with undercooling. There are some glass forming melts in which I does not reach a measurable level at any undercooling. This experience has shown that achievement of high undercooling and glass formation may require not only containerless processing but also special measures - such as atmosphere control, etching, or fluxing - to eliminate heterophase nucleants from the melt surfaces.

The conditions for forming glassy and microcrystalline solids and for impurity-trapping in thin overlays of melts quenched on their crystallized substrates will be discussed. The realization of metastable structures in this type of processing depends critically on the interfacial undercooling which is determined by the imposed thermal gradient, the thermal and atomic diffusivities, and the frequency of the interfacial rearrangements.

Also the current understanding of the nucleation resistance of metal melts will be reviewed.

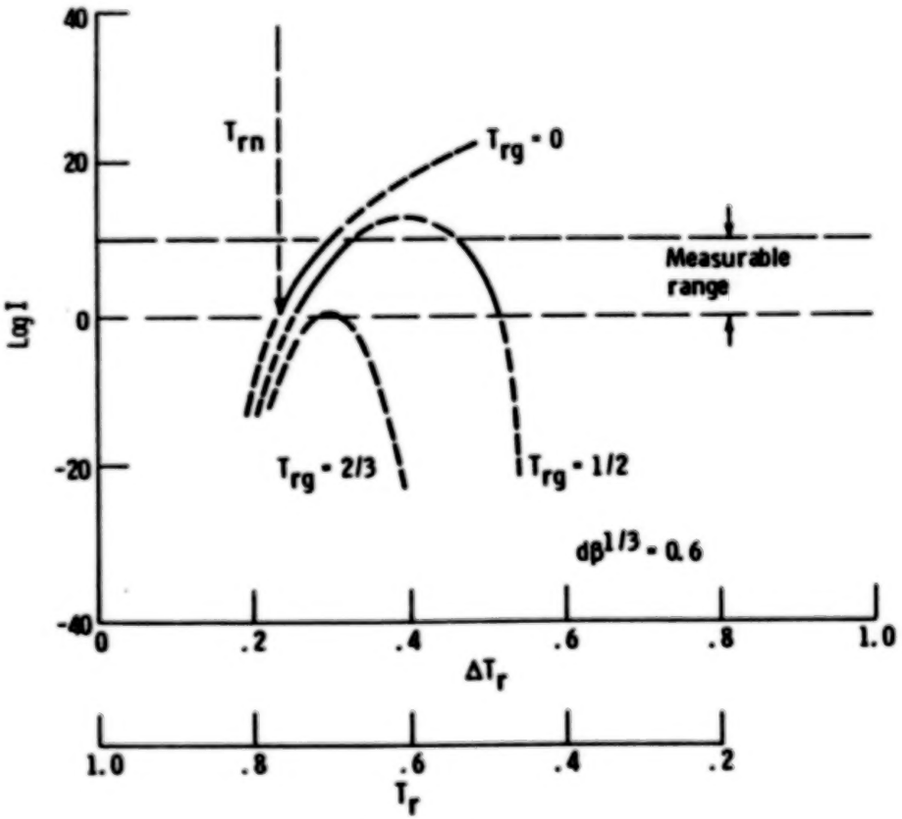

$$I = Ak_i(T) \exp\left\{\frac{-b\alpha^3\beta}{(\Delta T_r)^2 T_r}\right\}$$

α = Scaled work of interface formation = $(\bar{N}\bar{V}^2)^{1/3}\frac{\sigma}{\Delta H_m}$

$T_r = T_g/T_m$

$\Delta T_r = (T_m - T_g)/T_m$

β = Scaled entropy of melting

Figure 1.

Plane front solidification

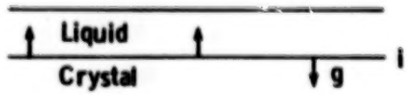

In linear kinetic regime

$$u \simeq u_0 \beta \frac{\Delta T_i}{T_i} \; ; \; u_0 = f k_i \lambda \; , \; \beta = \frac{\Delta S_m}{R} ; u = K(\text{grad } T)_i \frac{\bar{V}}{\Delta H_m}$$

At steady state

$$\Delta T_i \simeq \left[\frac{K(\text{grad } T)_i}{u_0}\right] \frac{\bar{V} T_i}{\beta \Delta H_m}$$

$T_m \rightarrow \frac{u_0 >> K(\text{grad } T)_i}{\text{---------}} T_i$ $\qquad$ $\frac{K(\text{grad } T)_i >> u_0}{} T_m$

--------- T_i

Sink temperature

T_i = Interface temperature
$(\text{grad } T)_i$ = Thermal gradient at interface
ΔT_i = Undercooling at interface
u = Velocity of interface
k_i = Frequency of interfacial rearrangement
K = Thermal conductivity
ΔS_m = Molar entropy of melting

Figure 2.

Impurity redistribution	Thermal activation and suppressibility at $T < T_g$	Upper limiting speed (a)	Occurrence
-	-	$u \lesssim u_s$ = sound speed ~ 4 km/sec	Pure metals and some alloys
+	+	$u = -D_i/C_i\,(\text{grad } C)_i$ $\therefore u \lesssim D_i/\lambda$ ~10 m/sec	Most alloys

(a)
D_i denotes diffusivity of impurity at interface, i; and
C denotes impurity concentration in melt

Figure 3.

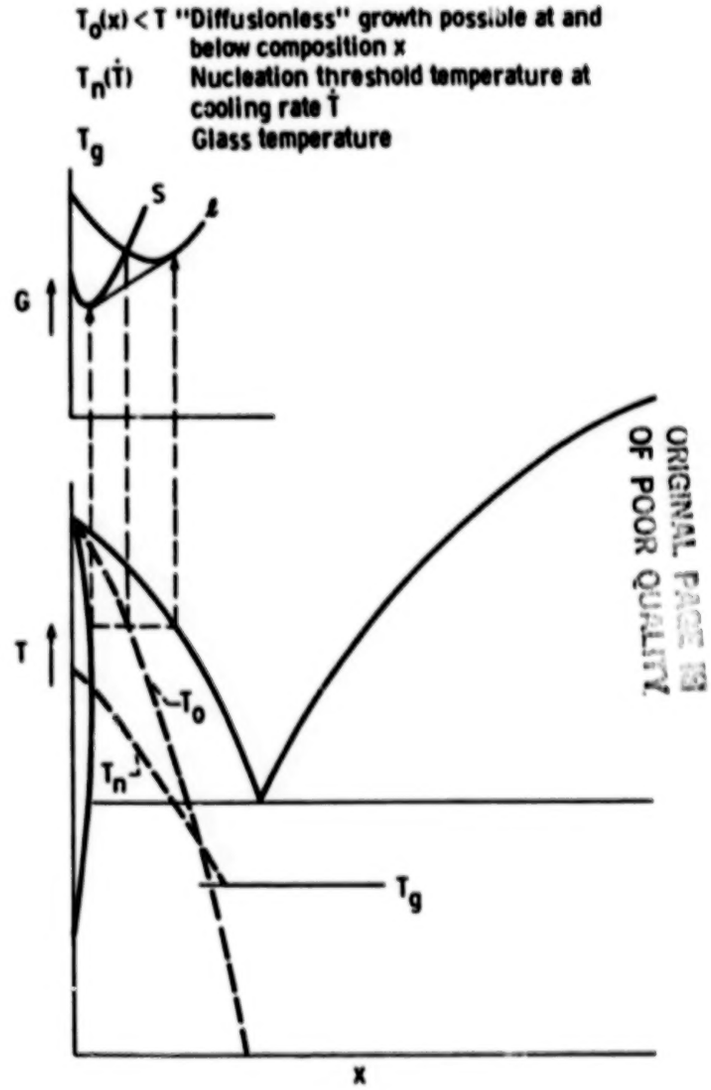

Figure 4.

Material	Reference crystal	$T_{rg} = T_g / T_g$ (a)	Cooling rate, $\dot{T}$, deg/sec
Common glass formers			
SiO_2	Quartz	0.835	$< 10^{-2}$
	Cristobalite	.745	
B_2O_3	--	.76	$< 10^{-2}$
GeO_2	Rutile	.65	$< 10^{-2}$
	Quartz	.63	
Se	--	.605	$< 10^{-2}$
o-terphenyl	--	.73	
Metal glass formers			
$Au_{77}Ge_{14}Si_9$	fcc solution	0.475	10^6
$Fe_{80}B_{20}$	bcc solution	~.49	10^6
$Fe_{95}B_5$	bcc solution	< .40	10^{12}
$Pd_{82}Si_{18}$	fcc solution	.60	< 800
$Pd_{77.5}Cu_6Si_{16.5}$	fcc solution	.63	< 800
$Ni_{40}Pd_{40}P_{20}$	fcc solution	.67	1

(a) T_ℓ denotes liquidus temperature; T_g denotes glass temperature.

Figure 5.

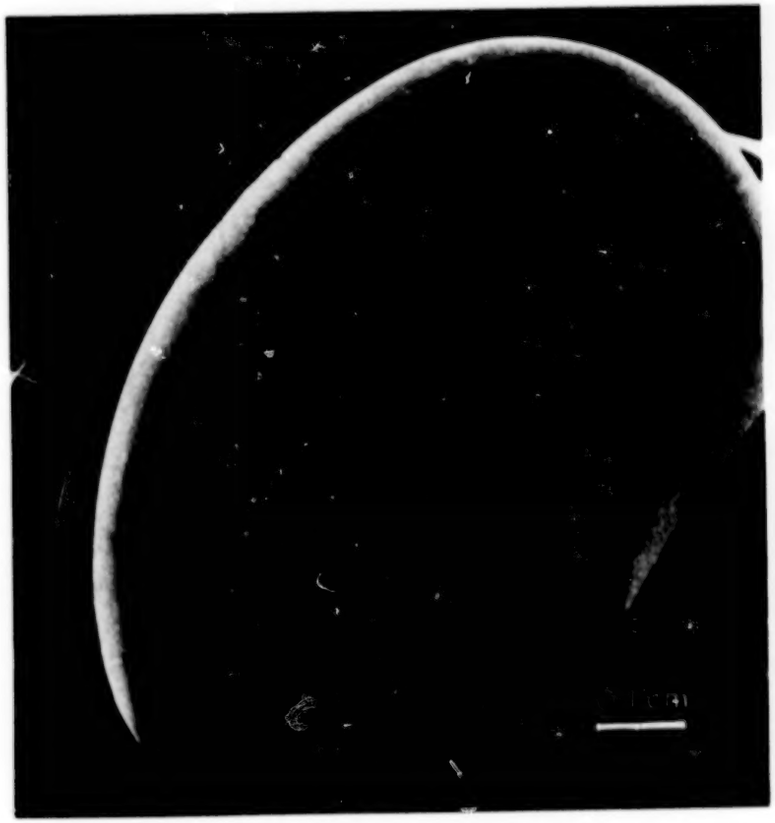

Figure 6. - 4-Gram glass ingot (hemispherical-minimum dimension 1 cm) of $Pd_{40}Ni_{40}P_{20}$ alloy formed by melt cooling ($\dot{T} < 1^0$/sec) under molten B_2O_3 flux.

N84 34591

BULK UNDERCOOLING

Theo Z. Kattamis
University of Connecticut
Storrs, Connecticut

In rapid solidification processing, such as melt-spinning and atomization, the requirement of rapid heat extraction limits the mass of the melt that can be quenched. In bulk undercooling there is no mass limitation. High growth velocities can be attained by substantially undercooling large masses of alloy melts prior to nucleation of the solid. Through proper melt conditioning, such as encasement in a glass slag aiming at eliminating heterogeneous nucleants, the degree of undercooling achieved in bulk specimens should approach that of droplets.

Through bulk undercooling the primary phase or the eutectic are morphologically changed, the dendritic and grain structures are drastically refined, the intradendritic minimum solute content is increased, the volume fraction interdendritic nonequilibrium eutectic is decreased, and the terminal solid solubility of the primary phase is extended, hence, chemical homogeneity is enhanced. Most of these features are expected to significantly and beneficially affect the mechanical and corrosion behaviors of the material. From this point of view undercooling studies are most important. From another point of view they provide fundamental information relevant to rapid solidification processes, since in most of them the melt undercools prior to nucleation.

Bulk undercooling methods and procedures will first be reviewed. Measurement of various parameters which are necessary to understand the solidification mechanism during and after recalescence will be discussed. During recalescence of levitated, glass-encased large droplets (5 to 8 mm diam) high speed temperature sensing devices coupled with a rapid response oscilloscope are now being used at MIT to measure local thermal behavior in hypoeutectic and eutectic binary Ni-Sn alloys. Dendrite tip velocities were measured by various investigators using thermal sensors or high speed cinematography. The confirmation of the validity of solidification models of bulk-undercooled melts is made difficult by the fineness of the final microstructure, the ultra-rapid evolution of the solidifiying system which makes measurements very awkward, and the continuous modification of the microstructure which formed during recalescence because of precipitation, remelting and rapid coarsening.

Some of the results of the investigation at MIT on Ni-25 wt % Sn and the eutectic Ni-32.5 wt % Sn alloys are

(1) In the hypoeutectic alloy the recalescence rate increases with undercooling, ΔT. For low undercoolings the recalescence time increases with ΔT, and reaches a maximum beyond which it decreases with increasing ΔT. It appears that the recalescence time is not limited by heat flow, but rather by solute transport.

(2) The solidification time decreases with undercooling.

(3) The maximum recalescence temperature decreases with undercooling and can be lowered below the eutectic temperature at an undercooling of 275 K.

Dendrite tip velocity was measured for various pure metals and alloys. The tip velocity R and the initial bulk undercooling, ΔT are related by $R = A(\Delta T)^n$, where A and n are constants. For a given undercooling R decreases with solute concentration.

The dependence of microstructure on undercooling and cooling rate after recalescence and its evolution during solidification of highly undercooled melts will next be analyzed. It was previously established that the dendritic structure is gradually refined with increasing undercooling and is eliminated at a critical undercooling of about 170 K. Below this undercooling the grain size is almost independent of ΔT. At $\Delta T = 170$ K the grains are drastically refined and become nondendritic with spherical coring. Beyond the critical undercooling the grain size decreases with ΔT. Nondendritic grain size also decreases with cooling rate after recalescence and in binary alloys, with increasing initial solute concentration in the alloy, as shown by current work at the University of Connecticut. The formation of observed microstructures and the roles played by mechanical disturbance and cavitation-induced nucleation, remelting during recalescence and coarsening during and after recalescence will be discussed. It will be shown that fine remelting of the supersaturated solid which forms early during recalescence and dendritic segmentation assisted by the presence of pressure waves, combined with accelerated coarsening during and after recalescence, could account for the observed microstructural transition, grain refinement, and grain size dependence on cooling rate after recalescence.

Solute partitioning at the solid-liquid interface and intradendritic solute distribution will be discussed as a function of undercooling and cooling rate after recalescence. Solidification models will be introduced and their predictions compared with experimentally measured solute distribution profiles. An explanation will be offered for the presence of high solute cores which are retained through quenching after recalescence at the center of nondendritic spherical grains or dendrite arms.

On the basis of observations made on bulk-undercooled specimens the effect of fluid flow on solidification microstructure and microsegregation will be discussed. Finally, predictions will be made as to how bulk-undercooled melts would solidify in a microgravity environment and to what extent reduced convection will affect final microstructure and distribution of alloying elements.

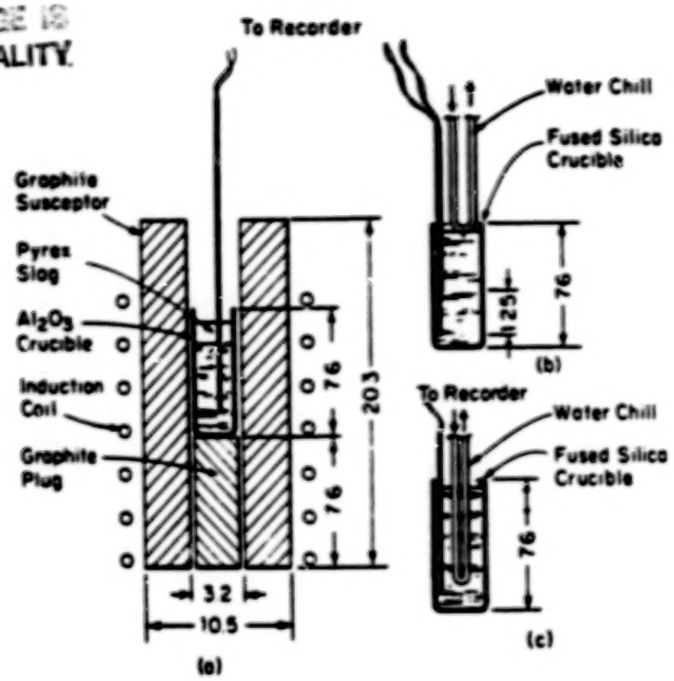

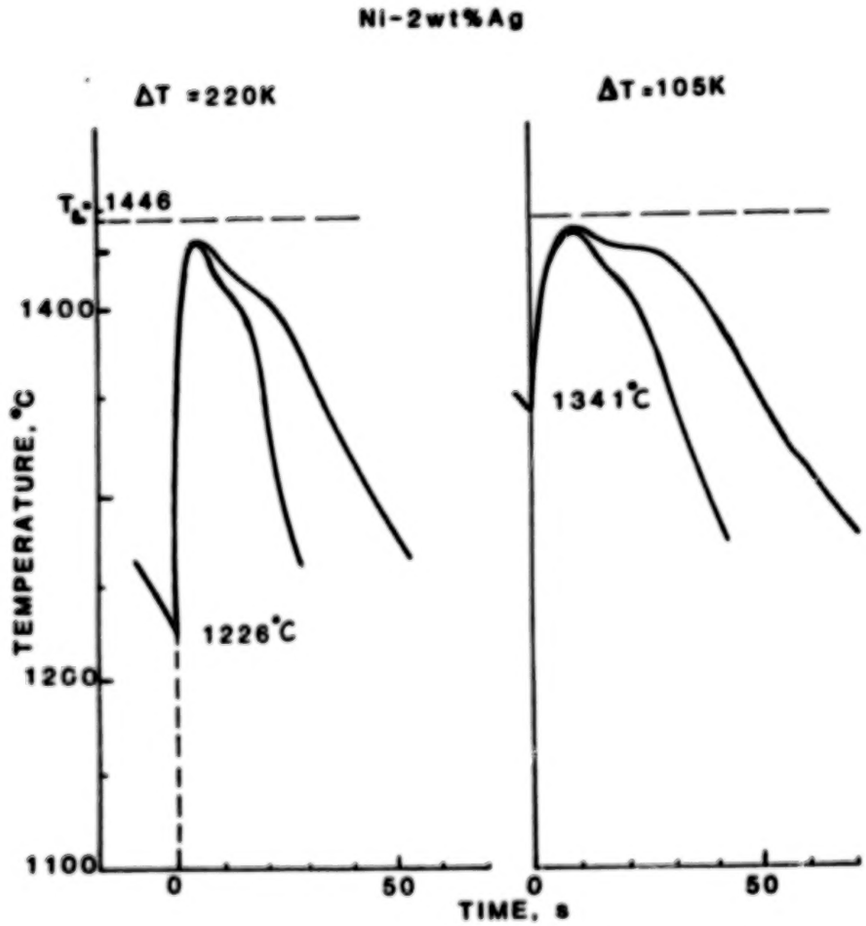

Thermal history of two Ni-2wt%Ag alloy specimens undercooled 105 K and 220 K, prior to nucleation of the solid, each cooled at two different rates after recalescence.

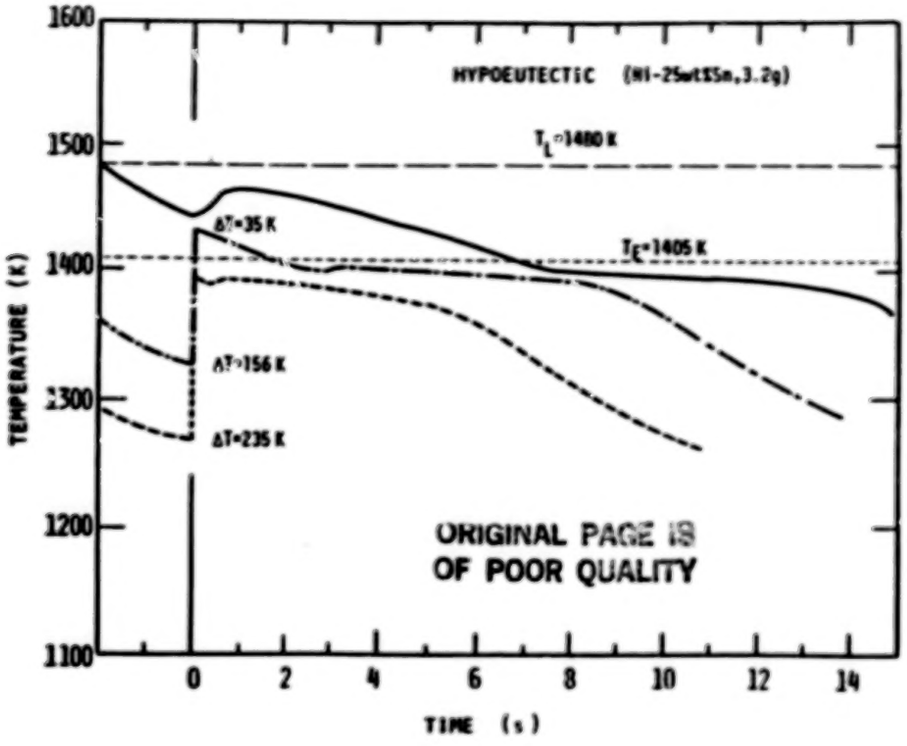

Thermal history versus initial undercooling. Hypoeutectic Ni-25wt%Sn alloy. From Wu, Piccone, Shiohara and Flemings.

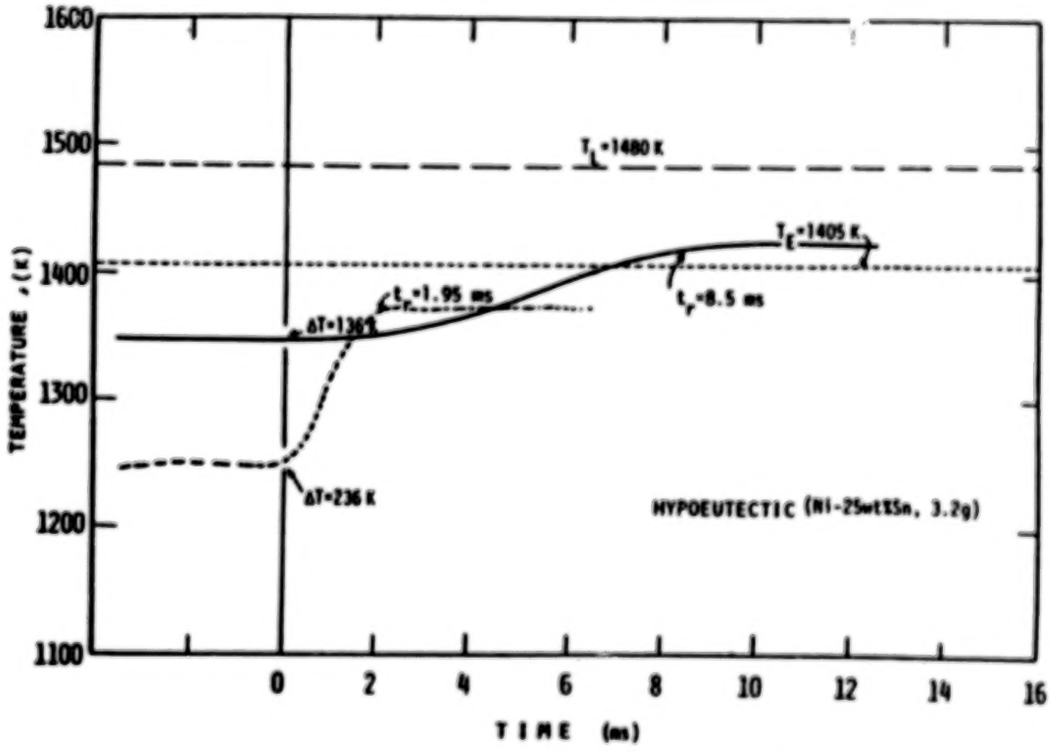

Thermal profiles during recalescence for two undercoolings. Hypoeutectic Ni-25wt%Sn alloy. From Wu, Piccone, Shiohara and Flemings.

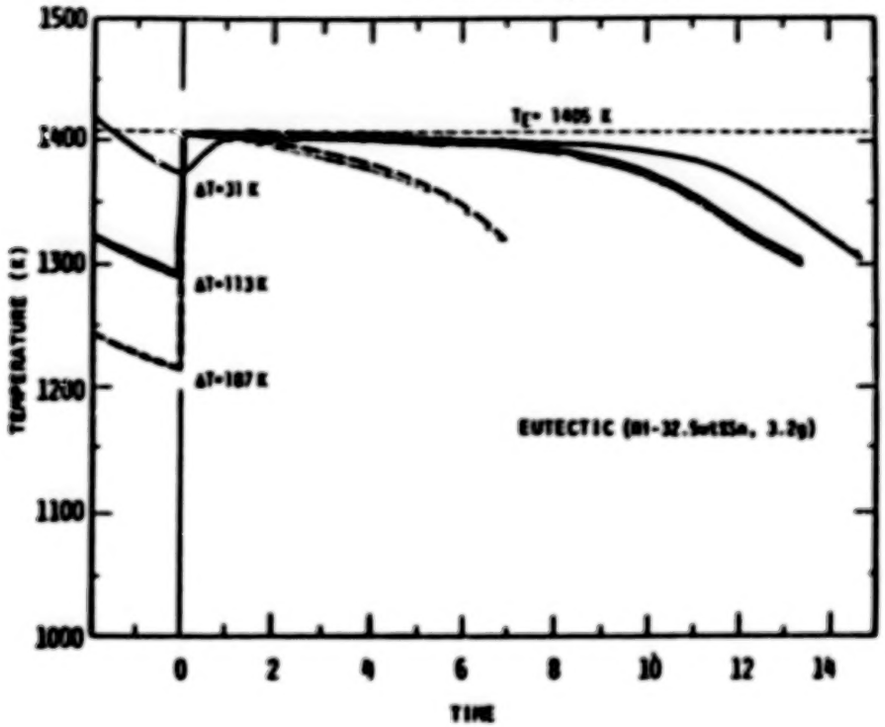

Thermal histories of three samples with different undercoolings. Ni32.5wt.%Sn eutectic alloy. From Wu, Piccone, Shiohara and Flemings.

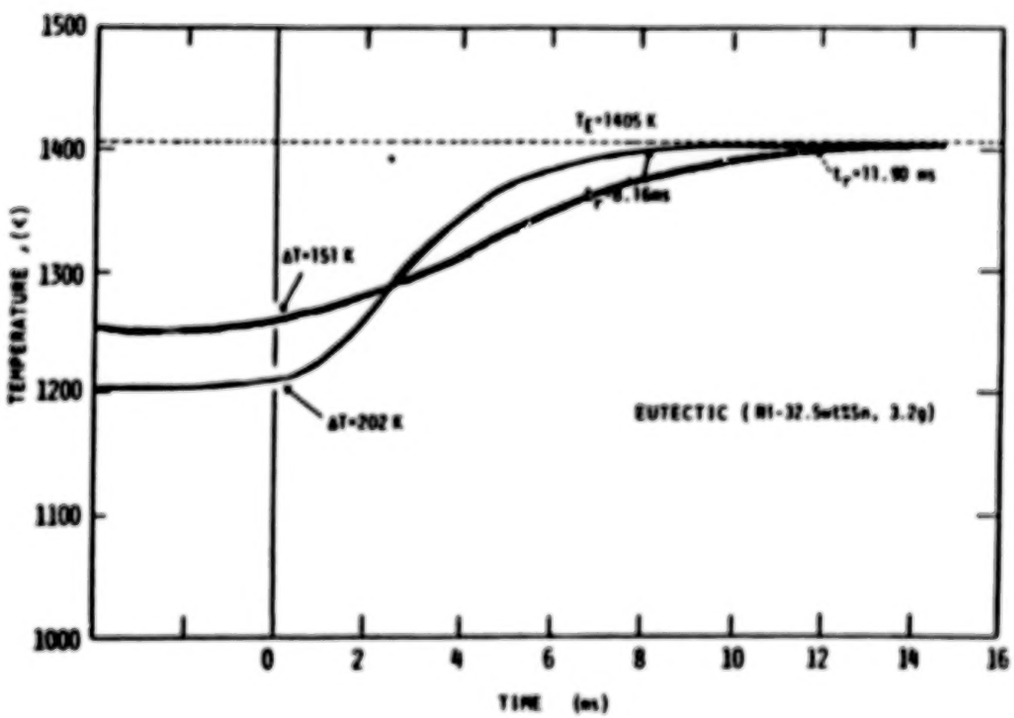

Thermal profiles during recalescence versus undercooling. Ni-32.5wt%Sn eutectic alloy. From Wu, Piccone, Shiohara and Flemings.

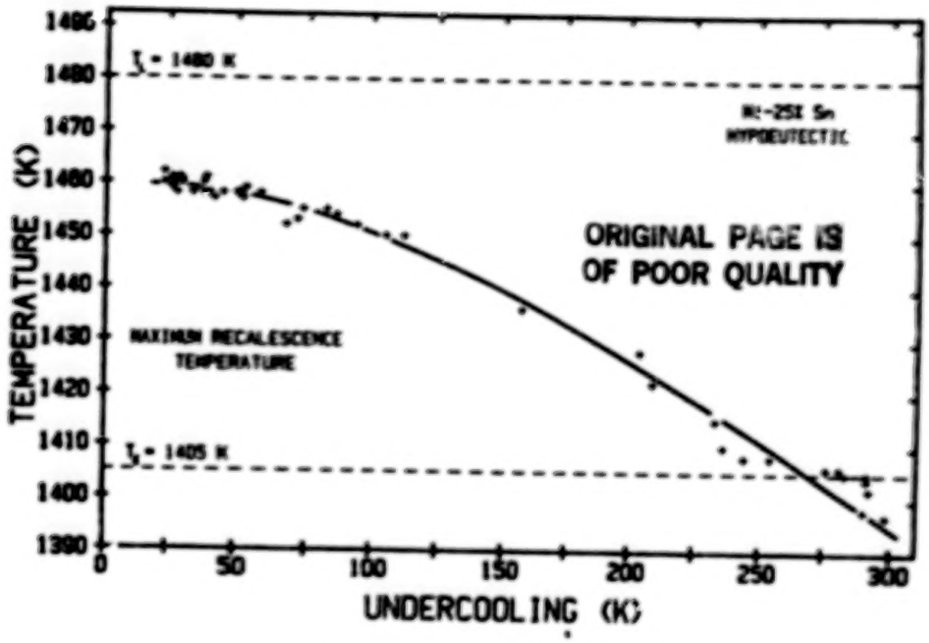

Maximum recalescence temperature versus undercooling. Ni-25wt%Sn hypoeutectic alloy. From Wu, Piccone, Shiohara and Flemings.

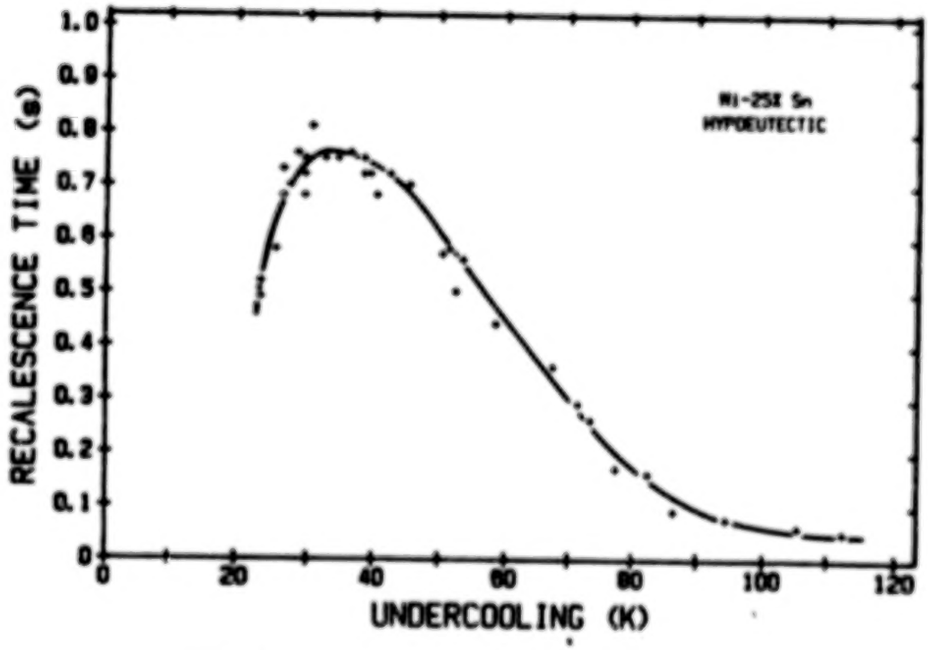

Recalescence time versus degree of undercooling. Ni-25wt%Sn hypoeutectic alloy. From Wu, Piccone, Shiohara and Flemings.

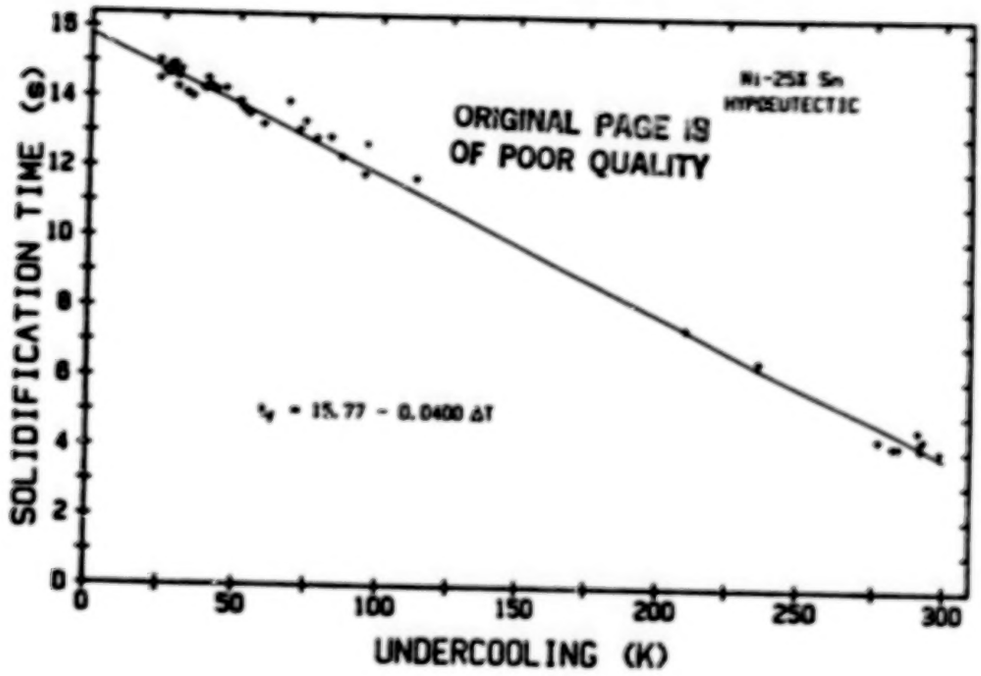

Solidification time versus degree of undercooling. Ni-25wt%Sn hypoeutectic alloy. From Wu, Piccone, Shiohara and Flemings.

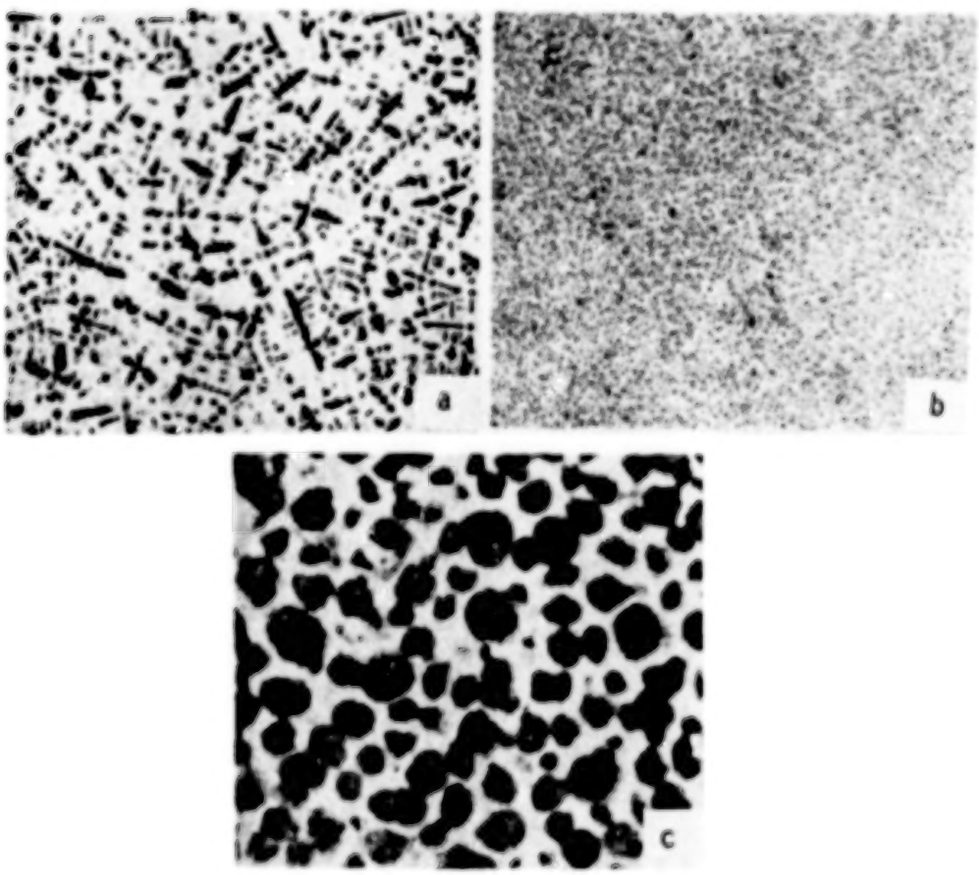

Photomicrographs of Fe-25wt%Ni alloy specimens undercooled: (a) 0 K, 12X ; (b) and (c) 250 K, cooled at about 0.4 K/s after recalescence, 150X.

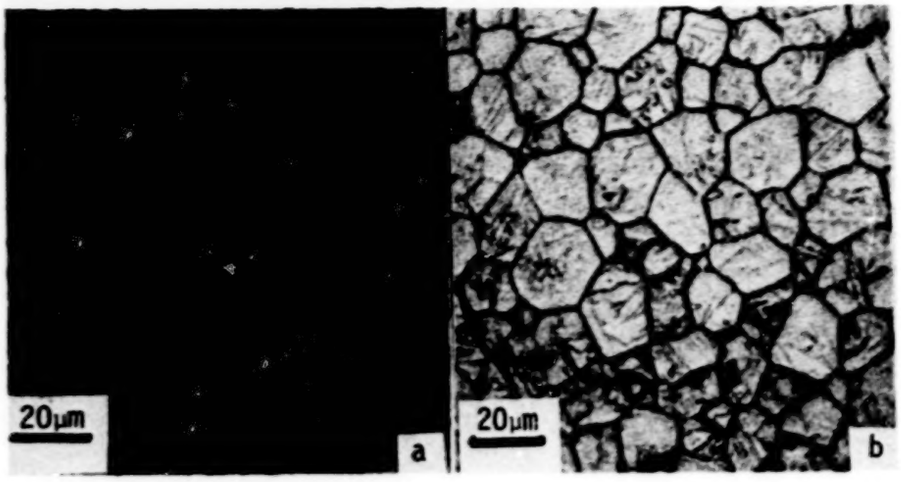

Photomicrographs of Ni-2wt%Ag alloy specimens undercooled 220 K and cooled at : (a) 5 K/s and (b) 1 K/s after recalescence.

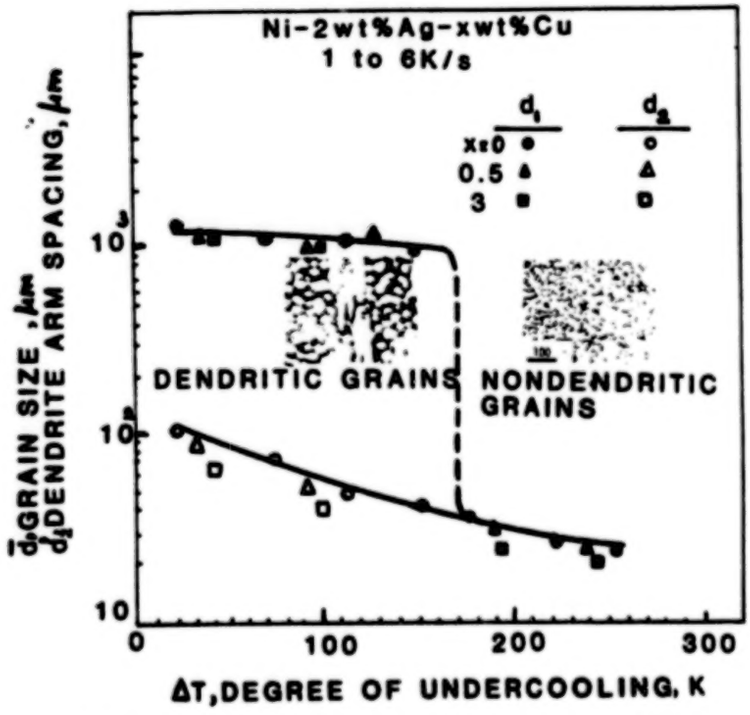

Dendrite arm spacing in dendritic specimens, and grain size in dendritic and nondendritic specimens versus degree of undercooling, cooling rate and composition. Ni-2wt%Ag-xwt%Cu alloy.

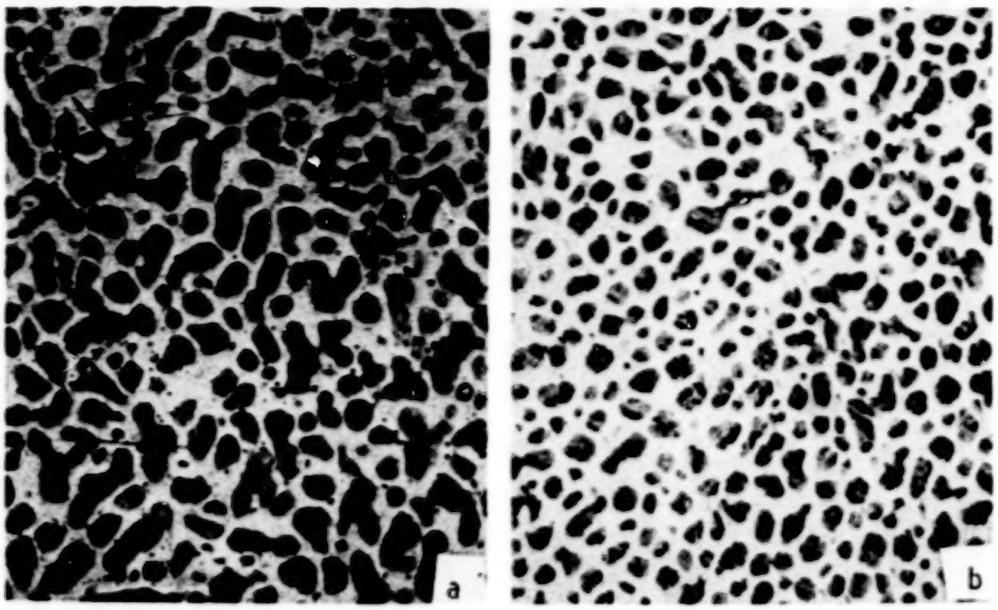

Photomicrographs of Fe-25wt%Ni alloy specimens undercooled : (a) 150 K, (b) 160 K, 60X.

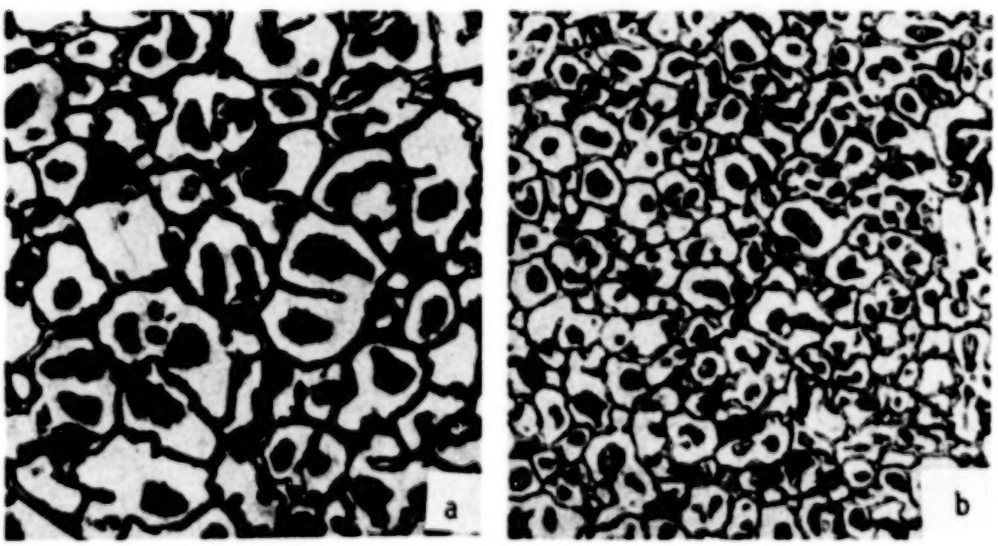

Photomicrographs of 440 C alloy steel. (a) Specimen cooled at about 10 K/min while vigorously stirred, 250X; (b) specimen undercooled 160 K and solidified at an average cooling rate of 10.5 K/min, 250X.

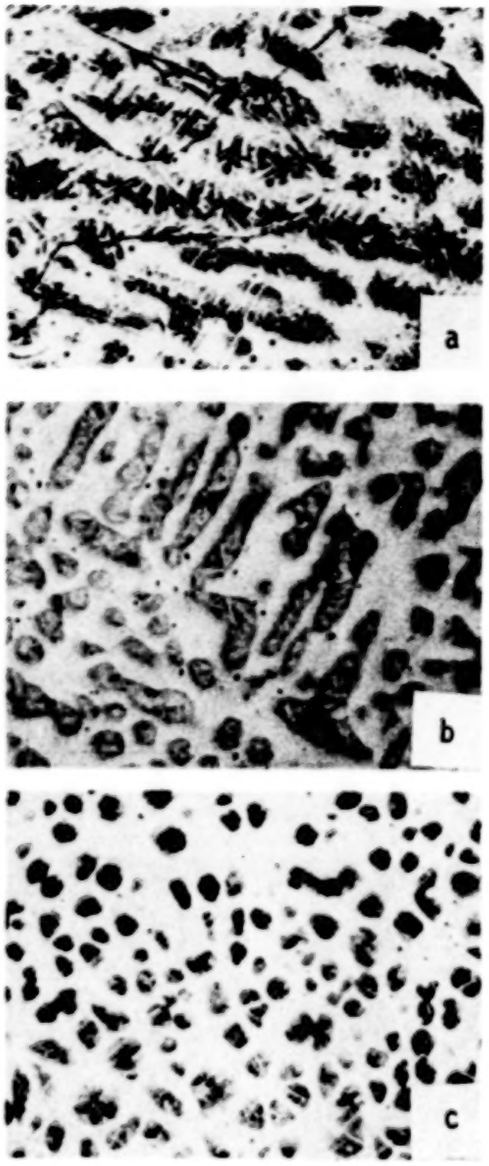

Photomicrographs of Fe-25wt%Ni alloy specimens undercooled 150 K , 55X. Average recalescence rates were: (a) 10 K/s, (b) 24 K/s and (c) 75 K/s.

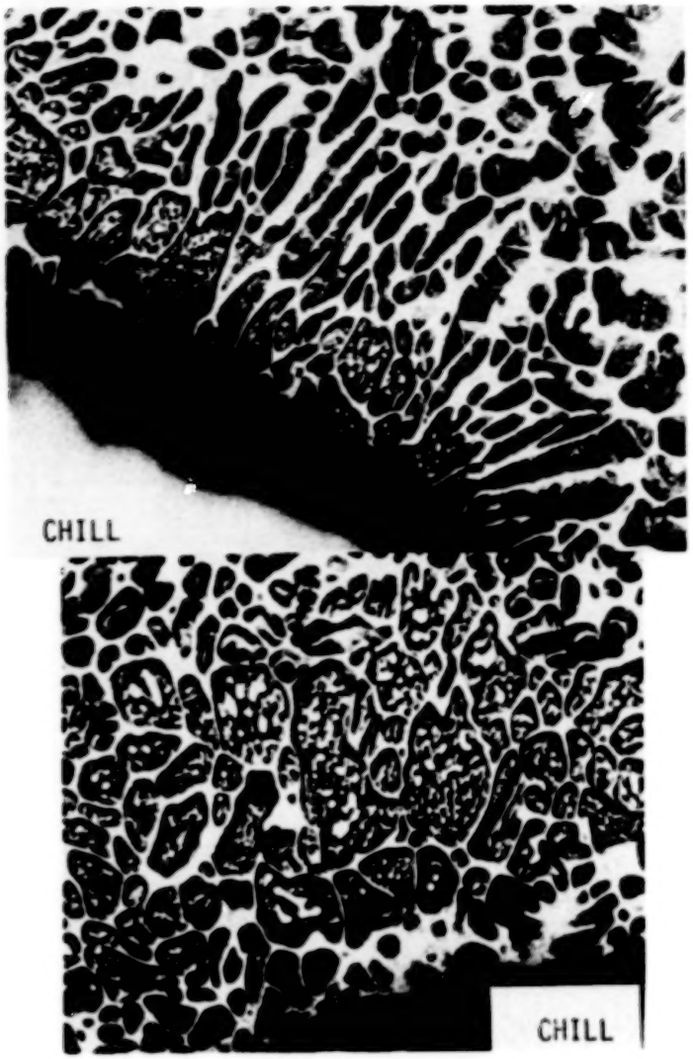

Retained remelting structure in Fe-25wt.%Ni alloy specimen undercooled 100 K and internally chilled, 100X.

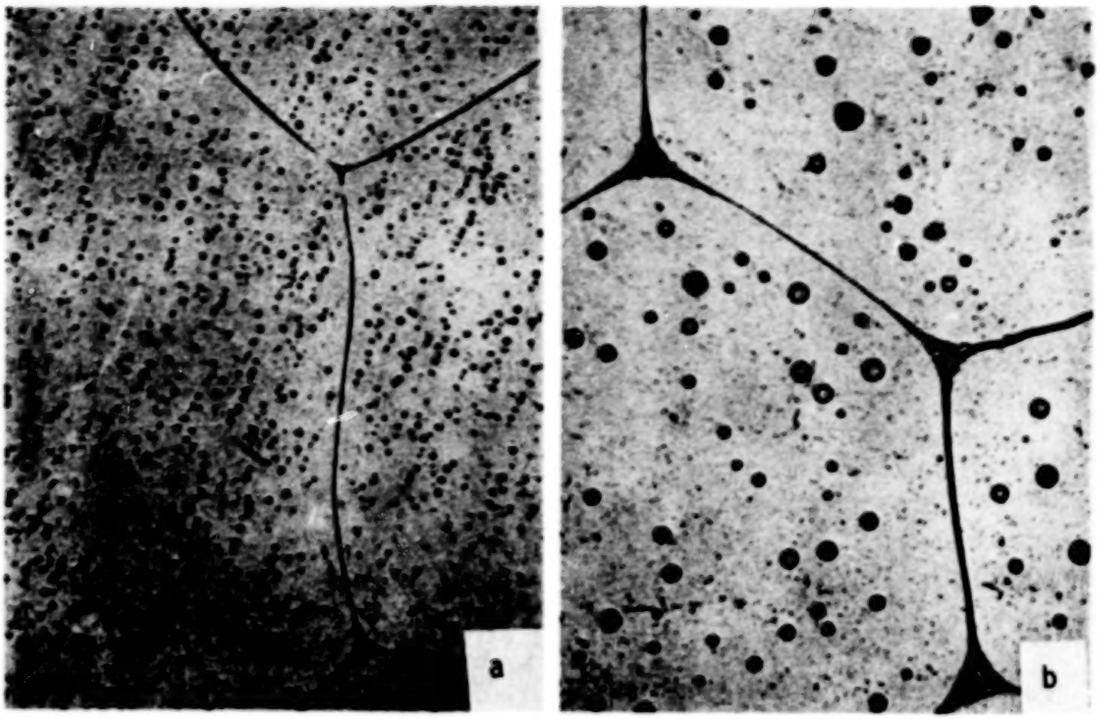

Homogenized Ni-2wt%Ag alloy specimens partially remelted and quenched. Heating rates were: (a) 50 K/s and (b) 10 K/s, 40X.

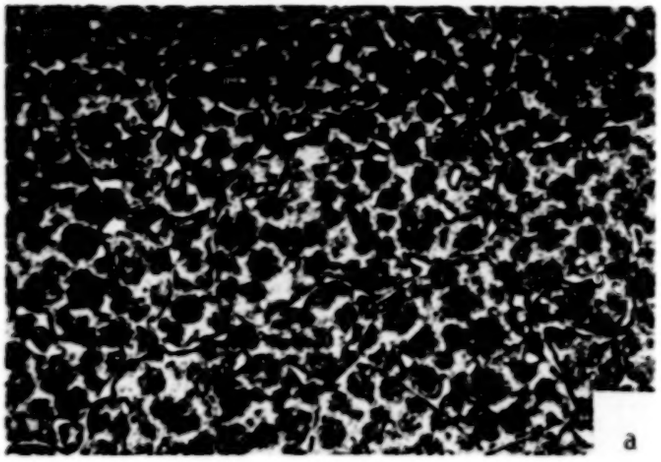

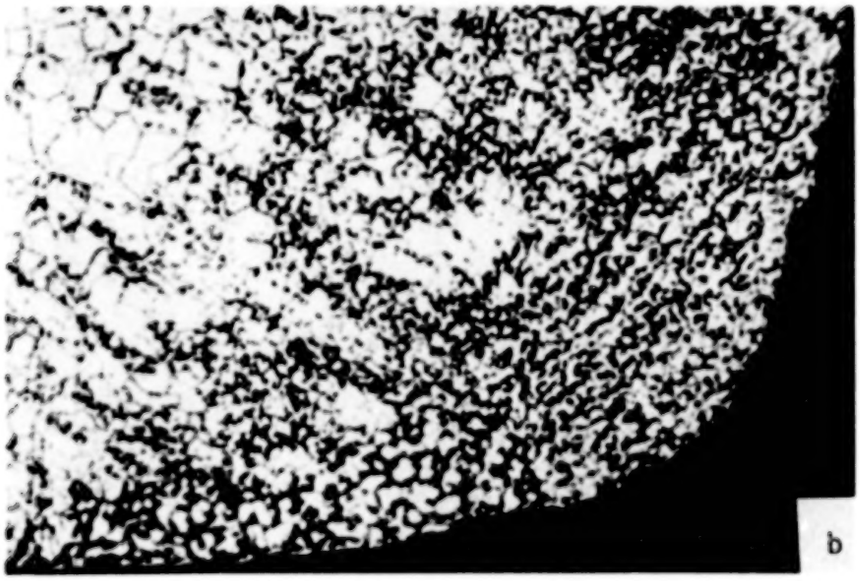

Photomicrographs of: (a) An Fe-25wt%Ni alloy specimen undercooled about 300 K , remelted at 350 K/s up to 1738 K and quenched, 110X; (b) Ni-2wt%Ag exploded wire tip.

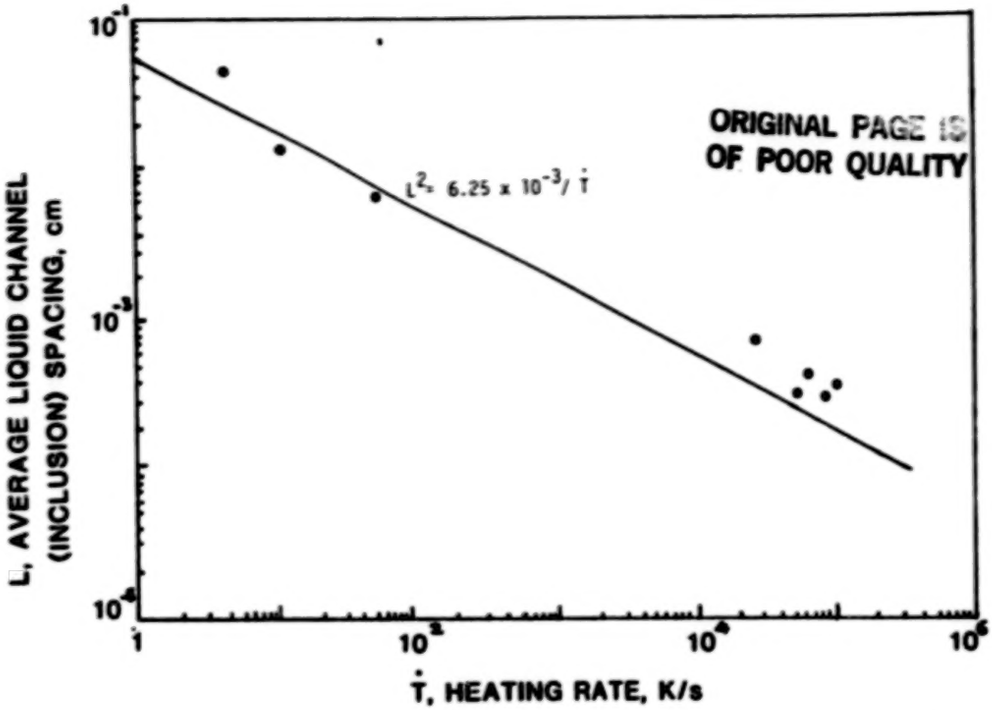

Average liquid channel or inclusion spacing versus heating rate. Ni-2wt%Ag alloy.

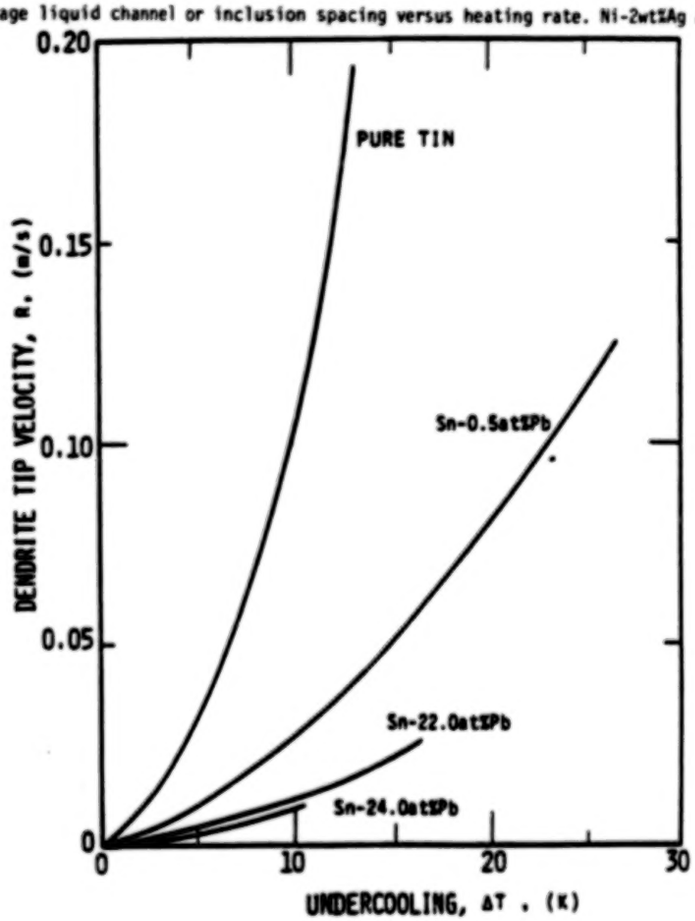

Primary tin dendrite tip velocity versus degree of initial undercooling for different compositions. Pb-Sn alloys. From Kobayashi and Shingu.

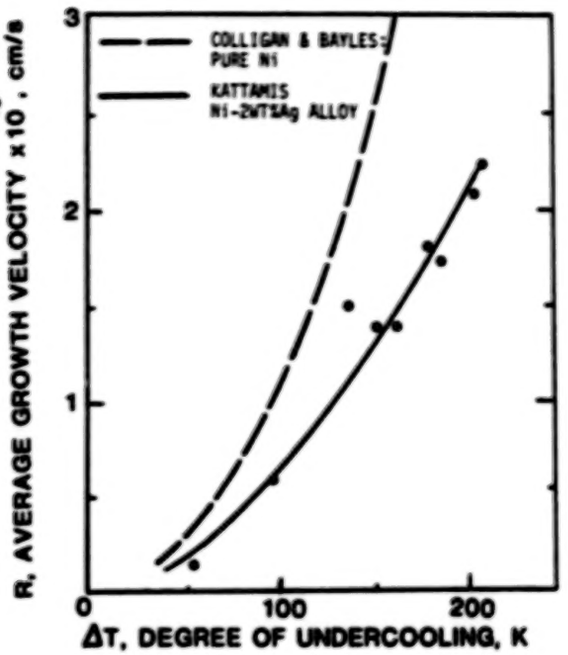

Average growth velocity versus initial bulk undercooling. Pure Nickel (Colligan and Bayles) and Ni-2wt%Ag alloy (Kattamis).

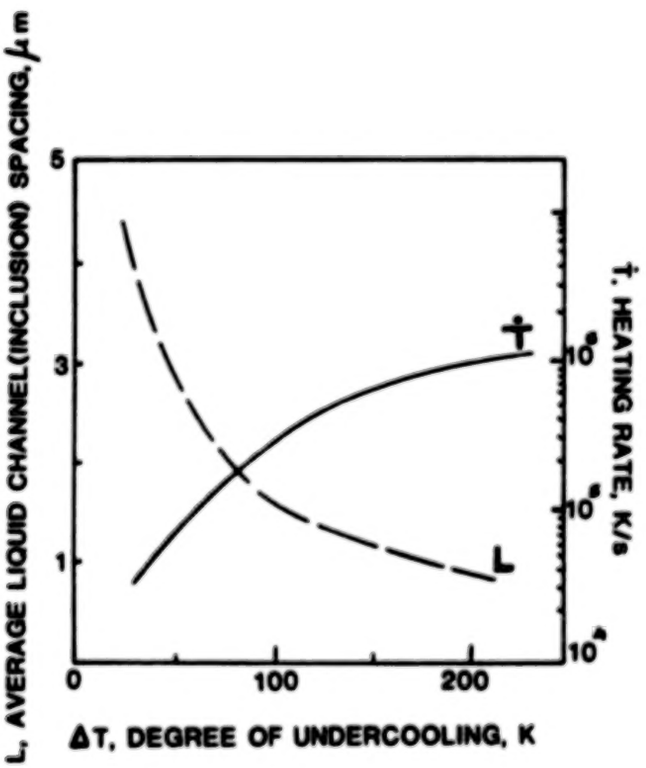

Average liquid channel or inclusion spacing and recalescence rate versus degree of undercooling. Theoretical curves. Ni-2wt%Ag alloy.

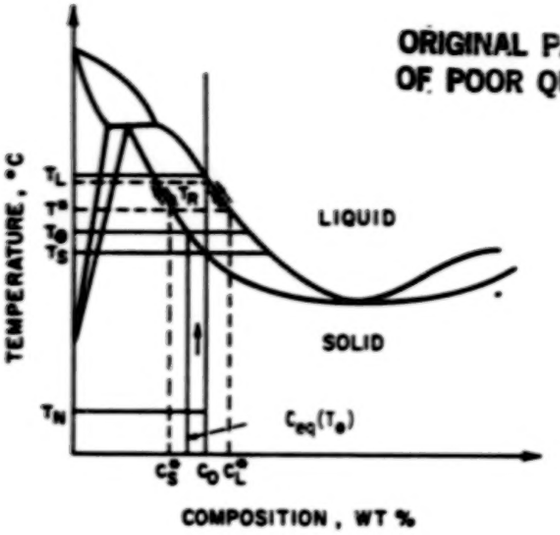

Hypothetical phase diagram used in the remelting analysis

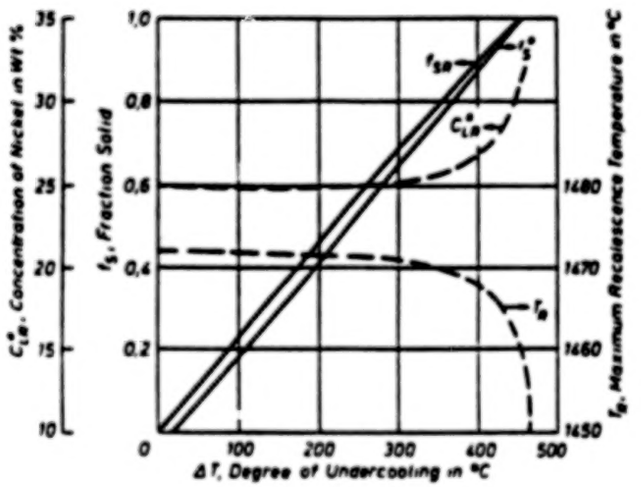

Fe + .5 wt % Ni, calculated values, versus degree of undercooling.
Tr - maximum recalescence temperature; f^o - fraction solid at the solidus temperature; f_{SR} - fraction solid at T_R; $^bC_{LR}$* - liquid composition.

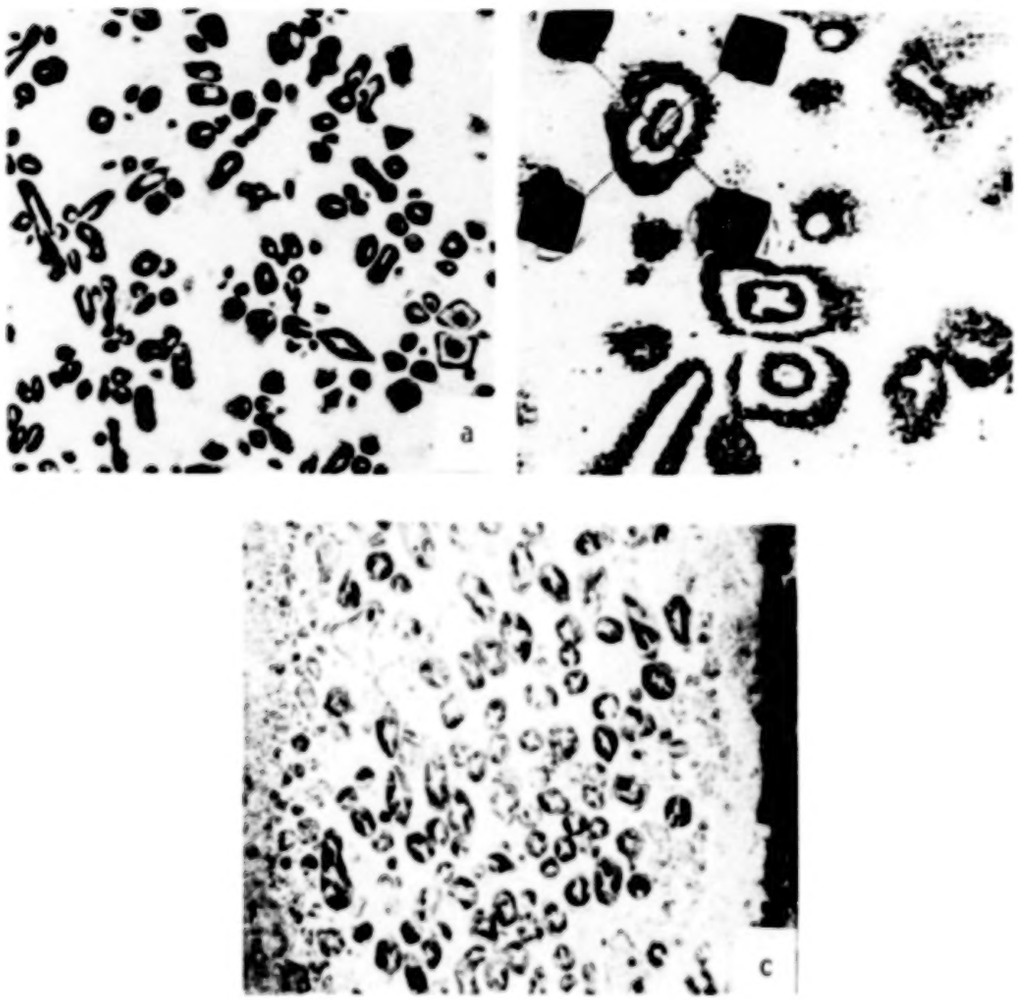

Photomicrographs of Fe-25wt%Ni alloy specimens: (a) and (b) Undercooled 100 K and internally chilled, 220X and 450X, respectively; (c) undercooled 150K and splat-cooled, 600X.

D3

THE POTENTIAL FOR BULK UNDERCOOLING AS AN INDUSTRIAL PROCESS

V. Laxmanan*
Case Western Reserve University
Cleveland, Ohio

INTRODUCTION

Dendritic solidification is a common occurrence in many commercially important casting processes and in controlled freezing experiments carried out for scientific investigations. An important example of dendritic solidification occurring at relatively slow growth rates is in the manufacture of single-crystal turbine blades used in the most advanced jet engines and also currently under evaluation for use in the main engines of the space shuttle. Such a "single-crystal" is actually composed of several dendrites, all growing in the preferred growth direction and with orientations within a few degrees (ideally, within a few fractions of a degree) of each other. However, even in this most advanced and carefully grown solidification structure significant micro and macro segregation occurs (ref. 1) with an attendant loss in anticipated high temperature properties. The "complexity" of the segregation pattern is intimately related to the complexity of the dendritic growth pattern propagating into the liquid during the solidification process, whereas, the "severity" of the segregation is influenced by the extent of solute redistribution (or "partitioning" of solute between the liquid and the solid phases as determined by the value of the partition ratio, k), which must inevitably occur in a multicomponent alloy, and, the complicating effects of fluid flow. In most terrestrial solidification processes, an important case of fluid flow is the influence of gravity acting on a liquid of varying density; density gradients being induced by both temperature and concentration gradients in the liquid. However, it must be pointed out that the complicating effects of fluid flow can produce unacceptably large compositional inhomogeneities even when the growth pattern propagating into the liquid is relatively simple, for example, a nearly flat solid-liquid interface advancing in a lightly doped semiconductor melt. Both micro and macro scale compositional variations have been reported during solidification of Si, GaAs, Ge, CdHgTe, InSb in terrestrial experiments but were found to be greatly reduced in experiments carried out in the Skylab (refs. 2 to 4), Apollo-Soyuz missions (ref. 5) and in the Salyut 6 Space Laboratory of the USSR (ref. 6). The author has recently proposed a series of experiments in the space shuttle designed to investigate the influence of gravity-induced fluid flow on the micro and macro segregation pattern accompanying dendritic growth. Figure 1 illustrates schematically the growth patterns propagating in the liquid during dendritic and plane front solidification.

In both the examples cited above the solidification rates (the velocity of the solid-liquid interface) are very small. For semiconductor crystals it varies between a few mm/hr to a few cm/hr. Single crystal turbine blades are grown at several cm/hr (ref. 7).

*Concurrently, NASA Lewis Resident Research Associate.

The main focus of this paper is, however, on solidification occurring in highly supercooled melts. Solidification rates in such melts are extremely high, an attractive feature from a commercial standpoint. Thus, the reported growth velocities for pure Ni and Co dendrites at a supercooling of 175 K are in excess of 180 km/hr (ref. 8). Rapidly quenched crystalline alloys produced by various atomization processes (e.g., centrifugal atomization or inert gas atomization) or melt spinning are examples of solidification processes, currently being intensively explored commercially, wherein extremely high solidification rates are achieved. Estimated dendrite tip growth rates are about 2 km/hr in a binary Al-4.5 wt % alloy, with a heat transfer coefficient of 6.4×10^5 W/m^2 K or 15 cal/cm^2 sK (ref. 9). In the limit, when the solidification rate exceeds a critical value, a glassy microstructure is obtained (refs. 10 and 11) even in highly alloyed melts, which under "normal" conditions would solidity to form one or more crystalline phases. Glassy metals, also called metallic glasses, are candidate materials for distribution transformers because of their very low energy losses (ref. 12) and are also being used in brazing and soldering applications (ref. 13).

The fundamental scientific argument behind the emergence of these various rapid solidification technologies is the simple fact that the scale of the microstructural pattern propagating into the liquid at very large growth rates is greatly refined. Thus, dendrite arm spacings reported in various rapidly solidified crystalline alloys approach micrometer and often sub-micrometer levels (ref. 14), with a corresponding reduction in the scale of the accompanying segregation pattern. Other benefits accompanying solidification at rapid rates, are the ability to incorporate into the solid solute elements which would be rejected into the liquid at lower growth velocities (e.g., Li in Al alloys; Pb in Zn or Al alloys) as well as the ability to nucleate metastable phases. In what follows, an attempt will be made to discuss in some detail the incentive(s) to explore undercooling or supercooling of large masses of liquid as a means to achieve rapid solidification rates. This is a route that has yet to be explored commercially, although historically the early experiments in this area were carried out in an industrial laboratory (refs. 8, 15, and 16). It is also interesting that the Fifth International Conference on Rapidly Quenched Metals, being held this year in West Germany, has a session devoted, for the first time, to solidification occurring at large undercoolings.

The various rapid solidification processes currently being investigated all suffer from the disadvantage of producing either atomized powders (mean particle size of about 150 to 200 μm) or ribbons which must be pulverized into a powder. To produce useful engineering components, these powders must be consolidated into fully dense bodies to achieve strength, toughness, and ductility by processes such as cold-pressing and sintering, hot mechanical pressing, hot isostatic pressing (HIP), and hot extrusion or dynamic compaction (ref. 17). An industrial process based on supercooling large masses of liquid, however, has the advantage of producing a bulk product, without the need to consolidate powders, while retaining the full benefits achieved by rapid solidification techniques. It is also conceivable that such a process will yield either near-net shape preforms or castings.

SOLIDIFICATION IN A HIGHLY SUPERCOOLED MELT

Dendritic growth in a number of commercially important processes such as electro-slag casting or remelting (ESC or ESR), vacuum arc melting (VAR) and continuous casting, in addition to the directionally solidified single crystal turbine blades mentioned earlier, occurs in the presence of an imposed positive temperature gradient in the bulk liquid ahead of the dendrite tips and within the interdendritic regions (figs. 2(a) and (b)). Good foundry practice also requires that solidification take place under a relatively steep thermal gradient and proceed progressively and directionally from the casting into a feed metal source (ref. 18). In all these processes, as also in melt spinning, the latent heat of fusion liberated during freezing as well as the sensible heat of the liquid phase is extracted through the fully solidified layer. Thus, the net heat flow is into the solid.

If, however, the liquid mass is allowed to supercool significantly below its liquidus temperature, extremely high solidification rates may be achieved when the melt nucleates, either spontaneously or following deliberate nucleation. This is because of the large decrease in free energy accompanying solidification from an initially supercooled melt. The latent heat of fusion is now released at a very rapid rate and must be transported away from the advancing solid-liquid interface at an equally rapid rate. Thus, at the typical dendrite growth velocities of the order of 180 km/hr mentioned earlier, the heat flux generated in the melt during freezing is $\rho_s HR$, where ρ_s is the density of the solid, H is the heat of fusion per unit mass, and R is the solidification rate, which for pure Ni is about 11.75 MW/cm^2 or 11.75×10^7 kW/m^2. Hence, if the initial melt supercooling is below a critical value, the heat of fusion liberated quickly raises the temperature of the advancing solid-liquid interface and of the remaining liquid to a value above the initial bath temperature T_∞, as shown schematically in figure 2(c). Here, it is assumed that solidification is dendritic and that the temperature of the bath far away from the advancing dendrite tips remains at the initial supercooled temperature, T_∞. Note that the dendrite tip temperature, T_t, is depressed below the liquidus temperature of the alloy, T_L, by an amount $\Delta T = (T_L - T_t)$. This depression in the tip temperature is often referred to as the "tip undercooling". The bulk liquid far away from the dendrite tip is depressed below T_L, by an amount $\Delta T_b = (T_L - T_\infty)$. In what follows, ΔT_b will be referred to as the bath "supercooling". The term "undercooling" will be used, in this paper, exclusively to describe the depression in the dendrite tip temperature (ref. 19).

Thus, dendritic growth in a "supercooled" melt occurs with negative temperature gradients in the bulk liquid ahead of the tips. The latent heat released at the advancing dendrite tips can, therefore, be transported away from the tip through the liquid phase. Note that in figure 2(c) it has been assumed that the temperature gradient within the interdendritic liquid is positive; in other words, some of the latent heat is transported away from the tip through the interdendritic liquid and, therefore, eventually through the solid. The thermal conditions within the interdendritic regions are, therefore, remarkably similar to those in solidification processes with an imposed positive temperature gradient (fig. 2(b)). Thus, during dendritic solidification in a supercooled melt, although there is a significant amount of heat flowing into the liquid phase, some of the heat released may be removed through the solid phase as well.

Figure 2(d) presents a slightly different viewpoint. Here, it is assumed that the thermal gradient within both the interdendritic regions and within the bulk liquid ahead of the dendrite tips is negative. Under these conditions all of the heat must necessarily be removed through the liquid phase.

Note that these general conclusions are equally applicable if the advancing solid-liquid interface is planar, cellular, or even nondendritic (e.g., cylindrical, rod, or spherical morphologies which are obtained with increasingly large bath supercoolings). In each case, the temperature of the advancing interface is depressed below T_L by a certain amount ΔT, which is a function of growth rate R, the prevailing temperature gradients, the radius of curvature at the advancing front, the liquid composition in equilibrium with the interface, and, finally, the bath supercooling, ΔT_b. A simple expression relating these quantities has been derived in appendix B. The application of this result to nondendritic morphologies has been discussed in reference 19.

Recent thermal measurements by Flemings and co-workers indicate that in a Ni-25 wt % Sn alloy droplet with an initial supercooling of about 236 K, the recalescence time is only about 2 ms (ref. 20). Thus, extremely high heat extraction rates are necessary to suppress recalescence and thereby "preserve" the initial supercooling of the bath throughout most of the solidification period. This, admittedly, is a very difficult task to achieve within 2 ms. The alternative is to attain very large initial supercoolings, ΔT_b, so that the maximum recalescence temperature and, hence, the maximum interface or dendrite tip temperature, T_t, never exceeds the equilibrium solidus temperature of the alloys, T_s (fig. 3).

The critical value of ΔT_b, the initial bath supercooling, required to avoid recalescence above the equilibrium solidus, T_s, is simply obtained as follows. The dendrite tip temperature or the "tip undercooling" ΔT, at the critical condition must equal the limiting value of $\Delta T_o = (T_L - T_s)$. Assume that following recalescence all of the liquid remaining has been raised from T_∞ to T_s. Let g_s be the volume fraction of solid formed. (Note that all of this solid was formed below T_s.) A simple heat balance yields, see also appendix A:

$$Lg_s = C_p(T_\infty - T_t) = C_p(T_\infty - T_s) \tag{1}$$

where L is the volumetric heat of fusion and C_p is the volumetric specific heat of the liquid. Here, it is assumed that all of the heat released flows into the remaining liquid (fig. 4). However,

$$\Delta T = (T_L - T_t) = (T_L - T_s) = \Delta T_o \tag{2}$$

Combining equations (1) and (2) yields

$$\Delta T_b = \Delta T + (T_\infty - T_t) = \Delta T_o + \frac{Lg_s}{C_p} \tag{3}$$

Note that the quantity L/C_p has the dimensions of temperature and is usually used as a scaling factor to normalize ΔT_b. Dividing equation (3) throughout by L/C_p yields a dimensionless bath supercooling usually denoted as $\Delta\theta$. Thus,

$$\Delta\theta = \frac{\Delta T_b}{L/C_p} = g_s + \frac{\Delta T_o}{L/C_p} \qquad (4)$$

If the alloy is completely solidified before recalescence raises the interface or dendrite tip temperature to T_s, the volume fraction solidified $g_s = 1$ in equation (4) above. The critical value of ΔT_b is then given by

$$\Delta\theta = 1 + \frac{\Delta T_o}{L/C_p} \qquad (5)$$

If the dimensionless supercooling $\Delta\theta > 1$, the bath is considered to be initially "hypercooled", whereas for $\Delta\theta < 1$, the bath is considered to be "hypocooled" (ref. 21).

Stated differently, in a hypercooled melt, solidification is completed before the temperature of the solid-liquid interface ever reaches T_s. Equation (5), however, indicates that, in an alloy melt, the dimensionless supercooling $\Delta\theta$ must exceed unity by an amount $C_p\Delta T_o/L$ (which depends on the freezing range of the alloy), for solidification to be completed below T_s. Recall that the solid forming below T_s is not subject to the thermodynamic constraints of solute redistribution imposed by the phase diagram and hence will be a solid of uniform composition, C_o, the composition of the initial alloy melt. Such a solid will have an "ideally uniform" distribution of all the alloying elements present in the initial melt. There is no microsegregation or macrosegregation in this case. Note that the growth morphology of the solid may be planar, dendritic, or nondendritic that it may appear "featureless" even at relatively high magnifications (refs. 11, 22, and 23).

For $\Delta\theta < 1$, there is some liquid remaining at the end of recalescence. Equation (4) must now be written as follows:

$$\Delta\theta = g_s + \frac{\Delta T}{L/C_p} \qquad (6)$$

where the dendrite tip "undercooling" ΔT is now less than ΔT_o, the equilibrium solidification range. The temperature of the solid-liquid interface (the dendrite tips) is thus greater than T_s. Microsegregation and also macrosegregation, can only be eliminated in this case if the solidification rates are high enough to cause a departure from "equilibrium partitioning" of solute elements between the solid and liquid phases (ref. 24). If the interface temperature, regardless of the morphology, remains below the so-called "T_o" temperature (this is the temperature at which the free energy of a solid of a given composition equals the free energy of a liquid of the same composition), thermodynamics indicates that "partitionless" solidifications without any solute redistribution is possible (refs. 24 and 25). Under these conditions, the solid formed from an initially "hypocooled" melt will also be completely free of all micro and macro segregation (appendix B).

THE TECHNOLOGICAL CONSTRAINTS TO ACHIEVING LARGE SUPERCOOLINGS

Two important technological requirements emerge from this description of solidification occurring in a supercooled melt. One is that in order to obtain

a solid which is "ideally" uniform in composition, the melt must be "hypercooled" before it is allowed to nucleate. Two, if the initial bath supercooling does not exceed the critical limit required for the onset of hypercooling, extremely rapid heat extraction rates must be achieved to avoid recalescence above the equilibrium solidus temperature of the alloy. The second requirement is dictated by the fact that solidification from an initially "hypocooled" melt will result in some residual microsegregation (and, perhaps, macrosegregation) depending on the level of the initial supercooling.

A third requirement, not immediately apparent, from the above description, is the need to exercise proper "control" on the heat extraction conditions, particularly if the melt is initially hypocooled. This is because under "uncontrolled" conditions which do not "preserve" the initial bath supercooling, a metastable (and, say, a desirable) phase may be nucleated at the lower; initial, bath temperature, and, with a progressive reduction in the bath supercooling as solidification proceeds, other, less desirable phases may nucleate and grow in the remaining liquid. Even when new phases do not nucleate in the remnant liquid, the morphology of the phase which has nucleated may change, to a less desirable one, with a progressive increase in the solidification temperature.

Each of the requirements outlined here will be discussed more completely in what follows.

Maximum Achievable Supercoolings

Flemings and Shiohara (ref. 20) have recently summarized the maximum supercoolings reported in a variety of alloys by a number of investigators. In most Fe and Ni base alloys, alloy systems of potential commercial interest, a maximum supercooling of at least 100 K has been obtained, and, in some specific compositions it is much higher, being a significant fraction of the supercooling required for the onset of hypercooling conditions. In type 316 stainless steel, for example, the maximum supercooling reported is 475 K; the hypercooling limit for pure Fe and Ni are, respectively, 329 K and 445 K, and, from equation (5) it appears that this steel was probably hypercooled. Thus, it seems possible to achieve, at least on a laboratory scale, supercoolings approaching the hypercooling limit in commercially important alloys.

Notable exceptions in the data summarized by Flemings and Shiohara are the commercially important Al and Cu alloys, although Cech and Turnbull (ref. 26) have reported supercoolings of 130 K and 236 K for pure Al and Cu, respectively, in microscopic droplets. Moak, Griesenauer, and Gelles (ref. 27) were, however, unable to achieve any supercooling in very high purity copper with larger samples. These authors were, likewise, unable to obtain any significant supercooling (maximum value of 10 K) in Narloy Z (Cu-3 wt % Ag-0.4 wt % Zr) in sample sizes of up to 1.5 g. In Cu-5 wt % Ag alloy, the maximum supercooling was close to 100 K but averaged 50 K in most experiments. More recently, Perepezko and coworkers (ref. 28) have used molten salt mixtures as carrier fluids to achieve substantial supercoolings in Al and Cu alloys.

Techniques for Supercooling Bulk Samples

The various techniques discussed in the literature (refs. 20, 28, and 29) to achieve significant supercoolings all depend on either isolating or eliminating potential heterogeneous nucleants from the melt. These nucleants may originate from impurities present in the raw materials used to make up the alloy, or may be the result of various mold-metal-environment reactions, or may actually form during the melting operation; oxides, sulfides, oxysulfides, and carbides for example. The most effective heterogeneous nucleation sites are, however, the walls of the container or the mold material itself, within which the alloy must be melted. Thus, the most effective way of supercooling bulk samples of up to several pounds, or larger, may be to isolate the molten alloy from the crucible walls by encasing it in a suitable glass or slag layer (refs. 15 and 29). This was the approach first used by Walker at the General Electric Research Laboratory, and, latter by Kattamis and Flemings at MIT. The glass probably dissolves the impurities present in the melt which act as active nucleants. However, repeated heating and cooling of the sample, a process often called "thermal conditioning", is known to aid in achieving a large supercooling, particularly after the first few cycles (fig. 5).

The actual processes operating during "thermal conditioning" are, as yet, not very well understood and perhaps differ for each alloy/glass/mold material combination. Suitable guidelines for the proper choice of the encasing inorganic glass and mold material, for each specific alloy of commercial interest, still need to be evolved. These should definitely prove to be a very fruitful area of research in industrial laboratories.

An alternative approach to supercooling bulk samples is to eliminate the crucible altogether and instead position the melt using electromagnetic acoustic and other nongravitational forces (refs. 30 and 31). This limits the potential heterogeneous nucleants to those arising from impurities present in the raw materials and those that actually form during the melting operation. Various "containerless" processing technologies are now sufficiently advanced but do suffer from a variety of limitations. Electromagnetic levitation, for example, requires a considerable amount of power input to generate the electromagnetic force needed to counteract the weight of the sample. This often implies an excessive amount of superheat and, hence, little control during melting or on the amount of subsequent supercooling. This limitation may, however, be overcome in the microgravity environment of space, since a much lower power input would be needed to counteract the weight of the sample. An electromagnetic levitation system is scheduled to fly aboard the space shuttle in September 1985 (Professor Merton C. Flemings, MIT, is scheduled to fly experiments on binary Ni-Sn alloys during this mission) and should offer a unique opportunity to levitate fairly large masses as well as exercise control on the degree of supercooling achieved.

Electrostatic and acoustic levitators (ref. 30) have been successfully used to levitate hollow quartz spheres heated to 500 °C. Temperature capabilities up to 1600 °C have been planned. There has, however, been very little work to date on melting and solidification of metal alloys in these systems.

Controlling Heat Extraction Rates in Bulk Samples

The second requirement of ensuring rapid heat extraction rates to suppress recalescence above the equilibrium solidus, has again been achieved on a laboratory scale. Thus Chu, et al., (ref. 32) were able to obtain a fully homogeneous solid solution in a Sn-5 wt % Pb alloy (note that the maximum equilibrium solid solubility of lead in tin is only 2.5 wt % Pb) by quenching an emulsified droplet in a vigorously agitated bath of CCl_4 and oil. (These droplets appeared to be "featureless", as discussed earlier, when examined at magnifications of up to 1000.) After being "aged" for 1 month at room temperature, however, the alloy showed substantial precipitation of the lead-rich phase. In this condition, the microstructure was very similar to that obtained in a slow cooled, emulsified droplet which supercooled about 100 K before nucleation.

The results of these experiments clearly indicate the benefits to be obtained by combining emulsification (that is proper "conditioning" of the sample to control the amount of supercooling before nucleation) with a suitable means of extracting heat externally. It is likely that rapid external cooling resulted in a higher degree of supercooling, thus suppressing formation of the lead-rich phase, or merely enabled heat to be removed more efficiently during solid state cooling. The important finding, however, from a practical standpoint, is that precipitation of the second phase(s) can now proceed in a controlled manner, so that the size, shape, and amount of these precipitates may be suitably tailored to optimize the mechanical or other physical properties of interest.

The importance of controlling heat extraction rates following nucleation is further illustrated by the following example. In binary Fe-C alloys with less than 0.51 wt % C (hypoperitectic compositions), Ono, et al., (ref. 33) observed that the bcc phase, δ-ferrite, nucleates first at the initial bath temperature and is followed by the nucleation of the fcc γ phase as the temperature increases during recalescence. In hyperperitectic alloys, with C contents between 0.51 and 1.20 percent, the metastable bcc phase is still the first phase to nucleate and is followed again by the nucleation of the stable fcc phase. Similar observations have been made by Kelly, et al., (ref. 34) and MacIsaac, et al., (ref. 35) in 303 stainless steel and 316 stainless steel, respectively. In both of these steels the metastable bcc phase nucleated, particularly at large initial supercoolings, but for lower supercoolings the alloys contained both bcc and fcc phases.

In the examples cited above, the primary benefit of rapid external cooling was in aiding the selection of the phase that would nucleate following supercooling of the samples. High heat extraction rates are, however, also vitally important to control the growth morphology of the phase that has been selected at the supercooled temperature. Morphological transitions from planar to cellular to dendritic structures have been observed in a number of rapidly solidified alloys: in Al-Si alloys (ref. 36) prepared by electrohydrodynamic atomization process (EHD); in electron-beam melted Ag-Cu alloys (ref. 37); and in melt-spun superalloys (ref. 14). As noted earlier, the more complex solidification morphologies are accompanied by a more complex residual microsegregation pattern. The critical processing parameters required to control these morphological transitions have recently been estimated by the author (ref. 22) for a simple binary alloy, assuming equilibrium partitioning of solute even for very large growth rates.

In alloys which are nominally two-phase after equilibrium solidification, for example, binary Ni-Sn, Ni-Sb (ref. 38), Ni-Mo (ref. 23), Co-Sn (refs.38 and 39), and Co-Sb (ref. 38) alloys of hypo, hyper, and eutectic compositions, laboratory scale experiments indicate that the morphology of the eutectic solid forming in these alloys is greatly influenced by the amount of initial melt supercooling. With increasing melt supercoolings, a greater amount of "irregular" or "anomalous" (ref. 40) eutectic is formed until at very large supercoolings (accompanied with rapid heat extraction) the structure is entirely the "irregular" or "divorced" type.

In summary, therefore, a viable industrial process based on supercooling large masses of liquid must be able to achieve, consistently, a significant amount of supercooling, as well as exercise control on the heat extraction rate following nucleation of the sample. It was estimated earlier that, for the typical dendrite growth velocities in a highly supercooled melt, the heat flux generated due to liberation of the heat of fusion during recalescence is of the order of $2MW/cm^2$ or $2x10^{10}$ W/m^2. Assume that a heat sink is available at a temperature of, say, 10^3 K below the temperature of the supercooled bath (fig. 6). (Note that liquidus temperatures of most alloy systems are of the order of 10^3 K. Higher temperature differences between the starting "melt" and the heat sink are only possible if the "melt" is a vapor or a plasma.) To completely suppress recalescence, the heat transfer coefficient between this sink and the supercooled liquid bath must be about $2x10^8$ W/m^2 K. This is about 2 to 3 orders of magnitude higher than the estimated heat transfer coefficients in various solidification processes (ref. 38), the maximum estimated value being about $2x10^6$ W/m^2 K for a 10 μm diameter droplet (ref. 34). The ability to extract heat externally, and rapidly, from a large mass of hypocooled liquid is, thus, necessarily limited.

These orders of magnitude calculations, however, clearly illustrate once again the importance of attaining very large bath supercoolings before nucleation. Various containerless processing technologies developed at the Jet Propulsion Laboratory (ref. 30), in particular, under the auspices of the National Aeronautics and Space Administration should, therefore, provide a valuable resource for both academic and industrial researchers in the quest for ever higher supercoolings.

THE TECHNOLOGICAL BENEFITS OF SUPERCOOLING BULK SAMPLES

Conventional ingot making or casting processes impose, in principle, virtually no size limitation. Thus, steel ingots weighing several hundred tons are common for use as rotors for the generators and turbines in electric power generating stations. These large ingots suffer, however, from serious micro and macro segregation as a result of their very long solidification times (ref. 41). Severe macrosegregation also persists in the smaller size scales commonly used in the superalloy or Al industries in processes such as ESR, VAR, or continuous casting. These will be discussed by others in this symposium. Since the prospects of supercooling such large masses of liquid appear remote, even in the distant future, a fundamental understanding of the mechanisms responsible for segregation in these size scales continues to be very important. In the absence of such understanding or control, casting processes requiring premium properties must necessarily begin with melts of a smaller

size scale. Moore (ref. 42) has suggested that the next generation of casting processes for tonnage steel production will involve thin slabs and small billets to achieve high quality and productivity. Specialty steels requiring superior electrical and magnetic properties (ref. 12) will probably use RST processing.

The potential benefits of developing industrial processes which rely on supercooling a large mass of liquid should be viewed in this larger context. A typical, and, perhaps, the only published, example of an application which beneficially exploits this concept is illustrated by a research program carried out at Battelle-Geneva in the late 1970's (ref. 43). The objective here was to assess the feasibility of supercooling two commercial superalloys, Mar-M-200 and Mar-M-509, for production of directionally solidified turbine blades. A variety of mold materials were investigated - recrystallized alumina, ZrO_2, fused silica, pyrex, and zirconium silicate bonded with waterglass - with the aim of attaining high initial supercoolings.

The alloys were synthesized from high purity raw materials, melted in an induction furnace, held isothermally at a temperature of between 1450 and 1500 °C for a few minutes and cooled at between 20 and 100 °C/min, while maintaining a temperature gradient of 10 °C/cm in the melt. Vacuum melting and repeated thermal cycling were found to improve the attainable supercooling. Some alloying elements such as Al were found to be totally detrimental. The mold material used was found to be of crucial importance. Thus, with Mar-M-509, a supercooling of 153 K was obtained in a fused silica mold but Mar-M-200 could not be supercooled in this mold. Shell molds made of zirconium silicate were, however, shown to favor a supercooling of up to 191 K in the latter alloy. The alloys were typically solidified into bars, 12 mm in diameter and 10 cm long, but, based on the initial results, a series of gas turbine blades was also prepared from supercooled Mar-M-200 melts. Tensile tests indicated that UTS and elongation at rupture were similar, or somewhat better than those obtained with conventional DS-200 alloy. Creep tests indicated that at 800 °C, the best time to rupture (403 hr) for the supercooled samples was effectively equivalent to that for a monocrystal. The overall creep performance was superior to conventional DS-200 alloy.

These results indicate that by a suitable choice of processing conditions it should be feasible to supercool medium-size melts (up to a few tens of kilograms and, perhaps, a few hundred kilograms) by merely extending the understanding gained in the laboratory. New innovations will no doubt be needed to produce the "ideal" solid of uniform composition, obtained only from "hypercooled" melts. However, it must be pointed out that a host of microstructures, whose engineering potential still remains to be explored, may be obtained from moderately supercooled or "hypocooled" melts. Thus, although the heat transfer coefficients required to completely suppress recalescence would probably be very difficult to realize in larger samples, useful practical applications of the refined and novel microstructures (refs. 10, 23, and 32 to 34) obtained from these melts still seems possible.

Finally, a very casual survey of the history of recent metallurgical innovations indicates that important new ideas have found their way from the academic laboratories to the industrial laboratories, where they were then extensively investigated. (The development of the single crystal turbine blade and some of the more recent microstructural innovations in these materials is,

probably, a good example of where just the opposite has occurred.) In the field of rapid solidification, one is immediately reminded of the contributions of Pol Duwez and his students at Caltech in the early 1960's. In his famous Campbell Memorial lecture (ref. 44), however, Duwez himself remarked that, because of size limitations, amorphous metals would probably only find applications in the field of electronics, or in very small electrochemical devices. The thicknesses of metallic glasses being cast into ribbons, in widths of up to 170 mm, are well within the size limitations recognized by Duwez. Yet, these amorphous materials are now being tested in large-distribution transformers because of both process innovations and innovative new approaches to the design and manufacture of the transformer itself. Interestingly, the very technological advances which were responsible for the production of metallic glasses in commercially important quantities (both here in the U.S. and overseas, Japan, in particular) have also spurred the development of a competing, rapidly quenched, crystalline alloy whose properties have been well known for almost a hundred years, Fe-6.5 wt % Si, for the same application. Recent work at Allied Corporation (refs. 45 and 46) has demonstrated the feasibility of producing wide ribbons of this alloy using the Planar Flow Casting process, whereas, Kawasaki Steel (ref. 47) has reported preparation of the same alloy by both single and twin-roler techniques. The magnetic properties of the rapidly quenched Fe-6.5 % Si alloy lie between those of the Fe-3.5 % Si alloys, currently being used extensively in transformers and motors, and the ferrous metallic glasses based on Fe-B-Si.

Another example of a recent metallurgical innovation is a class of forming or casting processes which have come to be known by the generic name of Rheocasting processes, which again originated in an academic laboratory, this time at MIT in the early 1970's (refs. 48 to 52). It has been confirmed through reliable sources that the process is now being used commercially by a major U.S. corporation whose identity must, for the moment at least, remain a mystery. Yet another interesting application of Rheocasting has recently been reported by Denholm, et al. (ref. 53). These authors were reinvestigating the Al-rich region of the Al-Fe-Mn ternary to determine more accurately the solubility of iron in commercial aluminum-manganese alloys. (This solubility limit determines the iron levels to be expected on recycling aluminum scrap.) Vigorous agitation of the partially solidified ternary Al-Fe-Mn melt resulted in large rounded aluminum crystals and also large polygonal intermetallic crystals of $(FeMn)Al_6$ and $FeAl_3$, microstructure typical of Rheocasting processes, which greatly aided in the accurate determination of Fe levels.

These two examples here illustrate the societal gains to be realized by a successful combination of the academic and industrial approaches to research and development. Our understanding of the supercooling behavior of liquid metals and alloys is, in a sense, very mature because of the pioneering contributions of researchers such as Professors Turnbull, Flemings, Kattamis, Perepezko and their coworkers in the academia. On a more fundamental level, the recent theoretical contributions of Langer and Muller-Krumbhaar (refs. 54 to 56), as well as the experimental and theoretical work of Glicksman, Trivedi and their coworkers (refs. 57 to 63), illustrate how much more remains to be understood. It appears, however, that the time is now ripe for the evolution of new processes which exploit gainfully the supercooling behavior of bulk samples. This would, nevertheless, require a powerful economic incentive, which is best provided by vigorous industrial participation.

CONCLUSIONS

It has been suggested that new industrial processes be evolved which exploit the supercooling behavior of large masses of liquid. Unlike other rapid solidification processes, such an approach offers the advantage of being able to produce a bulk product without the need for subsequent consolidation of ribbons, flakes, or powders, while at the same time retaining the full benefits achieved by rapid solidification techniques. These new processes must be able to achieve large melt supercoolings as well as exercise control on the rate of heat extraction following nucleation of the melt. However, significant engineering advantages are predicted even for moderate bath supercoolings and heat extraction rates.

APPENDIX A

Critical Supercooling Required For The Onset of Hypercooling

In writing the simple heat balance of equation (1), it has been assumed that the latent heat released during recalescence only flows into the remaining liquid, in other words, we have implicitly assumed adiabatic or isenthalpic conditions (ref. 34). Moreover, it has been assumed that there are no temperature gradients within the liquid remaining at the end of recalescence (fig. 4(a)). Equation (1) may, however, be reinterpreted for the thermal conditions shown schematically in figures 4(b) and (c). Here, it is assumed that heat flows into both liquid and solid phases during recalescence. For simplicity, the solid-liquid interface is taken to be planar. At the end of recalescence both liquid and solid are uniformly at a temperature T_t (fig. 4(c)). Writing a simple heat balance as before:

$$Lg_s = C_{pl} g_l (T_\infty - T_t) + C_{ps} g_s (T_\infty - T_t) \tag{7}$$

where C_{pl} and C_{ps} are the specific heats of the liquid and solid, respectively, g_s and g_l are the volume fractions of the solid formed and liquid remaining, and, Lg_s is the amount of heat liberated. Rewriting equation (7) results in

$$Lg_s = C_p (T_\infty - T_t) = (C_{pl} g_l + C_{ps} g_s) (T_\infty - T_t) \tag{8}$$

Comparing equations (1) and (8), it follows that C_p may be regarded as an "effective" specific heat of the liquid plus solid mixture remaining at the end of recalescence.

If the interface temperature, T_t, at the end of recalescence remains below T_s (in other words for $\Delta T > \Delta T_0$), the bath will be hypercooled, and there is no liquid remaining at the temperature T_s.

Note also that any liquid remaining at the end of recalescence is essentially isothermal. Hence, solidification of this liquid can only proceed if there is some heat flow through the solid. The system can no longer be adiabatic. Thus, the heat flow "path" must follow the general path, 3, described by Levi and Mehrabian (ref. 34, fig. 7).

APPENDIX B

Relationship Between The Bath Supercooling and the Dendrite Tip Undercooling

Assume that solidification into the supercooled liquid is dendritic. At the very early stages of recalescence, it may be assumed that the bulk liquid far away from the dendrite tips remain at the initial bath temperature, T_∞, as shown schematically in figures 2(c) and (d). The dendrite tip temperature, T_t, will be depressed below the equilibrium liquidus temperature, T_L, for the initial alloy composition, C_o, by an amount ΔT due to the compositional changes occurring in the liquid, as well as, curvature and kinetic effects (refs. 64 to 67). Thus,

$$\frac{\Delta T}{\Delta T_o} = \frac{\Delta C}{\Delta C_o} + \frac{2\ell_c k}{r_t} + \frac{\Delta T_k}{\Delta T_c} \tag{9}$$

where ℓ_c is a characteristic length called the capillary length (ref. 60), r_t is the radius of the dendrite tip, and, $\Delta C = (C_t - C_o)$ is the solute buildup at the dendrite tip, C_t being the liquid composition in equilibrium with the tip (fig. 8), ΔT_k is the kinetic undercooling, and $\Delta T_o = (T_L - T_s)$ is the equilibrium solidification range. Thus, of the total bath supercooling, ΔT_b, a portion, ΔT, is required to ensure that the dendrite tip is in "equilibrium" with the bath and satisfy kinetic effects. The remainder, $\Delta T_H = (T_t - T_\infty)$, is required to dissipate the heat of fusion generated at the tip. A simple heat balance at the tip yields

$$T_t = T_\infty + \frac{L}{C_p}\left(\frac{\lambda_t R r_t}{2\alpha_L}\right) \tag{10}$$

where α_L is the thermal diffusivity of the liquid, R the dendrite tip growth rate and λ_t is a dimensionless quantity related to the "effective" thermal diffusion distance in the bulk liquid (ref. 19). Equations (9) and (10) together yield a relationship between ΔT_b and the tip undercooling ΔT. As discussed earlier, the extent of microsegregation depends on the dendrite tip temperature (or tip undercooling) because of its influence on the composition of the solid formed at the tip. Experimental data obtained from directional solidification, usually carried out with a positive thermal gradient in the liquid, must be compared with data from supercooled melts at a constant value of the tip undercooling, ΔT.

The solute buildup ΔC at the dendrite tip is given by (ref. 64)

$$\frac{\Delta C}{\Delta C_o} = s + \frac{2p\lambda_c\, k(1 - s)}{1 - 2p\lambda_c(1 - k)} \tag{11}$$

where

$$s = \frac{\alpha k}{k - 1} = \frac{D_L G_i}{R\Delta C_o} \tag{12}$$

and

$$a = \frac{D_L G_i}{RC_o} \tag{13}$$

Here, λ_c is another dimensionless quantity, related to the "effective" solute diffusion distance in the bulk liquid ahead of the tip, G_i is the thermal gradient within the interdendritic liquid, and p is the Peclet number; $p = Rr_t/2D_L$, D_L being the diffusion coefficient of solute in the liquid. Finally, $\Delta C_o = C_o(1 - k)/k$. It is assumed that $G_i > 0$.

Note that these equations include an important morphological detail, the dendrite tip radius r_t. The dimensionless quantity λ_c must be considered a true constant except at large growth rates approaching the "absolute stability" limit of Mullens and Sekerka (ref. 68). The value of λ_c may be estimated by considering dendrite behavior at these large growth rates. It seems that $\lambda_c = 1/16 = 0.0625$, to be in agreement with the tip stablility parameter σ. (See later and refs. 55 and 69.) Very close to the Mullins and Sekerka limit, however, the dimensionless quantity λ_c must abruptly tend to zero. In this limit it has been shown that the tip radius becomes infinite, in other words, the interface becomes planar (refs. 65 and 66).

Moreover, as λ_c tends to zero at large values of R, the solute buildup given by equation (11) becomes negligibly small, even for equilibrium partitioning of the solute. Finally, λ_c has been shown to be intimately related to another dimensionless parameter, $\sigma_c = 2\ell_c D_L/Rr_t^2$ (ref. 66). This is remarkably similar to the "tip stability" parameter $\sigma^* = 2\alpha_L d_o/Rr_t^2$ obtained by Langer and Muller-Krumbhaar for dendritic growth in a supercooled pure melt (refs. 54 and 65). The tip stability parameter determines the largest, stable, dendrite tip radius for a given set of growth conditions and thus determines the size-scale of the dendritic growth pattern propagating in a liquid. It has been suggested by the author (ref. 19) that the value of σ_c or σ^* also, probably governs the transition from dendritic to the nondendritic (cylindrical and spherical) growth morphologies observed in supercooled melts. From a practical standpoint, σ_c determines the scale of the microsegregation pattern in the finally solidified alloy.

REFERENCES

1. Giamei, A. F., and Kear, B. H., Met. Trans, 1 (1970) 2185.

2. Gatos, H. C., in Materials Processing in Space, Proc. of a Special Conf. on Advances in Ceramics, Sep. 4-5, 1982, published by American Ceramic Society, 1983, ed., B. J. Dunbar.

3. Yue, J. T., and Voltmer, F. W., J. Crystal Growth, 29 (1975) p. 329.

4. Witt, A. F., Gatos, H. C., Lichtensteiger, M., Lavine, M. C., and Herman, C. J., J. Electrochem. Soc., 122 (1975) p. 276.

5. Witt, A. F., Gatos, H. C., Lichtensteiger, M., and Herman, C. J., J. Electrochem. Soc., 125 (1978), p. 1832.

6. Galazka, R. R., Warminski, T., Bak, J., Auleytner, J., Dietl, T., Okhotin, A. S., Borovikova, R. P., and Zubritskij, I. A., J. Crystal Growth, 53 (1981) 397.

7. Mclean, M., in Directionally Solidified materials for high temperature service, published by the Metals Society, London, 1983.

8. Colligan, G. A., and Bayles, B. J., Acta Met, 10 (1962) 895.

9. Masur, L. J., and Flemings, M. C., Proc. 4th Int. Conf. on Rapidly Quenched Metals, Sendai, 1981, p. 1557.

10. Boettinger, W. J., Proc. 4th Int. Conf. on Rapidly Quenched Metals, Sendai, 1981, p. 99.

11. Laxmanan, V., "Interface Morphology During Rapid Solidification," to be presented at the 5th Int. Conf. on Rapid Quenching and Solidification of Metals, Sep. 3-7, 1984, Eds., H. Warlimont and S. Steeb.

12. Gilman, J. J., Metals Progress, July 1979, pp. 42-47.

13. DeCristafaro, N., to be presented at the 5th Int. Conf. on Rapid Quenching and Solidification of Metals, Sep. 3-7, 1984, Eds., S. Steeb and H. Warlimont.

14. Jones, H., Mat. Sci. and Eng., 65 (1984) 145.

15. Walker, J. L., in G.R.St. Pierre (ed.), Physical Chemistry of Process Metallurgy, AIME, New York, (1961), 845.

16. Tarshis, L. A., Walker, J. L., and Rutter, J. W., Met. Trans. 2, (1971) 2589.

17. Grant, N. J., and Pelloux, R. M. in Rapid Solidification Technology, p. 361, ASM Sourcebook, Ed., R. L. Ashbrook, ASM, 1983.

18. Flemings, M. C., in Solidification Processing, p. 231-243, McGraw Hill, New York (1974).

19. Laxmanan, V., "Some fundamental aspects of solidification in a supercooled melt," to be presented at the 5th Conf. on Rapid Quenching and Solidification of Metals, Sep. 3-7, 1984.

20. Flemings, M. C. and Shiohara, Y., Mat. Sci. and Eng., 65 (1984) 157.

21. Cohen, M., Kear, B. H., and Mehrabian, R., in Proc. 2nd Int. Conf. on Rapid Solidification Processing: Principles and Technologies, Reston, VA, March 1980, Claitor's Publishing Div., Baton Rouge, LA, 1980, Eds., R. Mehrabian, B. H. Kear, and M. Cohen, p. 13.

22. Laxmanan, V., "Some fundamental considerations during rapid solidification processing," to be published in Proc. Symp. on Rapidly Solidified Metastable Materials, North Holland Publishing Co. (1984), eds. B. C. Giessen and B. H. Kear.

23. Tewari, S. N., and Jayaraman, N., unpublished research carried out at NASA-LeRC, Cleveland, Ohio.

24. Boettinger, W. J., and Coriell, S. R., Mat. Sci. and Eng. 65 (1984) 27.

25. Baker, J. C., and Cahn, J. W., in Solidification, ASM (1971) p. 23.

26. Turnbull, D. and Cech, R. E., J. Appl. Phys., 21 (1950) 804.

27. Moak, D. P., Griesenauer, N. M. and Gelles, S. H., in "Undercooling of Materials During Solidification in Space," Battelle, NAS 8-28749, Final Report, April 1975.

28. Perepezko, J. H., Mat. Sci. and Eng., 65 (1984) 125.

29. Kattamis, T. Z., and Flemings, M. C., Trans. AFS, 75, (1967), 191.

30. Barmatz, M., in Materials Processing in the Reduced Gravity Environment of Space, Elesevier Publishing Co., (1982), Ed., G. E. Rindone, p. 25.

31. Oran, W. A., Presented at the 15th National SAMPE Technical Conf., Oct. 4-6, 1983, Cincinnati, Ohio.

32. Chu, M. G., Shiohara, Y., and Flemings, M. C., Met. Trans. A15, (1984) 1303.

33. Ono, T., Takeo, T., Umeda, T., and Kimura, Y., in Proc. U.S. Japan Cooperative Science Program, Seminar on Solidification Processing, Dedham, MA, June 26-29, 1983, Eds. M. C. Flemings and G. Ohira, p. 359.

34. Kelly, T. F., Cohen, M. and Vander Sande, J. B., Met. Trans. A, 15A, (1984).

35. MacIsaac, D. G., Shiohara, Y., Chu, M., and Flemings, M. C., in Proc. Conf. on Grain Refinement in Castings and Welds, eds., G. J. Abbaschian and S. A. David, Met. Soc. AIME, Warrendale, PA, 1983, p. 87.

36. Mehrabian, R., Int. Met. Rev. 27 (1982) 185.

37. Boettinger, W. J., Shechtman, D., Schaefer, R. J., and Biancaniello, F. S., Met. Trans. A, 15A (1984) 55.

38. Ohira, G., in ref. 33 above.

39. Kattamis, J. Z., J. Mat. Sci. Lett., 5 (1970) 531.

40. Powell, G. L., and Hogan, L. M., J. Inst. Metals, 93 (1965) 505.

41. Flemings, M. C., Scan. J. Metallurgy, 5 (1976) 1.

42. Moore, M. R., Iron and Steel Maker, Dec. 1983, p. 22.

43. Lux, B., Haour, G., and Mollard, F., in Proc. 2nd Int. Conf. on Rapid Solidification Processing, see ref. 22 above.

44. Duwez, P., Trans. ASM, 60 (1967) 607.

45. Chang, C. F., Bye, R. L., Laxmanan, V., and Das, S. K., "Texture and Magnetic Properties of Rapidly Quenched Fe-6.5 wt Si Ribbon," submitted to IEEE Trans. on Magnetics.

46. Laxmanan, V., Chang, C. F., and Das, S. K., "Chill Roll Casting of Metal Strip," patent applied for by Allied Corporation, Morristown, NJ.

47. Kan, J., Ito, Y., and Shimanaka, H., J. Magnetism and Mag. Mat. 26 (1982) 127.

48. Spencer, D. B., Mehrabian, R., and Flemings, M. C., Met. Trans., 3 (1972) 1925.

49. Rheocasting, Metals and Ceramics Information Center Report, Jan. 1978.

50. Laxmanan, V., "Rheocasting of Superalloys," S. M. Thesis, Dept. of Mat. Sci. and Eng., MIT, June 1975.

51. Flemings, M. C., Riek, R. G., and Young, K. P., AFT Int. Cast. Met. J., 1 (1976) no. 3, p. 11.

52. Laxmanan, V., Flemings, M. C., Met. Trans. A, 11A (1980) 1927.

53. Denholm, W. T., Esdaile, J. D., Siviour, N. G., and Wilson, B. W., Met. Trans. A, 15A (1984) 1311.

54. Langer, J. S., and Muller-Krumbhaar, H., Acta Met., 26 (1978) 1681, 1689, 1697.

55. Muller-Krumbhaar, H., and Langer, J. S., Acta Met., 29 (1981) 145.

56. Langer, J. S., Rev. Mod Phys, 52 (1980) 1./

57. Trivedi, R., J. Crystal Growth, 49 (1980) 219.

58. Trivedi, R., J. Crystal Growth, 49 (1980) 93.

59. Somboonsuk, K., Mason, J. T., Trivedi, R., Met. Trans. A, 15A (1984) 967.

60. Trivedi, R., Met. Trans A, 15A (1984) 977.

61. Mason, J. T., Verhoeven, J. D., and Trivedi, R., J. Crystal Growth, 59 (1982) 516.

62. Glicksman, M. E., Mat. Sci and Eng., 65 (1984) 45.

63. Lipton, J., Glicksman, M. E., and Kurz, W., Mat. Sci. and Eng., 65 (1984) 57.

64. Laxmanan, "Dendritic Solidification I, II, III," submitted to Acta Met.

65. Laxmanan, V., "Dendritic Solidification at Very Large Growth Rates," submitted to Met. Trans. A.

66. Laxmanan, V., "Dendritic Solidification in a Bindary Alloy Under an Imposed Thermal Gradient: Minimum Undercooling Versus Tip Stability Criterion," submitted to Met. Trans. B.

67. Laxmanan, V., "Constitutional Supercooling at the Dendrite Tip," submitted to Met. Trans. A.

68. Mullins, W. W., and Sekerka, R. F., J. Appl. Phys., 35 (1964) 444.

69. Laxmanan, V., "The Constitutional Supercooling Principle During Dendritic Solidification," to be presented at the AIME Fall Meeting, Sept. 17-20, 1984, Detroit, Michigan.

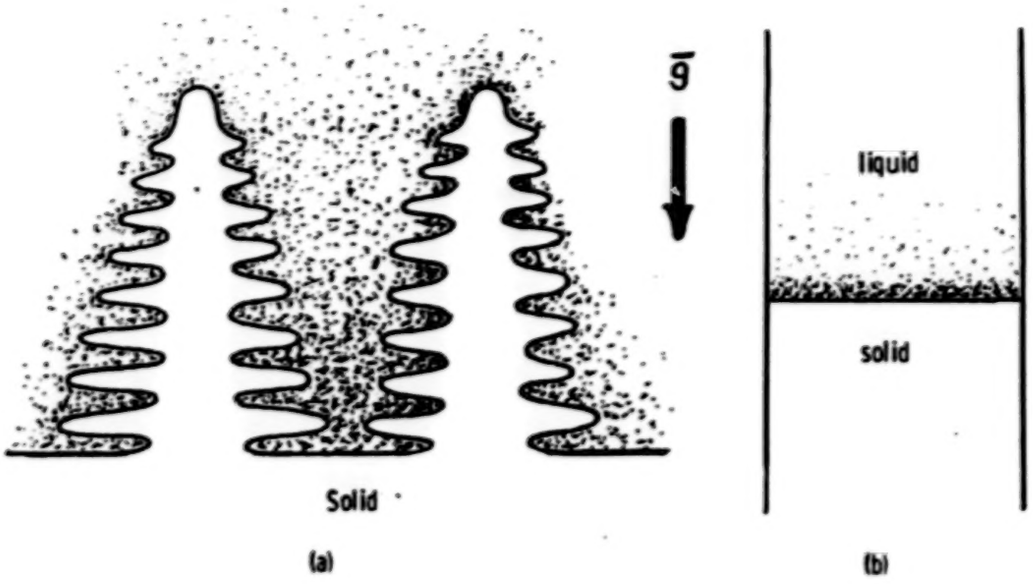

Figure 1. - Schematic illustration of the growth patterns propagating in a liquid during solidification in an alloy. (a) dendritic growth, (b) plane front solidification. Note shaded regions indicate segregated liquid.

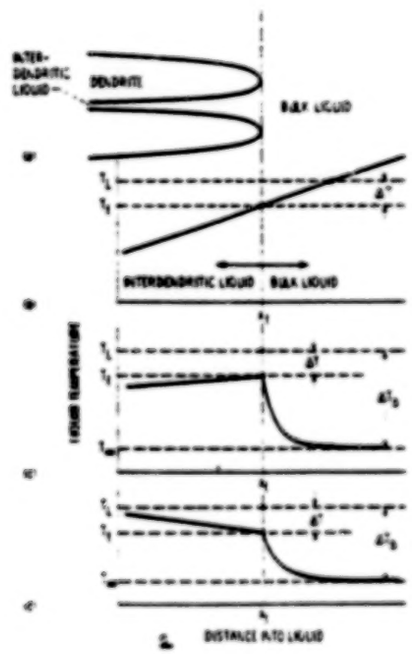

Figure 2. - Thermal conditions during dendritic solidification in an alloy melt (from ref. 66).

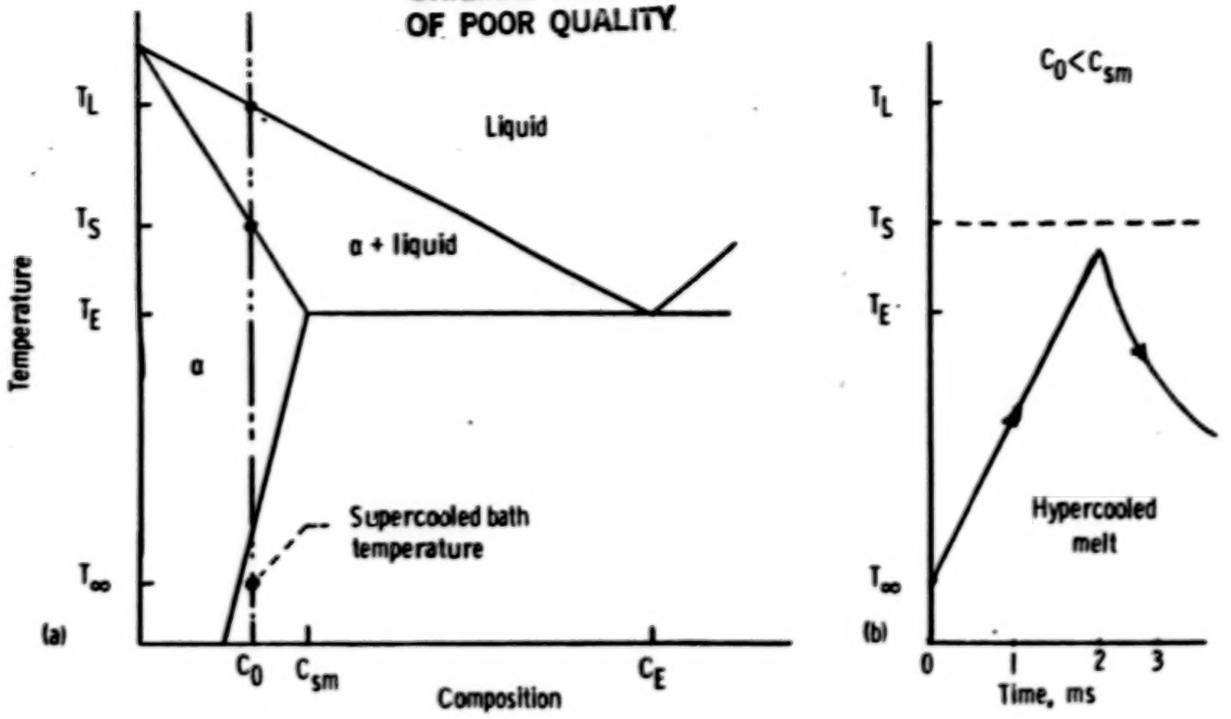

Figure 3. - (a) Phase diagram for a binary alloy indicating the equilibrium liquidus temperature, T_L the equilibrium solidus, T_S, and the supercooled bath temperature, T. For C_0 C_{SM}, equilibrium solidus is T_S. (b) Temperature-time profile after nucleation.

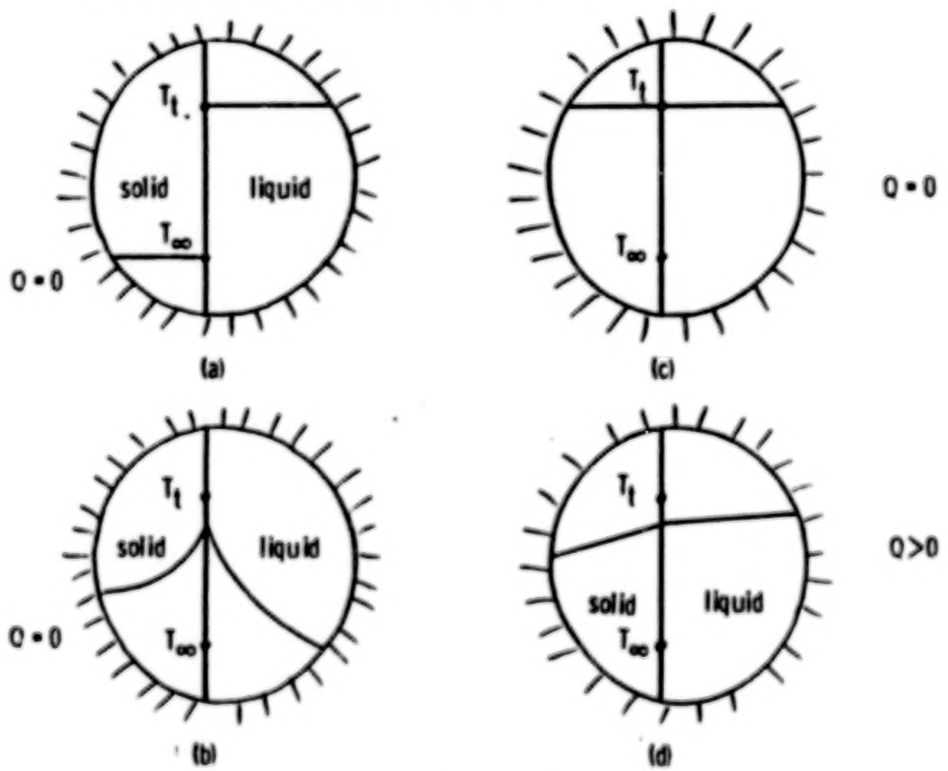

Figure 4. - Heat flow during solidification from a supercooled melt. (a) End of recalescence, no heat flow in solid, adiabatic, (b) During recalescence, adiabatic, heat flow in both liquid and solid, (c) End of recalescence, adiabatic heat flow in both liquid and solid, (d) After recalescence, heat flow to surroundings, net heat flow into solid.

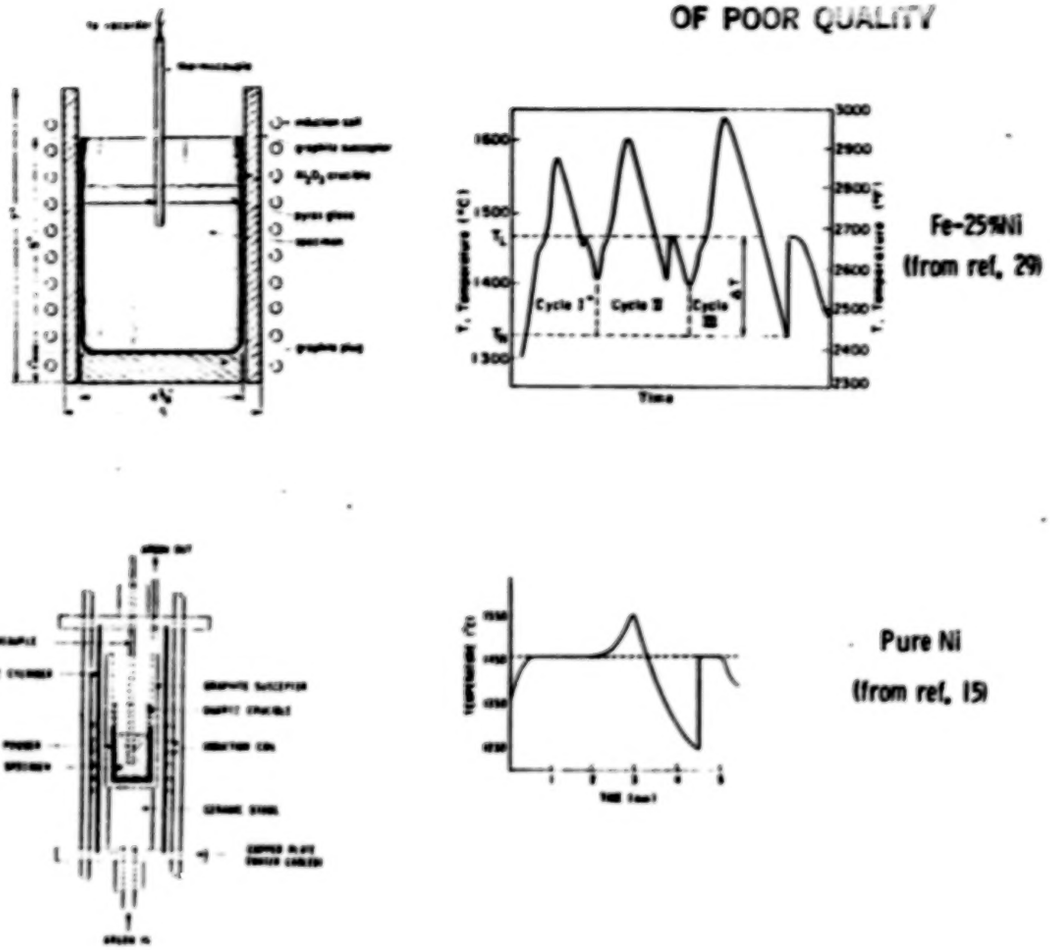

Figure 5. - Thermal "conditioning" to achieve large supercoolings.

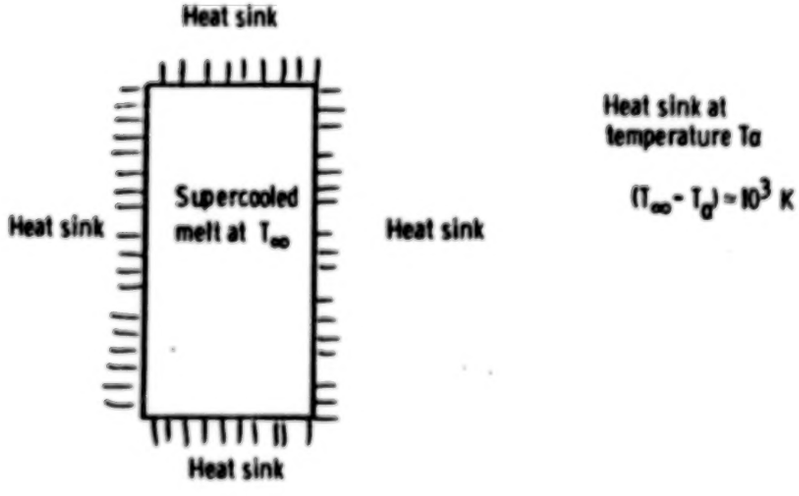

Figure 6. - Heat extraction from a supercooled melt after nucleation at temperature T. Heat sink is at temperature T_∞ below T_α.

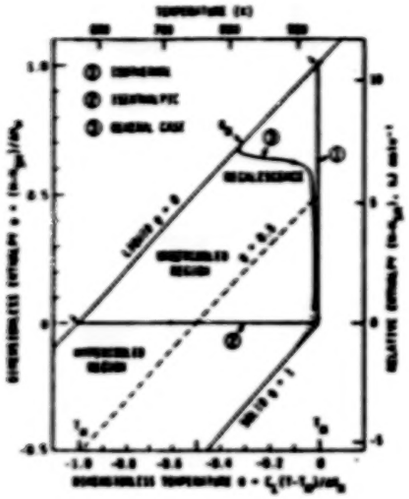

Figure 7. - Enthalpy-temperature diagram showing possible solidification paths. From Lovi and Mehrabian [36].

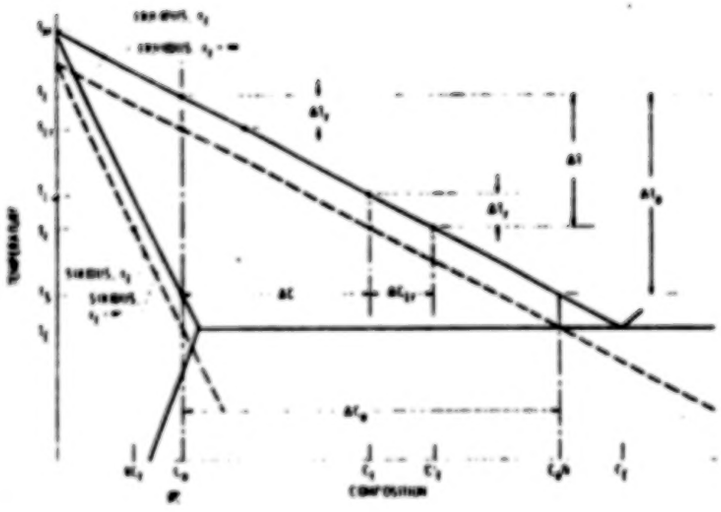

Figure 8. - Dendrite tip undercooling and solute buildup superimposed on a phase diagram (from ref. 66).

APPENDIX C

ORAL PRESENTATION FIGURES

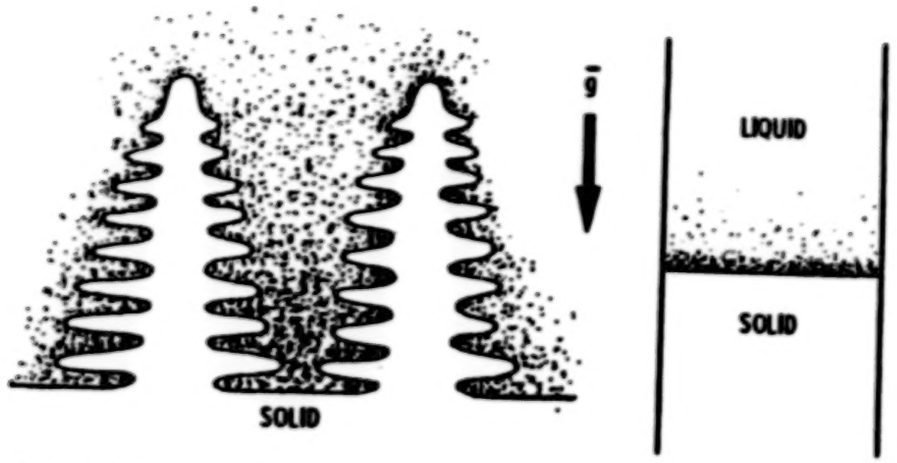

- SINGLE CRYSTAL TURBINE BLADES
  ~1-5 cm/hr
- MELT-SPUN CRYSTALLINE ALLOYS
  ~2 km/hr
- SEMI-CONDUCTOR CRYSTALS
  ~5 mm/hr - 25 mm/hr
- ATOMIZED DROPLETS
  ~2 km/hr
- SUPERCOOLED MELTS
  ~180 km/hr

FACTORS INFLUENCING SEGREGATION PATTERN IN SOLID

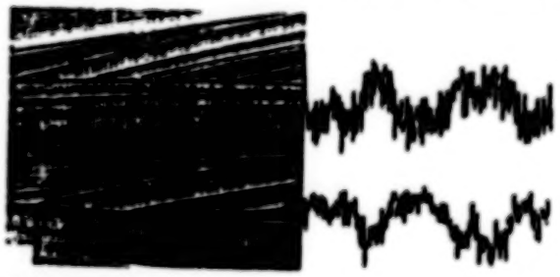

FROM GATOS et al.

- "COMPLEXITY" OF SEGREGATION PATTERN
- SEGREGATION PATTERN FAITHFULLY REPRODUCES THE COMPLEXITY OF THE GROWTH PATTERN PROPAGATING IN THE LIQUID

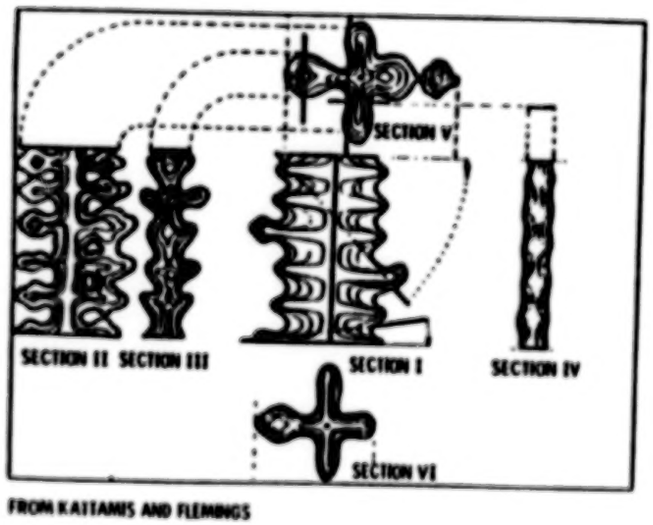

FROM KATTAMIS AND FLEMINGS

- "STRIATIONS" IN SEMICONDUCTOR CRYSTAL GROWTH
- "DENDRITIC" ISOCONCENTRATE CONTOURS IN METAL ALLOYS
- HIGH GROWTH RATES REFINE THE "SCALE" OF THE GROWTH PATTERN (REDUCED DENDRITE ARM SPACINGS)

FACTORS INFLUENCING SEGREGATION PATTERN IN SOLID

- "SEVERITY" OF SEGREGATION
  - RATIO OF MINIMUM TO MAXIMUM COMPOSITION WITHIN A DENDRITE
  - AMOUNT OF NON-EQUILIBRIUM EUTECTIC (MORE GENERALLY, ALL "SECONDARY" PHASES PRESENT IN THE INTERDENDRITIC REGIONS)
  - HIGH SOLIDIFICATION RATES REDUCE "SEVERITY" OF SEGREGATION BY REDUCING COMPOSITIONAL DIFFERENCES WITHIN DENDRITE
  - FLUID FLOW DUE TO GRAVITATIONAL EFFECTS ALSO AFFECTS "SEVERITY" OF SEGREGATION – MACROSEGREGATION

INFLUENCE OF REDUCED GRAVITY LEVELS ON SEGRAGATION BEHAVIOR

- WITT, GATOS, LICHTENSTEIGER, LAVINE AND HERMAN
  - SKYLAB, InSb DOPED WITH Te
  - APOLLO-SOYUZ, Ge DOPED WITH Ga
- YUE AND VALTIER
  - SKYLAB III, Ge DOPED WITH Ga, Sb, B
- GALAZKA, WARMINSKI, BAK, AULEYTNER, DIETL, OKHOTIN, BOROVIKOVA, AND ZUBRITSKU
  - SALYUT 6, CdHgTe
- BOTH MACROSEGREGATION AND MICROSEGREGATION WERE GREATLY REDUCED COMPARED TO EARTH-BASE SAMPLES

SEGREGATION IN EARTH AND SPACE GROWN CRYSTALS

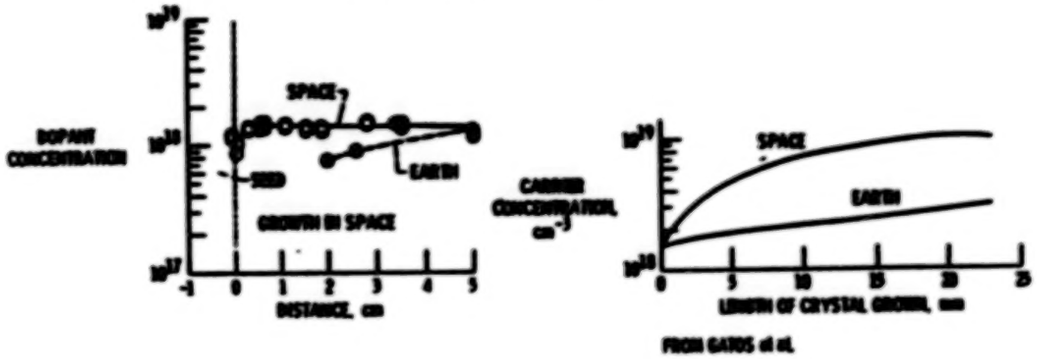

FROM GATOS et al.

SEGREGATION IN EARTH AND SPACE GROWN CRYSTALS

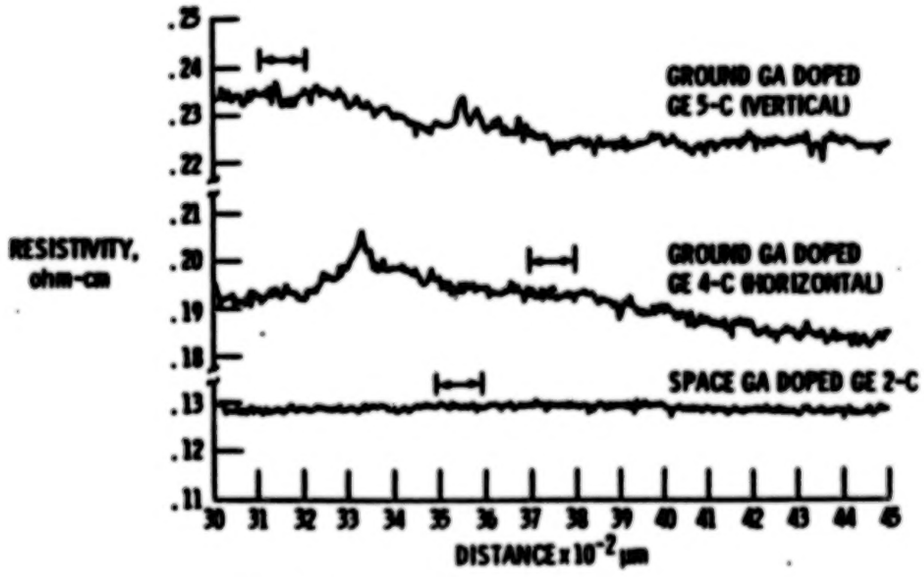

FROM YUE AND VOLTMER

MAJOR OBJECTIVES OF RAPID SOLIDIFICATION PROCESSING

- THERE ARE TWO MAJOR OBJECTIVES FOR RSP/RSR/RST
  - OBTAIN VERY HIGH SOLIDIFICATION RATES
  - PRODUCE AN ALLOY OF HOMOGENEOUS COMPOSITION

METHODS OF ACHIEVING HIGH SOLIDIFICATION RATES

- VARIOUS ATOMIZATION TECHNIQUES
  - CENTRIFUGAL ATOMIZATION
  - INERT GAS ATOMIZATION
  - ROTATING ELECTRODE PROCESS
- RIBBON MAKING PROCESSES
  - MELT SPINNING
  - PLANAR FLOW CASTING
  - MELT DRAG
- SELF-QUENCHING PROCESSES
  - LASER-BEAM MELTING
  - ELECTRON-BEAM MELTING

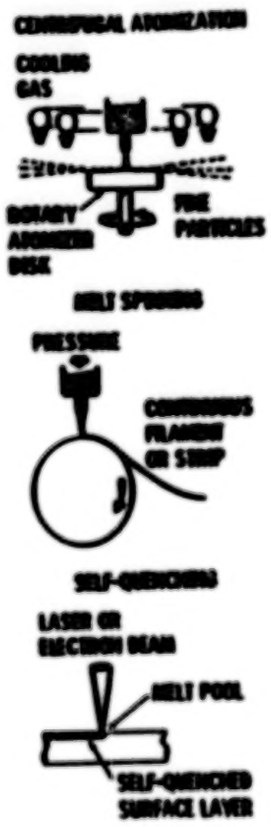

RATIONALE FOR HIGH SOLIDIFICATION RATES

CONSIDER THE FOLLOWING EXAMPLE. LET'S SAY, NEED 50 lb OF STEEL FOR USE IN A TRANSFORMER

- 4 in. THICK SLAB
  - SAND MOLD FREEZING TIME ABOUT 40 min
  - WATER COOLED COPPER MOLD ABOUT 6 min
  - CONTINUOUS CASTING (4 in. x 4 in. AT 175 in./min) CASTING RATE APPROXIMATELY 900 lb/min
- SLAB MUST UNDERGO REDUCTION TO FINAL SIZE
- IS ALSO PROBABLY SEGREGATED TO AN UNACCEPTABLE LEVEL
- PLANAR FLOW CASTING
  - CAN CAST 50 lb IN ABOUT 2 min OR LESS
  - RIBBON HAS FINAL DIMENSIONS
  - GREATLY REDUCED (NEARLY ABSENT) SEGREGATION

METHODS OF ACHIEVING HIGH SOLIDIFICATION RATES

SUPERCOOLING A LARGE MASS OF LIQUID IS AN ALTERNATIVE ROUTE TO ACHIEVING RAPID RATES OF SOLIDIFICATION

- PRODUCT WILL BE A PREFORM OR CASTING
- NO SUBSEQUENT CONSOLIDATION OF FLAKES, RIBBONS OR POWDERS

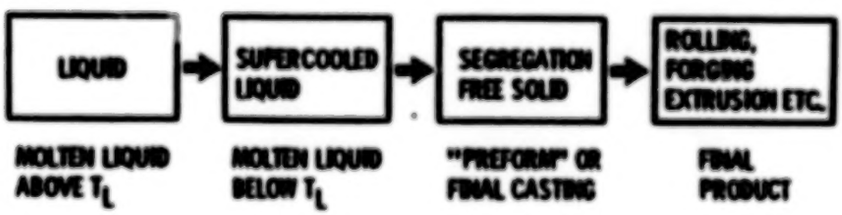

LIMITATIONS TO ACHIEVING LARGE SUPERCOOLINGS

- THE THEORETICAL UPPER LIMIT TO ACHIEVABLE SUPERCOOLING IS THE "HOMOGENEOUS NUCLEATION" TEMPERATURE
  - TURNBULL ($\sim 0.18\ T_M$)
  - PEREPEZKO ($\sim 0.18\ T_M$)
  - SPAEPEN AND THOMPSON
- THE PRACTICAL UPPER LIMIT TO ACHIEVABLE SUPERCOOLING IS GIVEN BY THE "HETEROGENEOUS NUCLEATION" TEMPERATURE

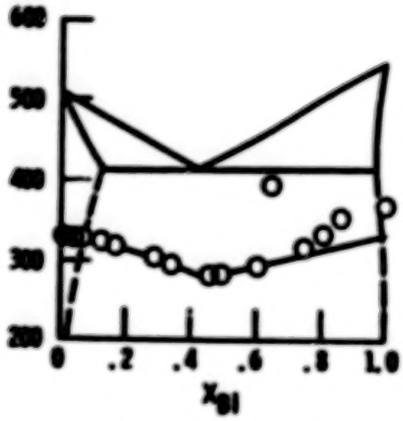

FROM SPAEPEN AND THOMPSON

SOURCES OF HETEROGENEOUS NUCLEANTS IN LIQUIDS

- RAW MATERIALS USED TO MAKE UP THE ALLOY
  - USE HIGH PURITY RAW MATERIALS
- MOLD-METAL-ENVIRONMENT REACTIONS
  - MOLD METAL REACTIONS
    - ALLOY CHEMISTRY
      (Al IN Ni-BASE SUPERALLOYS, Zr IN Cu-Ag-Zr ALLOYS)
    - MOLD MATERIAL
      (NON-WETTING CRUCIBLES)
    - INORGANIC GLASS OR SLAG ENCASING
  - METAL-ENVIRONMENT REACTIONS
    - VACUUM MELTING
      (CARBON "BOIL", CO BUBBLES IN STEEL MELTS)

TECHNIQUES FOR SUPERCOOLING LARGE LIQUID MASSES

- PROPER CHOICE OF MOLD-MATERIAL AND ALLOY CHEMISTRY
- ENCASEMENT OF MELT IN AN INORGANIC GLASS OR SLAG
- THERMAL "CONDITIONING" OF MELT BY REPEATED HEATING AND COOLING
- "CONTAINERLESS" PROCESSING
  - ELECTROMAGNETIC LEVITATION
  - ELECTROSTATIC LEVITATION
  - ACOUSTIC LEVITATION
  - HYBRID METHODS

ACOUSTIC LEVITATION

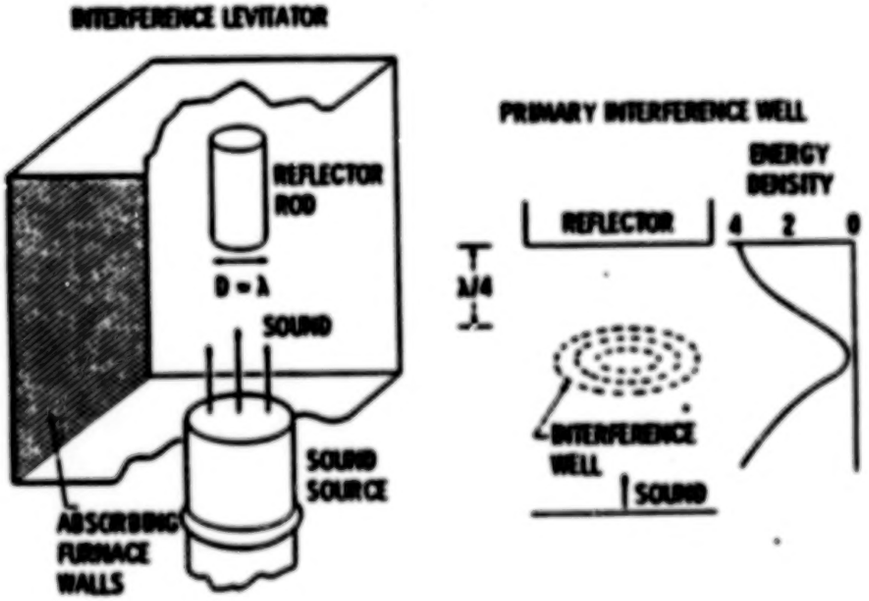

ELECTROMAGNETIC LEVITATION

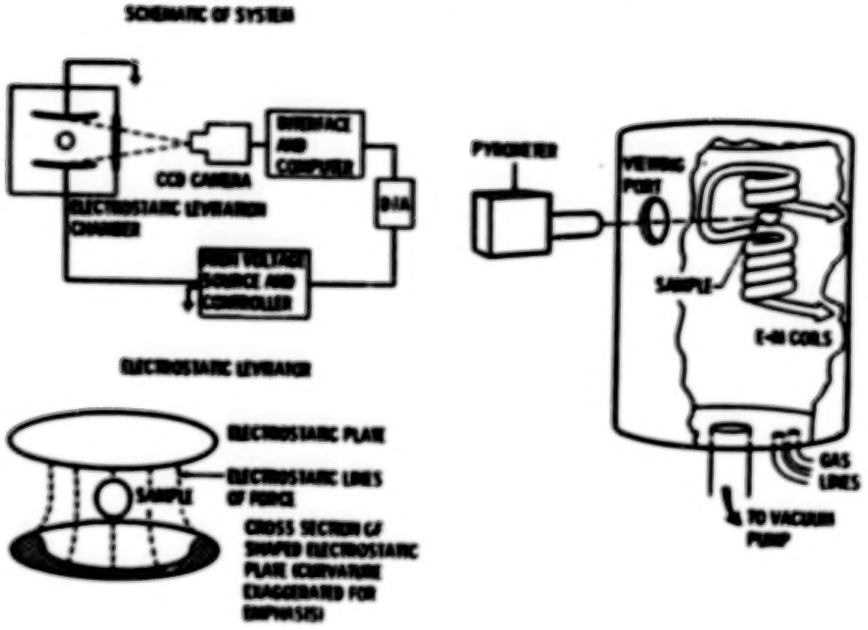

DEFINITION OF HYPERCOOLING AND HYPOCOOLING

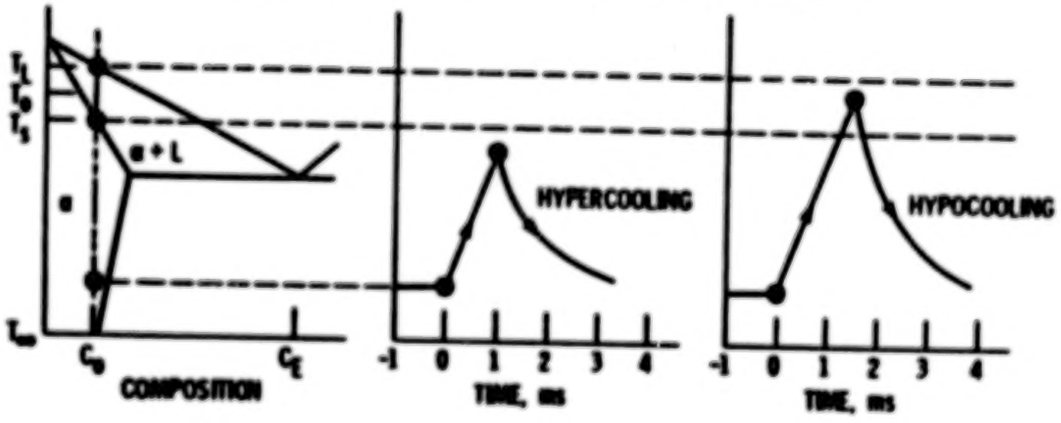

- HEAT FLUX GENERATED DUE TO SOLIDIFICATION

$$\rho_s HR = 11.75\ \text{mW/cm}^2 = 11.75 \times 10^7\ \text{kW/m}^2 \quad \left.\right\} \text{PURE Ni},\ R = 180\ \text{km/hr}$$

- RECALESCENCE TIMES FROM THERMAL MEASUREMENTS OF FLEMINGS AND CO-WORKERS ~ 2 ms

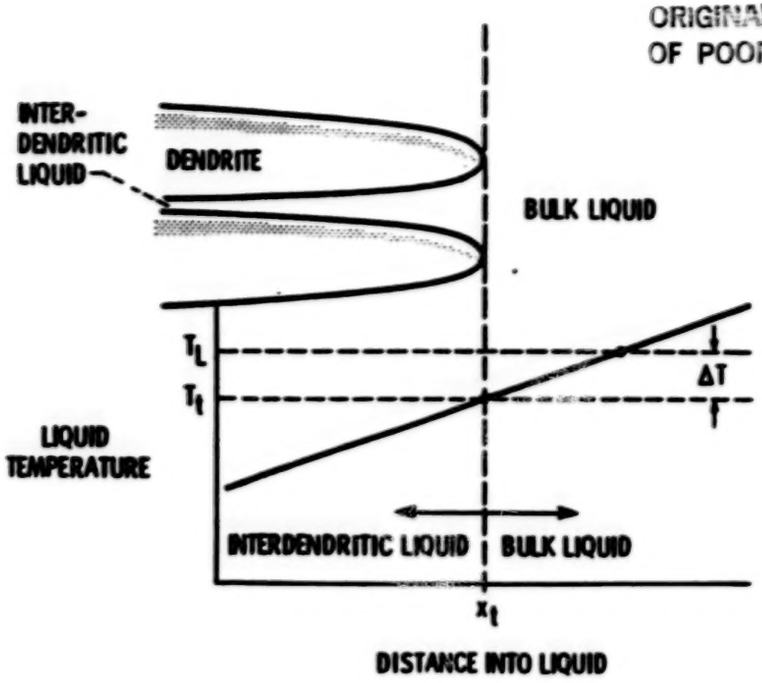

CONSTRAINED DENDRITIC GROWTH

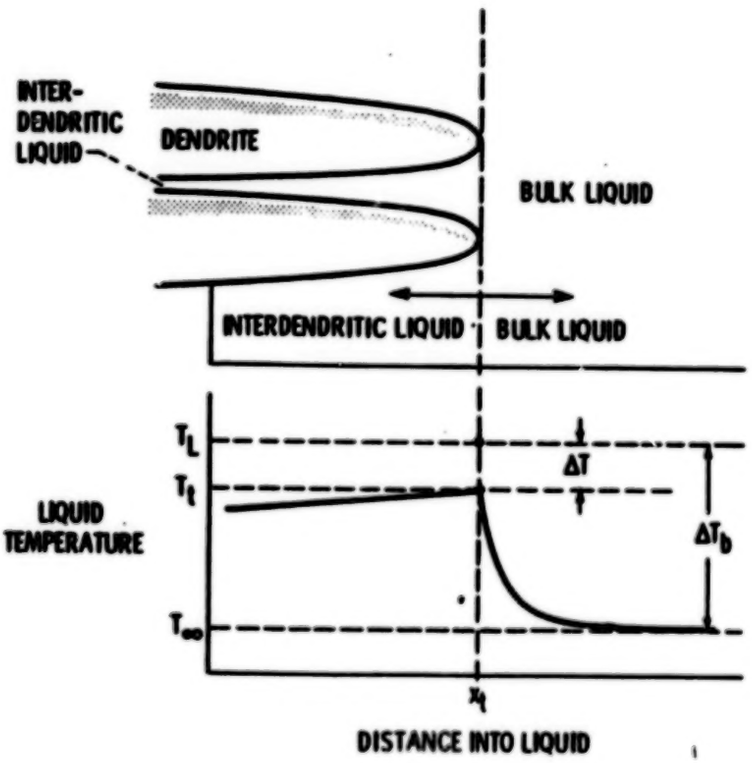

FREE DENDRITIC GROWTH

POSITIVE INTERDENDRITIC GRADIENT

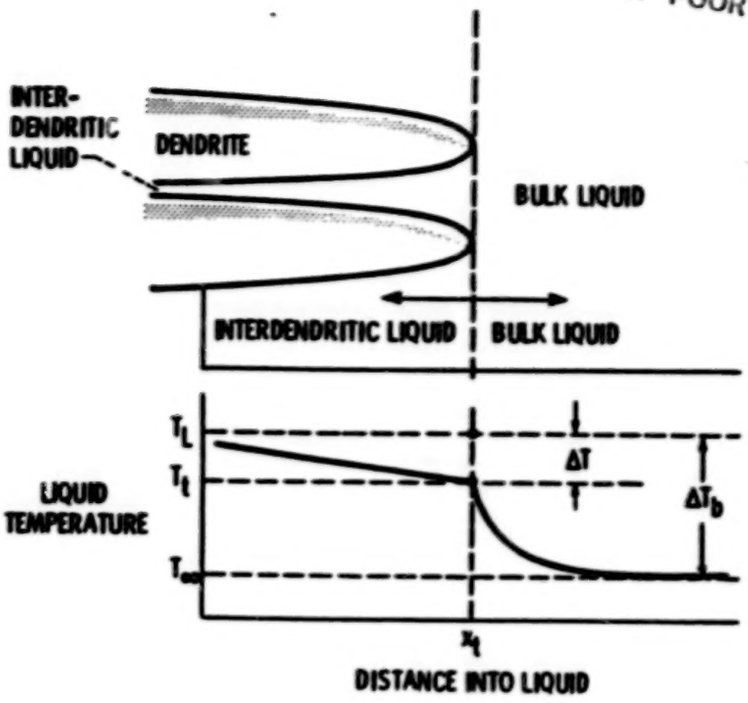

FREE DENDRITIC GROWTH

NEGATIVE INTERDENDRITIC GRADIENT

DENDRITE TIP UNDERCOOLING VERSUS BATH SUPERCOOLING

- BATH SUPERCOOLING $(T_L - T_\infty) = \Delta T_b$
- DENDRITE TIP UNDERCOOLING $(T_L - T_t) = \Delta T$
- MICROSEGREGATION IS STRONGLY INFLUENCED BY THE DENDRITE TIP UNDERCOOLING BECAUSE COMPOSITION OF THE SOLID FORMED AT THE TIP DEPENDS ON T_t,

$$T_t = f(R, G_t, r_t, C_o, \Delta T_b)$$

- COMPARISON OF DATA FROM DIRECTIONALLY SOLIDIFIED SAMPLES $(G_L > 0)$ AND SUPERCOOLED MELTS $(G_L < 0)$ MUST BE MADE AT CONSTANT VALUES OF ΔT

PROCESS REQUIREMENTS DURING SUPERCOOLING OF BULK SAMPLES

TO ACCOMPLISH THE TWIN OBJECTIVES OF

- HIGH SOLIDIFICATION RATES
- ALLOY OF HOMOGENEOUS COMPOSITION

THE FOLLOWING REQUIREMENTS MUST BE MET

- ACHIEVE LARGE INITIAL BATH SUPERCOOLINGS, ΔT_b
  - PREFERABLY "HYPERCOOLED" CONDITIONS ($\Delta T \geq \Delta T_o$)
- EXTRACT HEAT RAPIDLY TO SUPPRESS RECALESCENCE PARTICULARLY, IF "HYPOCOOLED" ($\Delta T < \Delta T_o$)
- EXERCISE "CONTROL" ON HEAT EXTRACTION CONDITIONS FOLLOWING NUCLEATION

CONTROL OF HEAT EXTRACTION RATES FOLLOWING NUCLEATION OF THE MELT

PROPER "CONTROL" OF HEAT EXTRACTION RATES IS REQUIRED

- TO AID IN "SELECTION" OF PHASE BEING NUCLEATED
  - FCC γ PHASE AND/OR BCC δ-FERRITE IN STEELS
- TO CONTROL GROWTH MORPHOLOGY OF PHASE WHICH HAS NUCLEATED
  - PLANAR/CELLULAR/DENDRITIC MORPHOLOGICAL TRANSITIONS
  - "IRREGULAR" OR "DIVORCED" EUTECTIC STRUCTURES
  - "NOVEL" MICROSTRUCTURES - GLASSY PHASE PLUS CRYSTALLINE PHASES
- TO ELIMINATE RESIDUAL MICROSEGREGATION IF HYPOCOOLED
- TO EXERCISE CONTROL ON PRECIPITATION OF SECOND PHASES FROM AN INITIALLY HOMOGENEOUS ALLOY EVEN IF HYPERCOOLED - SOLID STATE COOLING

ORIGINAL PAGE IS
OF POOR QUALITY

SUPERCOOLING DATA FOR BINARY Fe-C ALLOYS

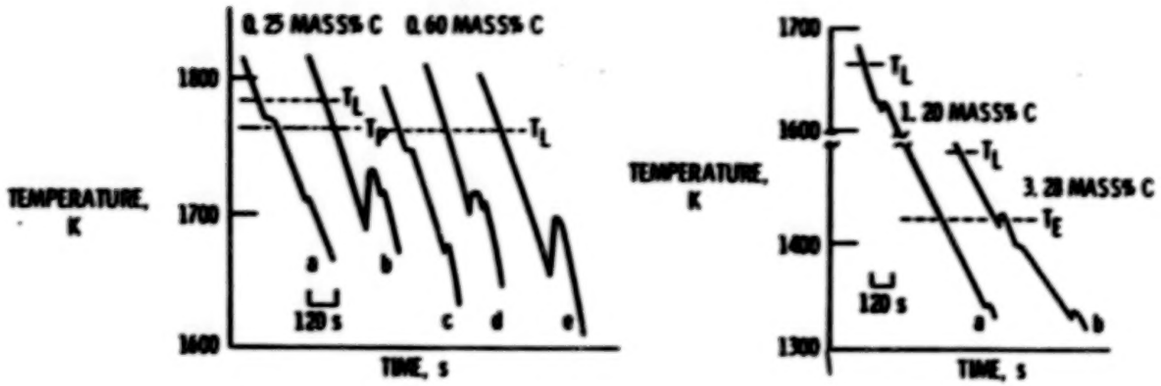

FROM ONO et al.

MAXIMUM REPORTED SUPERCOOLINGS

- IN MOST Fe AND Ni BASE ALLOYS A SUPERCOOLING OF AT LEAST 100 K HAS BEEN ACHIEVED
- SUBSTANTIAL SUPERCOOLING HAS BEEN ACHIEVED IN Al AND Cu BASE ALLOYS
  - 316 STAINLESS STEEL, 475 K (MACISACC et al.)
    - HYPERCOOLING LIMITS FOR PURE Fe AND Ni 329 K, 445 K
  - 4340 STEEL, 4330
  - 440 C
  - 304 STAINLESS, 303 STAINLESS
  - IN-738 LC
  - MAR-M-200, 191 K
  - MAR-M-509, 153 K

BATTELLE - GENEVA RESEARCH PROGRAM

- ALLOY CHEMISTRY IMPORTANT
  - Al WAS FOUND TO HINDER SUPERCOOLING
- MOLD MATERIAL IMPORTANT
  - MAR-M-509, 153 K IN FUSED SILICA
  - MAR-M-200, NO SUPERCOOLING IN FUSED SILICA
  - MAR-M-200, SUPERCOOLS IN $ZrSiO_4$ SHELL MOLDS TO THE EXTENT OF 191 K
- TENSILE TESTS
  - UTS AND ELONGATION SIMILAR OR BETTER THAN DS-200
- CREEP TESTS
  - PROPERTIES AT 800° C EFFECTIVELY EQUAL TO A MONOCRYSTAL OVERALL CREEP PERFORMANCE SUPERIOR TO DS-200

POTENTIAL APPLICATIONS OF BULK UNDERCOOLING AS AN INDUSTRIAL PROCESS

- RELATIVELY SMALL COMPONENTS CURRENTLY BEING FABRICATED VIA RSR/RST INVOLVING CONSOLIDATION OF FLAKES, RIBBONS, POWDERS
  - WILL REQUIRE ABILITY TO SUPERCOOL LIQUID MASSES UP TO SEVERAL 10's OF POUNDS, MAY BE A FEW HUNDRED POUNDS
  - IMPORTANT "ENGINEERING" ADVANTAGES EVEN FOR RELATIVELY SMALL SUPERCOOLINGS, MUCH LESS THAN THE HYPERCOOLING LIMIT
  - TURBINE BLADES, DISKS (?)
- NEW APPLICATIONS CURRENTLY OUTSIDE THE DOMAIN OF RSR/RST WHICH CAN BENEFIT FROM THE UNIQUENESS OF THE PROCESS

SOME RECENT METALLURGICAL INNOVATIONS

NEW IDEAS HAVE FOUND THEIR WAY FROM ACADEMIC LABORATORIES TO THE INDUSTRIAL LABORATORIES AND VICE VERSA

- POL DUWEZ EXPERIMENTS TO VERIFY HUME-ROTHERY RULES LEAD TO THE DISCOVERY OF AMORPHOUS METALS (CALTECH 60's)
  - PROCESS INNOVATIONS AND INNOVATIONS IN TRANSFORMER DESIGN HAVE LED TO METALLIC GLASSES NOW BEING CANDIDATE MATERIALS FOR DISTRIBUTION TRANSFORMERS
  - METALLIC GLASSES ARE BEING CAST AS RIBBONS UP TO 170 mm (~7 in.) WIDE
- THE SAME PROCESS INNOVATIONS THAT HAVE LED TO PRODUCING COMMERCIALLY IMPORTANT QUANTITIES OF METALLIC GLASSES HAVE MADE POSSIBLE Fe-6.5 wt % Si ALLOY
  - ALLIED - PLANAR FLOW CASTING
  - KAWASAKI STEEL - SINGLE AND TWIN ROLLER
- RHEOCASTING PROCESSES (MIT 70's)
  - DIE CASTING OF HIGH TEMPERATURE ALLOYS (Fe, Cu, Al BASE)
  - FORGING AND FORMING OPERATIONS
  - POTENTIAL OF MAKING STRIPS FROM THE SLURRY
  - A MAJOR US CORPORATION IS CURRENTLY REPORTED TO BE USING THIS PROCESS COMMERCIALLY
- RHEOCASTING HAS FOUND AN INTERESTING APPLICATION IN DETERMINING PHASE DIAGRAMS
- DENHOLM, ESDAILE, SIVIOUR AND WILSON (1980) Al RICH REGION OF Al-Fe-Mn TERNARY DIAGRAM
- LARGE ROUNDED PARTICLES OF Al CRYSTALS AND INTERMETALLICS, $(Fe,Mn)Al_6$ AND $FeAl_3$ HELPED DETERMINE Fe SOLUBILITY IN Al ALLOYS (IMPORTANT IN RECYCLING Al SCRAP)

POROSITY AND ENVIRONMENT

Thomas S. Piwonka
Materials and Manufacturing Technology Center
TRW, Inc.
Cleveland, Ohio

Until fairly recently, when the importance of grain structure and segregation became understood and methods became available to control them, the principal job of the foundryman was to control porosity, i.e., make sound castings. As a result, there was much effort expended to develop empirical rules which would satisfy this requirement, and foundries guarded their gating and risering designs jealously, as they were, indeed, their trade secrets.

The emphasis on soundness led to a great deal of experimental work devoted to the development of risering equations. Most of these followed Chvorinov's Rule (1), which related the surface area/volume ratio of the casting to that of its riser as a way of predicting which would stay liquid longer. Obviously, it was desirable for the riser to remain liquid if it was to provide a reservoir of molten metal to feed the porosity. A refinement which applied to steel castings and pure metals was introduced by Caine (2), but, although Chvorinov's Rule was somewhat helpful, it was of little practical use in the gating of mushy feeding alloys. In addition, it ignored the contribution which the evolution of dissolved gas made to porosity.

Significant progress was achieved when it was realized that porosity could be analyzed successfully by considering not only heat flow, but also fluid flow within the solidifying casting. First, Walther, Adams, and Taylor (3) investigated the problem for pure metals, then Piwonka and Flemings (4), and Campbell (5) extended the work to mushy freezing alloys, introducing the concept of treating flow in such alloys as flow through porous media. This view has recently been elaborated on by Lesoult and his coworkers (6). It has the advantage of showing relationships between pressure on the liquid metal, length of the mushy zone, solidification rate, pressure of dissolved gas, and physical properties of the alloys.

The general finding from these approaches is that sound castings may be produced by lowering pressure during melting (to allow dissolved gas to escape the melt) and increasing pressure during solidification (to force liquid metal into the mushy zone to feed shrinkage). Such techniques are especially effective if they are combined with chilling of parts of the casting to produce progressive solidification, which shortens the mushy zone and, hence, the distance that metal must travel to feed porosity.

Applications of this theory in practice include various types of pressure casting (7,8), centrifugal casting, centrifuging (particularly titanium alloy casting), and die casting (the Accurad process). Interestingly, directionally solidified superalloy castings are not necessarily completely sound: Their large mushy zone requires that high gradients be employed during their manufacture to shorten the freezing range enough to permit complete feeding to occur.

Despite the number of methods which have been developed to make use of applied pressure to improve casting soundness, most castings today are made using only the combination of metallostatic head and atmospheric pressure to feed castings. Both are important: solidification under reduced pressure (as in a vacuum chamber) invariably increases porosity over that found when the casting is solidified in air.

The problem of eliminating porosity in space, however, becomes a great deal more difficult precisely because there is no gravity. The only natural force encouraging fluid flow within the channels is surface tension. Although it is possible that proper combination of an alloy and casting geometry could produce Marangoni flows which give substantial feeding, it is unlikely. Thus, it is to be expected that shrinkage will remain where it occurs, unfed.

The same may be said for gas. Normally, gas which comes out of solution at a liquid-solid interface as a result of the difference in solubilities floats through the liquid and out of the riser. In space, unfortunately, the gas does not float, and remains in place as solid grows around it.

Thus, porosity will exist where it forms in a casting solidified in space, and Earth-based techniques to eliminate it will prove to be of no avail. Indeed, one is faced with an added problem: The site where solidification begins will determine the distribution of the final porosity. If nucleation begins uniformly at the mold walls, the porosity will be found at the center of the casting. However, if it begins at only one wall, or at the interior of the casting (as a result of an inclusion, or off of a core surface), the porosity will be found on the outside of the casting - which in this case will fail to fill the mold. Examples of both phenomena have been found by Larson (9), by Lacey and coworkers (10), and by Cybulsky and coworkers (11).

Thus, the application of solidification processes in space will present new challenges to both the investigator and foundryman to produce sound castings. It is by no means certain that methods can be found to do so without reimposing force fields which mimic gravity, and counteract all of the advantages which might otherwise accrue from space solidification.

1. N. Chvorinov, Giesserei, 27 (1940), p. 127.

2. J. B. Caine, "A Theoretical Approach to the Problem of Dimensioning Risers," Trans. American Foundrymen's Society, 56 (1948), p. 492.

3. W. D. Walther, C. M. Adams, and H. F. Taylor, "Mechanism for Pore Formation in Solidifying Metals," Trans. American Foundrymen's Society, 64 (2956), p. 658.

4. T. S. Piwonka and M. C. Flemings, "Pore Formation in Solidification," Trans. AIME, 236 (1966), p. 1157.

5. J. Campbell, "Hydrostatic Tensions in Solidifying Metals," Trans. AIME, 242 (1968), p. 264.

6. L. Ouichou, F. Lavaud, and G. Lesoult, "Influence of the Chemical Composition of Nickel-base Superalloys on Their Solidification Behavior and Foundry Performance," Superalloys 1980, American Society for Metals, p. 235.

7. E. E. Sprow, "Low-Pressure Casting for High-Performance Parts," Machine Design, Apr. 5, 1973, p. 122.

8. D. G. Chandley, "Advances in Investment Casting Technology," Solidification Technology, MCIC (1973), p. 189.

9. D. J. Larson, "Sphere Forming Experiment," Proc. Third Space Processing Symposium - Skylab Results," Vol. 1 NASA M745, 1974, p. 101.

10. L. L. Lacy, M. B. Robinson, and T. J. Rathz, "Containerless Undercooling and Solidification in Drop Tubes," NASA MSFC, Huntsville, AL, 1980.

11. M. Cybulsky, M. H. Johnston, and T. S. Piwonka, unpublished research, NASA Guest Investigator program, MSFC, 1981.

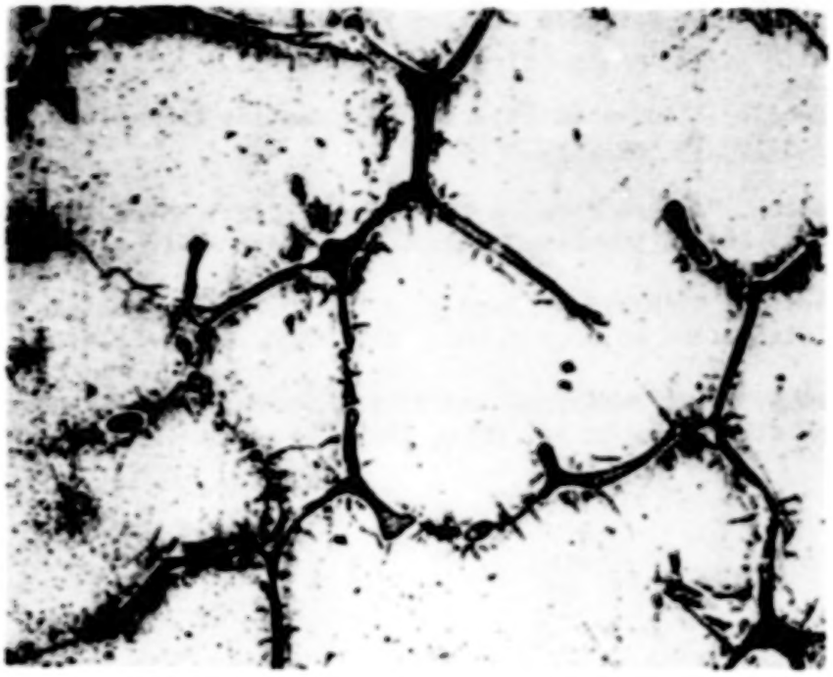

Figure 1. Typical appearance of interdendritic porosity in an Al-4.5% Cu alloy.

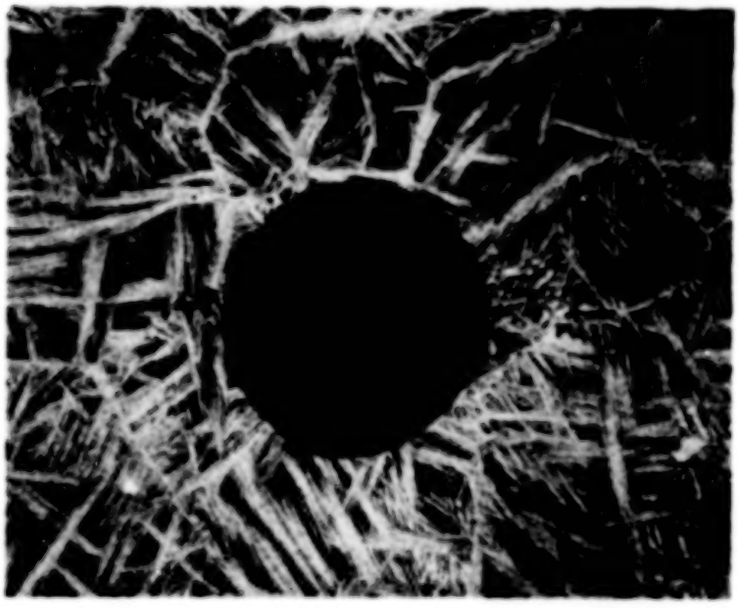

Figure 2. Gas and shrinkage porosity in a Ti-6Al-4V alloy, showing the combination of gas (the spherical void) and shrink (interdendritic voids).

Figure 3. Ground Based sample of Al-4.5% Cu alloy saturated with gas and solidified at 240°C/sec. Porosity is distributed evenly throughout the sample.

Figure 4. Microgravity sample of same material solidified at 240°C/sec. Porosity is evenly distributed throughout sample. (Large circular voids are drill holes for chemistry samples.)

Figure 5. Second microgravity sample solidified at 400°C/sec. Sample is sound, but failed to fill the mold. One possible interpretation is that shrinkage and gas occurred outside the casting instead of within it.

THE MOVEMENT OF PARTICLES IN LIQUID METALS UNDER GRAVITY FORCES AND THE INTERACTION OF PARTICLES WITH ADVANCING SOLID-LIQUID INTERFACE

F. Weinberg
University of British Columbia
Vancouver, British Columbia, Canada

A. Porosity

In general I agree with the previous speaker Dr. T.S. Piwonka that casting in space will not alleviate problems of shrinkage and gas porosity. Gravity forces enhance the removal of gas bubbles from the melt and contribute to the feeding of shrinkage porosity in castings.

Research in a microgravity environment could be directed toward casting materials with a high density of large pores - foamed metals. Microgravity would presumably allow the bubbles to nucleate and grow without movement in the melt. It is not clear how the bubbles would interact with each other.

There are a number of experiments which could be done in a microgravity environment which could contribute to an understanding of the growth and formation of gas porosity during solidification.

1. If a liquid metal containing dissolved gases is solidified directionally with a plane and a cellular interface will the gas be rejected at the interface in the same manner as a binary metal alloy? This cannot be established clearly in a normal gravity field as the gas will form bubbles which will float to the surface at an unknown rate.

2. In casting an aluminum alloy containing a high concentration of dissolved hydrogen in a chill mould, the concentration of pores is observed to be low in the centre of the casting[1]. This is attributed to gas bubbles growing and agglomerating in the centre and floating up to the top of the melt during solidification. Experiments in a microgravity environment would establish if this is correct. It might also clarify the source of nucleation in the centre of the casting.

3. Pores which form in directionally solidified aluminum containing hydrogen, vary appreciably in size, shape and density in the solid[1], Figure 2. This variation depends on the hydrogen concentration, freezing rate, fluid flow in the melt due to gravity, bubble movement and agglomeration also due to gravity, and other factors. If suitable experiments were conducted in a microgravity environment and compared to repeat experiments in a gravity field, the contribution of fluid flow and bubble movement in the melt to the porosity could be established.

B. Particle Movement Due to Gravity Forces

A metal particle in a liquid metal will tend to float or sink, depending primarily on the relative density of the particle with respect to the melt. The terminal velocity of the particle at steady state is given by Stokes Law which

depends on the density difference of the particle and melt, the liquid viscosity and the particle size[2]. If the particle is moving slowly initially, the transient velocity with time as the particle accelerates to steady state can also be determined[2]. However there is no treatment of particles which are at rest with respect to the melt. How large a density difference is required for metal particles to float or sink in a metal melt and to what extent do factors not considered in Stokes Law influence particle movement in a real system?

Experiments were undertaken to answer these questions[3] using copper particles in a lead-tin melt. The density of copper is between the density of lead and tin so that the copper density can be matched by the melt by adjusting the melt composition. Copper is wetted by a lead-tin melt and dissolves very slowly in the melt. The temperature dependence of the density of copper and two lead-tin melts are shown in Figure 3. At high temperatures copper is heavier than a Pb41%Sn melt and lighter at low temperatures.

In initial experiments the buoyancy of copper shot and pieces of high conductivity copper wire were examined in a lead-tin melt. In both cases the buoyancy varied greatly in a given melt due to porosity in the copper. The results indicated, that buoyancy forces are very sensitive to microporosity or any other factors which influence the particle density. Experiments were then carried out using a 5 mm vacuum grown single crystal cube of copper of 99.999% purity. The copper was irradiated to ^{64}Cu which enabled the position of the copper cube in the melt to be continuously monitored without disturbing the system, by using a scintillation counter situated below the melt.

The results are shown in Figure 4 in which the position of the cube is shown at different melt temperatures after vigorous stirring of the melt[3]. The density difference between the cube and the melt determining whether the cube floats or sinks is very small; less than 1 kg m^{-3} (0.001 g cm^{-3}).

In a series of experiments the position of the cube was monitored as the bottom of the melt was slowly cooled. The results are shown in Figure 5. The copper cube is observed to remain at the bottom of the melt through the density inversion to a melt density which is 12 kg m^{-3} higher than the copper. At this point the melt is vigorously stirred and the cube floats to the top. When the melt is reheated the cube remains at the top of the melt following the density inversion until the melt is stirred. These effects are attributed to surface tension forces when the cube is in contact with the crucible bottom and the meniscus at the top of the melt. A quantitative estimate of the acting surface tension forces could not be made.

In a separate series of experiments a pure tin melt was slowly solidified and the melt tumbled about a horizontal axis[3]. During solidification equiaxed grains formed and grew. The grains were uniformly distributed through the melt as a result of the tumbling action. After 27% of the melt had solidified, the residual melt was marked with a tracer, the tumbling stopped for 300 s and the system then rapidly quenched. During the stopped period the solid grains settled in the bottom part of the container as shown in Figure 6. The solid grains are white in the figure and the residual liquid black. Similar results were obtained for settling times down to 15 s and over a range of percent solidified before the tumbling was stopped. Examining the configuration of particles in Figure 6, it is apparent that

there are large spaces between the grains; in many cases the grains do not touch. Water models studies indicate that the grains should touch and pack reasonably closely within 10 s. It is not clear why the grains in the melt are so widely spaced in the present observations.

C. Interaction of Particles with an Advancing Solid-Liquid Interface.

Many investigations have been carried out on the interaction of particles with an interface in water base or organic transparent liquids during solidification. It has been clearly demonstrated that small particles may be rejected by a slowly advancing solid-liquid interface[4]. This has not been demonstrated for particles in a metal melt. Observations of solid particles concentrated in interdendritic regions and grain boundaries in metals suggests that the particles may be pushed to these locations during solidification. The present experiments were carried out to determine if this was the case[4].

Observations were made using iron particles 3 to 33μm in diameter in a lead melt. The density of iron (7700 kg m^{-3}) is appreciably lower than that of lead (10,600 kg m^{-3}). As a result the particles would float to the surface of the melt, if lead containing the particles was slowly solidified. This problem was overcome using the following procedure. Iron particles were distributed throughout a lead melt by vigorous mixing. The melt was then cast into a 11 mm diameter Vycor tube and rapidly quenched, such that the particles remained uniformly distributed throughout the lead. A zone 30 mm in length was melted with the rod positioned vertically, and the zone moved slowly down the rod. As the zone moved, iron particles were continuously released from the lower melting interface. These floated upward and interacted with the upper solidifying interface. After the zone had moved down 50 mm the liquid was rapidly quenched and the particle distribution determined on sectioned surfaces in the vicinity of the quenched interface as well as the solidified metal.

The results showed that particles were not rejected by a plane advancing interface for the full range of particles sizes examined[4]. This was the case with all the freezing rates examied down to 1.5×10^{-4} cm s^{-1}. With a cellular interface particles were observed to be concentrated in the intercellular regions. This is shown in the etched transverse section of a solidified sample, Figure 7, and in the bar graph in Figure 8 in which the number of particles is plotted as a function of particle size for the intercellular and matrix positions. The percentage of particles in the matrix as a function of the particle size is shown in Figure 9, the particle density in the matrix markedly decreasing with increasing particle size.

The concentration of particles in the cell walls is attributed to the dynamic interaction of the particle with the curved interface. This was investigated in two ways.

1) A liquid zone was moved horizontally along the lead rod containing iron particles. During solidification the rod was rotated at a rate which kept the particles from floating to the top of the melt.

2) A water model was observed in which nylon spheres in brine interacted with an interface, as shown in Figure 10.

In the water model the nylon spheres were observed to be concentrated in the intercellular regions, as shown in Figure 11, for both horizontal and vertical simulated growth. The mechanism by which this occurred was clearly evident from direct observations. When the spheres moving with a small velocity hit the surface, they rebounded in a direction determined by the point of contact as illustrated in Figure 12. Spheres A and B moved across the cell faces until they hit in a C position and became trapped in the intercellular region. In vertical solidification the movement of particles across the interface is enhanced by fluid flow across the interface. The velocity of rebound of an iron particle on a lead surface is very small. However fluid flow at the interface would move the particles across the interface leading to trapping of the particles in the intercellular regions similar to that observed in the water model.

The interaction of iron particles with a dendritic interface was examined by casting a Pb50%Sn alloy containing iron particles. Particles were observed to be concentrated between the dendrite branches as shown in Figure 13. Most of the particles were observed to be between secondary branches below horizontal primary branches. This shows that the particles are trapped between the dendrite branches as they float to the top of the melt during solidification.

In summary, the results indicate that metal particles are not rejected by an advancing solid-liquid interface in a metal melt. Concentrations of particles in a metal following solidification are due to other factors. Theoretical considerations indicate that the only force acting between an iron particle and an interface in lead is the Lifshitz-Van der Waals force. This force is attractive, which is consistent with the present experimental conclusions that particles are not rejected by an advancing interface in a metal.

REFERENCES

1. F. Weinberg and D.A. Hirschfeld, Metal Science, 1979, pp. 335-338.

2. R. Clift, J.R. Grace and M.E. Weber, "Bubbles, Drops and Particles", 1978 Academic Press, N.Y.

3. F. Weinberg, Metl. Trans. B, 1984, in press.

4. C.E. Schvezov and F. Weinberg, Metl. Trans. B, 1984, submitted for publication.

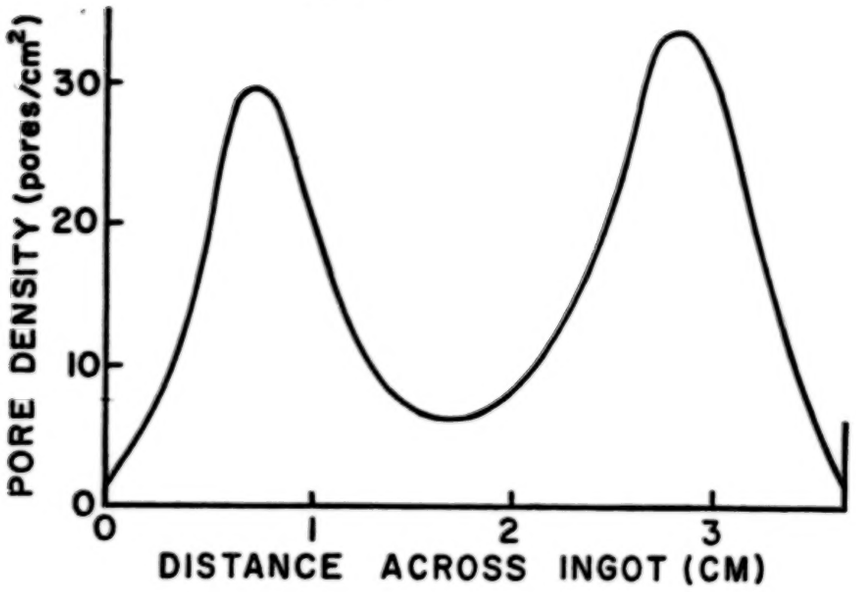

Figure 1: Pore distribution across an aluminum casting containing hydrogen. Pores counted were these visible at 5 X magnification.

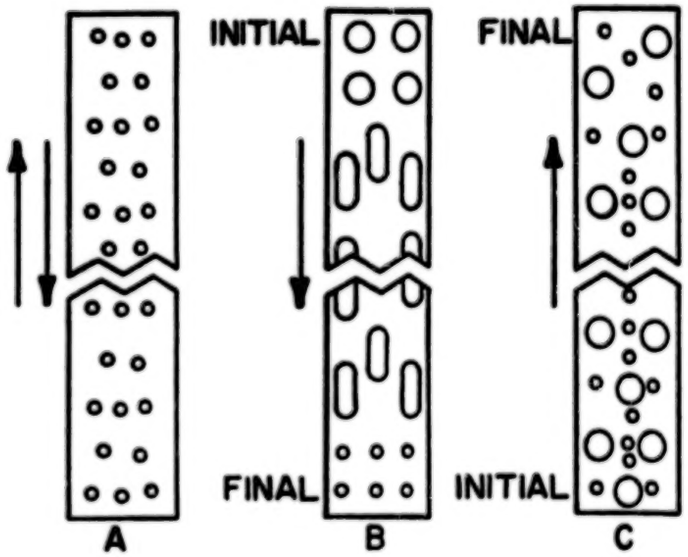

Figure 2: Schematic representation of porosity observed in directionally solidified high purity aluminum. (a) Low hydrogen concentration solidified in both up and down direction. (b) High hydrogen content solidified downwards. (c) High hydrogen content solidified upwards.

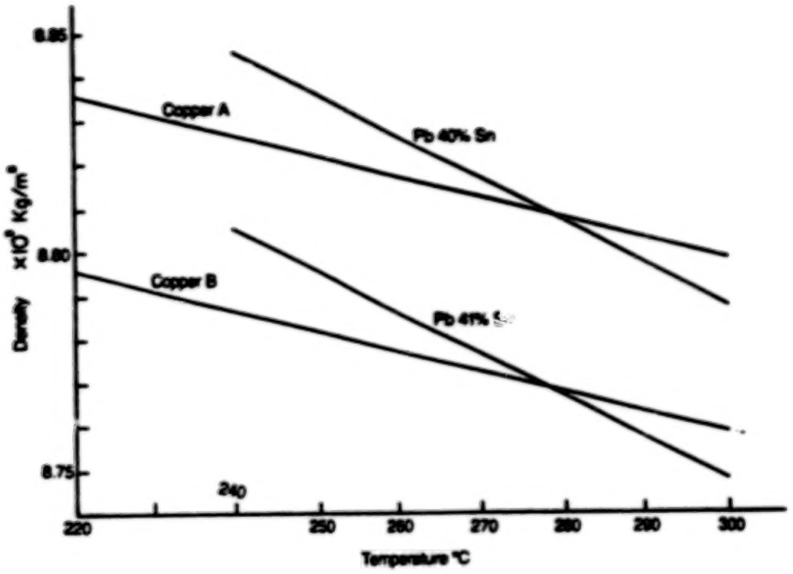

Figure 3: Density of copper and PbSn alloys as a function of temperature. Copper density at 20°C A = 8930 kg/m^3, B = 8890 kg/m^3.

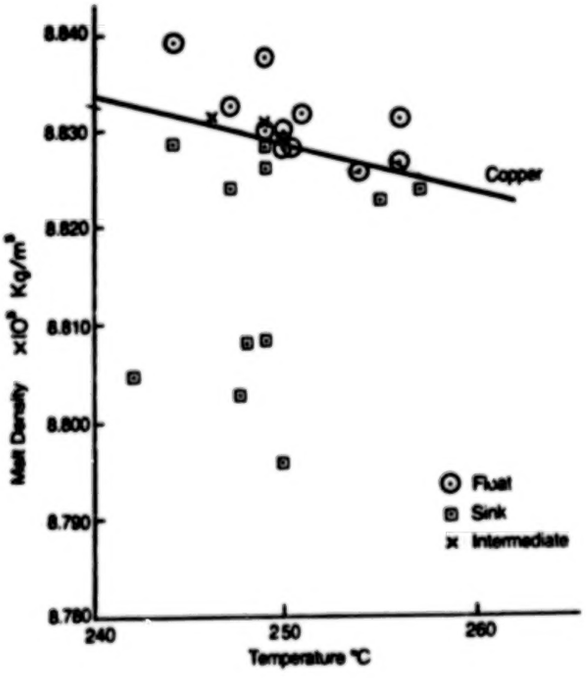

Figure 4: Position of a single crystal cube (float, sink or intermediate) in a PbSn melt as a function of melt density and temperature. The solid line is from published data for copper through the neutral buoyancy density at 250°C.

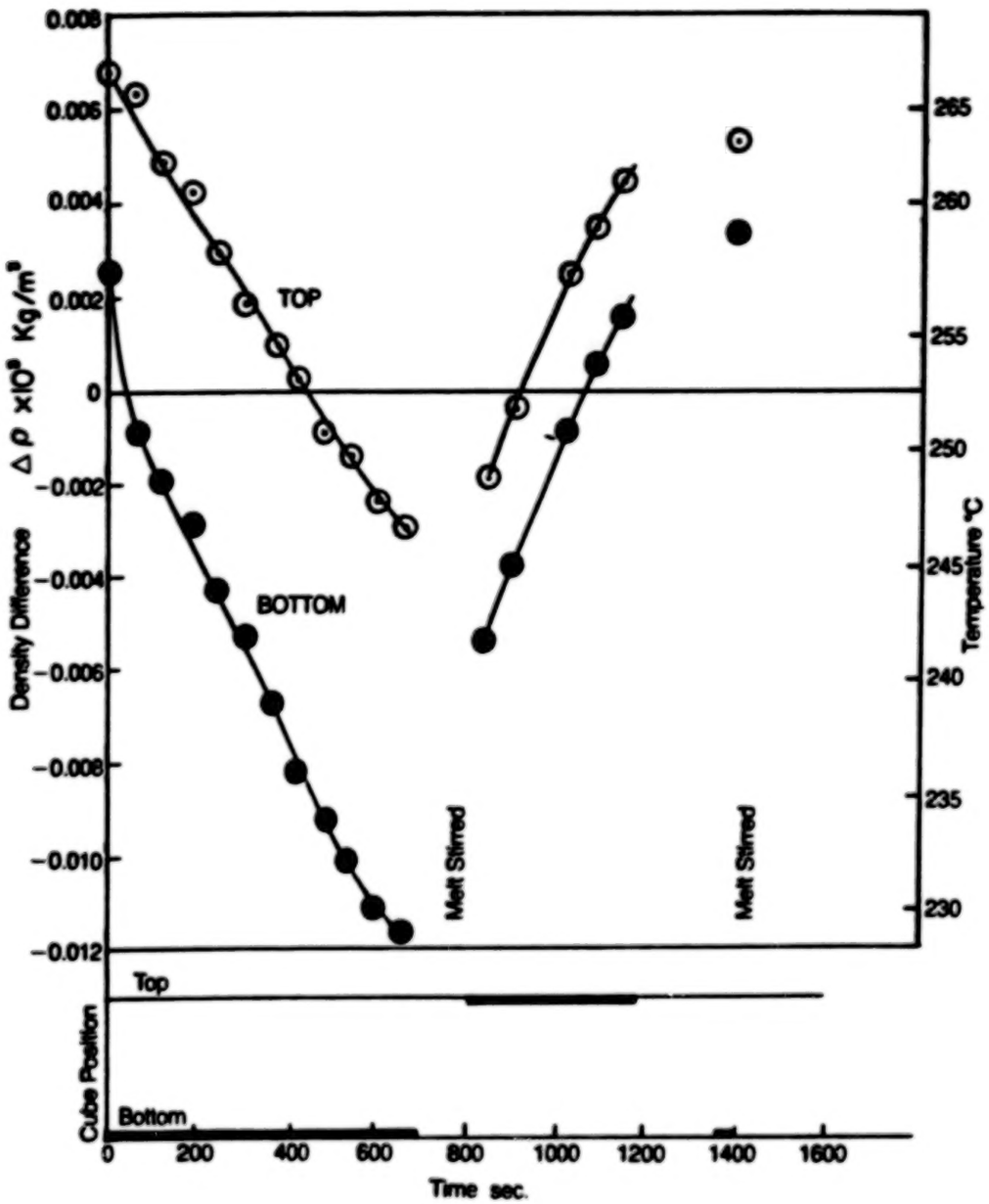

Figure 5: The density difference between a single crystal copper cube and a PbSn melt is plotted as function of time as the bottom of the melt was first cooled and then reheated. A negative density difference is for the copper density less than the melt density. The corresponding copper cube position, with time is shown in the lower part of the figure. The melt was stirred at the times indicated.

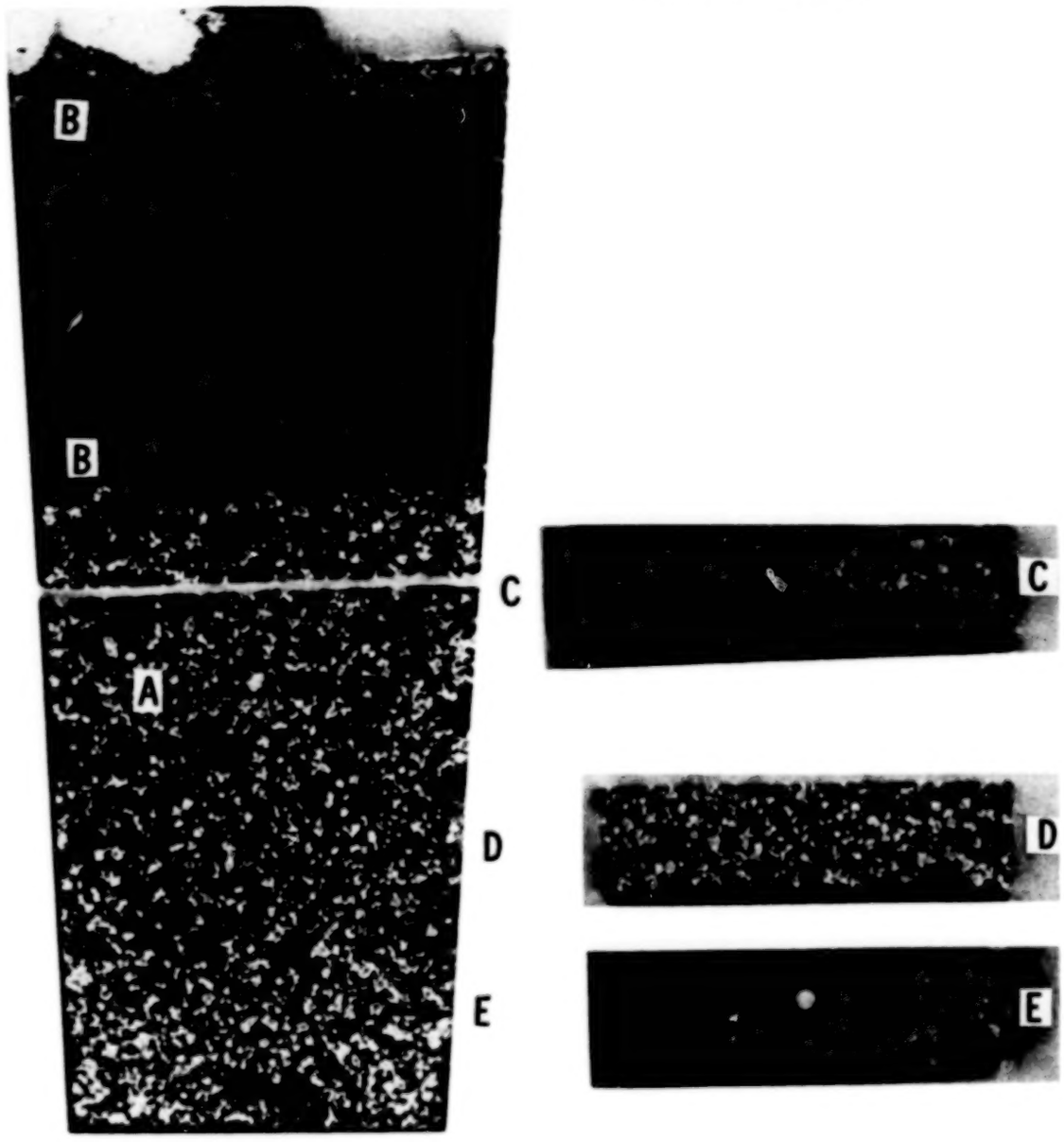

(a) (b)

Figure 6: (a) Autoradiograph of quenched partially solidified tin melt. Tumbling time 690 s (27% solid). Settling time 300 s. A grains from tumbling period. B grains from settling period. Mag. x 0.9.
(b) Autoradiographs of horizontal sections through the ingot at the heights indicated. Mag. x 0.9.

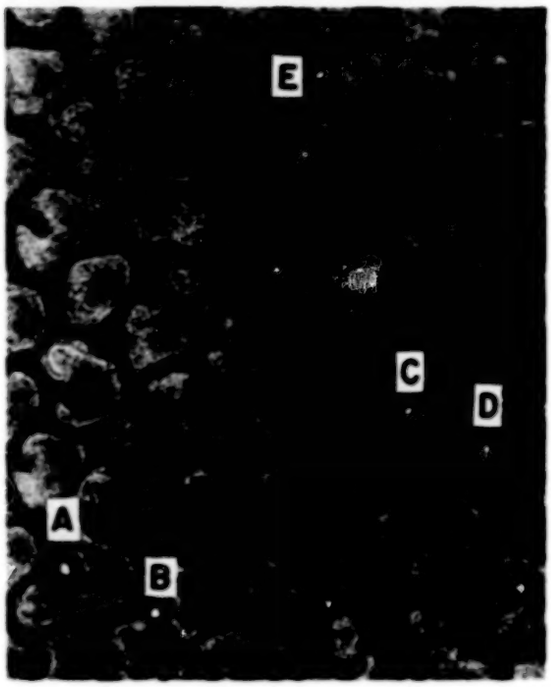

Figure 7: Transverse section of Pb 1 wt pct. Sb alloy containing iron particles A-E. (a) Mag. x 100 etched surface. $v = 1.7 \times 10^{-3}$ cm s^{-1}.

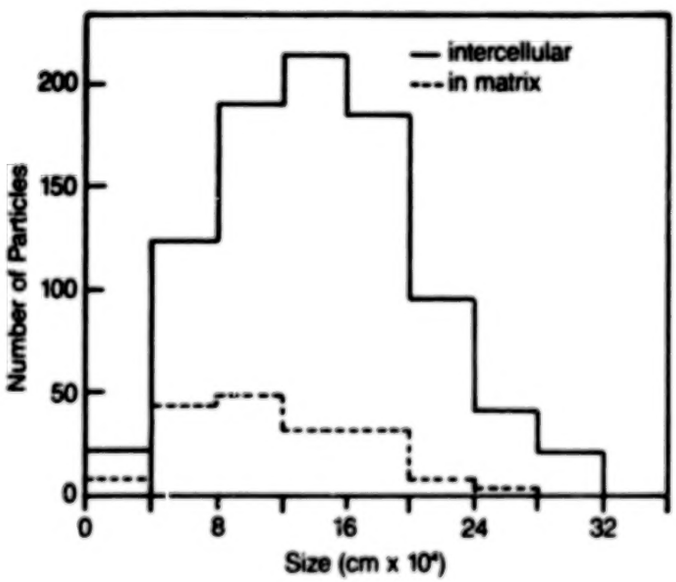

Figure 8: Size distribution of iron particles in Pb 1 wt pct. Sb solidified vertically with a cellular structure.

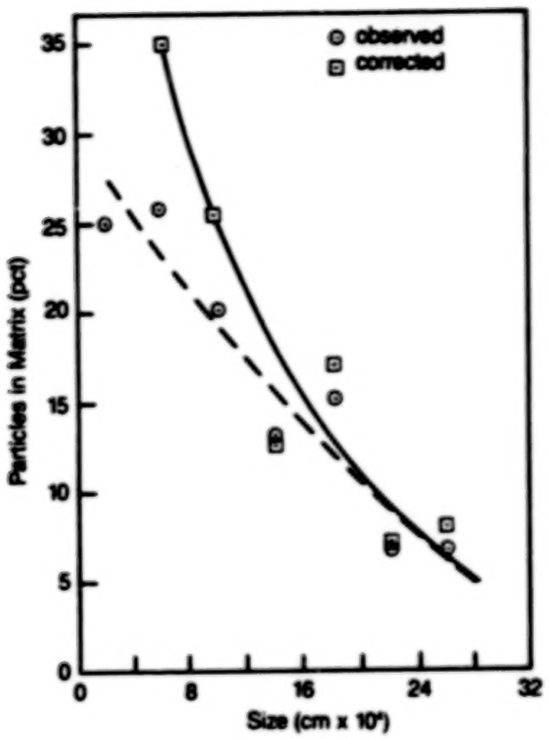

Figure 9: Percentage of particles in the cell matrix for vertical growth in lead as a function of particle size.

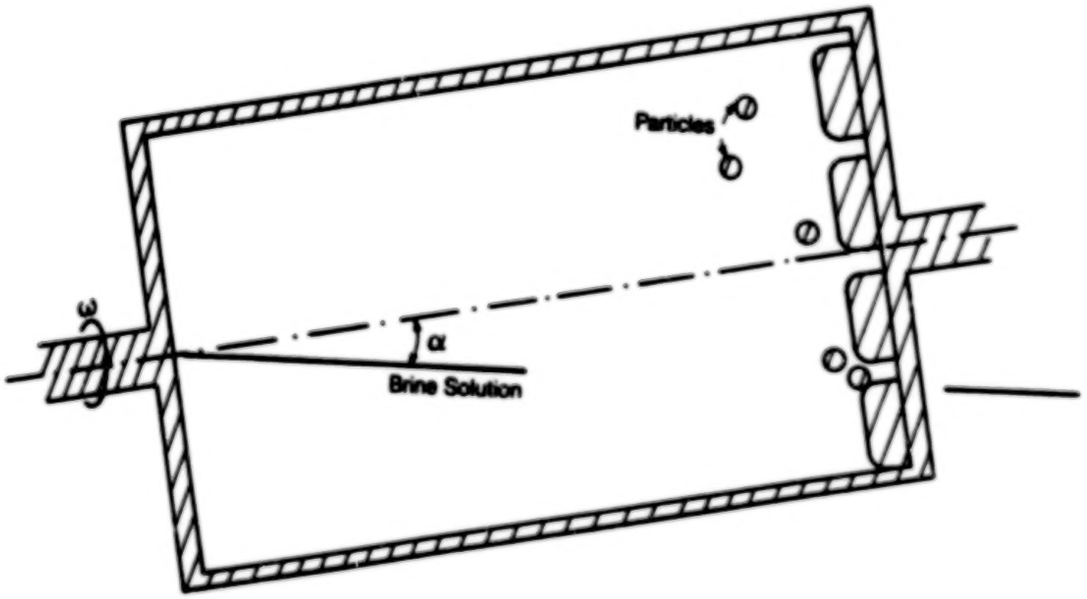

Figure 10: Water model. Lucite tube 170 mm long and 95 mm inside diameter. The cellular structure at C consists of lucite hexagons 20 mm in diameter and 4 mm apart.

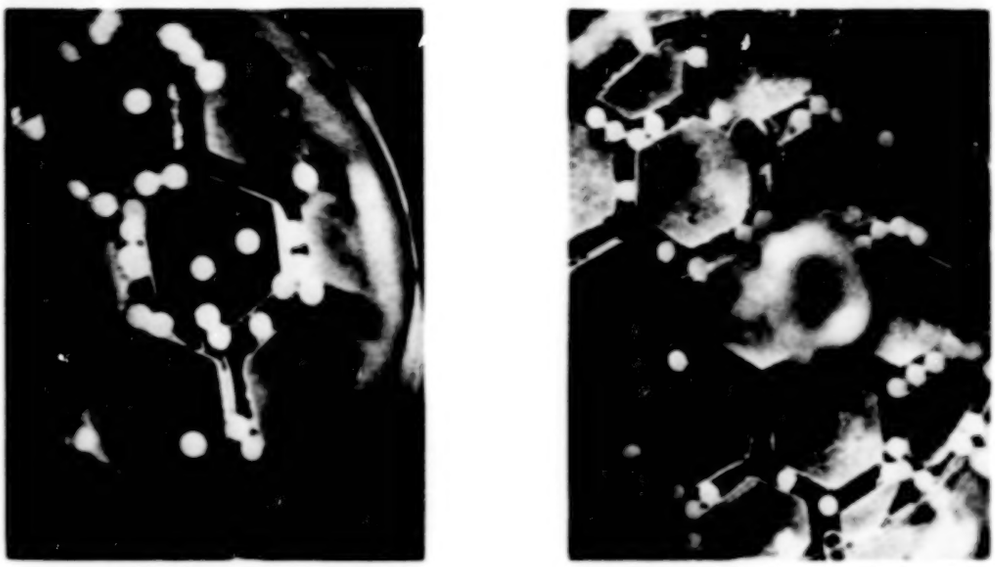

Figure 11: Photographs of cellular end of water model with nylon spheres segregated to intercellular regions. (a) Horizontal $\omega' = 0.5$ rps $\alpha' = 4'$ Vertical $\alpha' = 90°$.

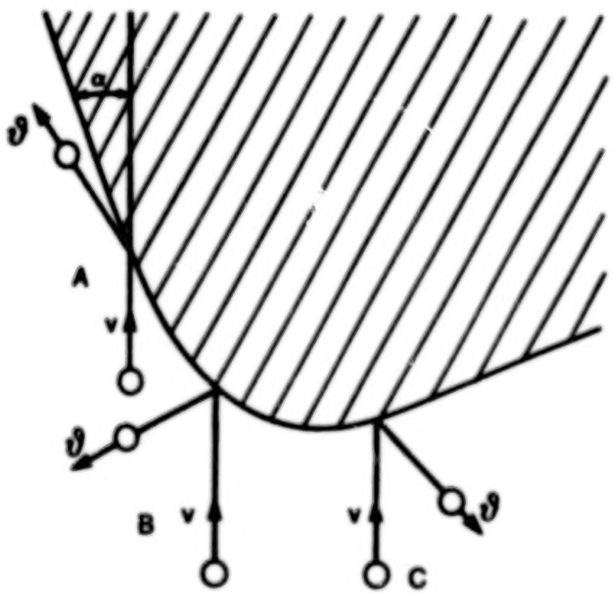

Figure 12: Schematic illustration of a sphere striking a cellular wall on the flat surface A, the curved surface B and the intercellular wall C. Sphere velocity before and after collision V and v respectively.

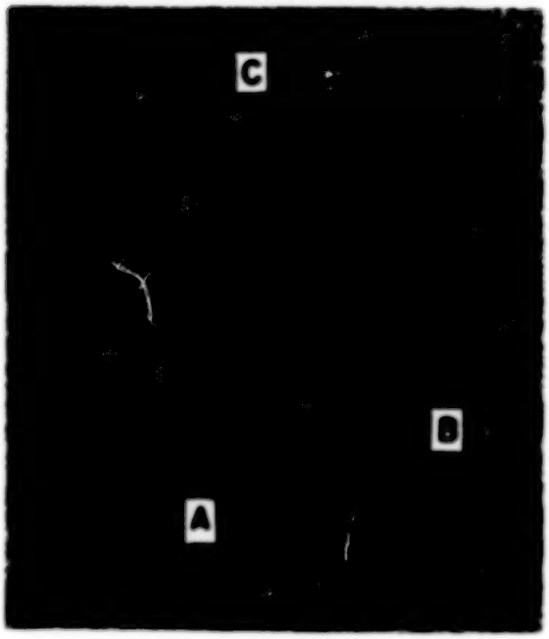

Figure 13: Cast Pb 50 wt pct. Sn alloy showing iron particles A-C in inter-dendritic regions. Etched. Mag. x 200.

CHANGES IN SOLIDIFIED MICROSTRUCTURES

John F. Wallace
Case Western Reserve University

SIGNIFICANCE OF CONTROL OF MICROSTRUCTURE

Utilization of knowledge of solidification principles frequently permits the attainment of solidified structures that exhibit the desired properties. For some purposes, such as high temperature applications, coarse grain sizes are preferred. In other cases, a fine grained morphology is optimum because of the improved yield strength and toughness of these structures at lower temperatures. Oriented or columnar grains exhibit anisotropic properties that can be either good or bad depending on the stress state existing in the component. The orientation of columnar grains parallel to the principal stress direction in superalloy blades is an example of a beneficial condition; the radial orientation of columnar grains in a centrifugal casting where hoop stresses are the highest stresses because of internal pressure within the bore of the tube is a poor state.

This presentation is primarily concerned with the change in the solidifying grains in a melt from columnar to equiaxed, as illustrated schematically in Figure 1 (1). This, perhaps oversimplified, sketch of the different columnar - equiaxed structures also shows a chill zone on the surface. It is well known that this chill zone may not form or may remelt after forming, so that it is frequently not present. The macroetched sections of transverse discs in Figure 2 illustrate some of the variations in structure that occur commercially. This refinement of the grains of the columnar and particularly the equiaxed grains of cast structures is also a change in solidified structure of some significance that is discussed in this paper. The two changes are interrelated since conditions that favor equiaxed grain refinements usually favor a change from columnar to equiaxed grains.

A few examples of the desirability of the change in solidified structure from columnar to equiaxed and from coarser to finer grain sizes are presented for commercial alloys. Table I illustrates the effect of grain size and orientation on the tensile properties of copper-zinc alloys (2). The longitudinal columnar grains exhibit the highest ductility but lowest strength; the transverse columnar grains have a higher strength but lower elongation. The equiaxed grains display the highest strength with intermediate ductility. The ductility of cast steels can also be improved by grain refinement. Some typical tensile properties from small unidirectionally solidified AISI 4335 steel castings are illustrated in Figure 3 (3). This figure shows the tensile properties of the grain refined, equiaxed steel castings and base, columnar steel produced from the same melt. The

variation in tensile properties at various distances from the chill end of the unidirectionally solidified section for both the base columnar structure and refined equiaxed steel casting are illustrated for tensile bars oriented in a vertical direction parallel to the solidification direction and in a horizontal direction perpendicular to this direction. The yield and tensile strength was uniform at about 208 and 250 ksi respectively for both the columnar and equiaxed or refined structures. The tensile ductility, as measured by the reduction in area, shows an improvement for the equiaxed, refined structure in both the vertical and horizontal direction. The refinement to an equiaxed grain also reduced the anisotropy (3). These effects on properties occur because of changes in the macro and microsegregation and distribution of the nonmetallic inclusions. In addition to its effect on the mechanical properties, grain refinement also reduces the hot tearing of the alloys during solidification (2-4). A coarse grained casting develops a coherent network of dendrites relatively early during the solidification period and provides higher localized areas of strain than a fine grained casting. Many of these effects carry over into the properties of wrought products.

MEANS OF CONTROLLING SOLIDIFIED STRUCTURE

The transition from columnar to equiaxed or free dendrites is affected by a large number of variables, such as the thermal gradient, rate of solidification, state of nucleation, variations in pressure, and characteristics of the alloy being solidified, particularly the equilibrium distribution coefficient. Because of its importance, a significant amount of research effort has been expended to control the columnar - equiaxed transition and to provide grain refinement during solidification. Several methods of accomplishing a transition from a columnar to one equiaxed structure are recognized and have been demonstrated. These methods are discussed and the effect of each described in the following paragraphs.

Constitutional supercooling of the segregated liquid metal ahead of the advancing columnar grains and the separate nucleation of dendrites in the supercooled liquid has long been recognized as a very effective means of changing the structure from columnar to equiaxed grains and producing grain refinement (5). The schematic drawings in Figure 4 illustrate the solid solutions susceptible to constitutional supercooling and the amount of constitutional supercooling attained with cellular, dendritic and free dendritic solidification. Conditions for interrupting columnar solidification are obviously improved by equilibrium distribution coefficients that differ greatly from unity and by the increased amount of constitutional supercooling obtained with free dendritic solidification. Examples of how effective the proper combination of constitutional supercooling and separate nucleation can be are shown in Figure 5 (4) for commercial aluminum alloys and Figure 6 for copper - tin alloys (2). Effective substrates for heterogeneous nucleation are a definite requirement for the proper functioning of this method as

shown by the columnar structures obtained in Figures 3, 5 and 6 without these substrates. These substrates for free dendrites are present in the supercooled region of the melt. To be effective, they should have epitaxy within 6% of the solidifying phase (6) as well as having a clean surface, solid, stable and of similar density as the melt. This mechanism in the opinion of the author is the most practical one for commercial use.

The detachment of dendrite arms and tips by melting off from the columnar wall, followed by their transport by convection to the melt ahead of the columnar wall is another method of changing columnar to equiaxed grain structure. The work conducted with the solidification of transparent organics of low $\alpha = \frac{L\xi}{RT_E}$ values of metals, so that these solidify with an atomically rough interface, have clearly demonstrated the feasibility of this mechanism (7). This melting off is demonstrated in Figure 7 (7). It is known that convection currents occur in solidifying melts of significant size, thereby contributing to alloy macrosegregation. The necks which attach the dendrite arms to spines are small and in a high temperature region. When the curvature of these necks is large, they are highly susceptible to melting and detachment. Any recalescence will produce many such detached arms. These arms have an ideal structure to serve as nuclei for solidification in the melt ahead of the columnar wall. The feasibility of this technique has also been demonstrated by calculations of heat flow and alloy segregation.

Mechanical vibration has been known as a means of providing grain refinement and the change from columnar to equiaxed grains for many years. When this refinement occurs in alloys with considerable solute content, the most probable mechanism is the rupture of dendrite arms and tips from the advancing columnar wall and their transport into the melt to serve as nuclei for free dendrites. This mechanism is aided by alloying elements that produce considerable segregation with significant constitutional supercooling. It has been shown that lower vibrational amplitude and frequencies will produce this structural change in solidifying alloys than in pure metals (8,9). The refinement of pure metals and eutectics require higher frequency X amplitude products (fa) and in this case the mechanism is believed to be cavitation that occurs in the melt. Figures 8a and 8b (9) are frequency - amplitude maps for grain refinement of pure metals and eutectics and dendritically solidifying alloys respectively. The practical problems encountered with mechanical vibration usually make the utilization of this technique a difficult one for attaining this refinement of the structure.

Another mechanism that has been demonstrated as effective in converting columnar to equiaxed structure has been the chilling of the open top surface of the solidifying melt. Small equiaxed crystals form at this surface and fall down into the molten metal region in front of the advancing columnar wall to form a free dendrite

zone. This behavior has been demonstrated with saturated ammonium chloride solution (7), aluminum alloys (10) and for steels in unpublished work by the author. The use of a trap door insert that may be closed to interfere with the falling down of these small free dendrites from the top surface was particularly effective in illustrating this mechanism (10). Figure 9 (7) demonstrates the appearance of the ammonium chloride crystals falling down from the chilled surface and Figure 10 (10) shows the dendritic nature of the so called comet type grains with their dendrite structure that have been trapped in the melt during the process of falling from the top surface to the equiaxed grain zone forming at the bottom of the cast section. This technique is limited to castings and ingots with chilled top surfaces. These conditions rarely prevail in castings produced a closed mold with insulated risers or ingots with a hot top and insulation at the top surface.

The inducement of flow in the solidifying metal can also be used for interrupting the solidification of the columnar region. This flow may be induced by oscillation of rotation during solidification or by the imposition of electromagnetic fields during solidification. This latter subject is discussed in detail by another paper in this symposium and therefore is not covered in this paper. Oscillation during rotation is effective, as demonstrated in Figure 11 (11). A timed program of oscillation-rotation-oscillation can be employed to provide a multiple combination of equiaxed and columnar grains. The oscillation which is conducted at relatively slow speeds separates the dendrite tips and arms from the spines so that they can serve as nuclei for free dendrites in the melt with minimal undercooling required. Continued rotation, on the other hand, interferes with the formation of the constitutionally supercooled zone and favors continued columnar grain solidification. The columnar grains are slightly tilted towards the direction of flow of the molten metal or away from the direction of rotation. Figure 11 shows the refinement and primarily equiaxed structure in A, the mostly columnar, coarse grained structure of the fully rotated structure in B, and combinations of rotation and oscillation with different timing in C and D. The process, although effective, does require suitable shapes of castings and considerable equipment.

In addition to the various methods listed above, it is also well known that rapid solidification will favor fine grains and with cold pouring can produce an equiaxed grain structure (11).

SUMMARY

The properties and casting behavior of metals can be significantly affected by their cast structure. This structure can be optimized by producing columnar versus equiaxed grains and coarse versus fine grains by controlling solidification conditions. The transition from columnar to equiaxed grains can be favored by: constitutional supercooling with effective nucleation of free dendrites;

melting off and transport of dendrite tips and arms; mechanical vibration; falling down of free dendrites from a chilled top surface; and induced flow in the solidifying structure by oscillation of rotation.

REFERENCES

1. Form, G. W. and Wallace, J. F.: "General Principles of Solidification of Metals", Trans. AFS Vol. 68 (1960) p. 145.

2. Wallace, J. F. and Kissling, R. J.: "Grain Refinement of Castings of Copper Alloys", Foundry, August and September, 1963, p. 54 and 74.

3. Wieser, P. F., Church, N. and Wallace, J.F.: "Grain Refinement of Steel Castings", Journal of Metals, June 1967, p. 44.

4. Kissling, R. J. and Wallace, J. F.: "Grain Refinement of Aluminum Castings", Foundry, June and July 1963, p. 45 and 78.

5. Chalmers, Bruce: "Shape and Sizes of Grains in Castings" Solidification ASM 1969, p. 295.

6. Bramfitt, B. L.: "Effect of Carbide and Nitride Additions in the Heterogeneous Nucleation Behavior of Liquid Iron", Metallurgical Transactions, Vol. 1, p. 1987, 1970.

7. Jackson, K.A. et al: "The Equiaxed Zone in Castings", Trans Met. Soc. AIME, Vol. 236, 1966, p. 149.

8. Southin, R. T.: "The Influence of Low Frequency Vibration on the Nucelation of Solidifying Metals", Journal of the Institute of Metals, Vol. 94, 1966, p. 401.

9. Campbell, J.: " Grain Refinement of Solidifying Metals by Vibration: A Review" Solidification Technology. The Metals Society, 1980, p. 61.

10. Southin, R. T.: "Nucleation of the Equiaxed Zone in Cast Metals", Trans. of Met. Soc. of AIME, Vol. 239, Feb. 1967, p. 220.

11. Bolling, G. F.: "Manipulation of Structure and Properties" Solidification ASM 1969, p. 341.

TABLE I –Effect of Grain Size and Orientation of Test of Columnar Grains on Tensile Properties of Cu-Zn Alloys[14]

Structure	Grains/in.²	Tensile Strength, psi	Elongation, per cent	Grain Shape and Size
		30 PER CENT ZINC-COPPER		
Alpha	56	34,600	58	Transverse columnar
	86	26,600	72	Longitudinal columnar
	1036	31,100	57	Small equiaxial
	3700	37,200	68	Small equiaxial
		40 PER CENT ZINC-COPPER		
Alpha + Beta	23	47,500	72	Longitudinal columnar
	66	50,100	44	Equiaxial
	112	50,600	51	Equiaxial
	426	49,600	46	Equiaxial
		47 PER CENT ZINC-COPPER		
Beta	26	50,600	64	Longitudinal columnar
	223	57,800	37	Equiaxial
	889	62,500	34	Equiaxial
	343	60,700	47	Transverse columnar

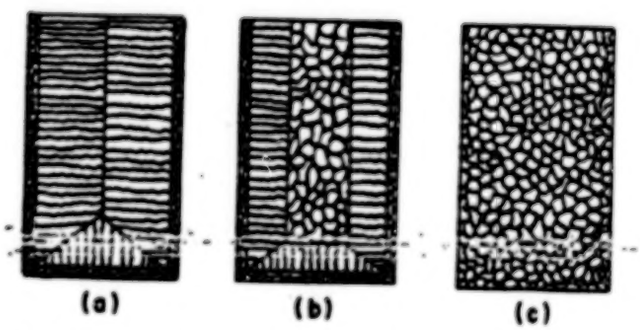

Fig. 1—Appearance of ingot structures: (a) wholly columnar except for chill zone; (b) partially columnar and partially equiaxed; and (c) wholly equiaxed. (1)

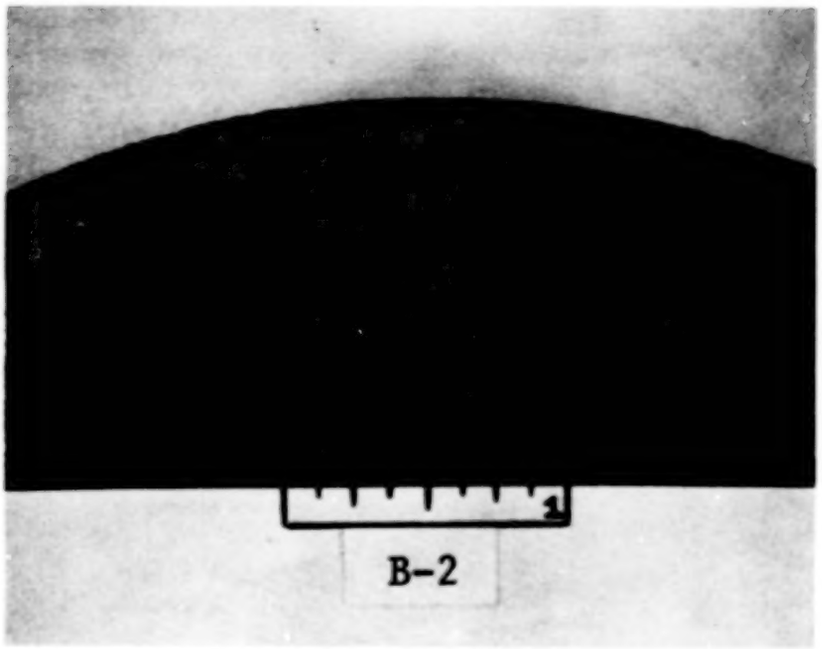

A.) Fine Columnar Rim; Medium Columnar Center; Thin, Fine Equiaxed Bore.

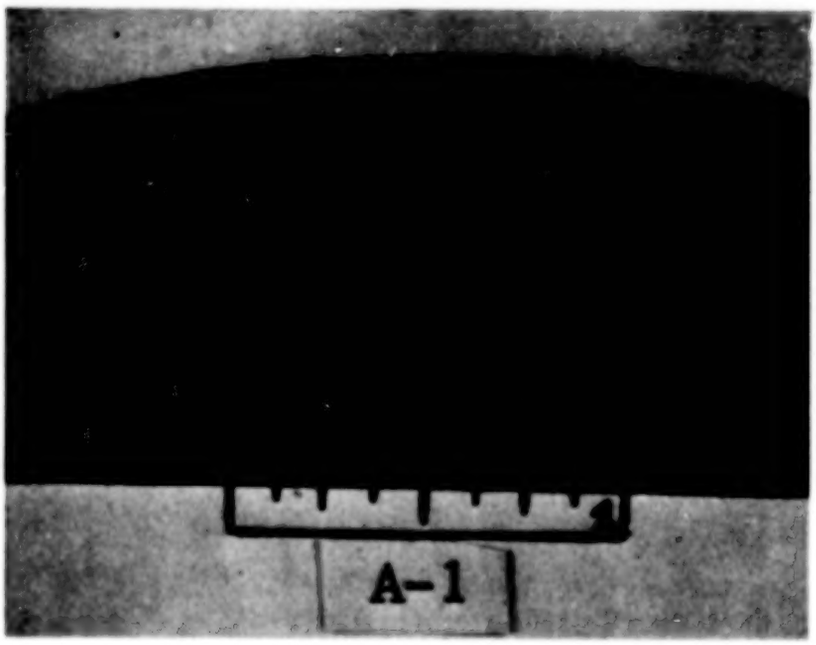

B.) Equiaxed Rim; Fine Columnar Band, Fine Equiaxed Thick Based at Bore.

Figure 2. Various microstructures in Centrifugally Cast Tubes.

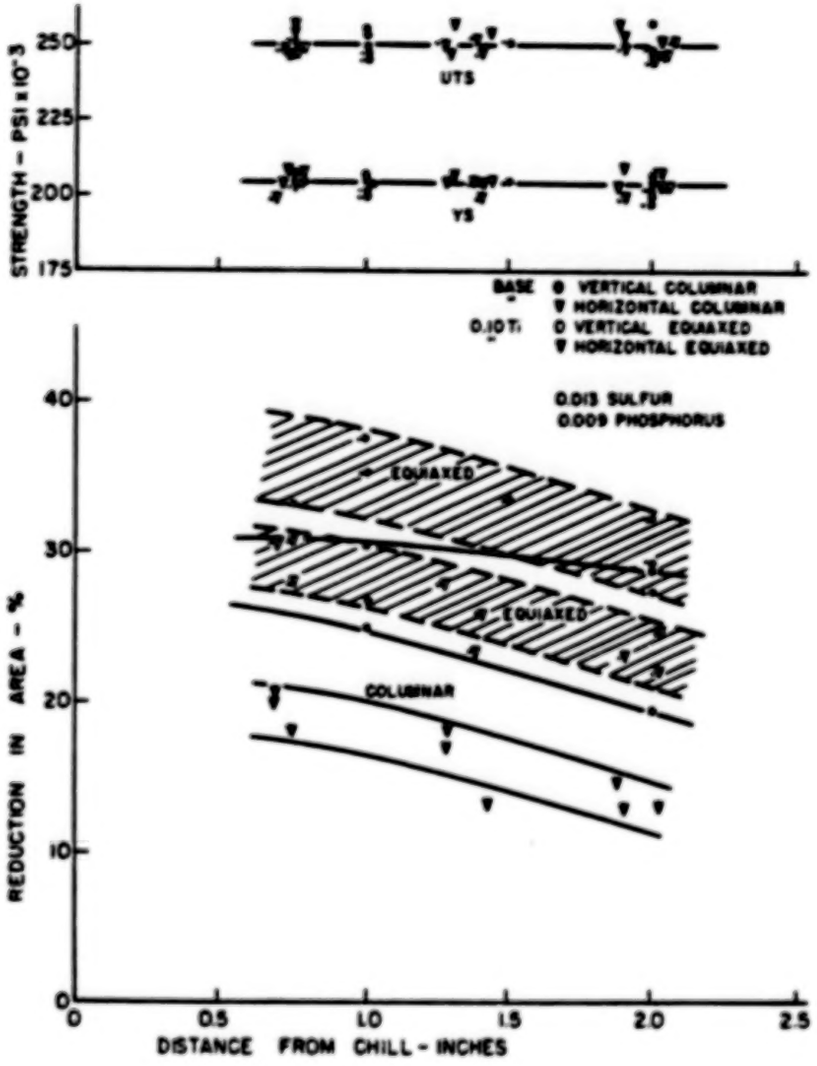

Figure 3. Effect of cast grain structure on properties of high strength unidirectionally cast 4335 quenched and tempered steel in base and grain refined condition (3).

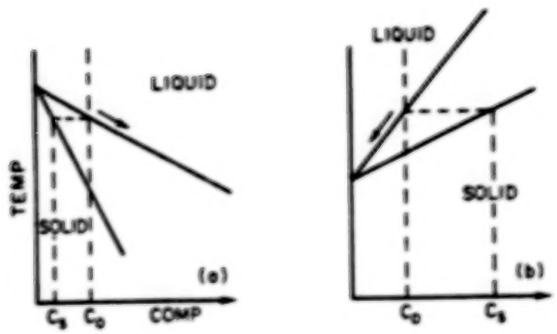

Schematic of phase diagrams that produce constitutional supercooling.

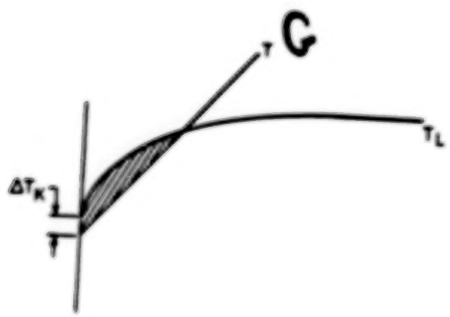

Thermal Gradient for Cellular Structure Showing Supercooled Region.

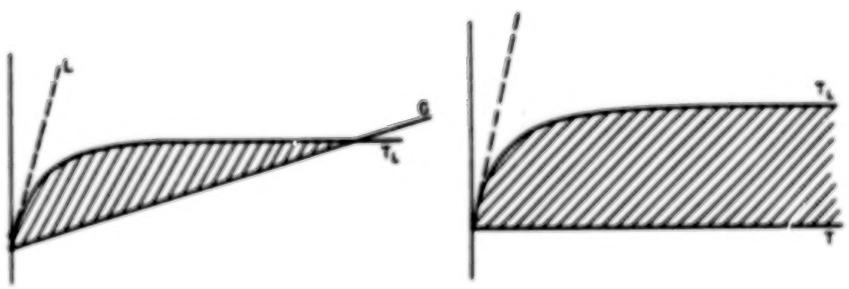

Thermal Gradient for dendritic structure showing Supercooled Region.

Thermal Gradient for free dendritic growth in an alloy showing Supercooled Region.

Figure 4. Constitutional Supercooling and Supercooled Regions for Different Structures (5).

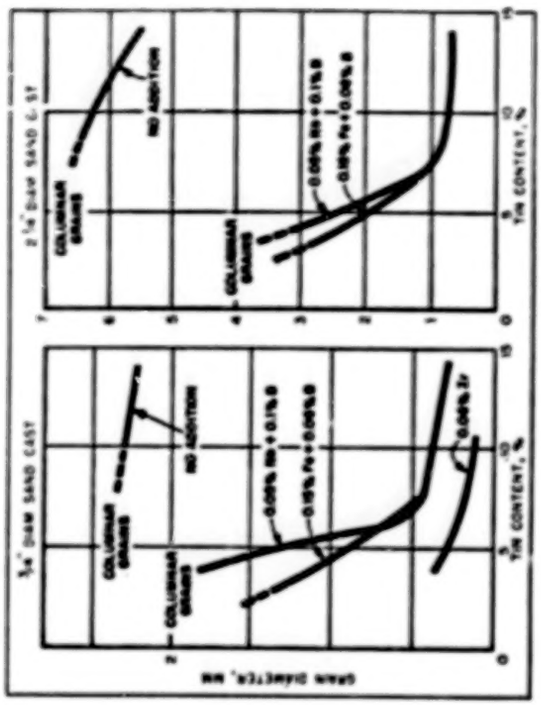

Figure 6. Effect of Grain Refining on the Structure of Cu-Sn Alloys. Influence of Constitutional Supercooling Shown by Various Alloy Contents (2).

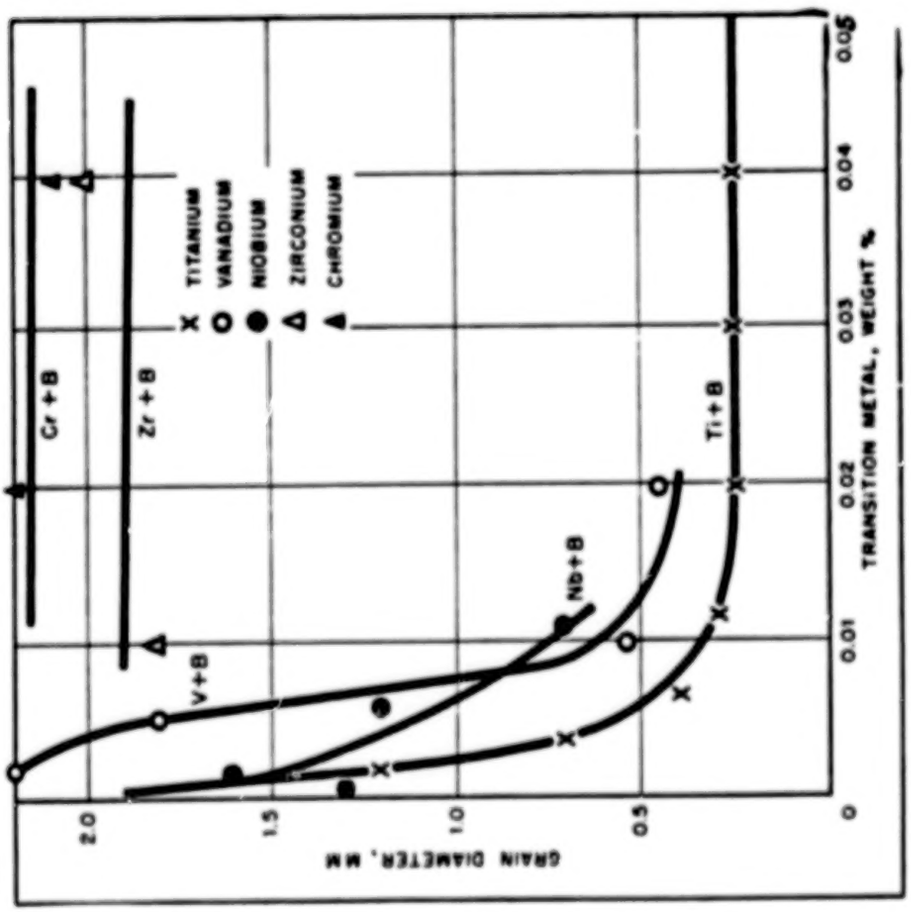

Figure 5. Effect of Various Grain Refining Additions on the Grain Size of 195 Al-Cu Alloy Cast in Light Sections. Effectiveness of Different Transition Metals Plus Boron Indicated (4).

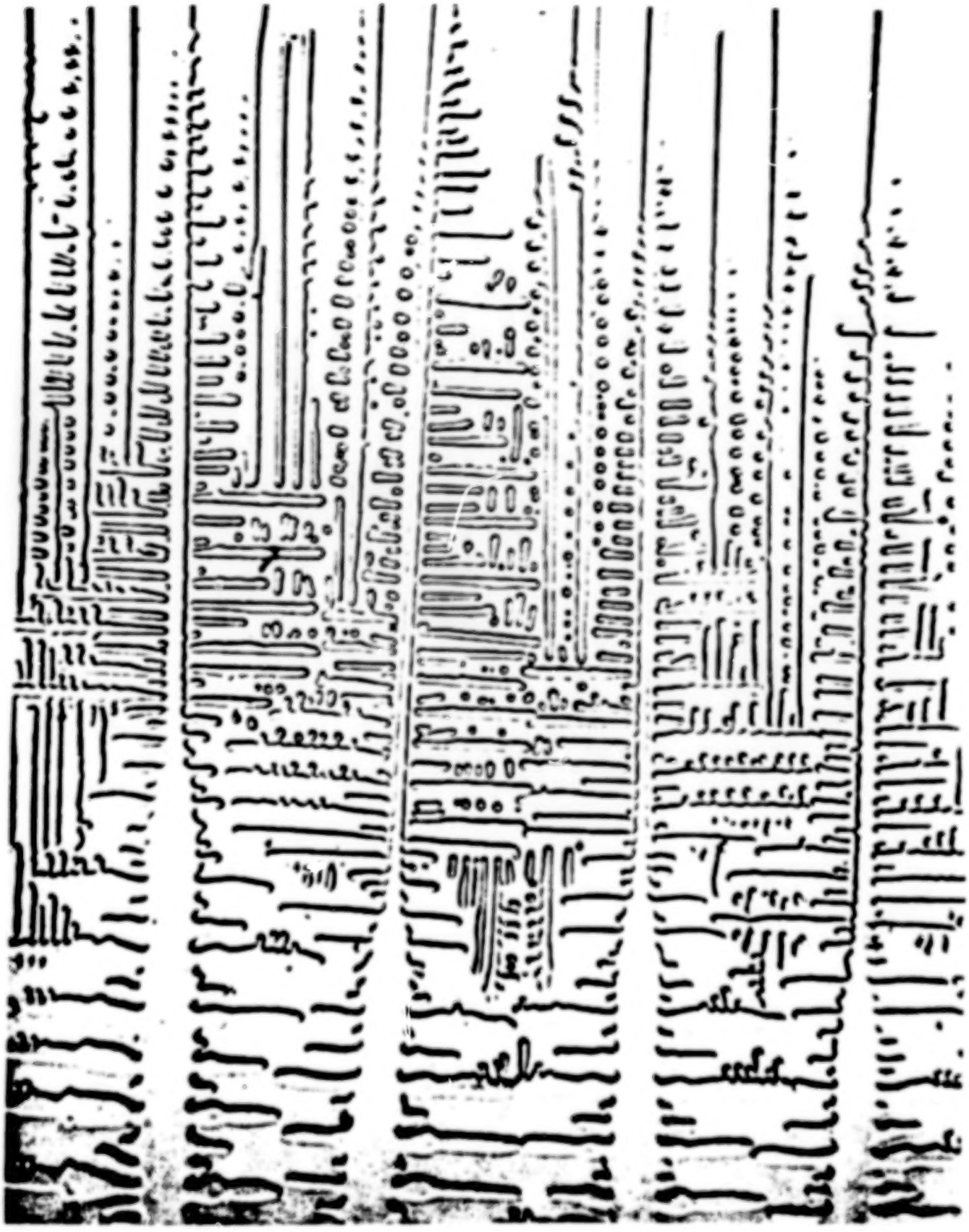

Figure 7. Separation of Dendrite Arms From Spine Shown in Carbon Tetrabromide and Salol Solidification with A Change in Solidification Rate 75X (7).

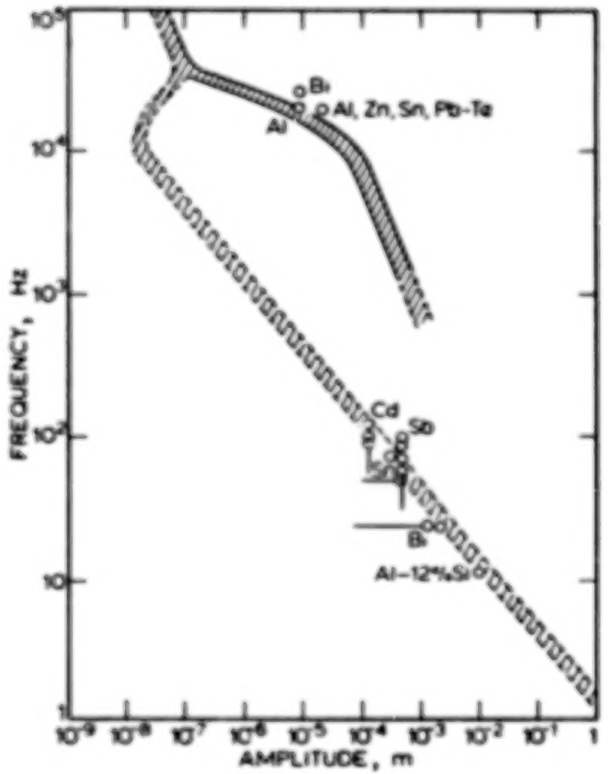

Figure 8a. Frequency/amplitude map of grain refinement data for pure metals and eutectics showing their coincidence with theoretically predicted cavitation conditions for sonic and supersonic vibration (9).

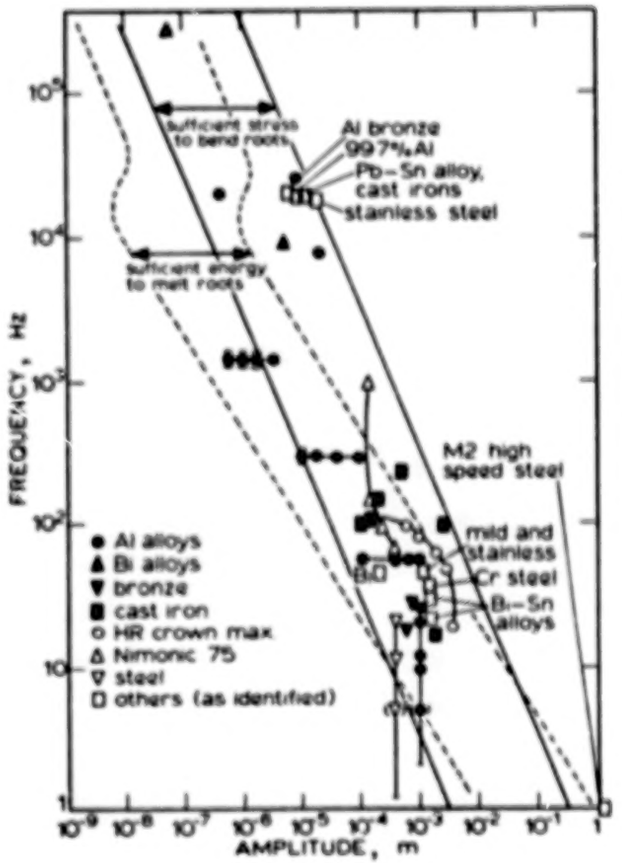

Figure 8b. Frequency/amplitude map of grain refinement data for dendritically solidifying alloys. Points in brackets denoted marginal refinement. All data are contained within lines of equal bending stresses experienced by dendrite roots (9).

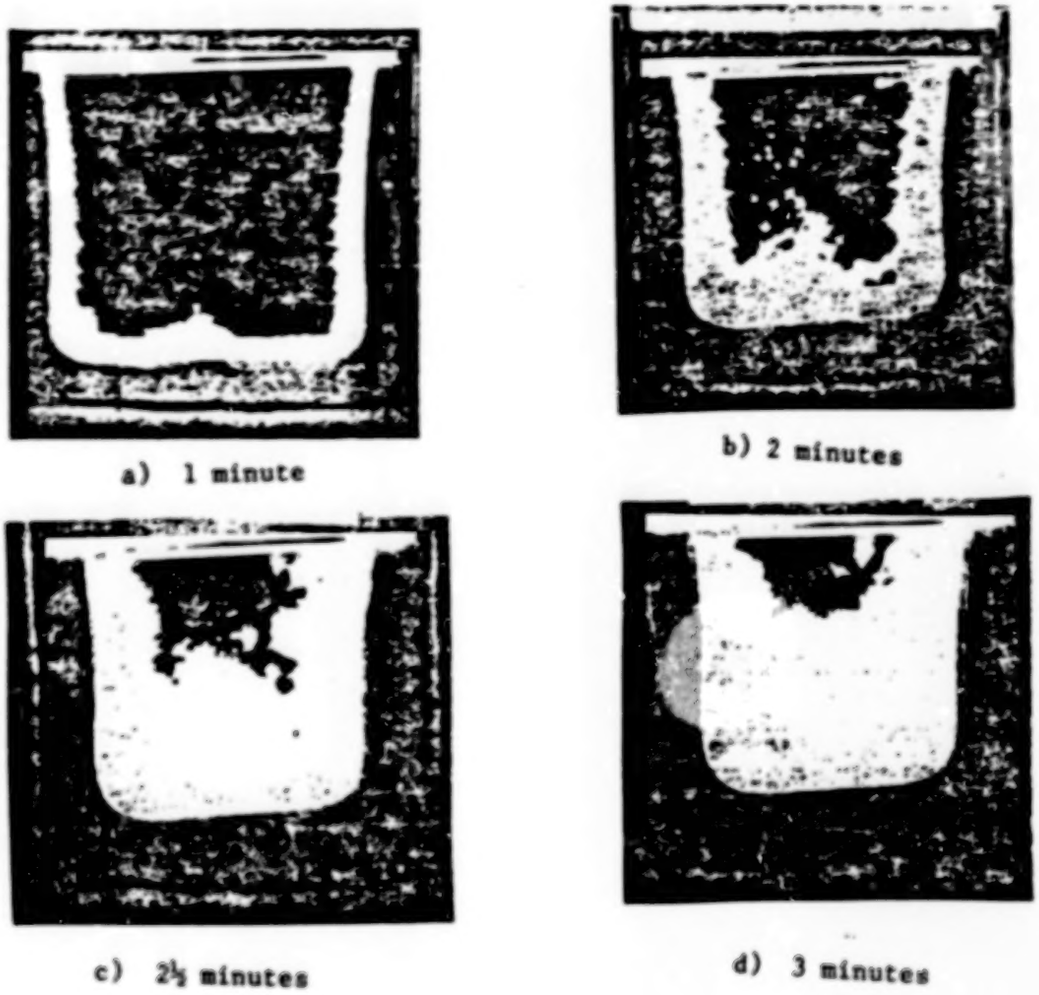

a) 1 minute

b) 2 minutes

c) 2½ minutes

d) 3 minutes

Figure 9. Casting of Ammonium Chloride - Water Solution, Saturated at 50°C, poured at 75°C Showing Times after Pouring (7).

A. 99.99% Al

Al - 0.1% Ca

Al - 2% Cu

Figure 10. Comet Grains Trapped During Falling From Top Chilled Surface Layer of Ingot (10).

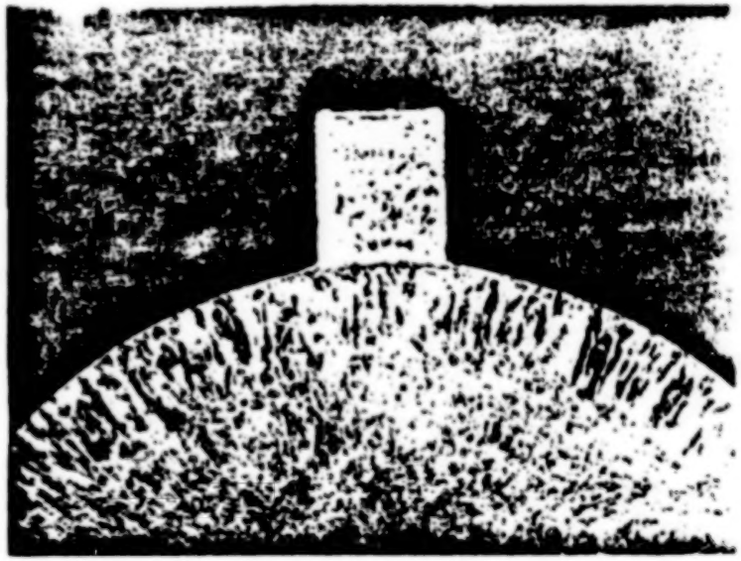

A. Completely Oscillated-Vane-Equiaxed Rim Fine Columnar; Body-Equiaxed.

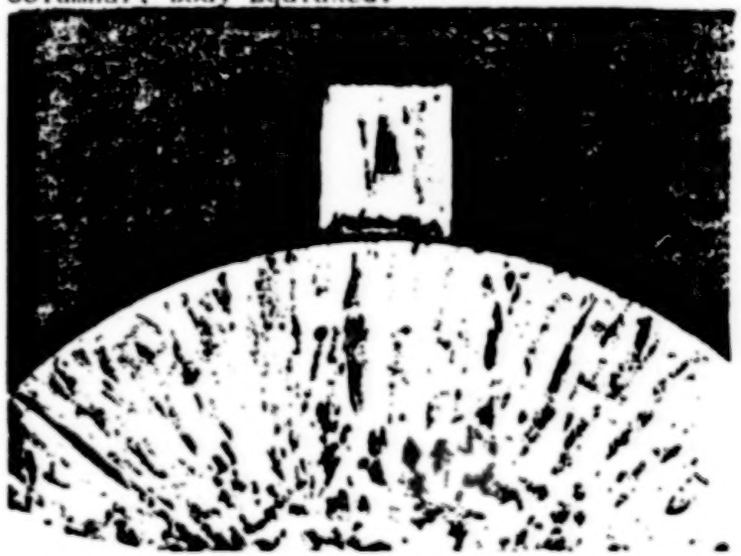

B. Rotated - Mostly Coarse Columnar

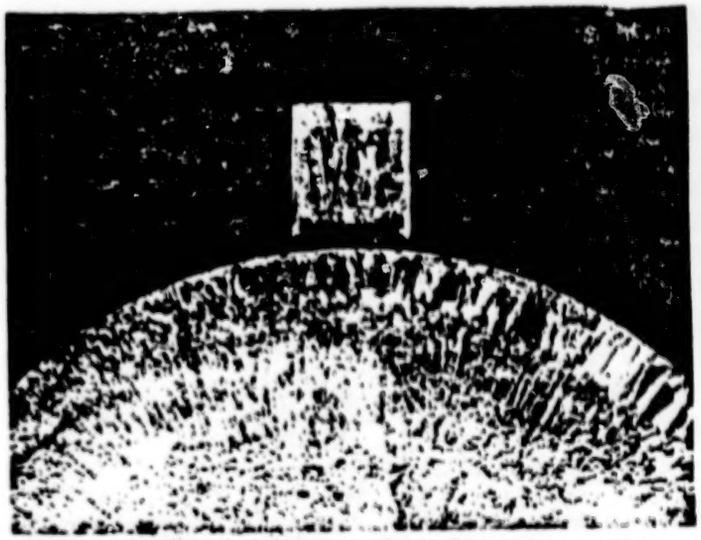

C. Rotated Through Vane Solidification, Then Oscillated-Vane-Coarse Columnar; Rim Fine Columnar; Body Equiaxed

D. Fully Rotated Mostly Coarse Columnar

Figure 11. Effect of Rotation -Oscillation Cycles During Solidification of Sn-3% Zn and Sn-1%Zn Alloys on the Macrograin Structure (11).

D7

SOLIDIFICATION STUDY OF SOME Ni- AND Co-BASE ALLOYS

Christian L. Jeanfils
Cabot Corporation
Kokomo, Indiana

As the understanding of ingot production processes improves, it is often found that the solidification behavior of the alloy itself should be known in more detail. An on-going research program aims to characterize the solidification of several Ni- and Co-based commercial wrought type alloys. The techniques used and the data items sought are

(a) Thermal analysis
  Liquidus
  Nonequilibrium solidus as a function of cooling rate
  Secondary reactions temperatures
  Incipient melting
  Progress of solidification as a function of temperature
(b) Optical Metallography
  Characteristic structures and secondary dendrite arm spacing as a function of cooling rate.
(c) X-ray Diffraction
  Identification of precipitates
(d) SEM/EDAX
  Measure of microsegregation

At this stage of the experimental program, the thermal analysis has received the most attention. The equipment is similar to that described by B. Carlsson and B. Calmer in the Jernkontoret Guide to the Solidification of Steels. The procedure consists of cycling a 20- to 50-gram alloy sample through its melt range and recording the temperature of the sample and the control thermocouple. The time derivative of the sample temperature assists in the identification of the transformation points. A mathematical function of the two recorded signals has values which are proportional to the rate of enthalpy change that is associated with the solidification or remelting. Its integral, a normalized enthalpy of the transformation, provides a measure of the progress of solidification as a function of time or temperature.

The Ni- and Co-based wrought type alloys usually contain significant amounts of one or more of the following alloying elements: Cr, Fe, Mo, W, Nb, Ti, Al, and C. A general observation for these alloys is that a large fraction of the liquid solidifies over a narrow temperature range. A typical value is 80 per- cent solidified at 30 °C below the liquidus. For the range of cooling rates adopted (0.05 to 1.0 °C/sec), the end of solidification occurs in a typical case 100 °C below the liquidus. The nonequilibrium solidus can be significantly below the temperature of incipient melting, even without a homogenization treatment. The hysteresis in the normalized enthalpy of transformation-temperature curve tends to be more pronounced at low fractions of liquid than near the liquidus.

The sample size is large enough to provide material for metallographic examination and for the extraction of precipitates. Samples corresponding to five cooling rates are produced for each alloy. The series of micrographs provides a rapid way to evaluate, by comparison of the microstructures, the cooling rate at various locations in an ingot. For the majority of the alloys considered, the secondary dendrite arm spacing is not strongly alloy dependent. Typical values are 50 μm at a cooling rate of 1.0 °C/sec and 100 μm at 0.05 °C/sec.

Most of these alloys form one or several types of primary precipitates. They are identified from x ray diffraction patterns obtained from the extraction residues. Because the relative stability of these precipitates varies with temperature and with local composition, alloy-specific experiments are sometimes needed to arrive at a clear understanding of the sequence of precipitate formation.

A few attempts were made to determine whether or not x ray line broadening could be used as a global measure of the microsegregation in the as-cast samples. These attempts were not successful because of the preferred orientation of the as-cast structure. The degree of microsegregation is measured by microchemical analysis with the SEM/EDAX. Currently, this part of the program is still at an early stage.

Two improvements are planned for the thermal analysis unit. One is to increase the data collection frequency above the current once every 10 sec so as to improve the resolution of minor reactions. A second one is to gain the ability to quench the sample during or immediately after solidification so as to better separate reactions and obtain a measure of the dendrite coarsening tendency of individual alloys.

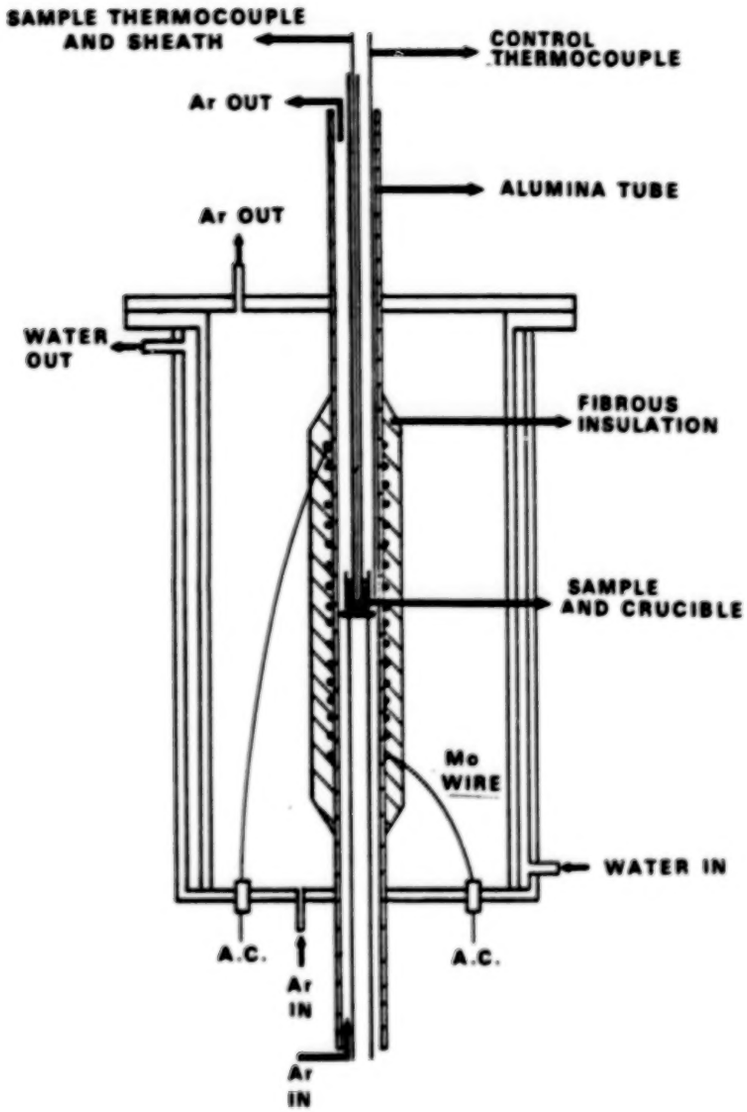

THERMAL ANALYSIS FURNACE

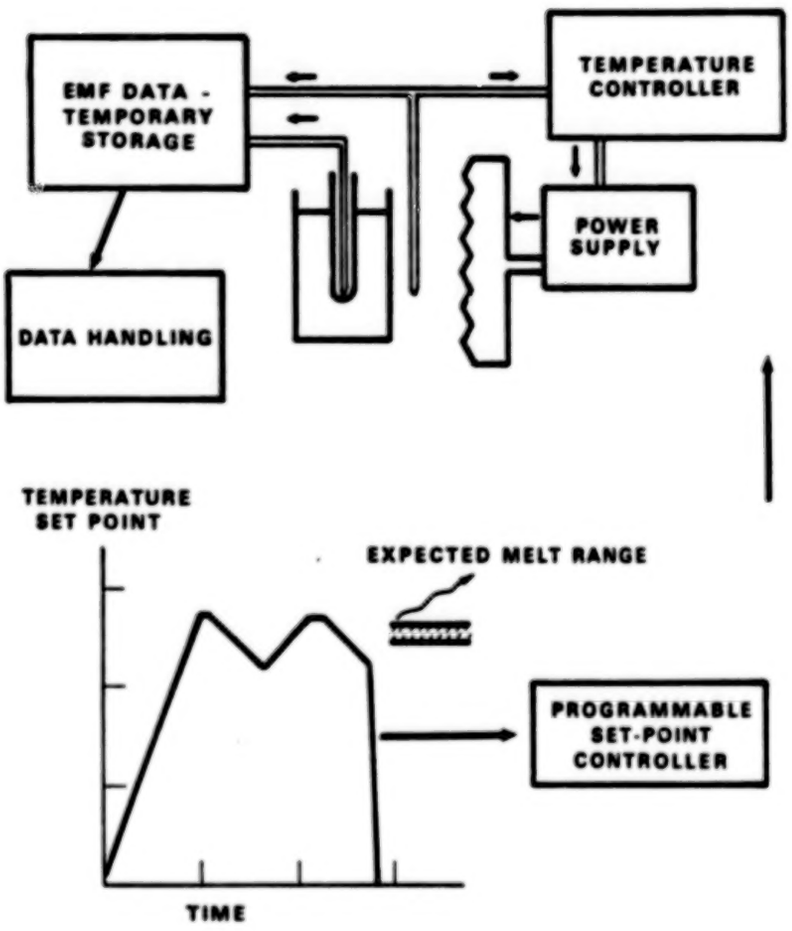

**THERMAL ANALYSIS FURNACE:
CONTROL AND DATA ACQUISITION**

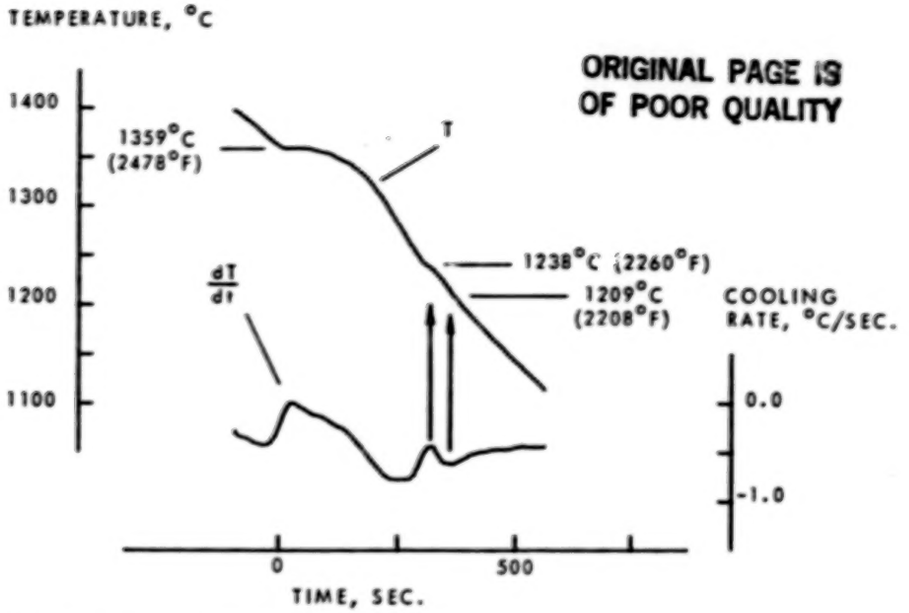

COOLING CURVE FOR HASTELLOY alloy X. THE COOLING RATE CURVE HELPS IN THE IDENTIFICATION OF TRANSFORMATION POINTS.

HEAT TRANSFER:

1. GOVERNING EQUATION:

$$(mc + m_r c_r)\frac{dT}{dt} + m\frac{d_L}{dt} = Q$$

WHERE: m AND m_r: MASS OF SAMPLE AND OF REFRACTORY, RESPECTIVELY

c AND c_r: SPECIFIC HEAT OF SAMPLE AND OF REFRACTORY, RESPECTIVELY

T: TEMPERATURE

L: HEAT OF FUSION/TRANSFORMATION

Q: TOTAL RATE OF HEAT INPUT

HEAT TRANSFER:

2. EXPRESSION TO ESTIMATE THE RATE OF HEAT INPUT:

ESTIMATOR OF $\frac{dT}{dt}$ OUTSIDE THE TRANSFORMATION RANGE:

$$u = E\left[\left(\frac{dT}{dt}\right) = u\left[\Delta T, T\Delta T, E_b(T), E_b(T_c)\right]\right.$$

$$E(Q) = (mc + m_r c_r)\, u$$

WHERE: T_c: CONTROL THERMOCOUPLE TEMPERATURE
ΔT: $T_c - T$
E ( ): EXPECTED VALUE
E_b( ): BLACK BODY EMISSIVE POWER

HEAT TRANSFER:

3. AMOUNT TRANSFORMED AS MEASURED BY ITS HEAT EFFECT: FUNCTION h_L

h_L IS DEFINED BY: $\frac{dh_L}{dt} = \frac{1}{L}\frac{dL}{dt}$

$h_L(o) = 1$ IF START FROM LIQUID:
$= o$ IF START FROM SOLID.

ESTIMATE OF $\frac{dh_L}{dt}$: $\frac{dh_L}{dt} = \left\langle \frac{mc + m_r c_r}{mL} \right\rangle \left(u - \frac{dT}{dt}\right)$

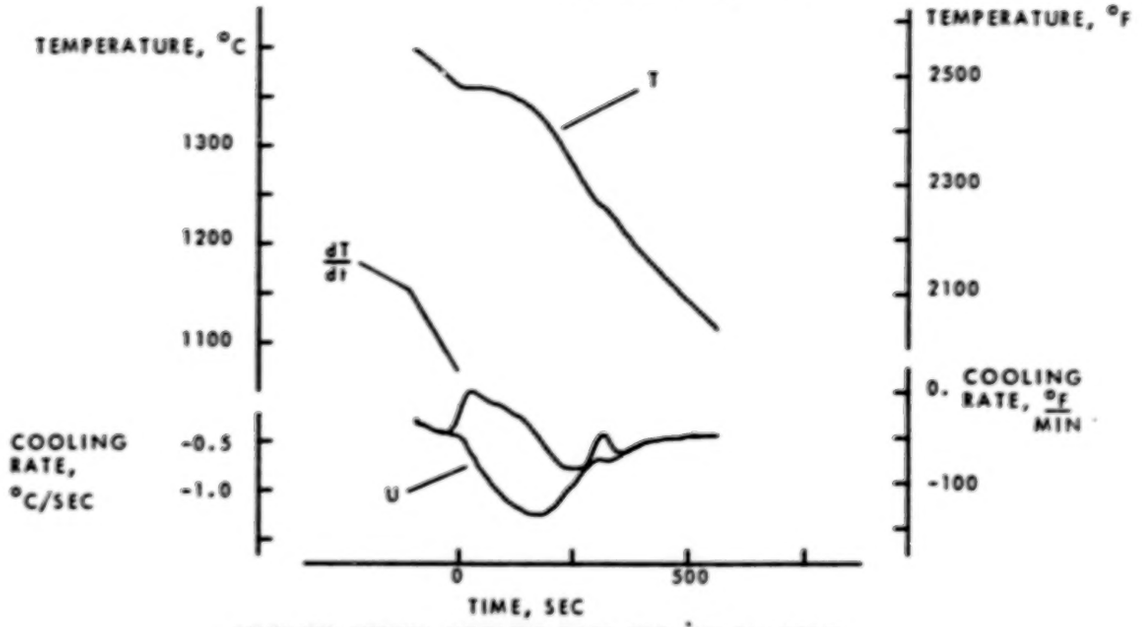

COOLING CURVE. COOLING RATE AND CALCULATED COOLING RATE U. HASTELLOY alloy X

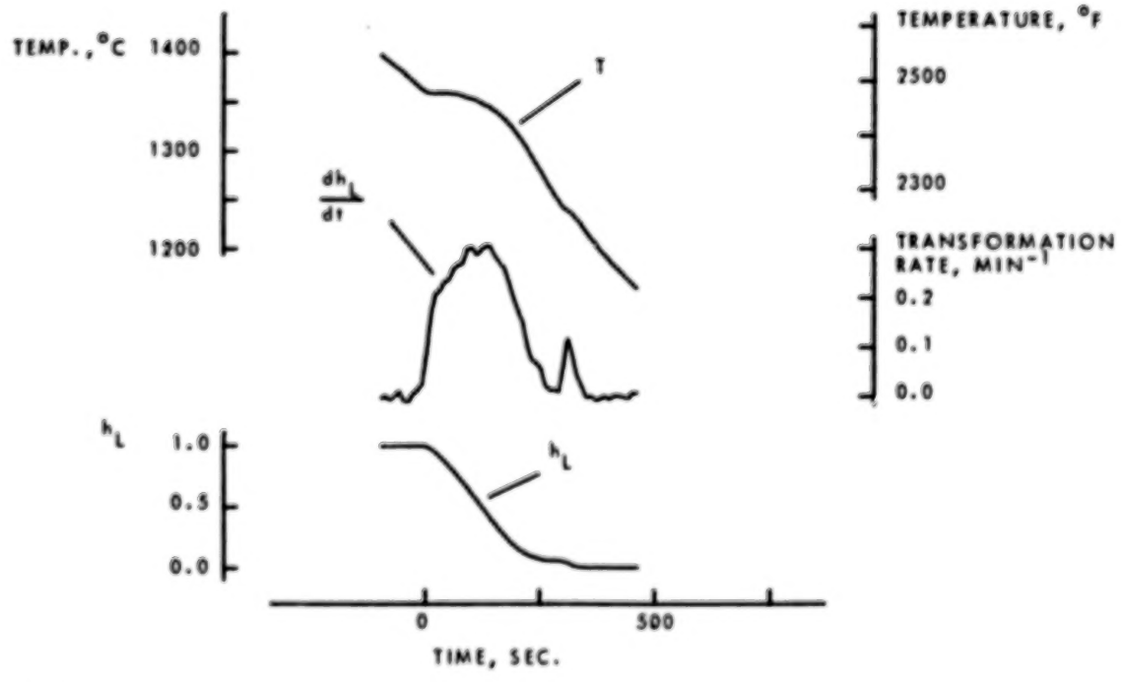

COOLING CURVE, TRANSFORMATION RATE AND h_L (1. - FRACTION TRANSFORMED). HASTELLOY alloy X.

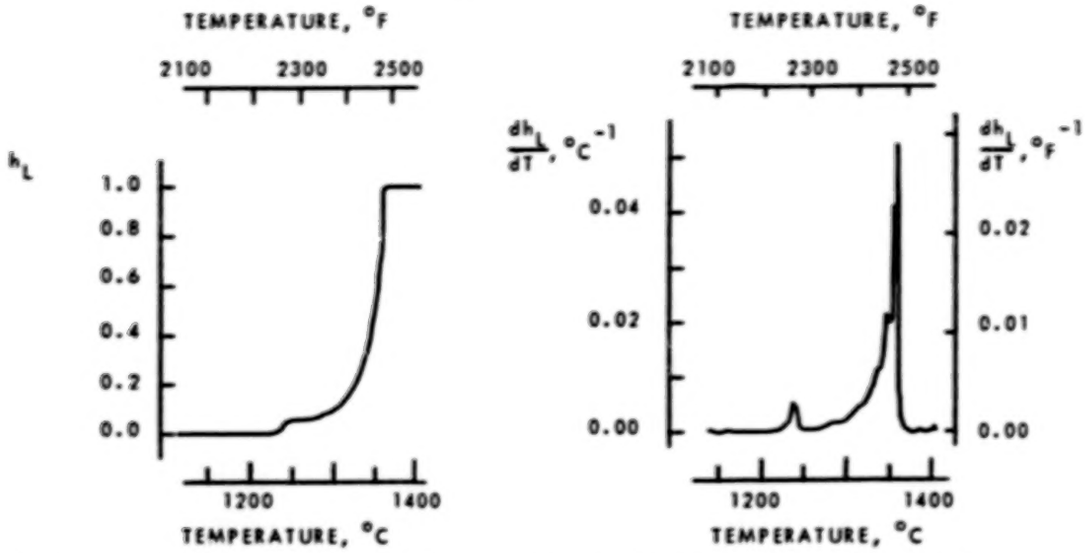

AMOUNT TRANSFORMED AS A FUNCTION OF TEMPERATURE. HASTELLOY alloy X COOLED AT 0.46°C/SEC (50°F/MIN).

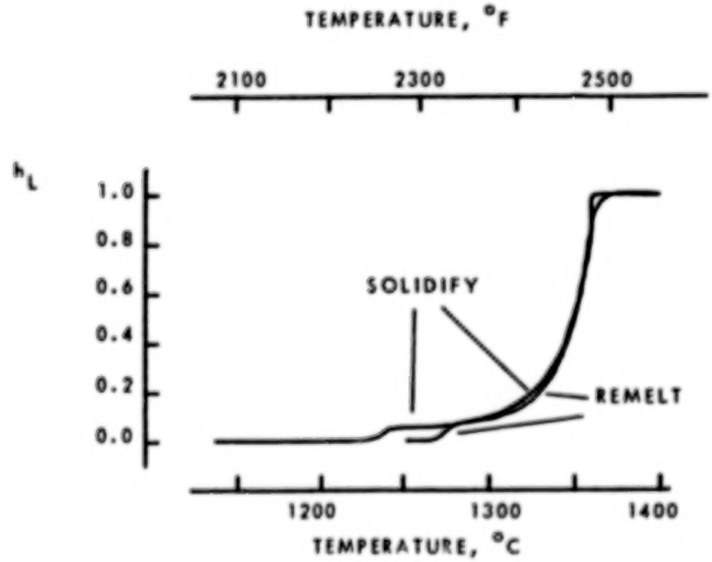

AMOUNT TRANSFORMED AS A FUNCTION OF TEMPERATURE. HASTELLOY alloy X FIRST COOLED AT 0.46°C/SEC (50°F/MIN) THEN REHEATED AT 0.23°C/SEC (25°F/MIN).

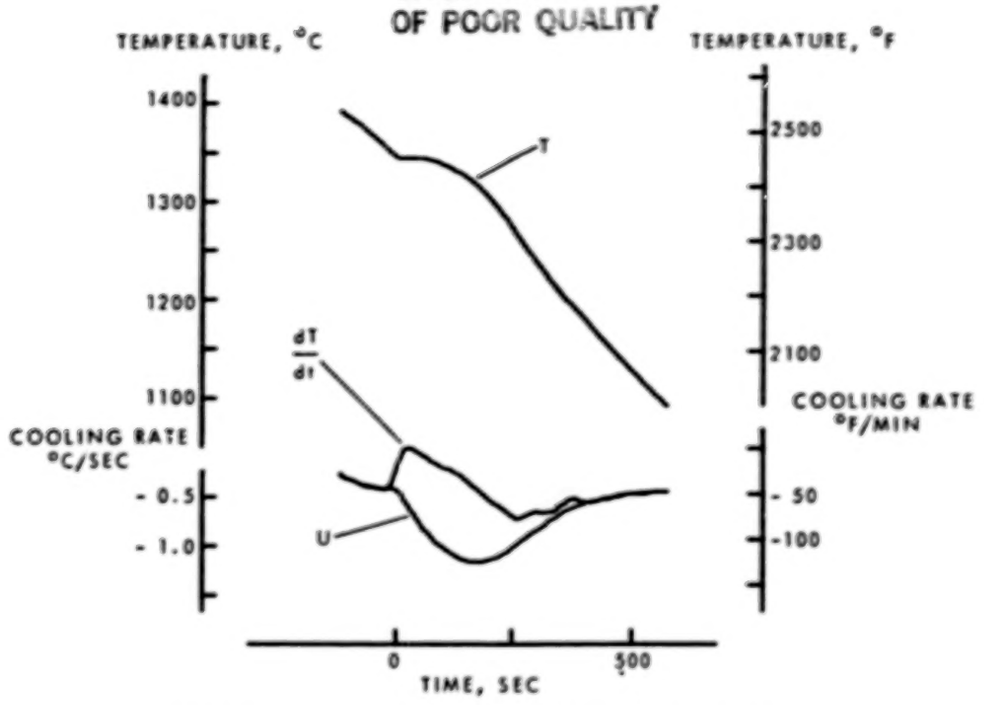

COOLING CURVE, COOLING RATE AND CALCULATED COOLING RATE U. HASTELLOY alloy G

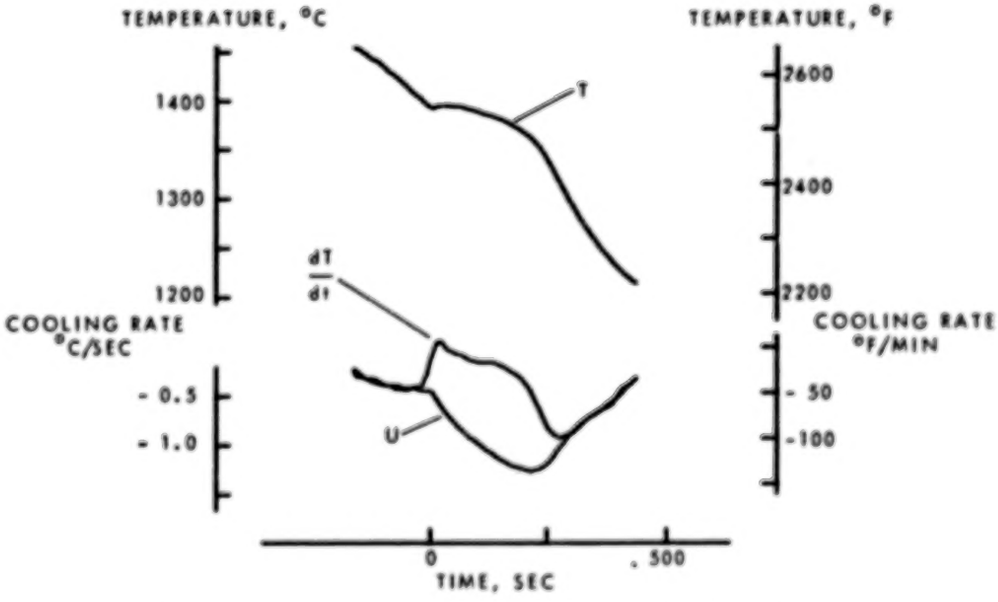

COOLING CURVE, COOLING RATE AND CALCULATED COOLING RATE U. HASTELLOY alloy B-2

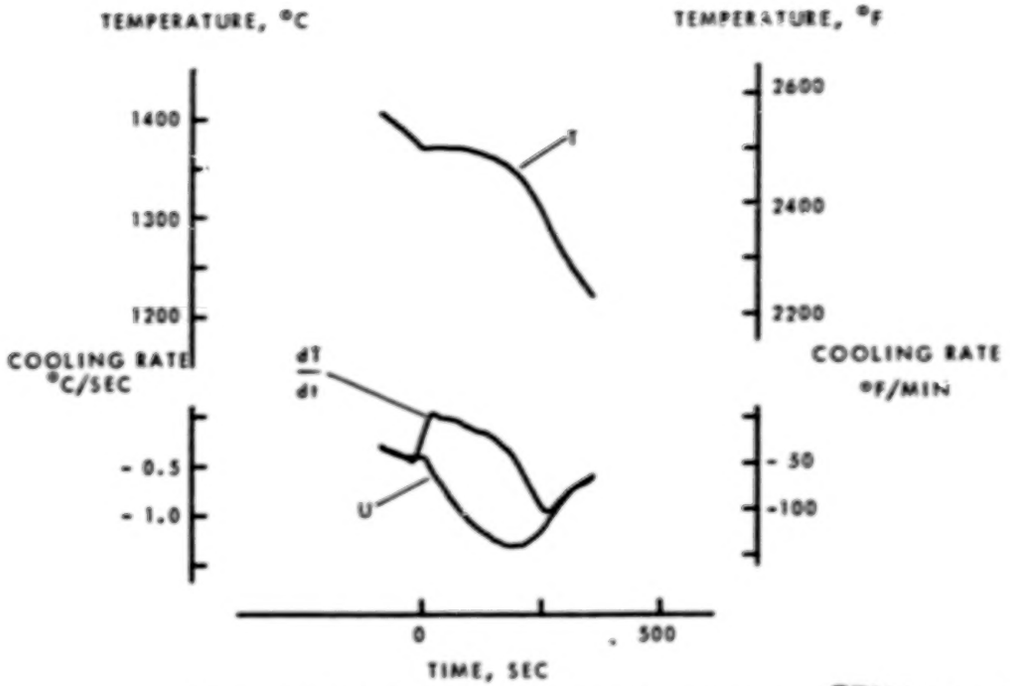

COOLING CURVE, COOLING RATE AND CALCULATED COOLING RATE U. HASTELLOY alloy C-276

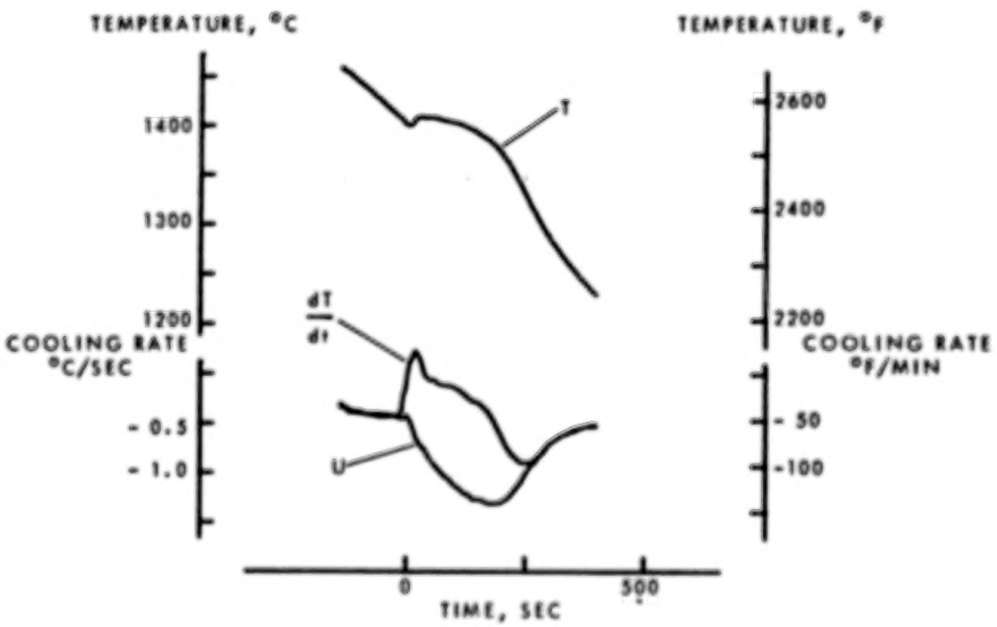

COOLING CURVE, COOLING RATE AND CALCULATED COOLING RATE U. HAYNES alloy NO. 25

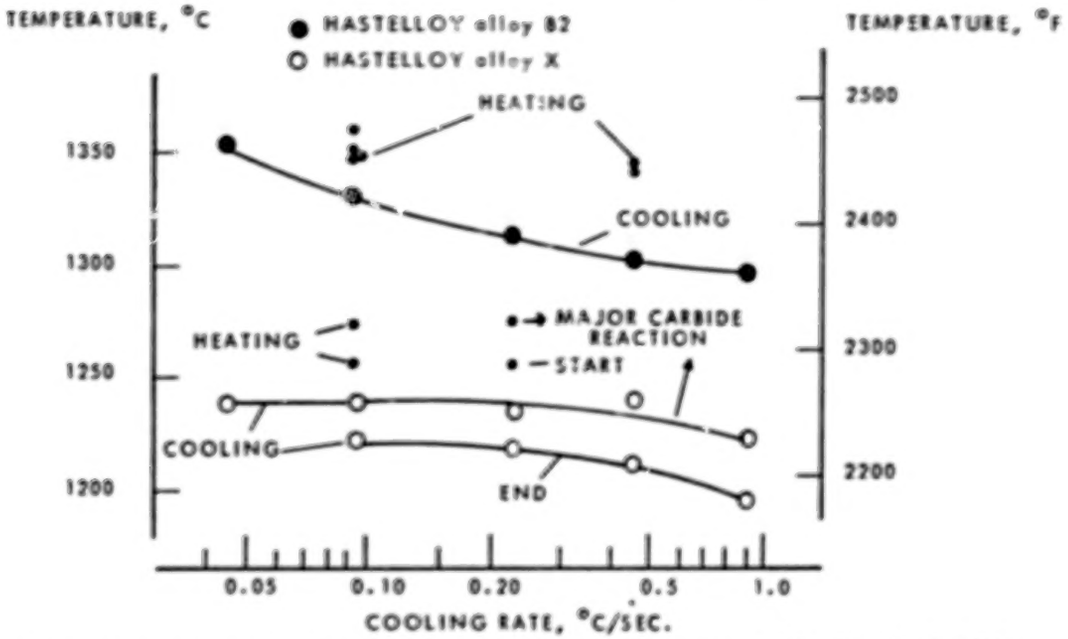

TEMPERATURE AT THE END OF TRANSFORMATION ON COOLING AND THE START OF TRANSFORMATION ON HEATING. (END OF SOLIDIFICATION AND INCIPIENT MELTING).

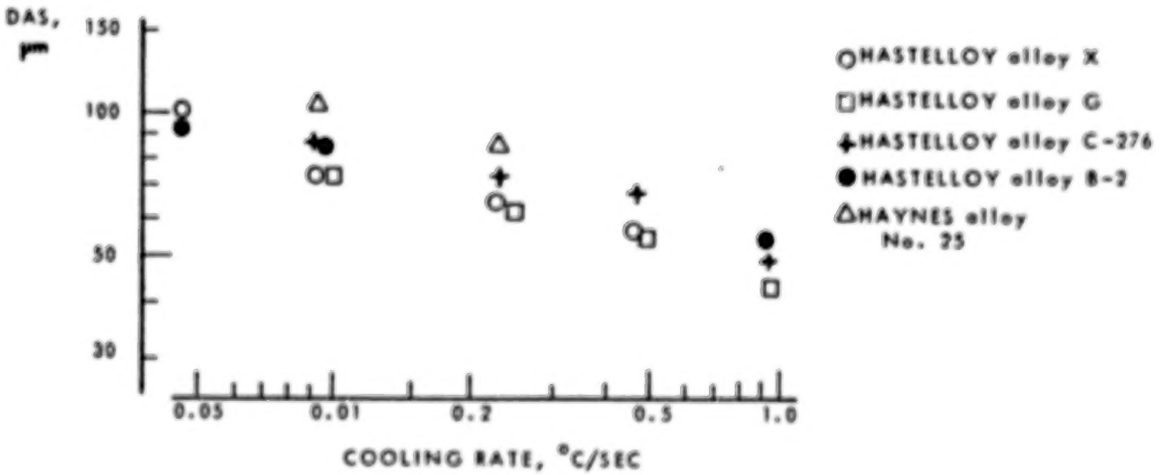

SECONDARY DENDRITE ARM SPACING AS A FUNCTION OF COOLING RATE.

MICROSEGREGATION DURING DIRECTIONAL SOLIDIFICATION*

S. R. Coriell and G. B. McFadden
National Bureau of Standards
Gaithersburg, Maryland

During the directional solidification of alloys, solute inhomogeneities transverse to the growth direction may arise due to morphological instabilities (leading to cellular or dendritic growth) and/or due to convection in the melt. In the absence of convection, the conditions for the onset of morphological instability are given by the linear stability analysis of Mullins and Sekerka. For ordinary solidification rates, the predictions of linear stability analysis are similar to the constitutional supercooling criterion. However, at very rapid solidification rates, linear stability analysis predicts a vast increase in stabilization in comparison to constitutional supercooling.

At high growth velocities, two solidification mechanisms can produce microsegregation-free crystalline alloys: planar growth under conditions of morphological stability and/or partitionless solidification. Even with equilibrium partitioning of solute, capillarity can stabilize a planar solid-liquid interface at high growth rates as long as the net heat flow is toward the solid. This type of stability, known as absolute stability, has been confirmed experimentally for Ag-Cu alloys (Boettinger, Shechtman, Schaefer, and Biancaniello). Another possibility for producing microsegregation-free alloys is partitionless solidification (distribution coefficient approaching unity) which can occur at high velocities and arises from the kinetics of interface motion. The effect on morphological stability of the velocity dependence of the distribution coefficients has recently been treated (Coriell and Sekerka). Under certain conditions oscillatory instabilities can occur and lead to a three-dimensional segregation pattern in which periodic solute variations in the two transverse directions are modulated by a periodic variation in the direction of growth.

Under slightly unstable conditions, cellular nonplanar interfaces develop. We calculate steady state two-dimensional cellular shapes by finite difference techniques. We assume local equilibrium at the solid-liquid interface, that the thermal properties of the melt and crystal are identical and that the cells are periodic and two-dimensional. For a specified interface shape, we solve the partial differential equations for temperature in the crystal and melt and for solute concentration in the melt. The solutions are constructed such that all boundary conditions except the Gibbs-Thomson equation are satisfied. The Gibbs-Thomson equation is then used in an iterative fashion to find the correct interface shape. An artificial time dependence is introduced which accelerates the convergence of the iterative scheme. Numerical results have been obtained for an aluminum alloy containing silver for solidification velocities of 0.01 and 1.0 cm/s, which correspond to the constitutional supercooling and absolute stability regimes, respectively. At a growth velocity of 1.0 cm/s, it is ob-

*Supported in part by the Microgravity Science and Applications Division, National Aeronautics and Space Administration and by the Defense Advanced Research Projects Agency.

served that the minimum in interface concentration does not occur at the maximum in interface shape (inverse coring).

During solidification of a binary alloy at constant velocity vertically upwards, thermosolutal convection can occur if the solute rejected at the crystal-melt interface decreases the density of the melt. Such convection can also lead to segregation even if the interface remains approximately planar. We assume that the crystal-melt interface remains planar and that the flow field is periodic in the horizontal direction. The time-dependent nonlinear differential equations for fluid flow, concentration, and temperature are solved numerically in two spatial dimensions for small Prandtl numbers and moderately large Schmidt numbers (McFadden, Rehm, Coriell, Chuck, and Morrish). For slow solidification velocities, the thermal field has an important stabilizing influence: Near the onset of instability the flow is confined to the vicinity of the crystal-melt interface. Further, for slow velocities, as the concentration increases, the horizontal wavelength of the flow decreases rapidly, a phenomenon also indicated by linear stability analysis. The lateral inhomogeneity in solute concentration due to convection is obtained from the calculations. For a narrow range of solutal Rayleigh numbers and wavelengths, the flow is periodic in time.

REFERENCES

Mechanisms of Microsegregation-Free Solidificatio, W. J. Boettinger, S. R. Coriell, and R. F. Sekerka, Mat. Sci. Eng. 65, 27 (1984).

Oscillatory Morphological Instabilities Due To Non-Equilibrium Segregation, S. R. Coriell, and R. F. Sekerka, J. Crystal Growth 61, 499 (1983).

Nonplanar Interface Morphologies During Unidirectional Solidification of a Binary Alloy, G. B. McFadden and S. R. Coriell, Physica D, in press.

Convective and Interfacial Instabilities During Unidirectional Solidification of a Binary Alloy, S. R. Coriell, M. R. Cordes, W. J. Boettinger, and R. F. Sekerka, J. Crystal Growth 49, 13 (1980).

Thermosolutal Convection During Directional Solidification, G. B. McFadden, R. G. Rehm, S. R. Coriell, W. Chuck, and K. A. Morrish, Met. Trans., in press.

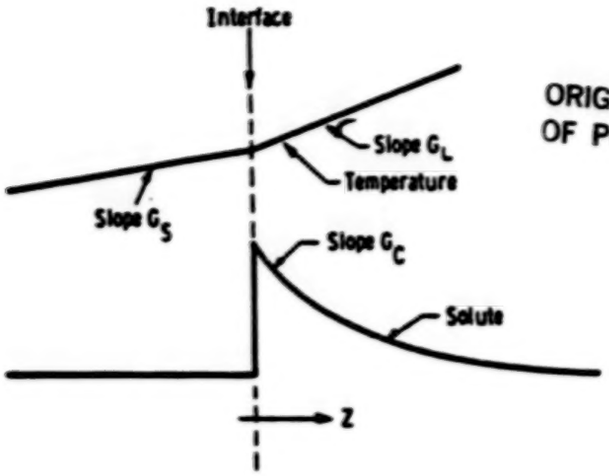

Temperature and solute profiles ($k < 1$) as a function of distance z from the solid-liquid interface for constrained growth of a dilute binary alloy at velocity V.

$$\mathbf{v}\cdot\mathbf{n}(\rho_s - \rho_L) = (\mathbf{u}\cdot\mathbf{n})\rho_L$$

$$(\mathbf{v}\cdot\mathbf{n})L_v = (-k_L\nabla T + k_s\nabla T_s)\cdot\mathbf{n}$$

$$(\mathbf{v}\cdot\mathbf{n})(c_s - c) = (\rho_L/\rho_s)D\nabla c\cdot\mathbf{n}$$

$$T_s = T = T_m + mc - T_m\Gamma\mathcal{K}$$

$$c_s = kc$$

$$f = f(z)\exp(\sigma t + i\omega_x x + i\omega_y y)$$

$$\sigma = \sigma_r + i\sigma_i$$

$\sigma_r > 0$ Unstable

$\sigma_r < 0$ Stable

$\sigma_i \neq 0$ Oscillatory

RESULTS FOR Q S S $(\dot{\delta}/\delta = 0)$

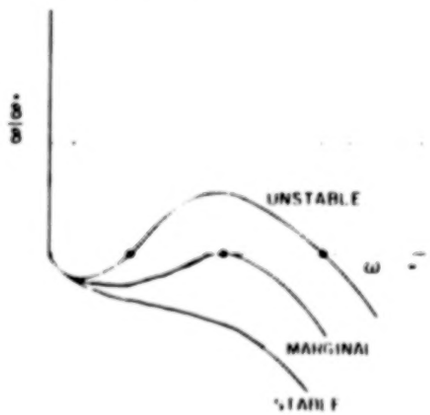

STABILITY CRITERION

$$G^*/(mG_C) > \mathcal{J}(A,k)$$

$$G^* = (k_S G_S + k_L G_L)/(k_S + k_L)$$

$$G_C = VC_\infty(k-1)/(Dk)$$

$$A = [k^2/(1-k)](\Gamma V/D)[T_M/(-mC_\infty)]$$

LINEAR STABILITY FOR Al – Cu

TEMPERATURE GRADIENT 200K/cm

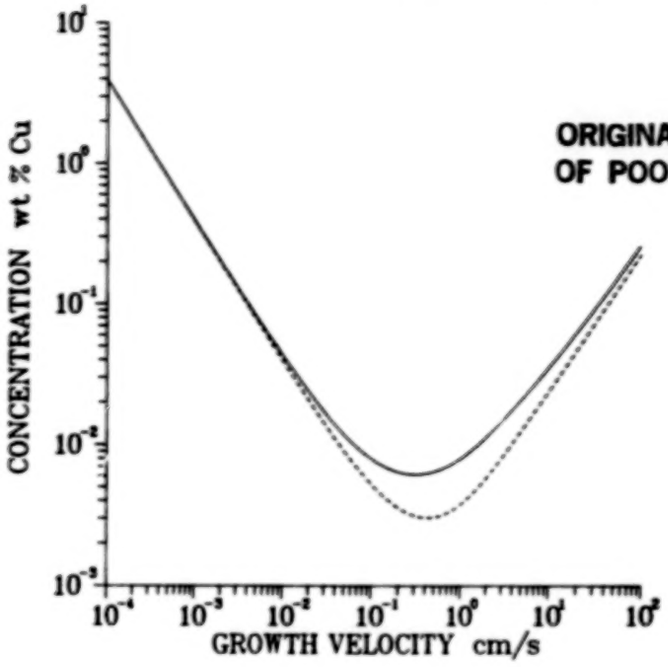

LINEAR STABILITY FOR Al – Cu

TEMPERATURE GRADIENT 200K/cm

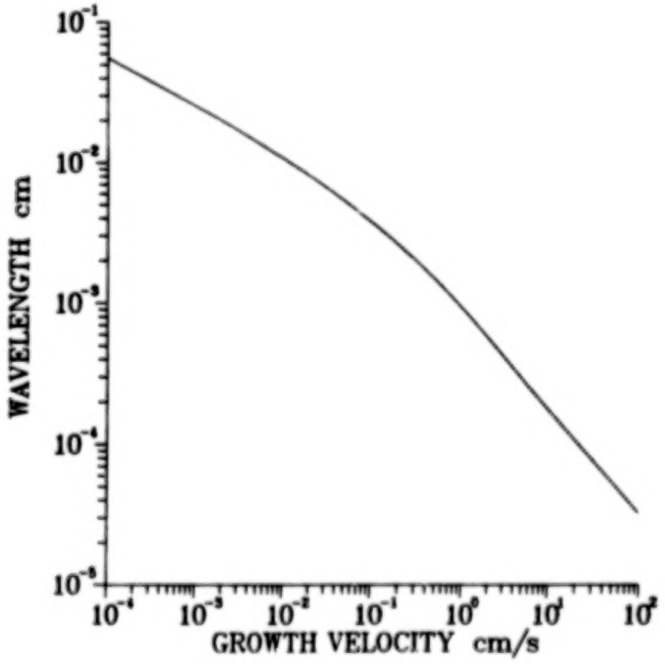

$A = 10^{-6}$ $k = 0.3$ $I = 10^{3}$

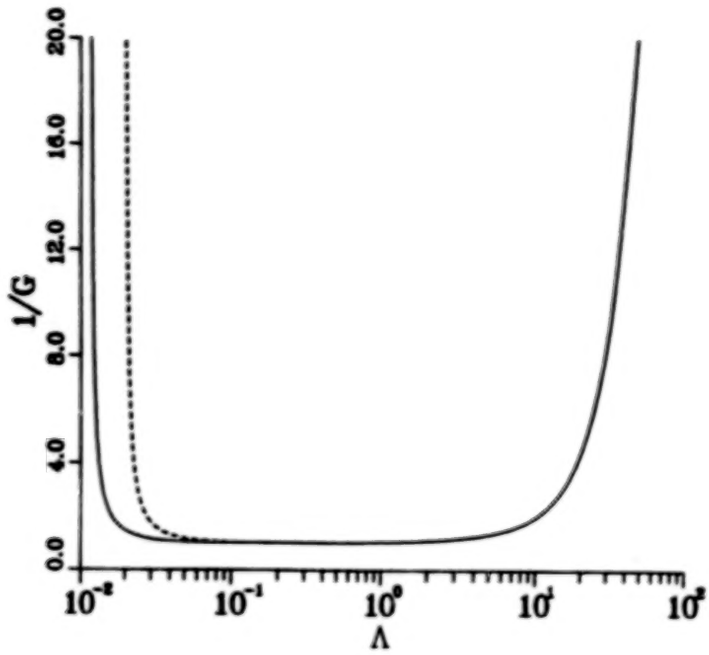

DEPARTURE FROM LOCAL EQUILIBRIUM

$$T_e = T_M - T_M \Gamma K + mC_I$$

$$V = \beta(T_e - T_I,\ C_I, T_I)$$

$$C_{SI} = C_I k(V,\ C_I, T_I)$$

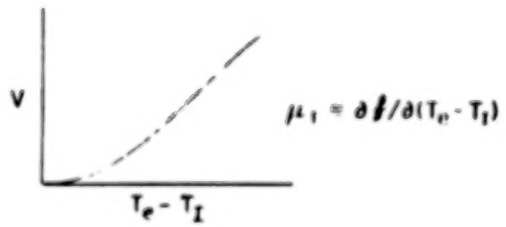

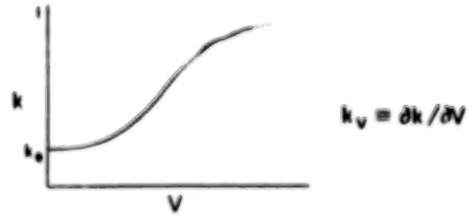

NEW STABILITY CRITERION

EXPLICIT DEPENDENCE ON

$$H \equiv V(\partial k/\partial V)/(1-k)$$

$$M \equiv (k_S + k_L)V/(LD\mu_T)$$

LET $\Sigma = \sigma D/V^2$

$\eta = \omega D/V$

Σ OBEYS A CUBIC EQUATION
SUBJECT TO

$$\mathcal{R}e\,(\Sigma^2 + \eta^2 + \tfrac{1}{4})^{1/2} > 0$$

COMPLEX $\sigma \Longrightarrow$ OSCILLATORY INSTABILITIES

$$\sigma = \sigma_R + i\sigma_I$$

$$\exp[\sigma t + i\omega_x x + \omega_y y] \rightarrow \exp(\sigma_R t)\,\mathrm{Cos}(\omega_x x)\,\mathrm{Cos}(\omega_y y)\,\mathrm{Cos}(\sigma_I t)$$

1. OCCUR AT SOLUTE CONCENTRATION FAR BELOW THOSE NEEDED FOR NON-OSCILLATORY
2. OCCUR ($H < 1$) **BETWEEN** CLASSICAL STABILITY CRITERION AND MODIFIED C.S
3. SUPPRESSED BY LARGE M (SMALL μ-)
4. 3-DIMENSIONAL SEGREGATION

$$\Delta C \propto \mathrm{Cos}(\omega_x x)\,\mathrm{Cos}(\omega_y y)\,\mathrm{Cos}(\sigma_I z/V)$$

Banded Microstructure at Intermediate Interface Velocity

Boettinger, et al.

LINEAR STABILITY FOR Al–Ag

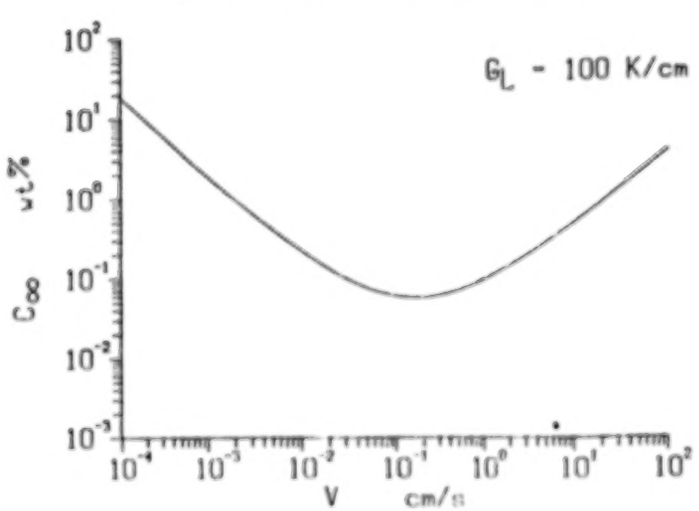

INTERFACE QUANTITIES

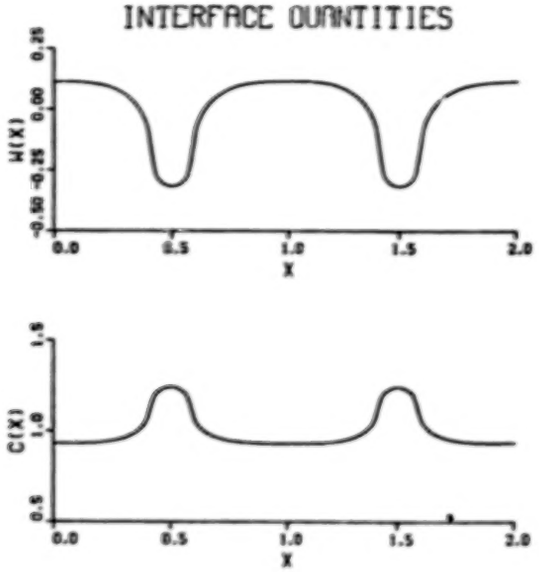

C_{∞}=.235, V=.01 CM/S, λ=.006 CM

CONVERGENCE OF INTERFACE

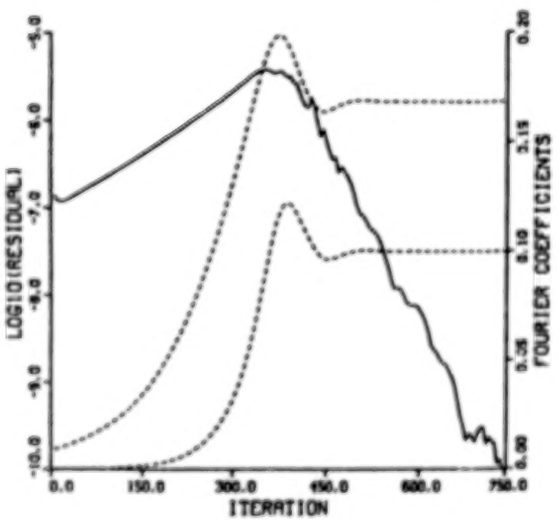

C =.235, V = .01 CM/S, L = .006 CM

INTERFACE SHAPE FOURIER COEFFICIENTS

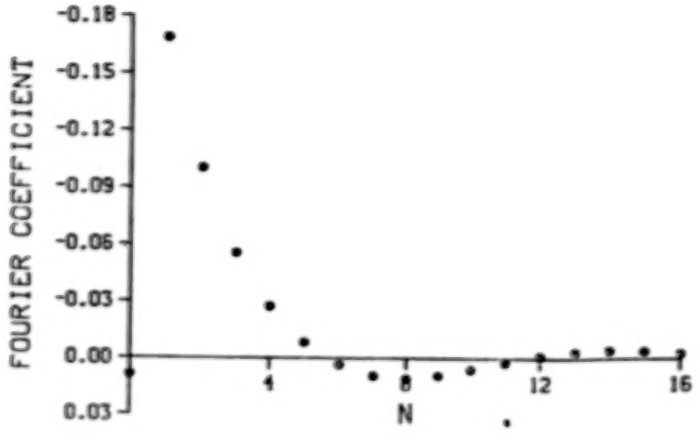

C_{oo}=-.235, V=.01 CM/S, λ=.006 CM

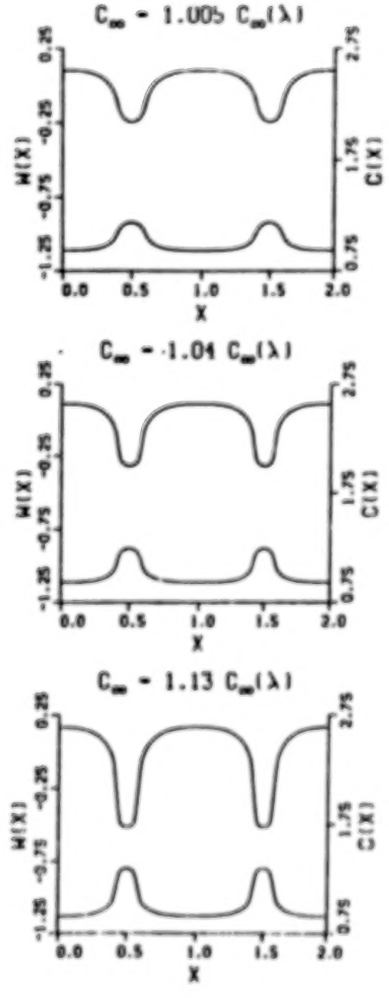

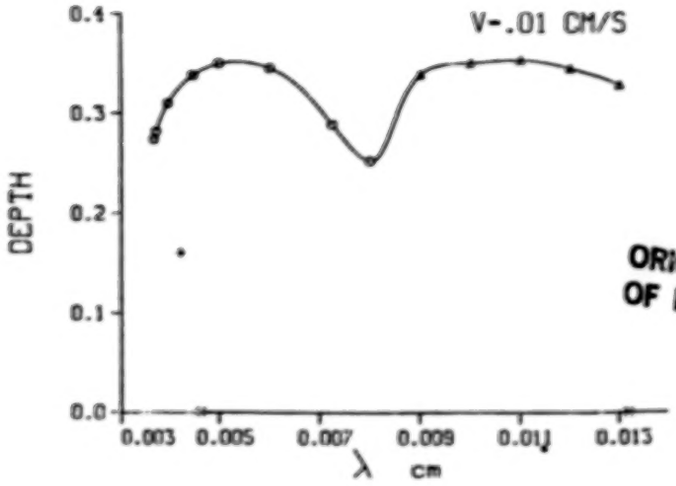

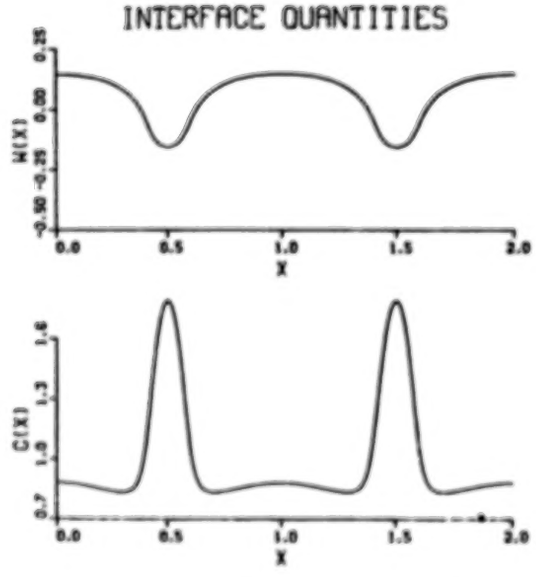

C_{∞}=.115, V=1.0 CM/S, λ=.0005 CM

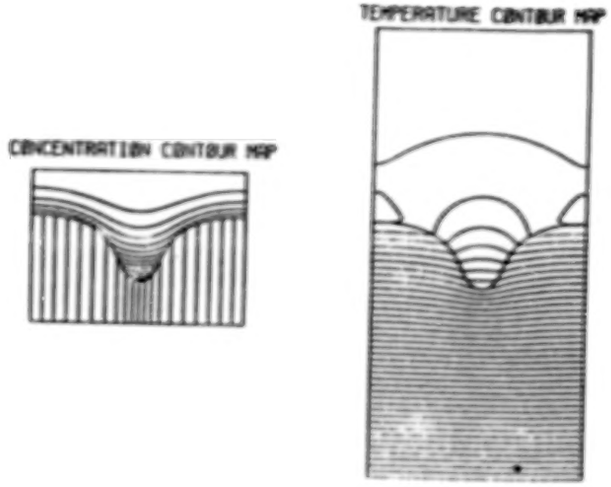

C =.1150. V = 1.000 CM/S. L =.0005 CM

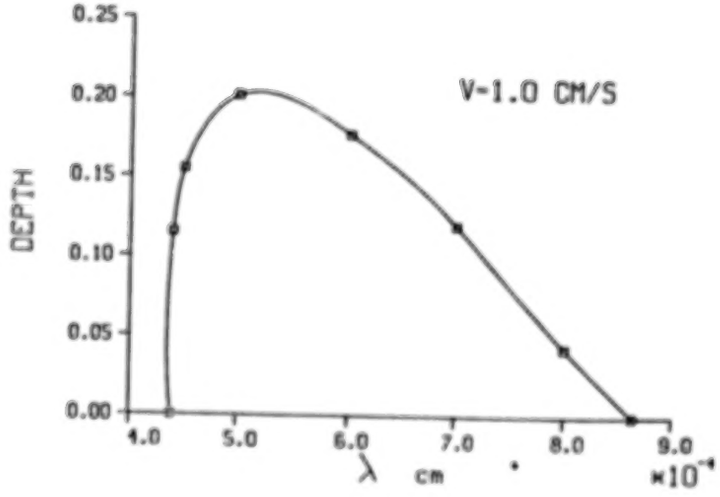

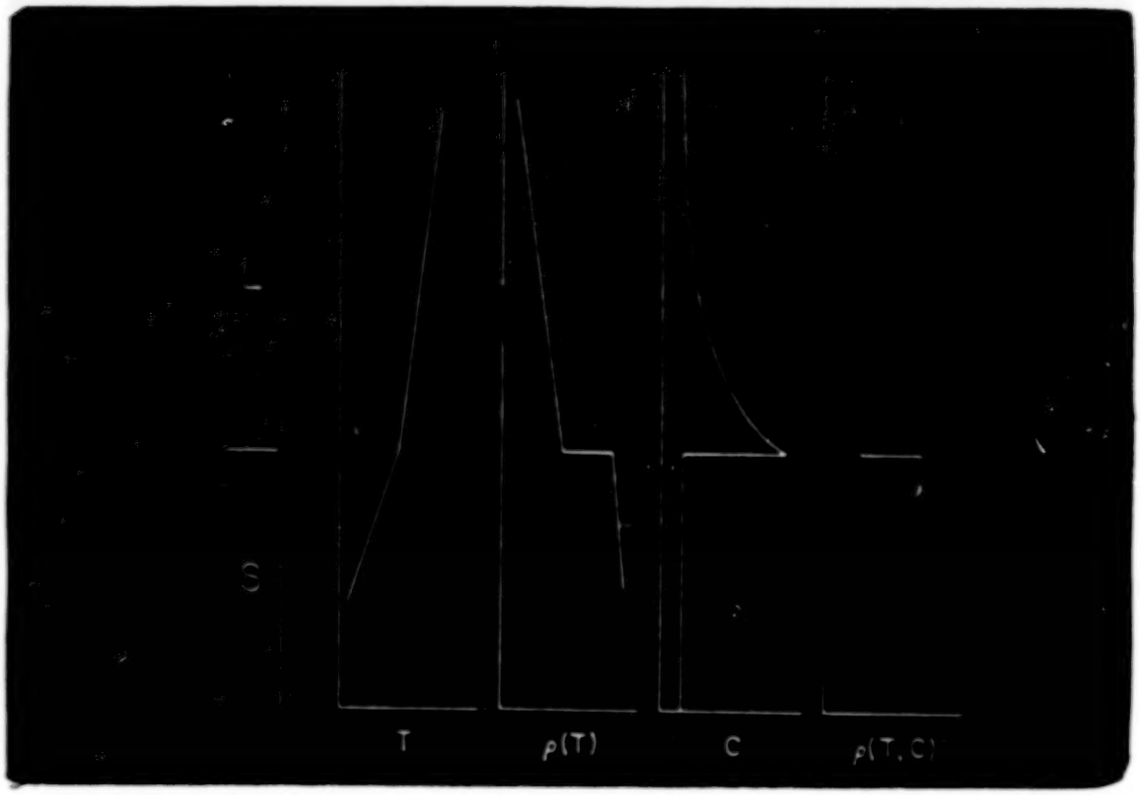

SOLUTE LESS DENSE THAN SOLVENT

$$\rho = \rho_0 \{1 - \alpha T - \alpha_c C\}$$

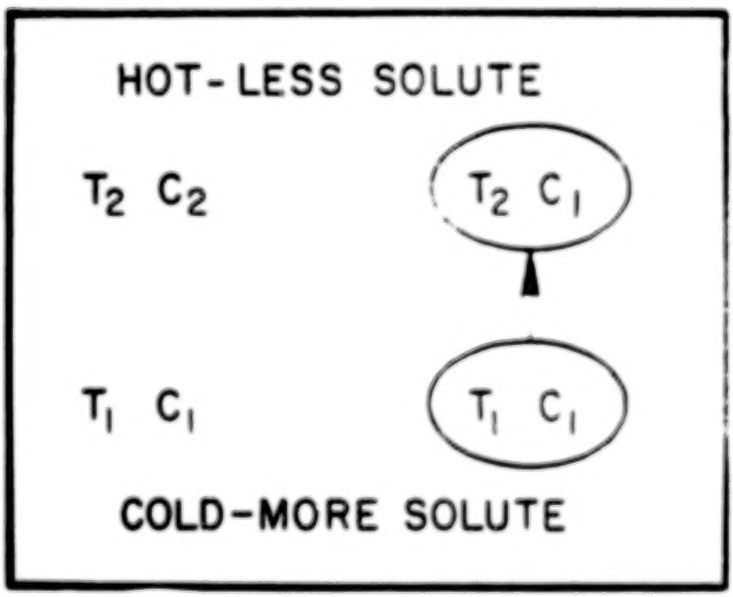

$\alpha > 0$

$\alpha_c > 0$

$(\partial \rho / \partial z) < 0$

$D < K$

LINEAR STABILITY FOR LEAD–TIN
TEMPERATURE GRADIENT 200 K/cm

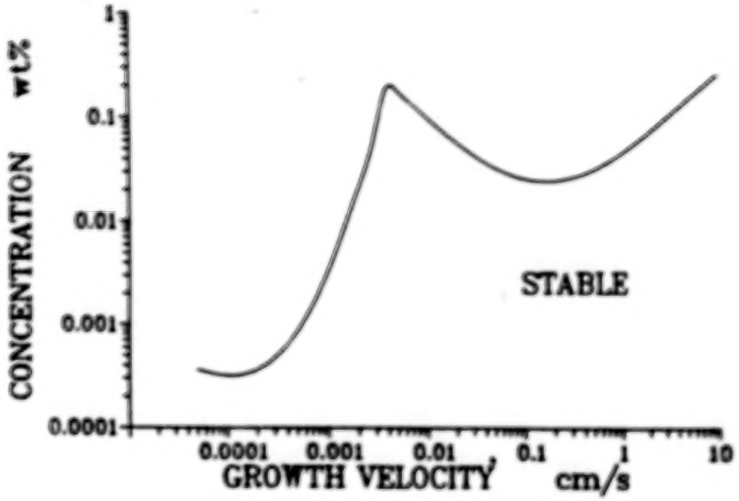

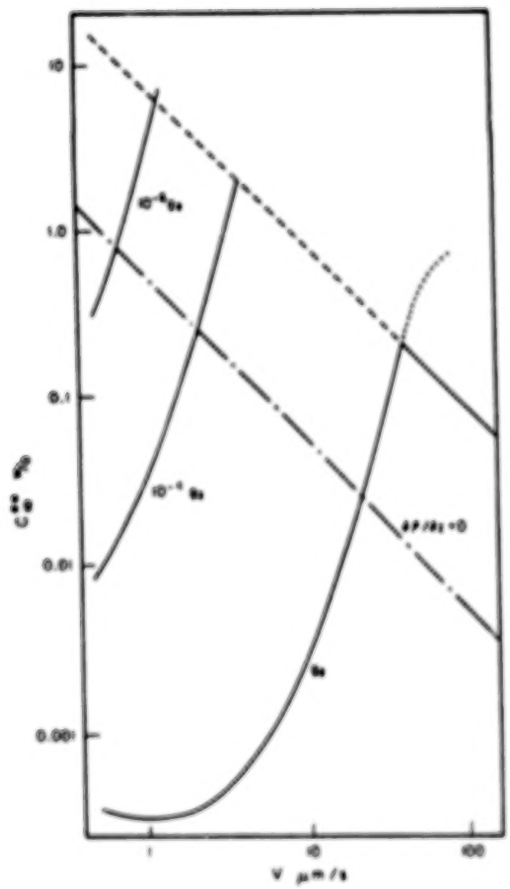

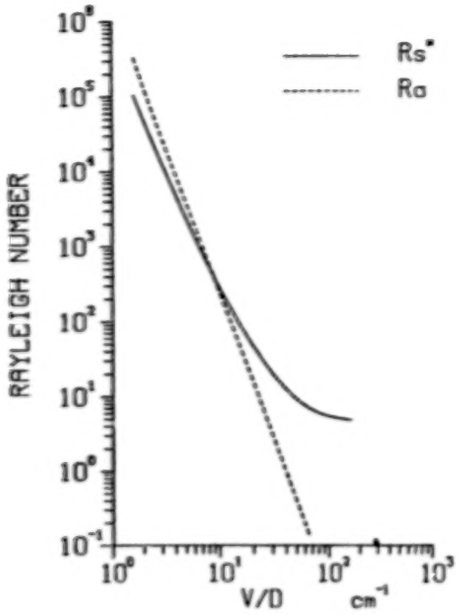

LINEAR THEORY FOR D/V = .015 CM

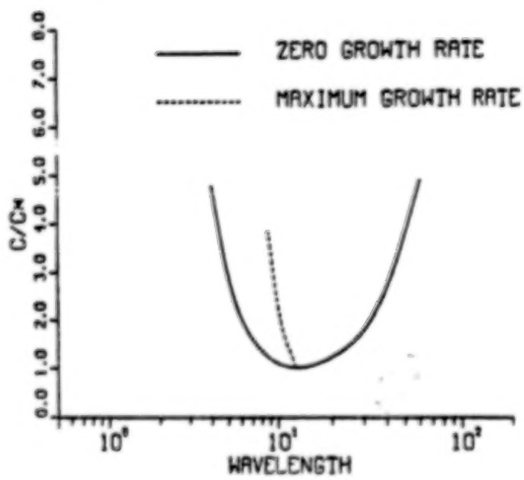

LINEAR THEORY FOR D/V = .15 CM

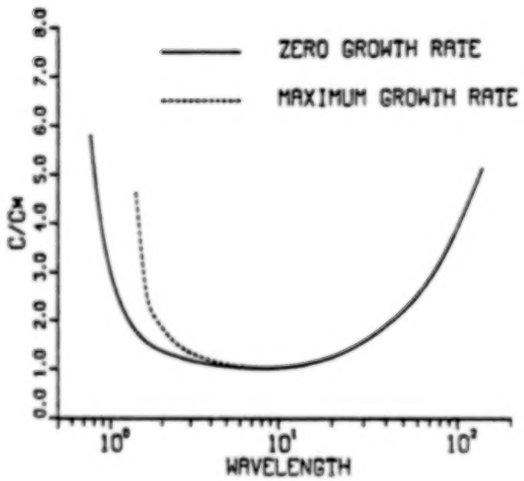

NONLINEAR CALCULATIONS FOR D/V = .15 cm
Sc = 10. Pr = .01

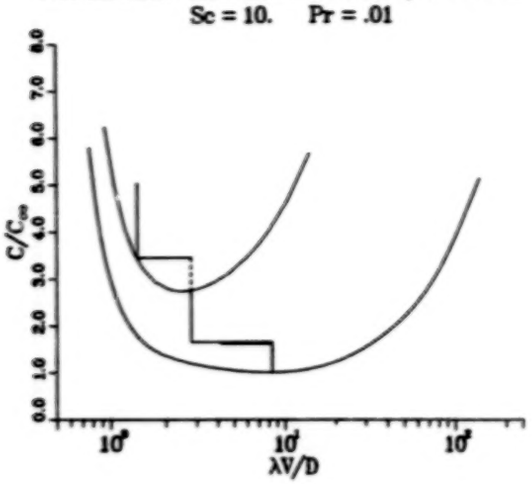

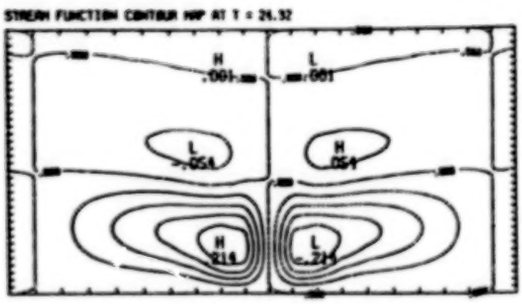

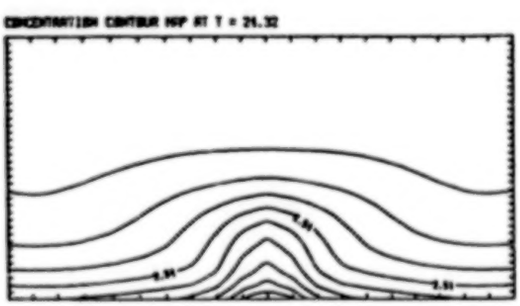

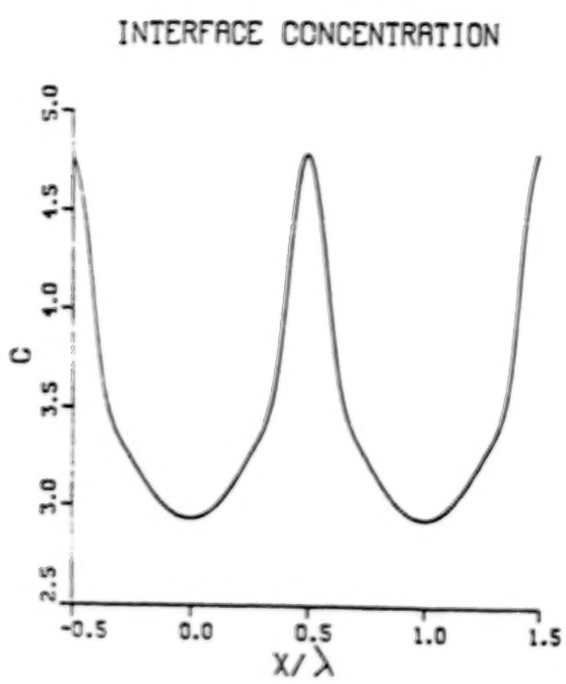

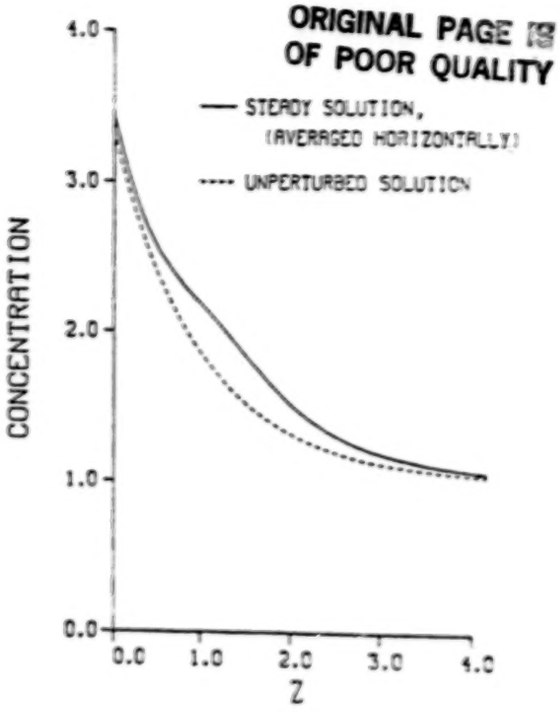

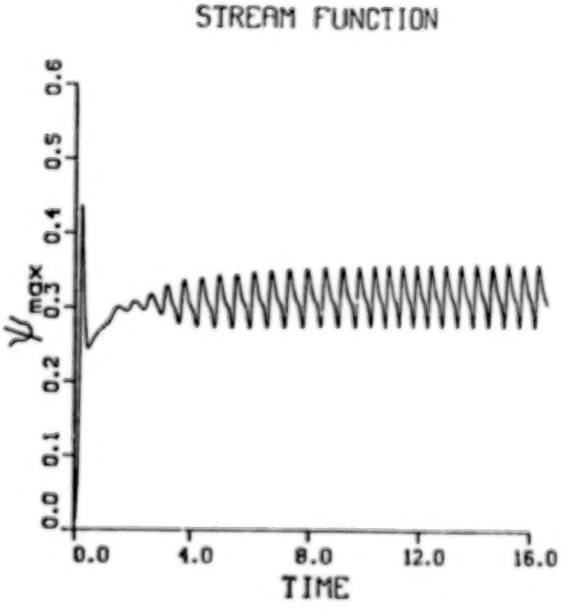

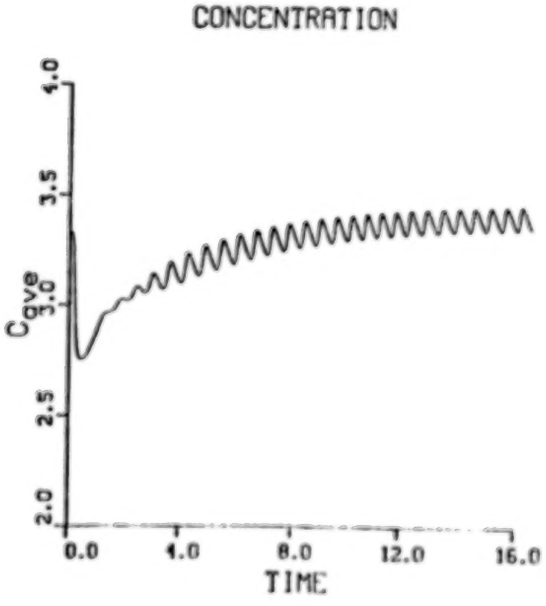

STREAM FUNCTION CONTOUR MAP AT T = 16.65

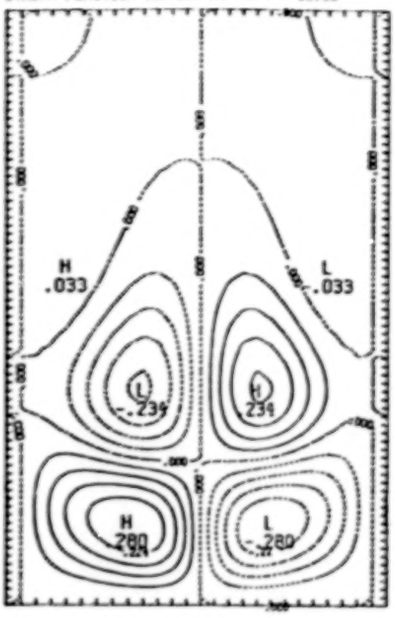

STREAM FUNCTION CONTOUR MAP AT T = 16.75

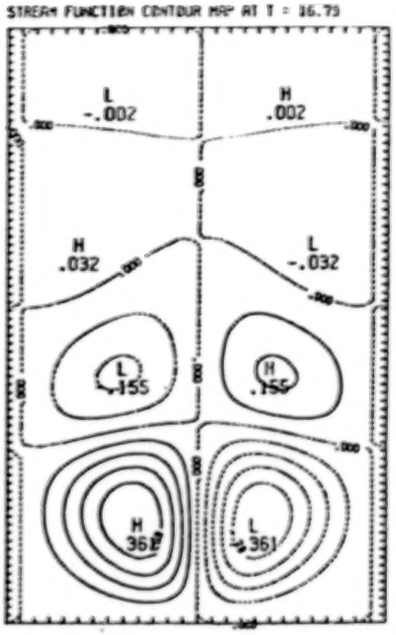

STREAM FUNCTION CONTOUR MAP AT T = 16.93

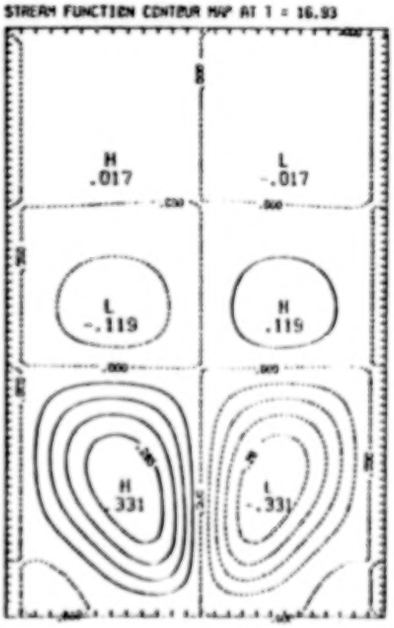

STREAM FUNCTION CONTOUR MAP AT T = 17.00

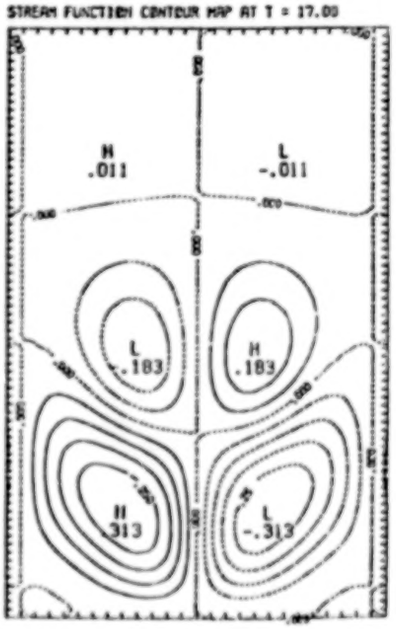

STREAM FUNCTION CONTOUR MAP AT T = 21.96

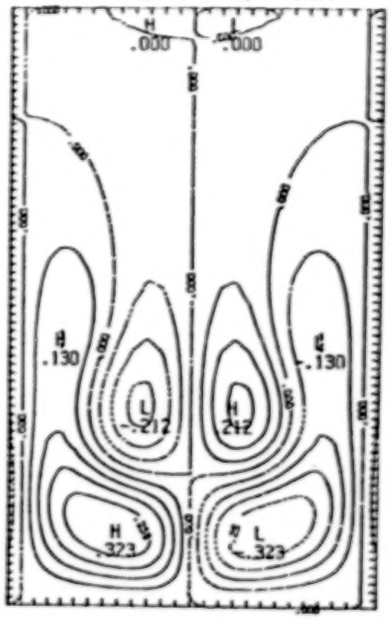

CONCENTRATION CONTOUR MAP AT T = 21.96

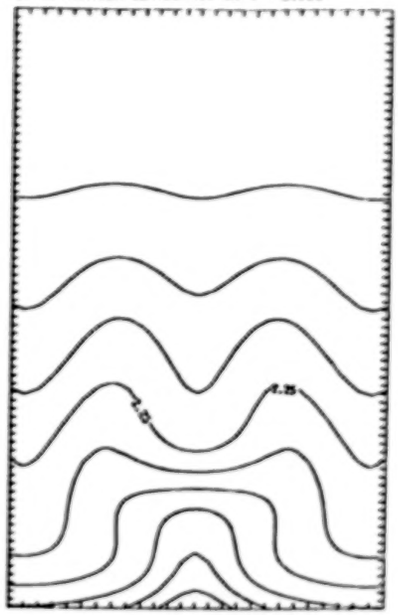

STREAM FUNCTION CONTOUR MAP AT T = 10.21

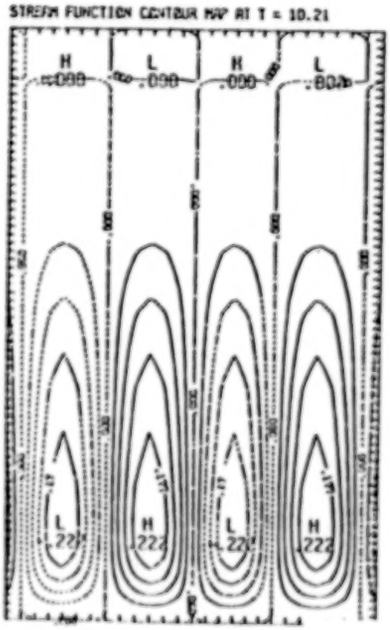

CONCENTRATION CONTOUR MAP AT T = 10.21

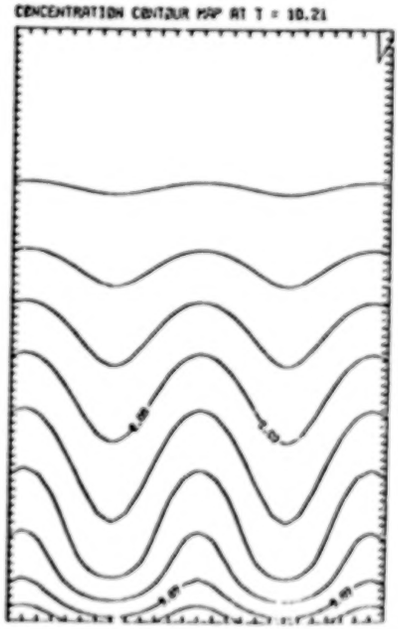

ORIGINAL PAGE IS
OF POOR QUALITY

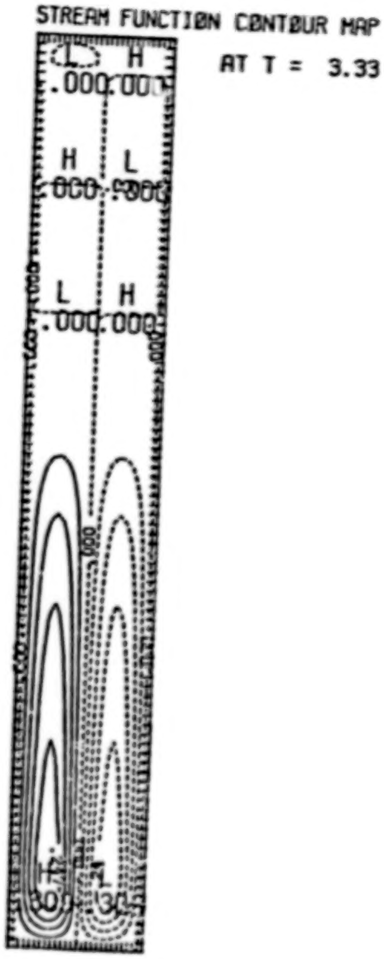

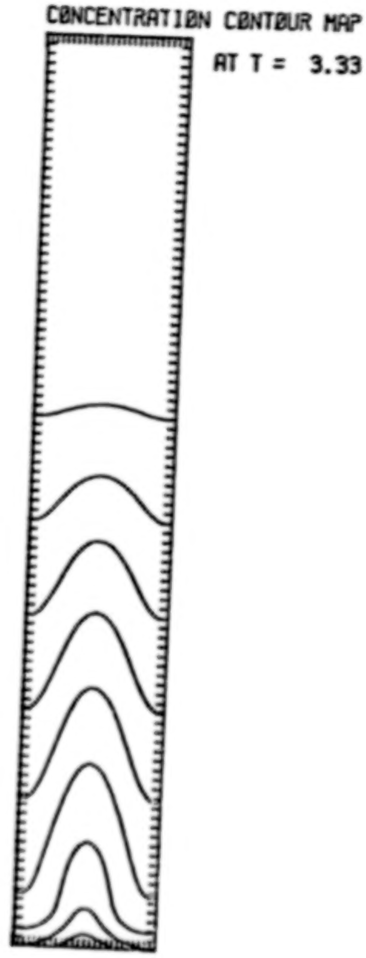

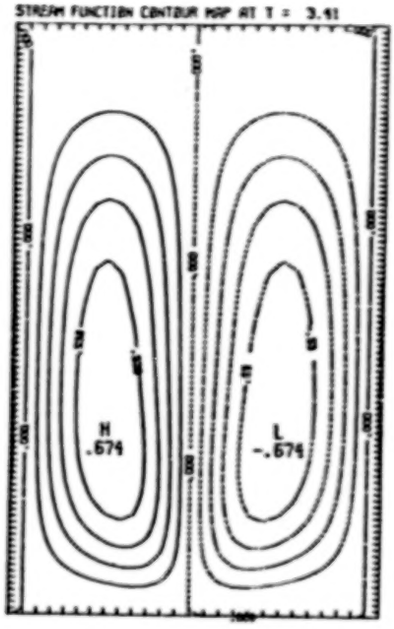

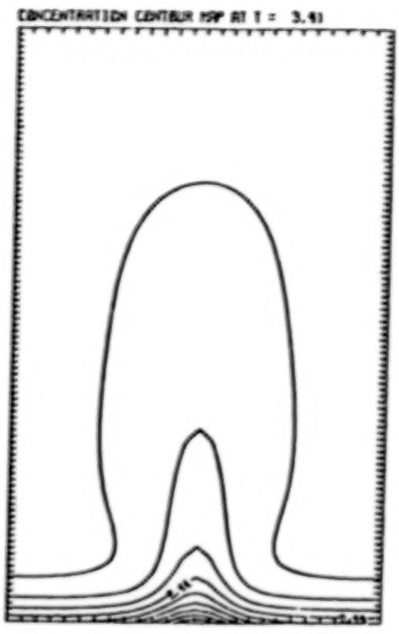

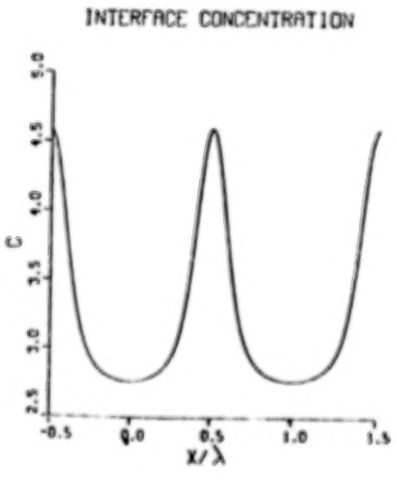

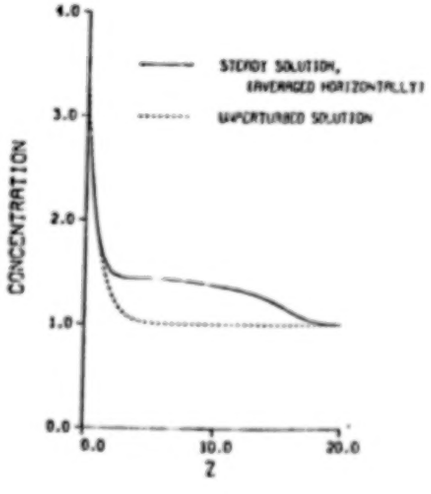

RS= .33438+004 RA= .12679+004 SC= 1.0000 Pr= .0100 LY/D= 2.4644

STREAM FUNCTION CONTOUR MAP AT T = 5.6549

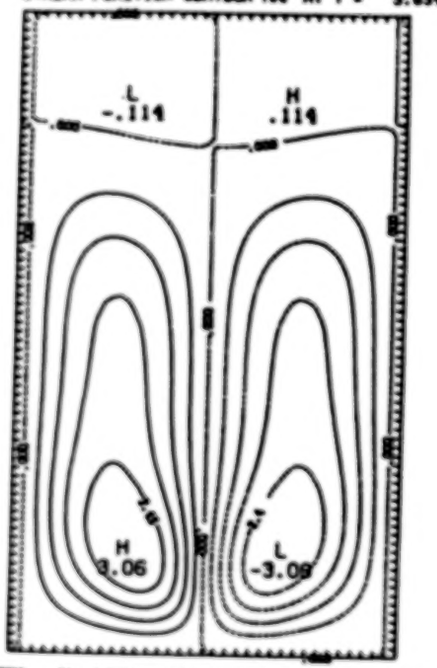

RS= .33438+004 RA= .12679+004 SC= 1.0000 Pr= .0100 LY/D= 2.4644

STREAM FUNCTION CONTOUR MAP AT T = 9.4741

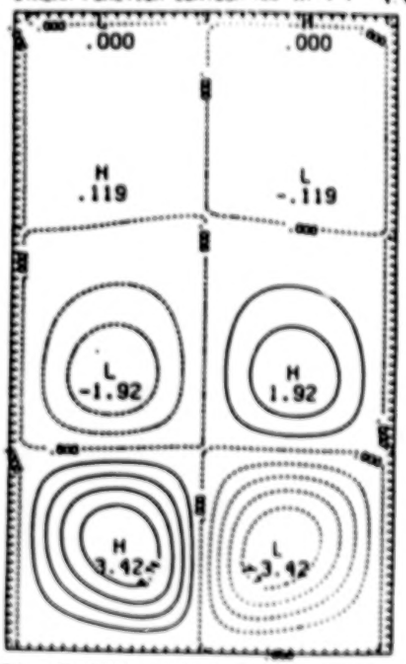

CHARACTERIZATION OF MACROSEGREGATION IN ESR IN-718

J. A. Domingue, K. O. Yu and H. D. Flanders
Special Metals Corporation

INTRODUCTION

Precipitation hardened superalloys used at elevated temperatures in highly stressed gas turbine rotor parts present a scientifically as well as commercially significant problem in macrosegregation during solidification processing. By nature of their design applications, these materials must be uniform and homogeneous to a high degree in order to insure performance; yet, by the very nature of their highly alloyed constitutions, these same materials are among the most segregation prone of industrial metallic systems. Consumable melting of the primary alloy ingot is generally a prerequisite to thermomechanical processing of large turbine parts such as disks. Some cost effective engines employ high strength and temperature capability, but highly segregable, difficult to forge nickel-base alloys manufactured by advanced processes such as powder metallurgy. Due to its excellent forgeability, P/M has not yet been required for nickel-iron base IN-718, which is perennially the highest commercial volume superalloy, by favor of an ample supply of low cost revert and progress in recycling technology. Also, current stabilization of fuel prices has slowed the demand for temperature capability-efficiency greater than that offered by IN-718. In this case, consumable melting is still seen as the most viable route, with vacuum arc remelting (VAR) being the sole qualified process currently in production in North America.

Nominal Composition of IN-718 by weight percent is

B	0.003	Cr	18.1	Mo	3.0	Al	0.5	Ni	Balance
C	0.03	Fe	17.5	Cb	5.3	Ti	1.0	(Si	$\leq$ 0.20)

Ingots are typically 432 mm (17") to 508 mm (20") diameter cylinders weighing up to 2700 kg (6,000#) and 4550 kg (10,000#) respectively. Even larger diameter forging stock is desirable. However, beyond 400 mm, IN-718 ingots are increasingly prone to gross positive macrosegregation of columbium ("freckles") and exaggerated microsegregation (remnant dendritism in forged billet and articles), unless the solidification is adequately controlled. Reasonable control in the VAR process, by optimizing melt rate and maximizing heat transfer across the ingot-mold gap, has been in effect for about two decades,[1] although some forged billets do exhibit remnant dendritism and negative columbium segregation. (Negative segregation is considered by the authors to be for the most part outside the scope of this discussion. This is because the most commonly proposed mechanisms, involving formation of columbium lean fragments and their entrapment in the solidifying ingot, are particular to the VAR process, rather than to the nature of solidification of IN-718.) However, other factors have contributed to a recent surge of interest in applying solidification theory to superalloys.

Advances in recent years towards understanding of fracture mechanics and fatigue-defect sensitivity of superalloys have generated a new era of "clean metal" technology, with concurrent exploration of consumable melting processes alternative to VAR. One such alternative receiving major consideration is electroslag refining (ESR). This process affords an efficient cleansing mechanism by means of selective chemical dissolution of non-metallic inclusions from the electrode into the slag layer. With this significant benefit comes a drawback of similar significance. Solidification proceeds within a "skin" of solid slag, which acts as a thermal insulator to reduce solidification rate as it expands and alters the shape of the molten core within the solidifying ingot - precisely the conditions favorable to remnant dendritism and freckles. ESR also has more attendant variables or degrees of freedom than VAR, such as slag chemical and physical properties, amount of slag, skin thickness and withdrawal vs static mold.[2,3] Therefore, modeling ESR in order to predict optimum melt parameters is inherently more difficult than VAR. Modifying any variable, including melt rate, usually affects several of the other variables with results not necessarily foreseeable. Indeed, the experimentation described herein was to some extent by trial and error, although the isolated effects of the individual variables on solidification rate could be estimated.

EXPERIMENTAL

Cylindrical electrodes were ESR'd in static molds from either 356 mm or 432 mm diameter to 432 or 508 diameter ingots, respectively. Modifications were made in:

Melt Rate.

Slag Formulation - By convention among ESR melters the four most common components are given in weight percent in the order

$$CaF_2/CaO/MgO/Al_2O_3$$

The popular industrial formulation consisting of seventy percent calcium fluoride (fluorspar) and fifteen percent each of calcium oxide and aluminum oxide is, for example, designated

70/15/0/15

Other fluorides are listed by chemical formula immediately after fluorspar and other oxides are listed after alumina.

Slag Charge
Initial - desired slag pool depth.
Feeder - proportional to anticipated skin thickness to maintain constant depth.

Longitudinal ingot specimens for macrostructural evaluation were obtained by first cutting approximately twelve inch sections, then cutting to expose the maximum cross section (through the center) and yielding a nominally one inch thick vertical slab. The macro-grain etchant clearly highlighted the longitudinal solidification grain growth pattern, from which, using standard metallographic techniques, could be determined:

grain size, morphology and orientation (growth angle).

pool profile and depth.

Macrodendritic pattern and macrosegregation were elucidated with an etchant which selectively dissolves the columbium-rich precipitates concentrated in freckles and in interdendritic regions. The eroded areas appear black; whereas columbium lean regions, like primary dendrite arms and negative segregation, have bright metallic luster.

The forged billets were ASTM grain size 5 or finer. Therefore, macro-grain etching was foregone. Sampling for the segregation etch was limited to transverse sections, usually 12.7 mm (0.5") thick disks, due to the potential commercial or experimental value of the billets.

RESULTS AND DISCUSSION

Effects of melt rate are to be seen in Figure (1) where a 432 mm diameter electrode was ESR'd through 70/15/0/15 into a 508 mm diameter mold. A relatively standard melt rate (for that diameter for most specialty steel alloy systems) was maintained until about half of the electrode mass was consumed. Then the rate was reduced to one-half the initial value.

Initially a fine columnar grain pattern emanates from the water-cooled baseplate, but due to the poor thermal conductivity of the alloy this pattern soon disintegrates. For a short time thereafter the pattern is similar to VAR, with columnar grain growth starting out at near 90° from the mold wall (horizontal) and terminating in a central equiaxed grain zone. This transitional region approximates the "U"-shaped pool and mushy zone condition common for VAR melting.[4,5] At the top of the bottom section in Figure 1 the typical ESR pattern begins to emerge, with near axially oriented grains emerging from the mold wall and gradually becoming more horizontal. This gives the "V"-shaped pool and mushy zone characteristic of standard ESR ingots. The emergence of the "V" structure is concurrent with the emergence of macrosegregation, seen as the random looking dark spots in Figure (1a) at the upper portion of the second section (counting from the bottom). The macrosegregation can at times become concentrated near the center (the apex of the "V"), as seen in Figure (1a), third section.

The substantially reduced, second half melt rate produced the axially oriented grain pattern in Figure (2a). The reduced power input effected this by:

1) Thickening of the slag skin from 0.6 mm to 3.5 mm which prevented effective heat transfer across the shrinkage gap to the mold wall.

2) Longer time in proximity to the slag pool for any cross section of the ingot and therefore a greater axial thermal gradient.

Random macrosegregation is eliminated with such a situation, but at the expense of extremely coarse dendritic structure and poor ingot surface, shown as rough edges in Figure (2). The tendency to accumulate columbium rich interdendritic material towards the ingot center also persists as axially oriented dark streaks.

Establishing a "U"-shaped pool and mushy zone in ESR does not necessarily eliminate macrosegregation. The 508 mm diameter ingot shown in Figure (3) was ESR'd through commercially pure fluorspar (part of a clean metal program to lower slag oxygen and nitrogen activity) at two melt rates intermediate to those in the case of Figures (1) and (2). The initial axial fine columnar grain structure in Figure (3a) is similar to that shown in Figure (1a). However, the high melting

point, low electrical resistivity and poor thermal conductivity of calcium fluoride combined to yield such a thick slag skin that pool slag depth rapidly decreased. Radiant heat loss from the top allowed the extensive equiaxed grain zone to develop. This was exaggerated with the programmed drop in melt rate beginning at about 660 mm from the bottom in Figure (3). In a situation of diminishing returns, addition of large amounts of slag temporarily regenerated the slag pool; but much of this fresh cold slag simply froze against the mold wall, aggravating the thick skin problem and expanding the molten ingot core. Eventually all molten slag was depleted and the melt was terminated when arc-melting began. Indeed, the ingot top has features characteristic of VAR, such as columnar grains growing from the top downwards and a shrinkage cavity a few inches below the top surface. Figure (3a) shows the progressive grain angle change indicating deepening pool as the melt proceeded. In Figure (3b) the pattern of columbium segregation follows the columnar-equiaxed grain transition and clearly outlines the "U"-shaped pool and mushy zone. Note that segregation occurred despite the fine equiaxed grain size, which is probably just a consequence of pool convection. Composition of a freckle and that of an area with normal etch response are given in Table I. The substantial difference is in columbium.

In Table II[6] the dendrite arm spacing values of several 508 mm VAR ingots are contrasted with those from a 432 mm ESR ingot which had the typical "V"-shaped pool profile. Despite the shorter radius, the ESR ingot had comparable values at mid radius and center. Furthermore, a considerable gradient from edge to mid radius occurs with the ESR ingot. The estimations of mushy zone thickness for the ESR ingot and the highest and lowest melt rate VAR ingots of Table I are given in Table III[6]. It can be seen that at the center, the ESR ingot had a mushy zone deeper than the VAR ingot which was melted at a faster rate. This extension of the mushy zone is thus correlated with an observed increase in the frequency of freckles in ESR IN-718, most probably due to the greater opportunity for interdendritic fluid flow.

The dark-etching, columbium-rich areas in Figures (1b), (2b) and (3b) contain excessive amounts of a Laves phase which has the nominal composition $Fe_2(Cb, Ti)$. This phase is metastable and can be dissolved by "homogenization treatment" at temperatures close to the solidus. In reality, the diffusion rate for columbium is impractical, so that as cast ingots with uneven distribution of Laves develop uneven distribution of the various $Ni_3(Cb, Ti, Al)$ and Ni_xCb[4] strengthening phases during precipitation treatment. These appear as dark bands in the as-forged microstructure, which extends across grain boundaries in the fine grain billet. In other words, no reasonable amount of deformation can remove this pattern. Regions of excess columbium will also develop more of the deleterious δ hexagonal form of Ni_3Cb.

Figure (4) shows a freckle as a white streak virtually denuded of the darker dendrites on either side of it. (Columbium-lean regions appear dark in SEM images of IN-718.) The freckle is thus much larger than the dendrite arms in this part of the ingot and must be considered as a true case of macrosegregation. The predominance of columbium-rich phases is seen with increasing magnification. A honeycomb-like Laves network weaves through the brighter tetragonal Ni_xCb in Figure (5) needles extend in Figure (6) from the Laves phase, which is also hexagonal. Ni_xCb particles in proximity to Laves and δ are coarser than average, allowing the typical rice-grain morphology of that phase to be seen in Figure (7).

Severe segregation appears, of course, on a macro scale even in forged fine grain billet, because it is these precipitated phases which are attacked by the macro etchant. Figure (8) shows the transverse freckle pattern from the ingot in

Figure (3). The transverse billet sections in Figures (9) through (11) are from 432 mm diameter ingots. Figure (9) shows center accumulation of columbium amid remnant dendritism which would develop from an ingot structure like Figure 2. Only remnant dendrite pattern is seen in Figure (10). Figure (11) appears homogeneous, evidence that static mold ESR can produce IN-718 free of macrosegregation and gross microsegregation when the process variables are "fine-tuned."

Although macro-evaluation is encouraging, at the present state of the art ESR microstructure appears less homogeneous than VAR. However, there are preliminary indications that the defect cleanliness attainable with ESR may provide a worthwhile trade-off in substantially improved fatigue performance at the expense of slight deterioration of tensile and creep properties.

CONCLUSION

Aspects of macrosegregation theory, such as dendrite arm spacing, pool profile and mushy zone depth have proved beneficial to developing consumable melting processes for IN-718, especially ESR. Aspects of microsegregation theory, such as correlation of dendrite arm spacing with heat transfer mechanisms and local solidification time, have been used to minimize remnant dendritism in both ESR and VAR IN-718. Specifically, ESR IN-718 must be optimized by developing practices which maximize ingot cooling rate and minimize the steepness of the solidus and liquidus isotherms. At present, however, the knowledge concerning macrosegregation in consumable melted IN-718 is in the form of correlations. Since the isotherm steepness is undoubtedly involved, investigations which include a microgravity environment might separate microsegregation effects from macrosegregation effects. Accounting for the effects of gravity and density differences between the metal pool and the interdendritic fluid, in combination with the pool and mushy zone profiles, would conceivably lead to improved melting-solidification practices for IN-718, and allow prediction of macrosegregation tendency to be incorporated into high temperature alloy design.

REFERENCES

1. U.S. Patent No. 3,353,585, "Method for Controlling the Cooling of Cast Metal", Inventor - J. M. Wentzell, assigned to Special Metals Corporation, Issued November 21, 1967.
2. "Electro-slag Refining," W. E. Duckworth and G. Hoyle, Chapman and Hall LTD, London, U.K., 1969.
3. "Electroslag Process, Principles and Practice", G. Hoyle, Applied Science Publishers London, U.K., 1983.
4. W. J. Boesch and H. B. Canada, J. Metals, 34-38, October, 1969.
5. K. O. Yu, Proc. Vacuum Metallurgy Conf. on Specialty Metals Melting and Processing, AIME, 1984.
6. K. O. Yu and H. D. Flanders, Proc. Vacuum Metallurgy Conf. on Specialty Metals Melting and Processing, AIME, 1984.
7. K. O. Yu, C. B. Adasczik and W. H. Sutton, Proc. Int. Conf. on Vacuum Metallurg, Iron and Steel Inst. of Japan, 1982.

Table I

Approximate Ingot Compositions in Weight Percent as Determined by Scanning Electron Microscopy-Energy Dispersive X-Ray Analysis (SEM-EDS)

Element	Inside Freckle	Outside Freckle
Al	0.43	0.67
Si	0.16	0.12
Ti	1.33	0.97
Cr	17.36	18.58
Fe	15.23	17.62
Ni	52.55	53.19
Cb	9.43	5.46
Mo	3.51	3.38

Table II

Measured Secondary Dendrite Arm Spacing of ESR and VAR IN-718 Ingot[6]

Melting Rate kg./hr.	DAS (μM) Center	Mid-Radius	Edge
	VAR 508 mm (20 in.) Dia.		
182	132	117	103
177	130	118	99
222	120	120	107
227	116	113	99
284	123	124	115
286	107	108	103
322	114	113	104
	ESR 432 mm (17 in.) Dia.		
273[a]	117	107	76
273[b]	108	111	71

a 210 mm (8.25 in.) from bottom.
b 1230 mm (48.5 in.) from bottom.

TABLE III

Estimated Mushy Zone Shapes of ESR and VAR Processed IN-718 Ingots[6]

Ingot Type		VAR	VAR	ESR	
Powder Input (KW)		125	200	240	
Melt Rate (kg/Hr.)		180	322	273	
Ingot Diameter (mm)		508	508	432	
Dendrite Arm Spacing (μm)	C	131	114	113	
	E	101	104	74	
Mushy Zone Thickness* (mm)	C	123	146	167	(152)**
	E	57	115	48	(40)**

Mushy Zone Shape

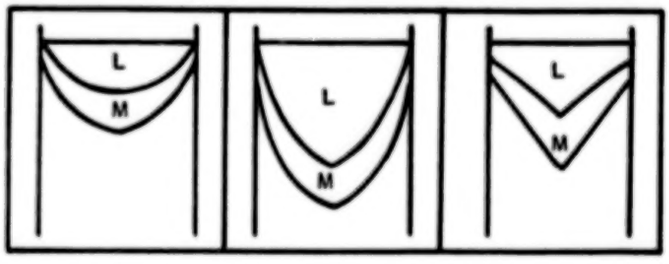

*Calculation based on the relationship of $d = 33.85\ \dot{\varepsilon}^{-0.338}$. Where d is secondary dendrite arm spacing (μm) and $\dot{\varepsilon}$ is average cooling rate in mushy zone (K/sec.).
**Obtained from previous thermal computations.(7)

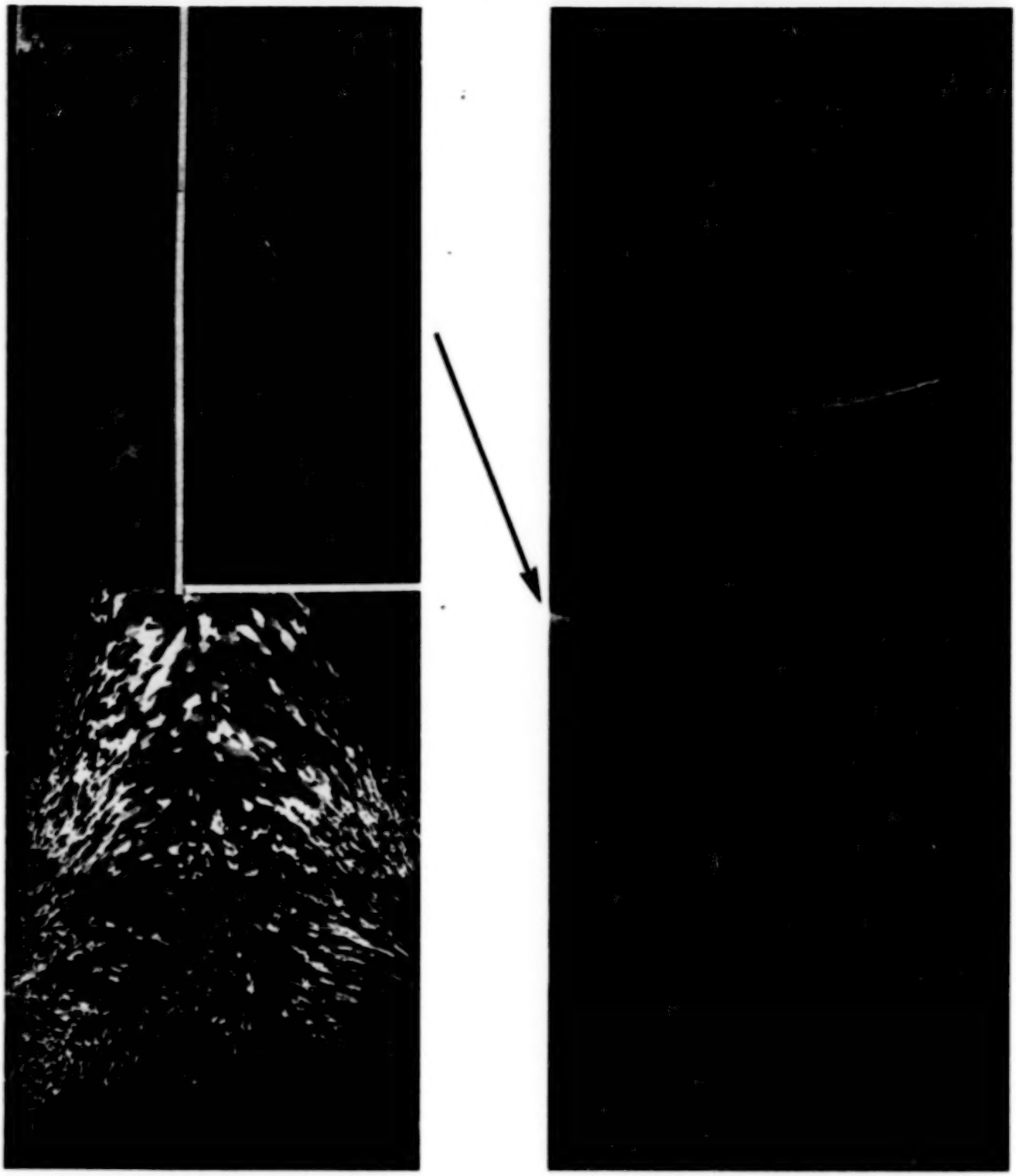

Figure 1. Standard Melt Rate, 0 to 132 cm x 508 mm.
(Crack is associated with factors other than segregation)

a) Grain-Etch Condition.

b) Segregation-Etch of Part of the Top Two Sections of (a) (Diffused dark are etchant stain)

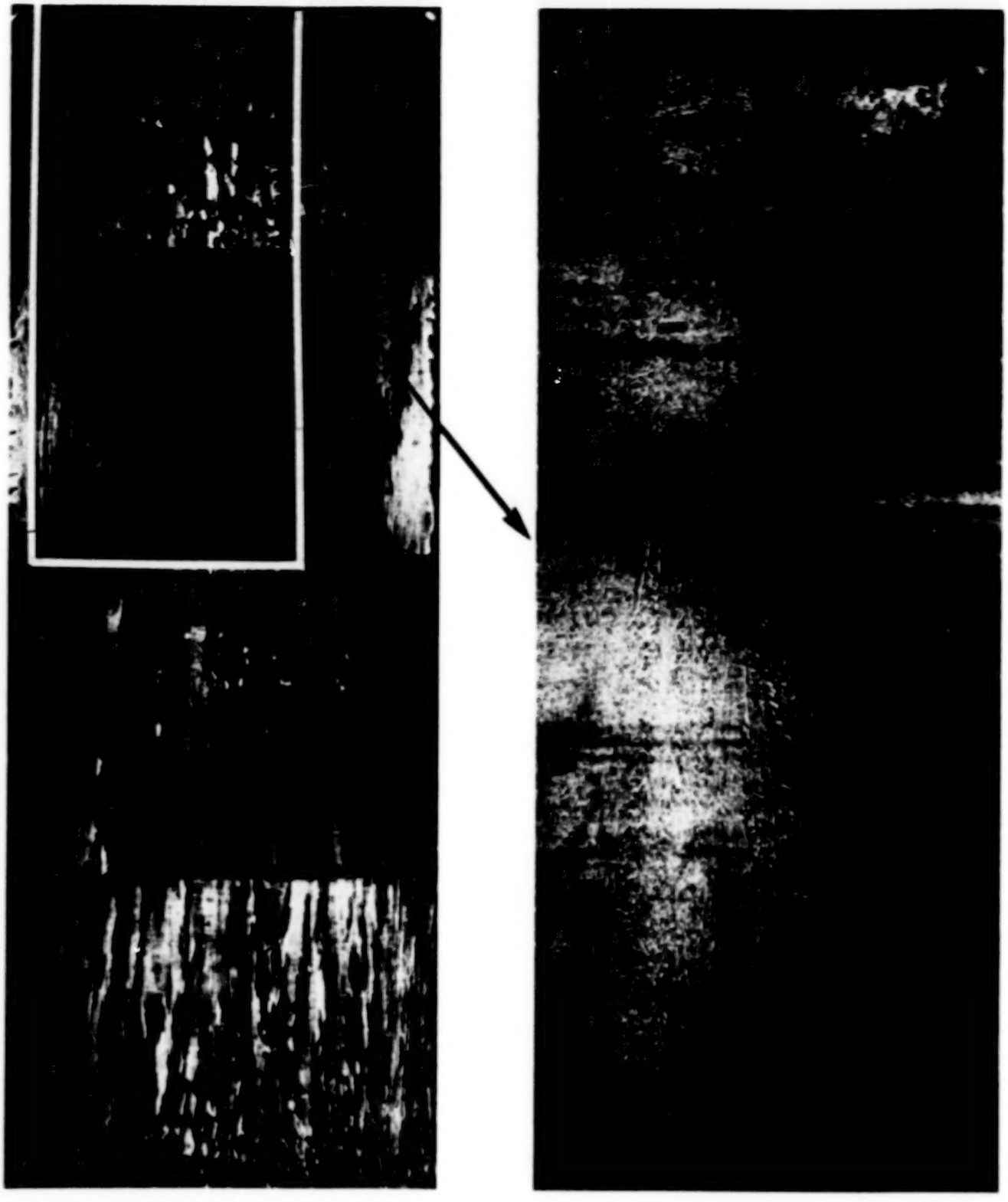

Figure 2. Low Melt Rate, 132 to 263 cm x 508 mm.

a) Grain-Etch Condition

b) Segregation-Etch of Part of the Top Two Sections of (a) (Horizontal streaks in top section are stains)

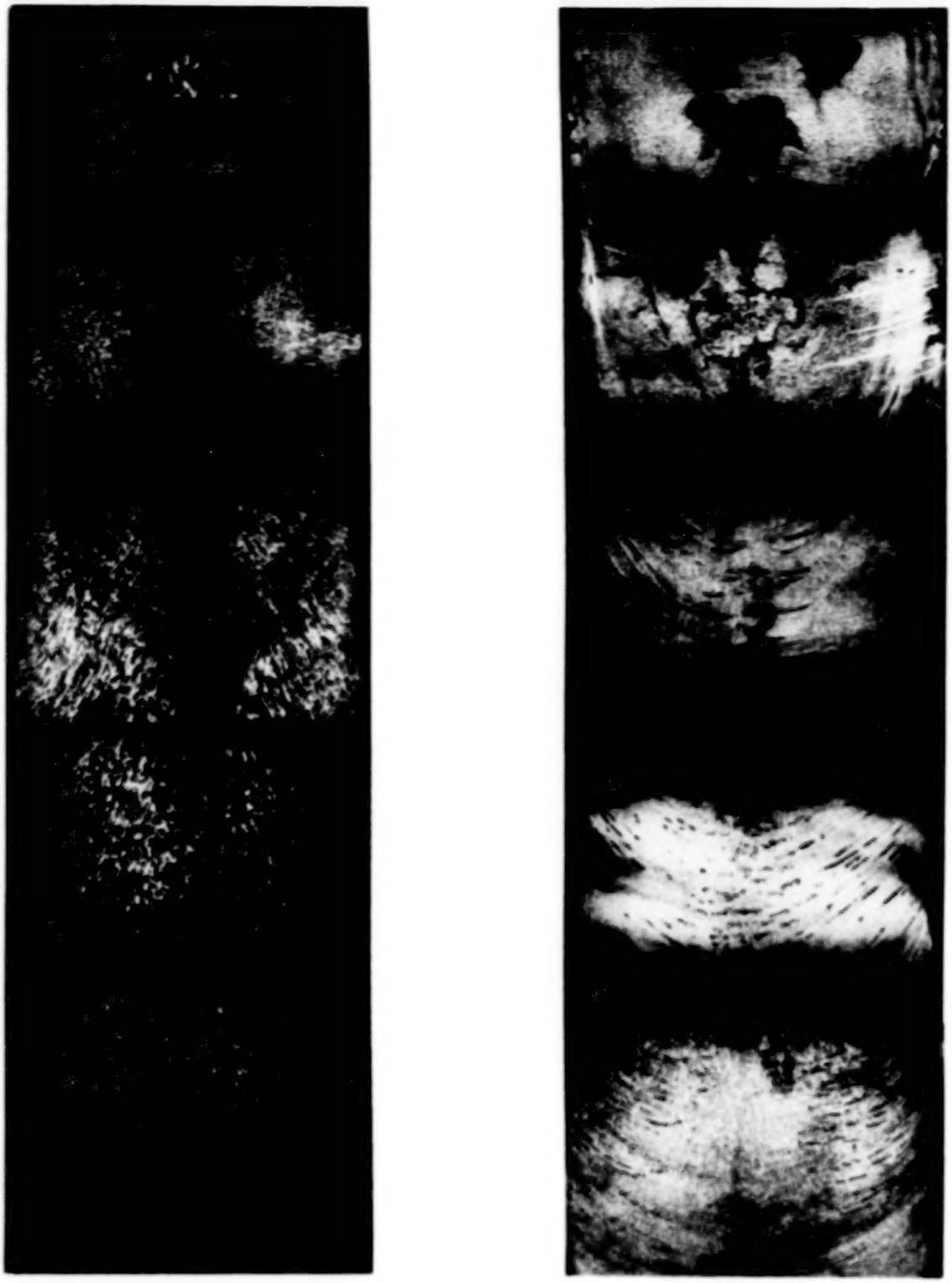

Figure 3. Intermedite Melt Rate, CaF_2 Slag. 159 cm x 508 mm.

a) Grain-Etch Condition

b) Segregation-Etch (Vertical stain in mid-height section)

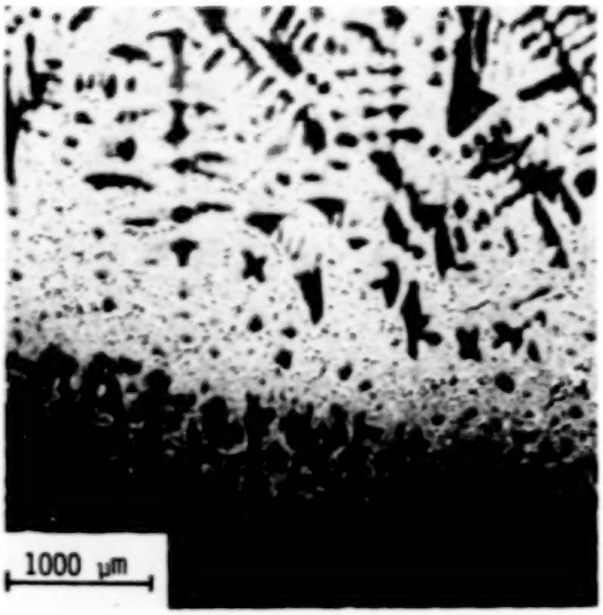

Figure 4. SEM Micrograph of One of the Dark Regions in Figure (3b)

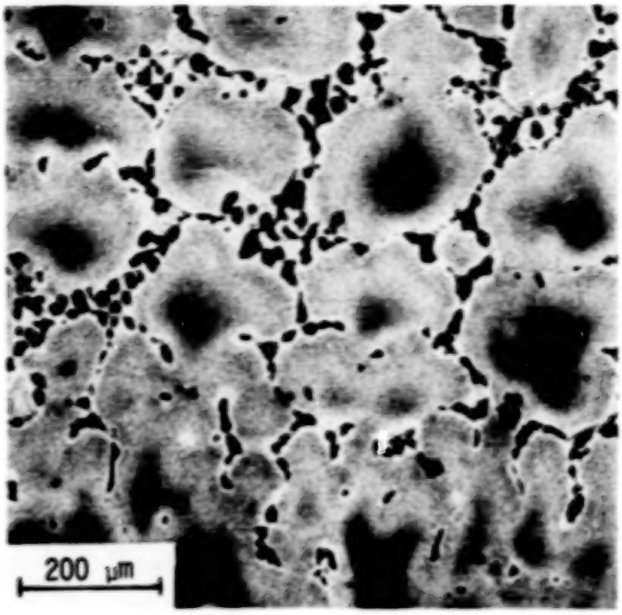

Figure 5. Blowup of Figure (4) Showing Laves Phase Network

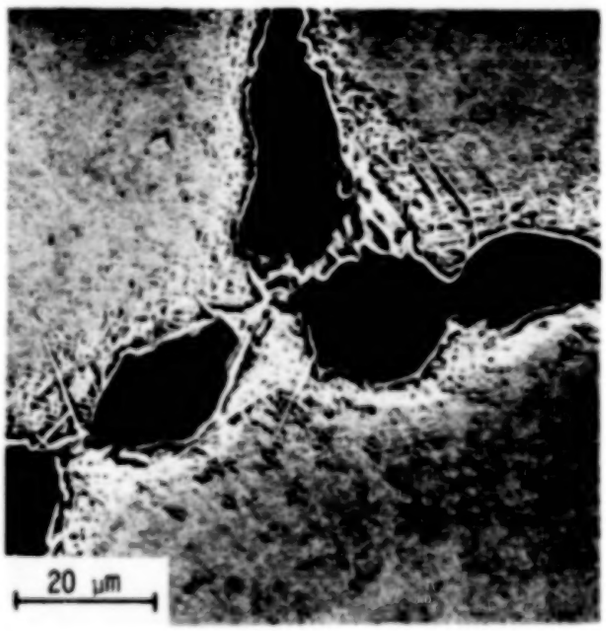

Figure 6. Blowup of Figure (5) Showing δ and Ni_xCb Around Laves Phase

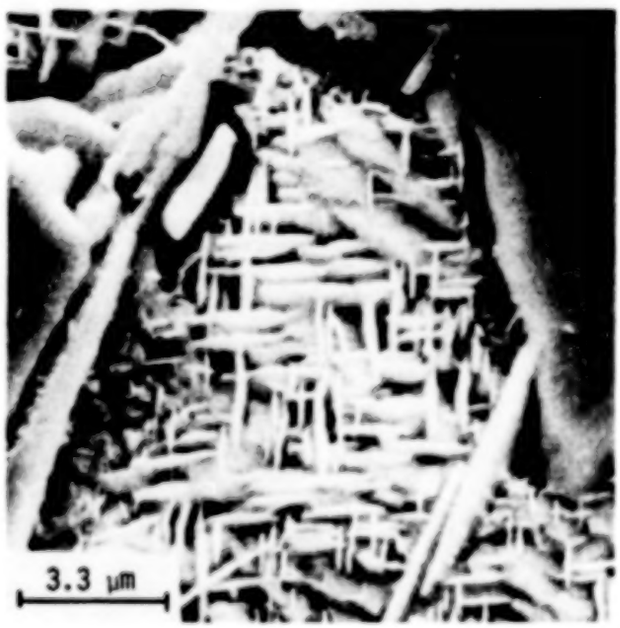

Figure 7. Blowup of Figure (6) Showing Ni_xCb Morphology

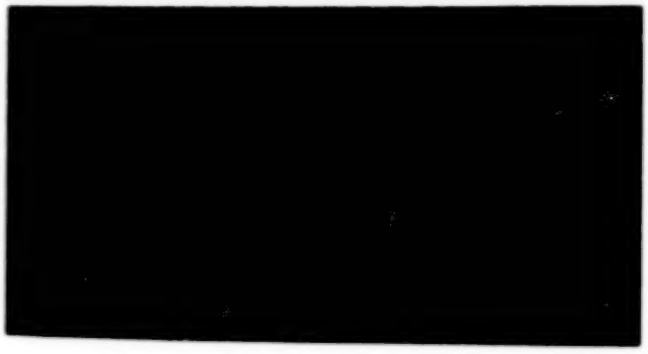

Figure 8. Oblique View of Third Section of Billet in Figure (3a). Note mid radius freckles in transverse face.

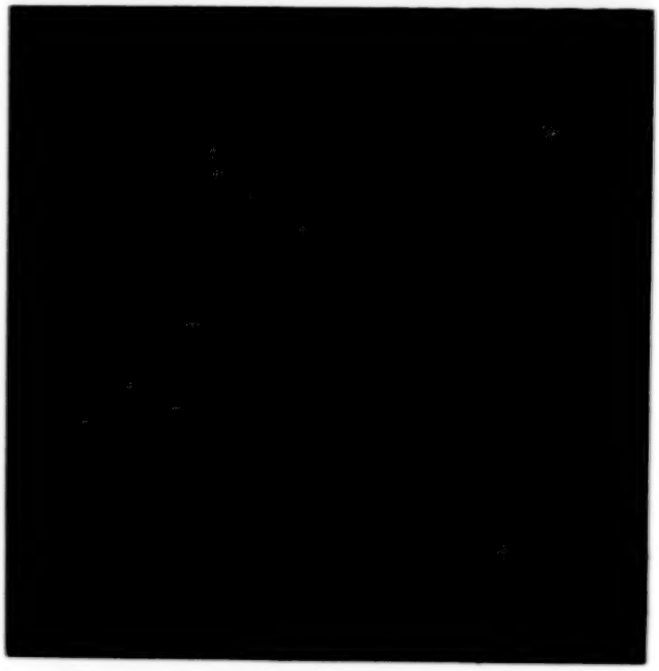

Figure 9. Center Concentrated Freckles and Remnant Dendritism in 152 mm (6") Diameter Forged ESR Billet.

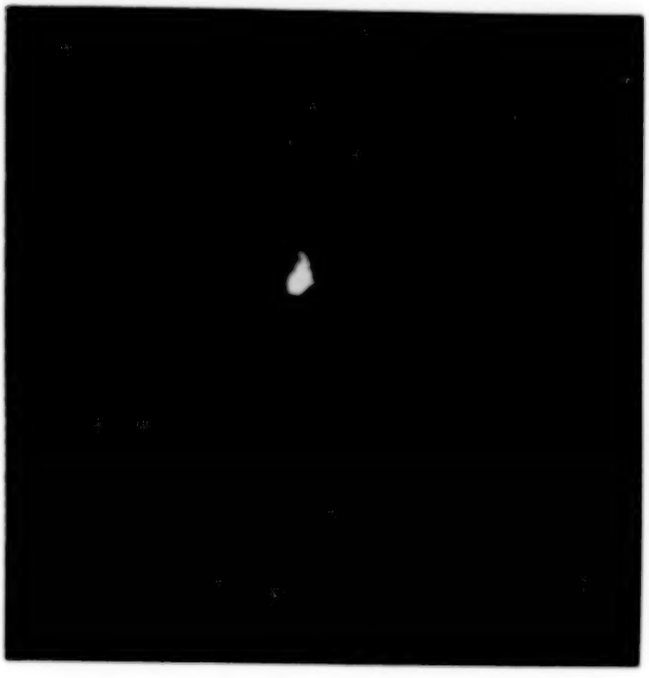

Figure 10. Remnant Dendritism in 381 mm (15") Diameter ESR Billet. (Bright Spot is Scratch on Specimen.)

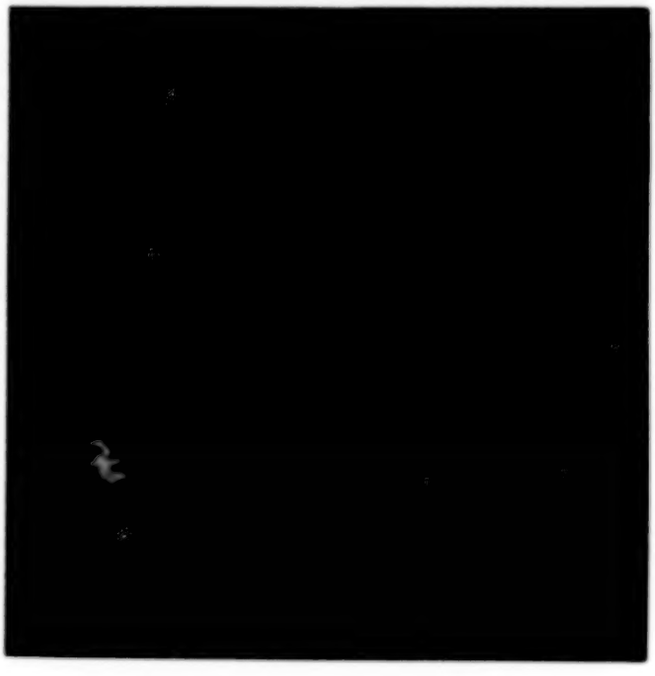

Figure 11. Optimized Macrostructure in 381 mm Diameter ESR Billet. (Bright Spots are Scratches.

D10

SOLIDIFICATION STRUCTURES GROWN UNDER INDUCED FLOW AND CONTINUOUS CASTING OF STEEL

Alexander A. Tzavaras
University of Pittsburgh
Pittsburgh, Pennsylvania

I. INTRODUCTION

The advent of steel continuous casting, in the sixties, revived interest on the use of induced flow as a means to control solidification structures in strand cast steel. Research work in this area revealed that some of the quality problems in strand cast steel stemming from columnar growth could be controlled, at least partially, by Electro Magnetic Stirring (EMS). Most of the research work reported have focused on the fragmentation and multiplication mechanisms.

II. EFFECTS ON STRUCTURES

Induced flow has been shown to change the normal morphology of dendrites. Figure 1. A,B,C. Velocities higher than those found in convection currents are normally associated with turbulence. Turbulent flow tends to round off the dendritic arms, and thus modify the morphology of the normal dendrites because the dendritic elements grow always into the flow. In such structure (Flow Modified or Thamnitic) no primary or secondary dendrite arms are discernible. Figure 1.B. This morphology is found both in equiaxed and in unidirectionally grown solidification structures.

Induced flow sweeping the solid-liquid boundary of a unidirectionally growing alloy, with velocities higher than those required to form flow modified solidification structures, reduces the growth rate of the solid and forms a cellular-like structure, which has been called fibrous because of its morphology. Figure 1.C.

III. SEGREGATION EFFECTS

Limited electromagnetic stirring (EMS) has been used extensively since the late seventies in steel strand casting as a refining technique; however solid grown under intense stirring conditions shows both negative and positive segregation which has been considered unacceptable by some steel producers. Fig. 2.A.B.

The severity of this type of segregation depends on the changes in the velocity of the liquid. Also, the peritectic reaction affects substantially the size of the columnar dendrites. Fig. 3. Thus the intensity of effective stirring varies with the composition of the steel being stirred. Some grades require more intense stirring that others, to control center segregation for instance. Extensive low density EMS has been shown to control effectively center segregation by reducing the size of the equiaxed dendrites, which appears to be a critical parameter in center segregation control. Pseudorimmed steel has been cast continuously by stirring in the mold area.

IV. EFFECTS ON INCLUSIONS

In steel the inclusion size and population is strongly affected by induced flow (EMS). Laboratory and industrial data show substantial reduction in inclusion size and content, but the overall effect of flow on inclusions is affected by the particular type of flow patterns utilized in each case.

V. BENEFITS FROM EMS

Productivity and quality have been raised substantially in steel strand casting by utilizing EMS. In the future more benefits are expected from the use of EMS, in combination with sensors and microprocessors that will improve the available controls for the solidification process.

A

B

C

Figure 1. Solid liquid interface of unidirectionally grown steel (4335)

A. Unidirectional growth without induced flow.
B. Unidirectional growth with induced flow of medium intensity.
C. Unidirectional growth with induced flow of high intensity

Mag ~100X

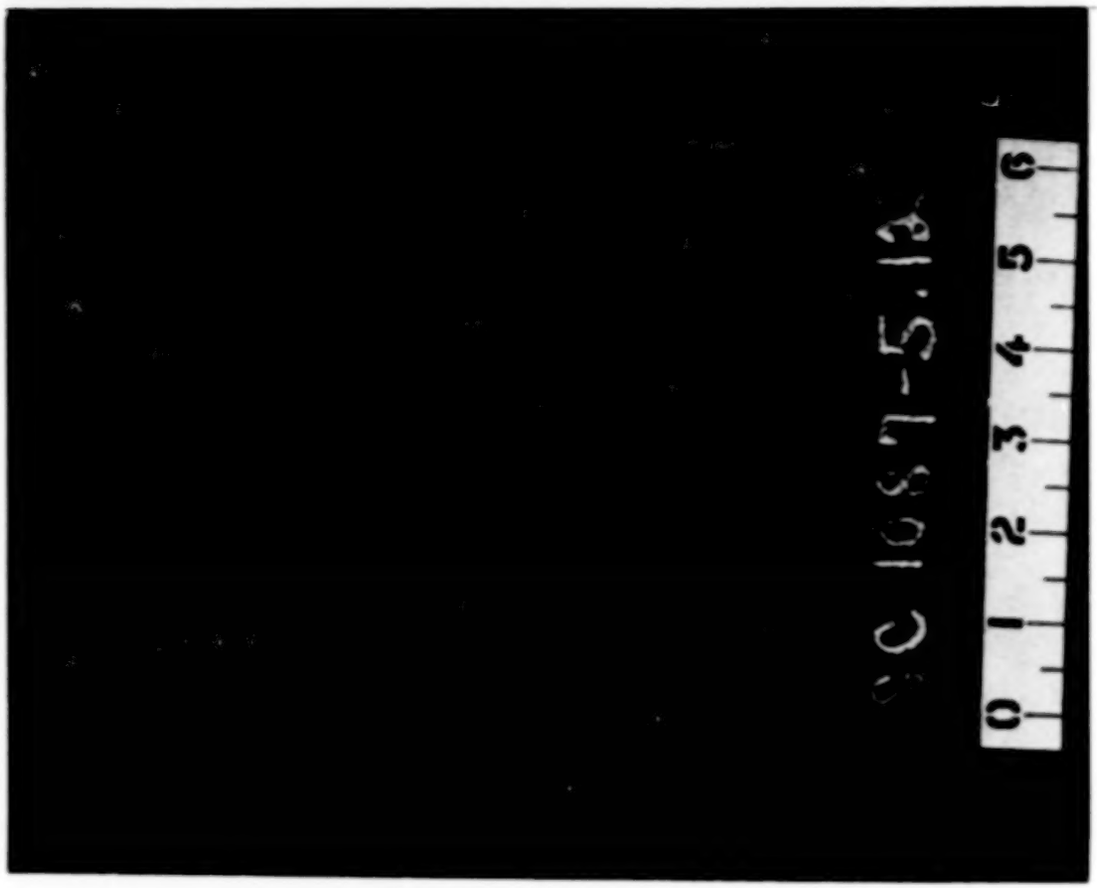

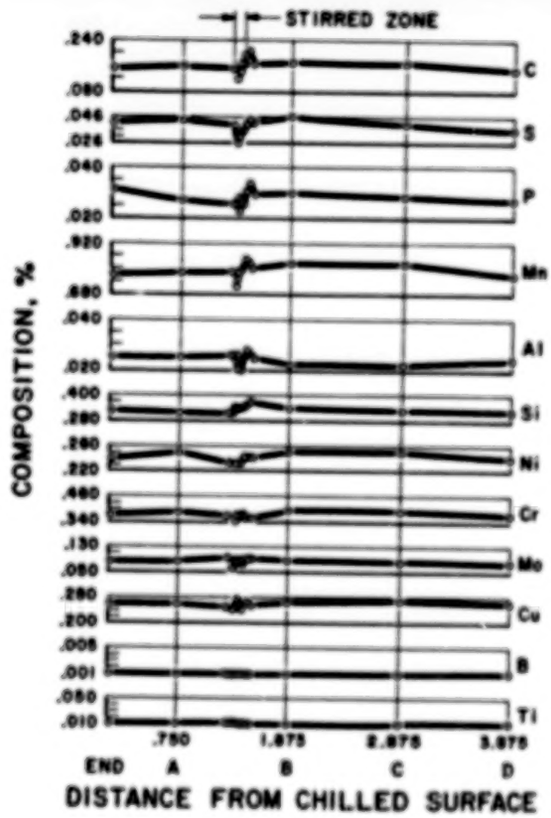

-B-

Figure 2. Intense limited stirring causes the formation of the "white band" (see A) which denotes area of negative segregation This negative segregation zone is followed usually by a positive segregation zone. (see B).

A. Etched cross section of a billet stirred intensly. Note the white band.

B. Measurement of segregation across the white band.

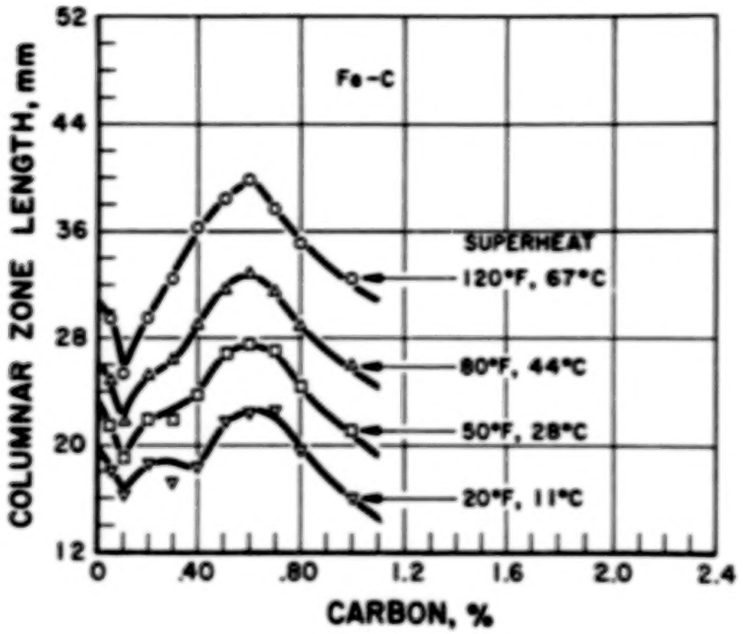

Figure 3. The size of the columnar growth depends not only on the superheat with which the steel is cast but on the peritectic reaction also, as shown in the above graph. (Courtesy of Dr. D. J. Hurtuk).

D11

N84 34600

MACROSEGREGATION IN ALUMINUM ALLOY INGOT CAST BY THE SEMICONTINUOUS DIRECT CHILL METHOD

H. Yu and D. A. Granger
Alcoa Technical Center
Alcoa Center, Pennsylvania

Macrosegregation in the DC casting process places serious constraints on the size and composition of ingot made by this method. As a result, the concentration of alloying elements is seen to vary substantially throughout the thickness of large commerical-size ingot. Figure 1 shows a typical copper macrosegregation pattern across the thickness of a DC commercial-size Al-Cu alloy sheet ingot. Ingot surface exudation, subsurface enrichment, and the depleted zone can be accounted for by the developed macrosegregation prediction theories. Ingot centerline negative macrosegregation, however, cannot be predicted theoretically unless mass transfer by convection currents within the molten metal pool is taken into consideration. Because of the complexity of molten metal convection currents in the continuous casting process, macrosegregation theories developed using static casting are generally found to be inadequate.

A satisfactory theoretical model of the semicontinuous DC casting method must be capable of predicting the positive segregation observed at the subsurface and negative segregation commonly found at the center of large commercial-size aluminum alloy ingot.

In this study, qualitative analysis of commercial-size aluminum alloy semicontinuous cast DC ingot has been carried out. In the analysis, both positive segregation in the ingot subsurface and negative segregation at the center of the ingot were examined.

Ingot subsurface macrosegregation was investigated by considering steady-state casting of a circular cross-section binary alloy ingot shown in figure 2. Nonequilibrium solidification was assumed with no solid diffusion, constant equilibrium partition ratio, and constant solid density (ref. 1 and 2).

With the frame of reference fixed in space, the continuity equation in the mushy zone is:

$$\nabla \cdot (\rho_L V_L g_L) - \rho_S V_S \cdot \nabla g_L = 0 \qquad (1)$$

where: ρ_L = liquid density
V_L = liquid velocity
g_L = liquid volume fraction
ρ_S = solid density
V_S = solid velocity = casting rate, U = a constant.

By considering the conservation of solute in the mushy zone, the following equation is obtained.

$$C_L \nabla \cdot (\rho_L V_L g_L) + \rho_L V_L g_L \cdot \nabla C_L + \nabla \cdot (V_S \rho_S g_S \overline{C}_S) = 0 \qquad (2)$$

where: C_L = solute concentration in liquid
$\overline{C}_S$ = average solute concentration in solid

$$= \frac{\rho \int_0^{g_{SE}} C_S dg_S + \rho_{SE}(1 - g_{SE})\, C_E}{\rho_S g_{SE} + (1 - g_{SE})\, \rho_{SE}} \qquad (3)$$

C_S = solute concentration in solid
C_E = eutectic solute concentration
g_S = solid volume fraction
g_{SE} = eutectic solid volume fraction
ρ_{SE} = eutectic solid density

Substituting equation (1) into equation (2), and for constant ρ_S and k, equation (2) becomes:

$$V_L \cdot \nabla C_L = - \left(\frac{C_L}{g_L} V_S \cdot \nabla g_L\right) \frac{(1 - k)}{(1 - \beta)} \qquad (4)$$

where $\beta = 1 - \frac{\rho_L}{\rho_S}$

k = equilibrium partition ratio = C_S/C_L

For the continuous casting of a cylindrical ingot, equation (4) becomes:

$$V_{L_r} \frac{\partial C_L}{\partial r} + V_{Lz} \frac{\partial C_L}{\partial z} = - \frac{(1 - k)}{(1 - \beta)} \frac{C_L}{g_L} U \frac{\partial g_L}{\partial z} \qquad (5)$$

Macrosegregation is determined by evaluating equation (5) at the ingot surface, where:

$V_{Lr} = 0$
$V_{Lz} = U$

$$U \left.\frac{\partial C_L}{\partial z}\right|_{r = R} = - \frac{(1 - k)}{(1 - \beta)} \frac{C_L}{g_L} U \left.\frac{\partial g_L}{\partial z}\right|_{r = R}$$

or:

$$\left.\frac{\partial C_L}{\partial g_L}\right|_{r = R} = - \frac{(1 - k)}{(1 - \beta)} \frac{C_L}{g_L} \qquad (6)$$

By making use of the equilibrium partition ratio and the fact that $g_S + g_L = 1$, local solute concentration in the solid is determined from equation (6).

$$C_S = kC_L^o (1 - g_S)^{-\frac{(1-k)}{(1-\beta)}} \quad (7)$$

where: C_L^o = solute concentration in liquid prior to solidification

The degree of macrosegregation under the ingot surface can be calculated from equation (3) together with equation (7). For constant solid density, $1 - \beta < 1$ and $k < 1$ such as with copper and magnesium in the Al-Cu-Mg alloy system, it can be shown that $\overline{C}_S > C_L^o$ or positive macrosegregation of Cu and Mg occurs under the ingot surface.

Away from the ingot surface, macrosegregation calculations would be more difficult. Macrosegregation prediction requires consideration of the transport equations of the solid phase, mushy zone and molten metal pool of the ingot. Both experimental evidence and order of magnitude estimates can be used to explain the occurrence of negative macrosegregation at the center of the large commercial-size DC ingot. Figures 3 and 4 show typical centerline negative macrosegregation of Cu and Mg in an Al-Cu-Mg alloy DC ingot 1.5 times the standard commercial size. Positive centerline macrosegregation of Ti, which comes from the added grain refiner, in the same ingot is shown in figure 5. Experimental observations suggest that "isothermal dendrites" are a major contributor to this centerline negative macrosegregation.

Two important characteristics of ingot structure are (1) the grain shape and size and (2) dendrite cells. The grains are typically equiaxed, about 300 μm in diameter. Many of the grains exhibit a dendritic structure with an average cell size (excluding coarse dendrites) of 95 μm. Of particular note, though, are those "grains" which appear nondendritic and which comprise about 30% of the volume. These grains are believed to be coarse dendrites that originated at the start of solidification and were swept into the ingot crater where they grew slowly at a temperature close to the alloy liquidus. These cells are termed "isothermal dendrites" and are illustrated in figure 6.

When the well-known relationship between dendrite cell size and cooling rate (ref. 3)

$$d = k\,\theta^{-0.34}$$

where: d = dendrite cell size (μm)
k = an alloy dependent constant (0.002)
θ = is the cooling rate (°F/sec)

is used to estimate ingot cooling rate, it is clear that the coarse and fine cells observed at the center of the ingot have different origins. The average average cell size of the smaller dendrites indicates a cooling rate of approximately 0.3°C/sec (0.6°F/sec) which is the expected rate at the center of the ingot. The larger dendrites clearly grew much more slowly and did not freeze in-situ when the center of the ingot solidified.

Further evidence to support this contention is provided by the copper distribution across a coarse dendrite obtained by electron probe microanalysis and illustrated in figure 7. A step scan, using 5 μm intervals, was made across a

coarse dendrite. As shown in the figure, the copper concentration peaks at the boundary of the cell then rapidly falls to a uniform level of about 0.7% Cu. The copper concentration in this plateau region is the value that would be expected for a dendrite growing in a pool of liquid of an average composition of 4% Cu. In contrast, a dendrite growing in-situ at the center of the ingot has both a higher C_{min} and shows a characteristic copper concentration profile; i.e., no plateau region, as shown in figure 8.

At the center of the ingot, there is a positive segregation of titanium (fig. 5). Since Ti is a peritectic-forming element with aluminum, it will be concentrated at the center of the α-Al dendrites. Therefore, a local enrichment in titanium can only be established through a concentration of primary aluminum dendrites. Thus, the positive segregation of this element at the center of the DC cast ingot is strong evidence that the eutectic element (Cu) depletion is associated with the incorporation of coarse, isothermal dendrites enriched in titanium.

The linear intercept method gives a volume fraction of 32% coarse dendrites at the ingot center, and probe traverses across these dendrites indicate about 50% of the dendrite grew with a C_{min} of approximately 0.7% Cu. Therefore, the volume fraction at 0.7% Cu is about 16%, leaving 84% at 4.0% Cu, assuming that the remaining dendrites grew from liquid of close to average composition. From these approximations, it is predicted that the average composition at the ingot center is (0.11% + 3.36% Cu) 3.47% Cu, an underestimate that suggests some flow of enriched liquid to feed shrinkage.

Cu and Mg macrosegregations of a standard commercial-size Al-Cu-Mg alloy DC sheet ingot are shown in figures 9 and 10, respectively. It can be seen from figures 3, 4, 9, and 10 that negative macrosegregation at the center of a DC ingot increases with increasing ingot size and casting rate. Solute density apparently has little influence, since both Cu and Mg show similar macrosegregation patterns across the ingot thickness. The importance of natural convection currents in the ingot molten metal pool can be estimated by considering the dimensionless fluid flow equations with the Boussinesq approximation.

$$\nabla \cdot V = 0 \tag{8}$$

$$(V \cdot \nabla)\, V = \frac{\mu}{\rho U L} \nabla^2 V - \nabla P + \frac{\bar{g}\beta\, (T_o - T_l)\, L}{U^2} \tag{9}$$

where: V = dimensionless molten metal velocity
P = dimensionless pressure
μ = molten metal viscosity
ρ = molten metal density
U = ingot casting rate
L = ingot molten metal pool depth
$\bar{g}$ = gravitation
T_o = bulk molten metal temperature
T_l = liquidus temperature
$\beta = -\frac{1}{\rho} \left(\frac{\partial \rho}{\partial T}\right)_p$

It is well known in ingot casting that the depth of the ingot molten metal pool increases with increase in ingot size and casting rate. For a large commercial-size DC ingot, $\bar{g}\beta (T_o - T_1) L/U^2$ shown in equation (9) is >>1, indicating that flow in the ingot molten metal pool is dominated by natural convection. In an ingot 1.5 times the standard commercial size, the natural convection velocity can be 2 orders of magnitude larger than the ingot casting rate.

Temperature distribution in the molten metal pool can be examined using the dimensionless energy equation

$$V \cdot \nabla T = \frac{K}{\rho C_p L U'} \nabla^2 T \qquad (10)$$

where: T = dimensionless temperature
K = molten metal thermal conductivity
C_p = molten metal specific heat
U = natural convection velocity α $2\bar{g}\beta (T_o - T_1) L$ (11)

$K/(\rho C_p L U')$ in equation (10) is <<1 for a large commercial-size ingot. Heat transfer in the molten metal pool is highly convective. Temperature in the molten metal pool is rather uniform except in the thermal boundary layer in the vicinity of the liquidus isotherm. This is confirmed by the experimental data presented in figure 11. The thermal boundary layer thickness, δ_t, can be shown to thicken towards the bottom of the molten metal pool, where its thickness increases with the depth of the molten metal pool.

$$\delta_t \alpha \sqrt{\frac{K L^{1/2}}{2\rho C_p \bar{g}\beta (T_o - T_1)}} \qquad (12)$$

The thermal boundary layer thickness at the bottom of the molten metal pool, in an ingot 1.5 times the standard commercial size, can approach 25.4 mm (1 in).

Results of the order of magnitude estimate of natural convection current and thermal boundary layer development in ingot molten metal pool are consistent with experimental observations of the presence of isothermal dendrites. Isothermal dendrites formed early in the solidification process (at the time of initial shell formation) are detached and carried by the strong natural convection current into the molten metal pool. They grow isothermally at a temperature close to the alloy liquidus within the thermal boundary layer and finally become entrapped in the solidifying ingot at the bottom of the pool. The thermal boundary layer provides an environment for the growth of isothermal dendrites which cannot exist at the higher bulk temperature of the ingot pool. Isothermal dendrites comprise a significant volume fraction at the center of the ingot and help to increase the severity of negative macrosegregation there. Equations (11) and (12) show that the deeper the molten metal pool, the stronger the natural convection current, and the thicker the thermal boundary layer. This is consistent with the increase in negative segregation at the center for larger size ingot and at higher casting rates. Mass transport in the ingot molten metal pool plays an important role in accounting for the negative macrosegregation at the center of the large commercial-size ingot. It is, therefore, necessary to include such phenomena in the development of a successful mathematical model to predict macrosegregation under these circumstances.

REFERENCES

1. Flemings, M. C., Nereo, G. E.: Macrosegregation, Part 1, Trans. Met. Soc. AIME; 239, 1967, 1449-1461.

2. Mehrabian, R., Keane, M., Flemings, M. C.: "Interdendritic Flow and Macrosegregation; Influence of Gravity," Met. Trans.; Volume 1, 1970, 1209-1220.

3. Spear, R. E., Gardner, G. R.: "Dendrite Cell Size," A.F.S. Transactions; 71, 1963, 209-215.

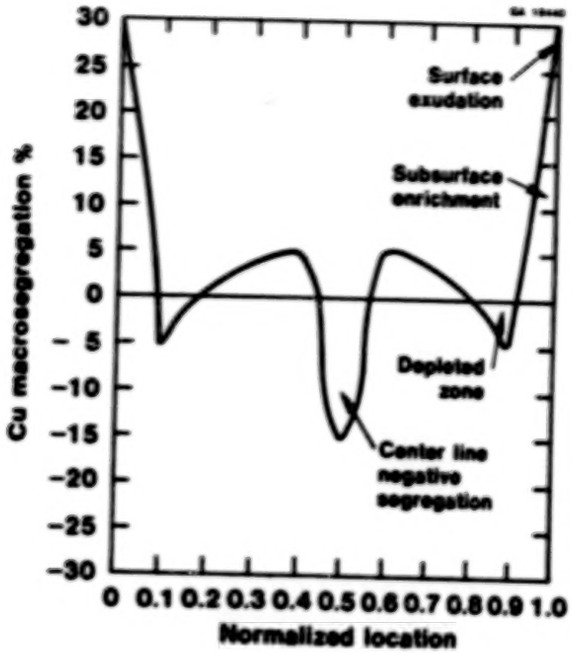

Typical Macrosegregation Across the Thickness of a Commercial Size Al-Cu Alloy DC Sheet Ingot
Figure 1

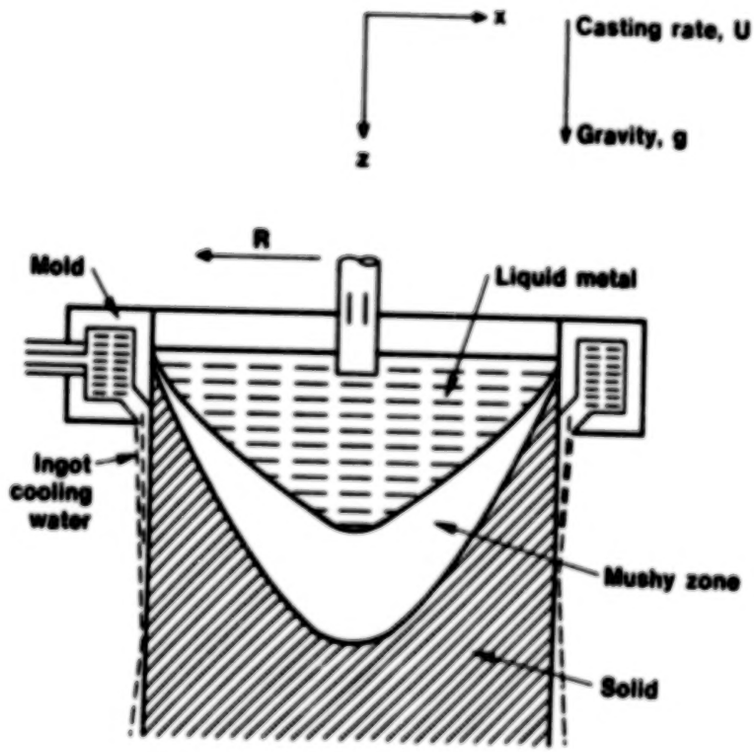

DC Ingot Casting
Figure 2

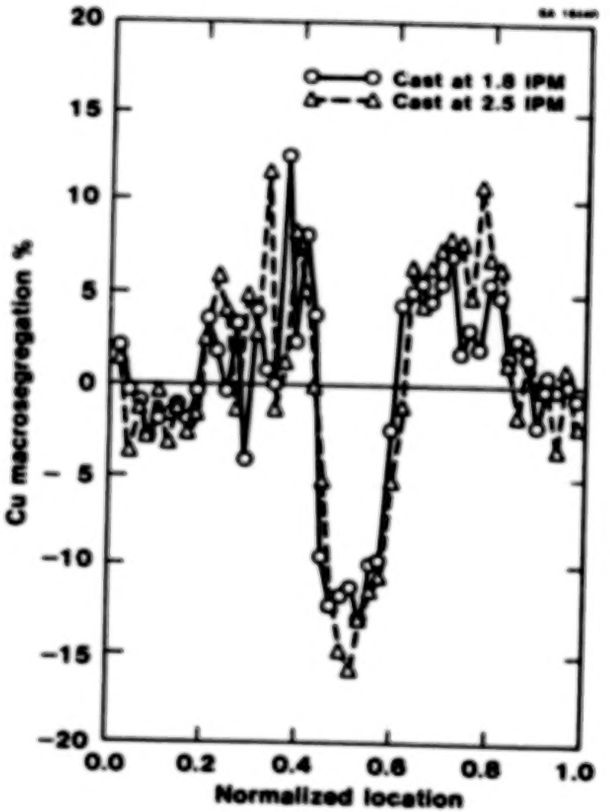

Cu Macrosegregation Across Ingot Thickness
Al-Cu-Mg Alloy DC Ingot
(1.5 times Standard Commercial Size)
Figure 3

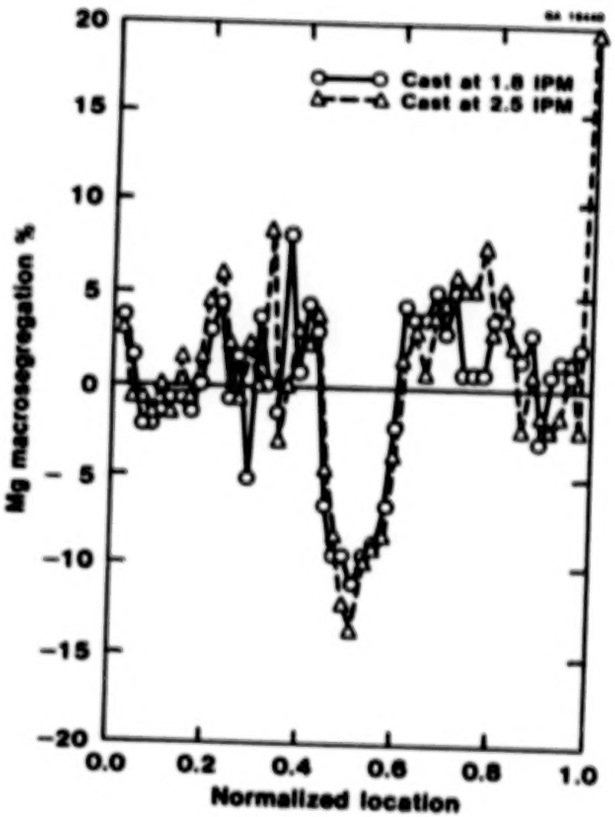

Mg Macrosegregation Across Ingot Thickness
Al-Cu-Mg Alloy DC Ingot
(1.5 times Standard Commercial Size)
Figure 4

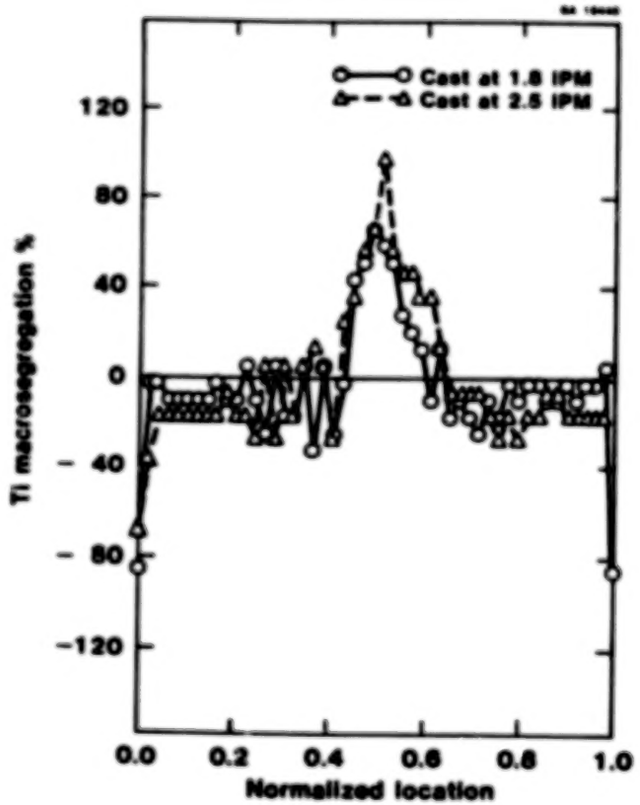

Ti Macrosegregation Across Ingot Thickness Al-Cu-Mg Alloy DC Ingot (1.5 times Standard Commercial Size)
Figure 5

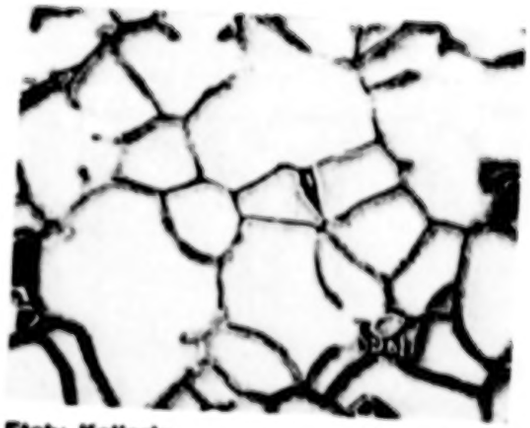

Dendrite Cells at the Center of a Large D.C. Cast Al-Cu-Mg Alloy Ingot Showing a Mixture of Coarse (Non-Dendritic) and Fine Cells.
Figure 6

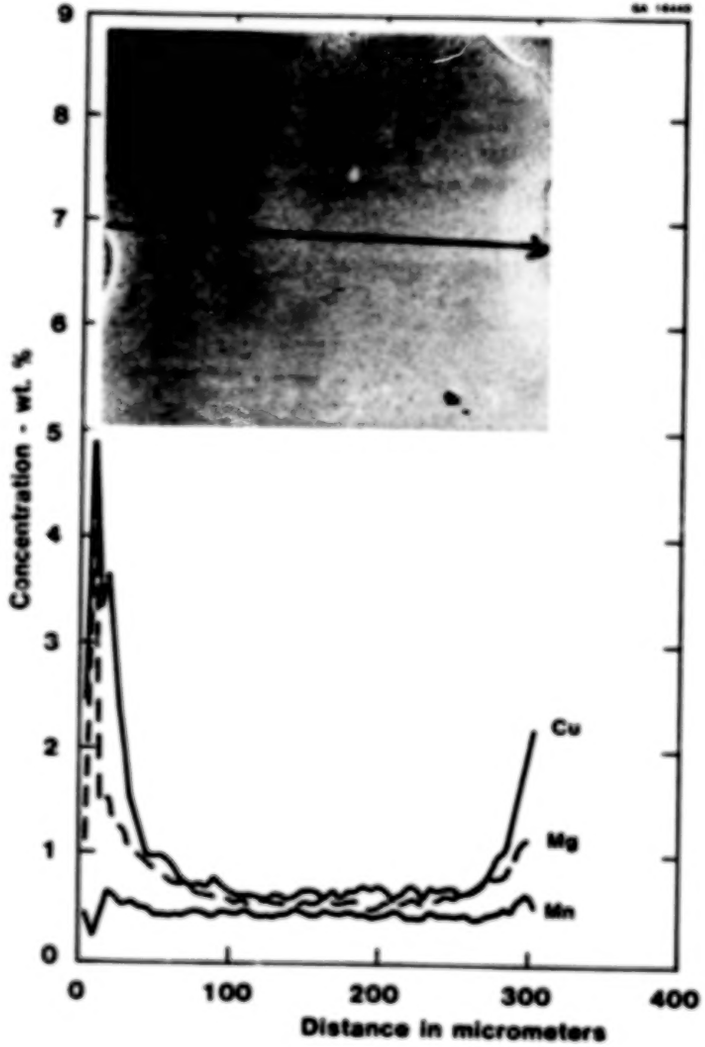

Microsegregation Across One Large Dendrite at Center of As Cast Al-Cu-Mg Alloy DC Ingot
Figure 7

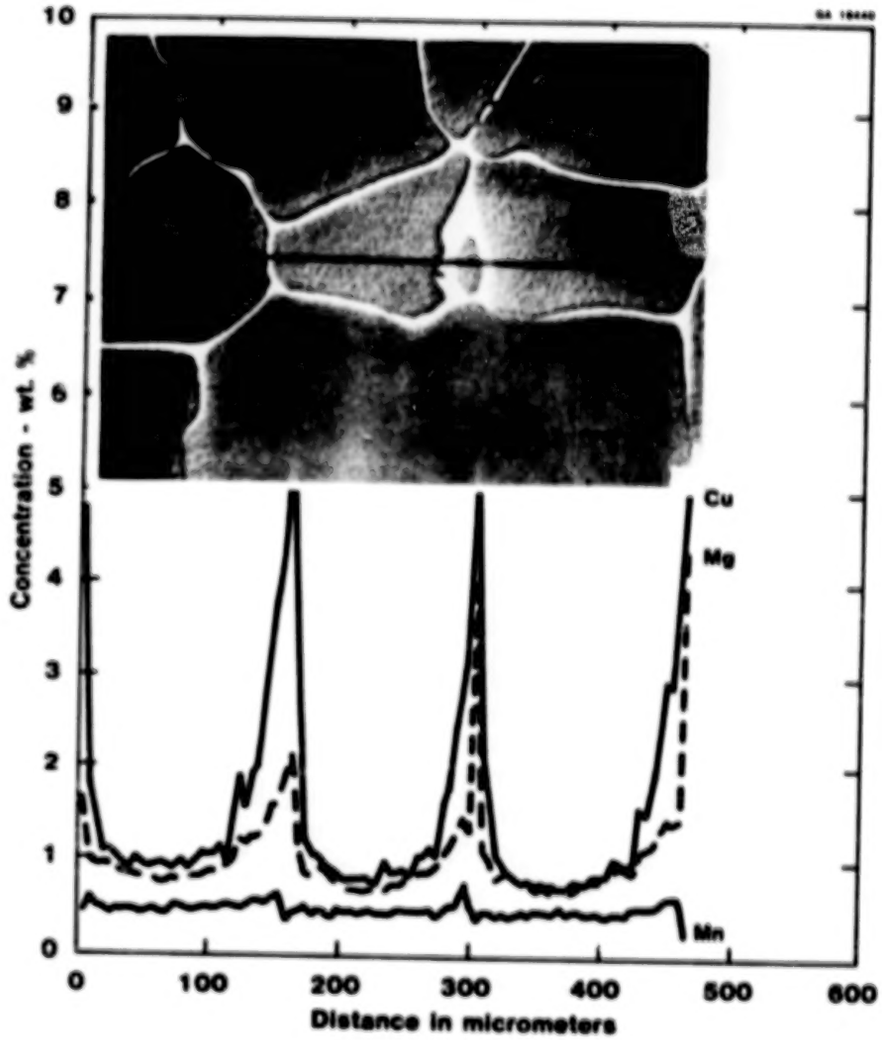

Microsegregation Across Three Medium Dendrites at Center of As Cast Al-Cu-Mg Alloy DC Ingot
Figure 8

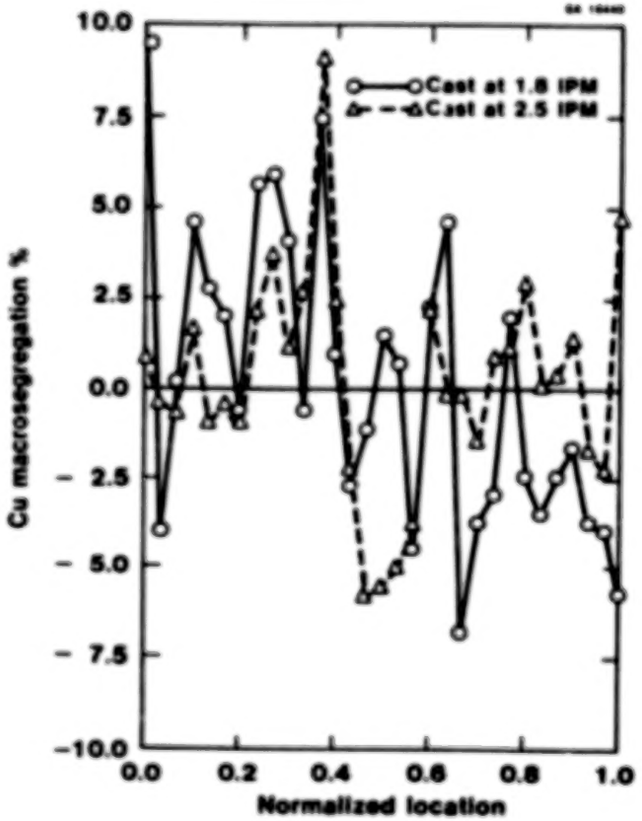

Cu Macrosegregation Across Ingot Thickness
Al-Cu-Mg Alloy DC Ingot
(Standard Commercial Size)
Figure 9

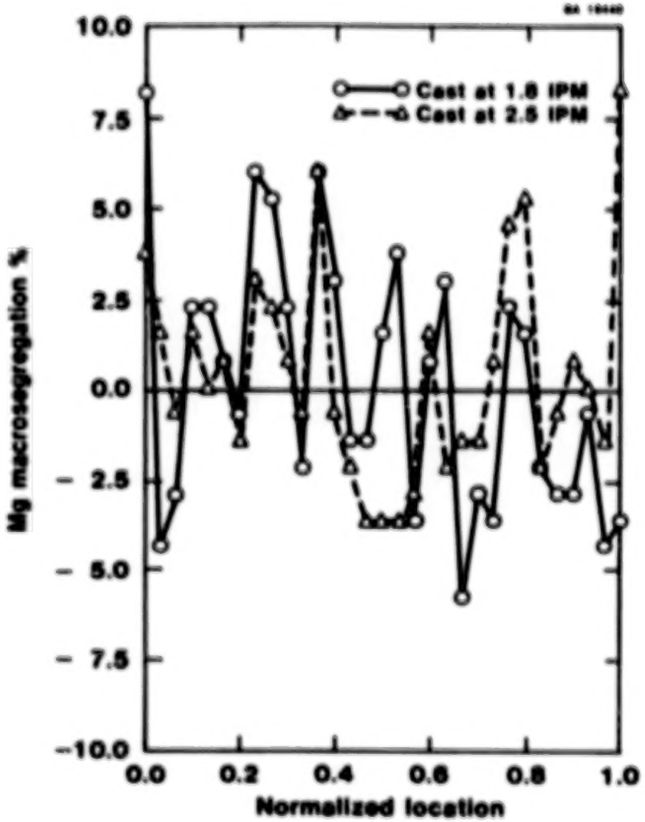

Mg Macrosegregation Across Ingot Thickness
Al-Cu-Mg Alloy DC Ingot
(Standard Commercial Size)
Figure 10

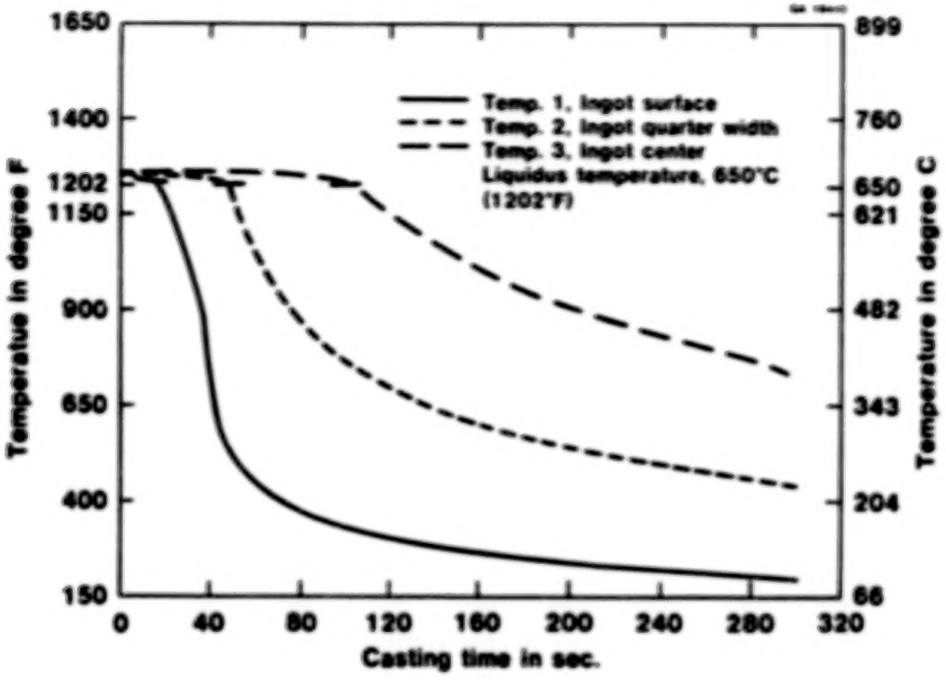

Temperature Profile of a Circular Cross-Section Commercial Size Level Transfer Ingot
Figure 11

N84 34601

D12

A REVIEW OF OUR PRESENT UNDERSTANDING OF MACROSEGREGATION IN INGOTS

Robert Mehrabian
University of California
Santa Barbara, California

Our present understanding of the mechanisms responsible for macrosegregation occurring in ingots produced by electroslag remelting (ESR), vacuum arc remelting (VAR), direct chill (DC), and continuous casting is reviewed. A detailed description is given of laboratory experiments on model Sn-Pb and Al-Cu alloys. The experimental findings are compared with theoretical predictions. Data are also presented on a high-temperature Ni-27 wt % Mo alloy ESR ingot and 2000 series aluminum alloy DC ingots. Comparison is made to theoretical predictions where appropriate.

Macrosegregation in ingots results primarily from interdendritic fluid flow in the "mushy" zone, although other mechanisms may also contribute in special cases (as floating and settling of solid particles or mass flow of liquid plus solid). Driving forces for the flow include contractions occurring during solidification, the force of gravity acting on a fluid of variable density, and penetration of bulk liquid in front of the liquidus isotherm, due to fluid motion in this region, into the mushy zone. In recent work on axisymmetric laboratory ingots, bulk flow in the liquid region (the metal pool) was coupled to interdendritic flow during solidfication. Results of this work indicate that natural convection in the liquid metal pool had little effect on interdendritic fluid flow. These results are neither conclusive nor can they be applied to large ingots where natural convection can be very strong. More work in this area is necessary.

Our understanding of the mechanisms responsible for the different macrosegregation patterns observed has improved significantly in the past 15 years. However, predictive theoretical models that can be used in on-line control of process variables for the economic production of ingots with acceptable homogeneity have yet to be developed. Theoretical work to date has been confined to one-dimensional heat flow and two-dimensional fluid flow or two-dimensional heat and fluid flow in axisymmetric ingots. The basic "solute distribution" equation, used to predict the extent of macrosegregation, has been primarily used for binary alloys, although ternary and some special higher order alloys have also been treated. Detailed quantitative comparisons of theoretical predictions have been made with ingots cast under controlled laboratory conditions. Agreement between computer calculations and experimental results on these ingots is good. The influence of the important solidification parameters, such as the shape and depth of the mushy zone and the local solidification time, on macrosegregation has thus been quantitatively demonstrated. For example, it had been shown that macrosegregation theory predicts not only surface-to-center variations in compositions, but also predicts conditions under which a severe type of segregation, called "freckles" forms.

Correlation of theory to segregation in commercial ingots is still qualitative. Heat flow models have been developed to relate the shape of the liquid metal pool and mushy zone to the casting parameters, but none of these models has incorporated the constitutive equations for the flow of interdendritic

liquid necessary to predict macrosegregation. It is time to couple multicomponent "solute distribution" equations to computerized phase diagram models for establishing solidification "paths," and to sophisticated computer codes for heat and fluid flow calculations in order to develop the necessary predictive models for commercial ingots. Finally, the calculation of interdendritic fluid flow requires the selection of permeability values as a function of volume fraction solid and structure in the mushy zone. Few permeability measurements have been made to date, and this area remains a major weak link between theory and experiment.

MECHANISM RESPONSIBLE FOR MACROSEGREGATION

- Interdentritic fluid flow
- Floating and settling of solid particles
- Mass flow of liquid plus solid

INTERDENDRITIC FLUID FLOW

- Solidification contraction
- Force of gravity acting on a fluid of variable density
- Fluid motion in the bulk liquid penetrates into the mushy zone

"SOLUTE REDISTRIBUTION EQUATION"
FOR A BINARY ALLOY

$$\frac{1}{g_L}\frac{\partial g_L}{\partial T} = -\frac{\rho_L}{\rho_S(1-k)}\left(1 - \frac{\vec{n}\cdot\vec{V}}{\vec{n}\cdot\vec{U}}\right)\frac{1}{C_L}\frac{\partial C_L}{\partial T}$$

WHERE

$$-\frac{\vec{n}\cdot\vec{V}}{\vec{n}\cdot\vec{U}} = \frac{V\cdot\nabla T}{\frac{\partial T}{\partial t}}\,.$$

g_L = VOLUME FRACTION LIQUID,

C_L = LIQUID COMPOSITION,

k = EQUILIBRIUM PARTITION RATIO,

n = UNIT VECTOR NORMAL TO ISOTHERMS,

t = TIME

T = TEMEPRATURE,

U = ISOTHERM VELOCITY,

V = INTERDENDRITIC FLUID FLOW VELOCITY,

ρ_L = LIQUID DENSITY, AND

ρ_S = SOLID DENSITY.

MACROSEGREGATION CRITERIA

IT IS CONVENIENT TO VIEW THE DIMENSIONLESS PARAMETER, $-(\vec{n} \cdot \vec{V})/(\vec{n} \cdot \vec{U})$ AS LOCAL FLOW VELOCITY PERPENDICULAR TO ISOTHERM RELATIVE TO ISOTHERM VELOCITY. MACROSEGREGATION CRITERIA CAN THEN BE ESTABLISHED FROM THE FOLLOWING EQUATION:

$$1 - \frac{\vec{n} \cdot \vec{V}}{\vec{n} \cdot \vec{U}} \gtrless \frac{\rho_S g_L + g_E (\rho_{SE} - \rho_S)}{\rho_L g_L}$$

FOR THE CASE OF THE:

= NO SEGREGATION

> NEGATIVE SEGREGATION

< POSITIVE SEGREGATION

AN INTERESTING AND IMPORTANT EFFECT OCCURS WHEN:

$$1 - \frac{\vec{n} \cdot \vec{V}}{\vec{n} \cdot \vec{U}} < 0$$

IN THIS CASE, FLUID FLOWS IN THE SAME DIRECTION AS THE ISOTHERMS AND FASTER THAN THE ISOTHERMS; THUS FLOW IS FROM COOLER TO HOTTER REGIONS WITHIN THE MUSHY ZONE. THIS TYPE OF FLOW RESULTS NOT IN SOLIDIFICATION BUT IN REMELTING. THIS IS THE BASIC MECHANISM OF FORMATION OF CHANNEL-TYPE SEGREGATES, INCLUDING "FRECKLES"

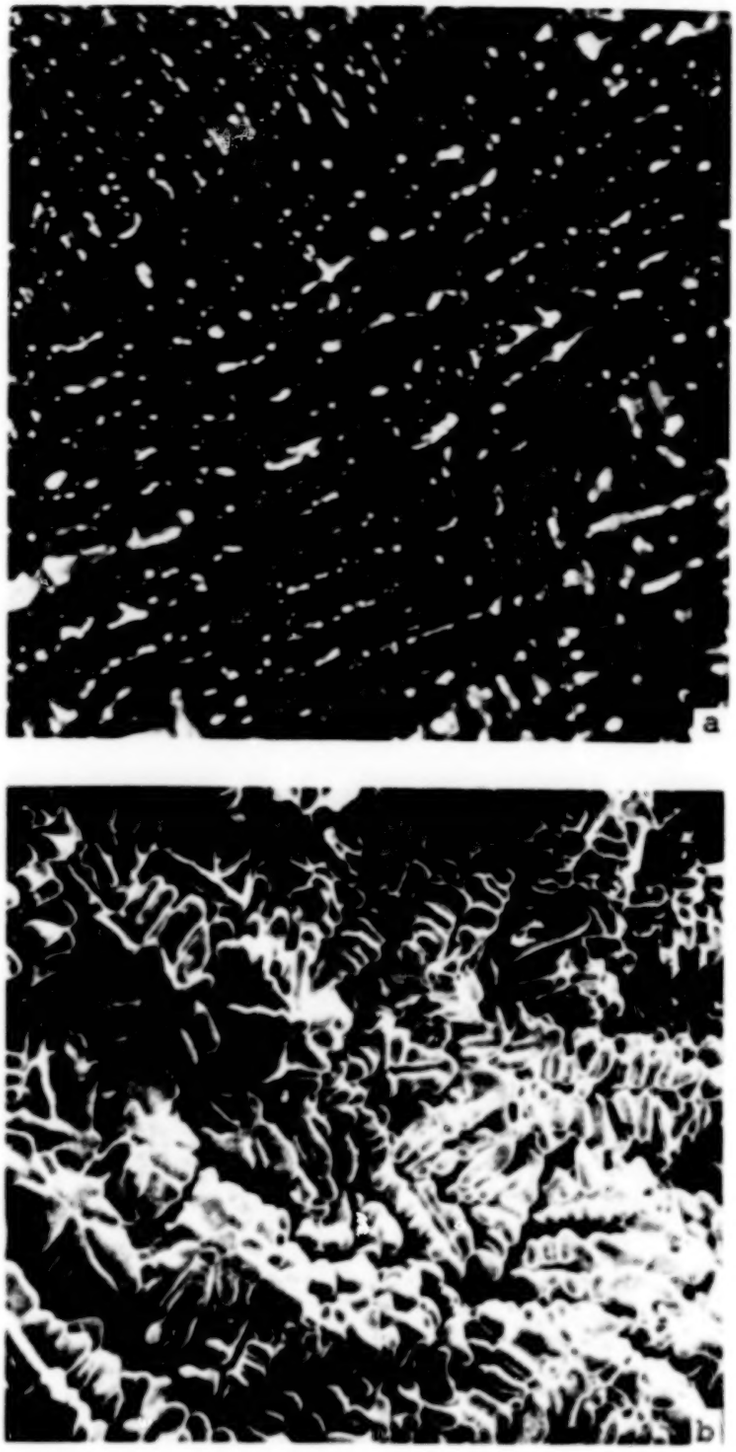

Views of transverse sections of porous dendritic networks of partially solidified Al-4%Si samples. (a) Stereo-photograph of a columnar network structure, x150; (b) SEM view of an equiaxed network structure, x22.

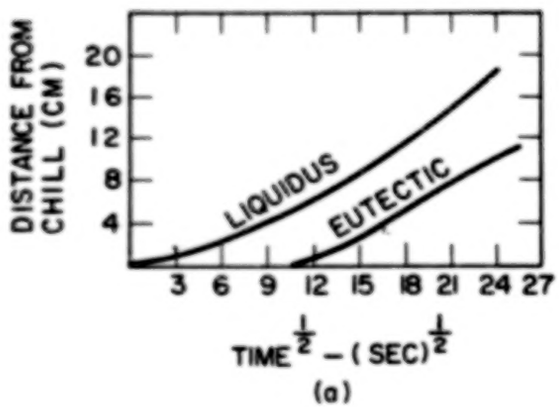

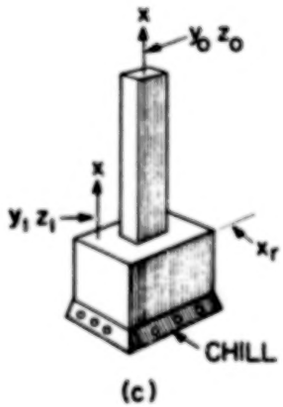

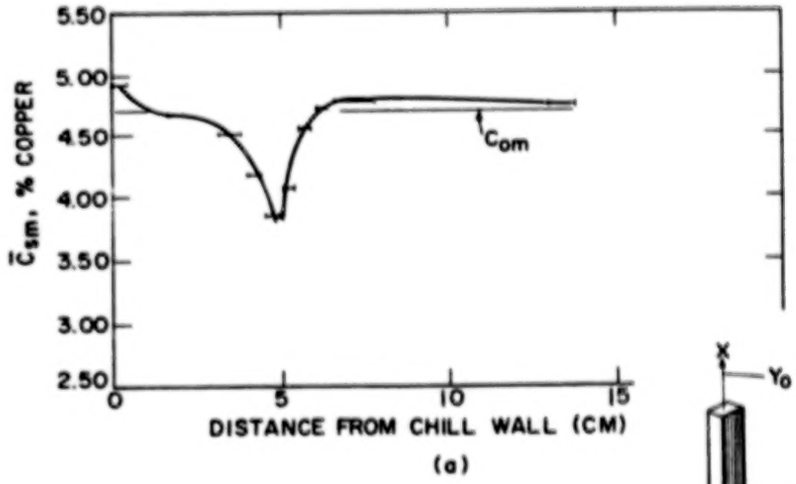

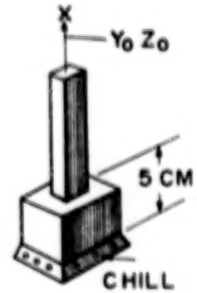

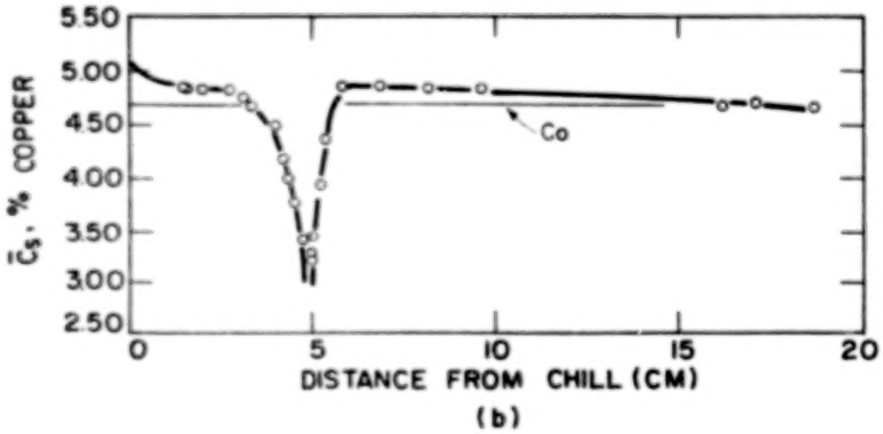

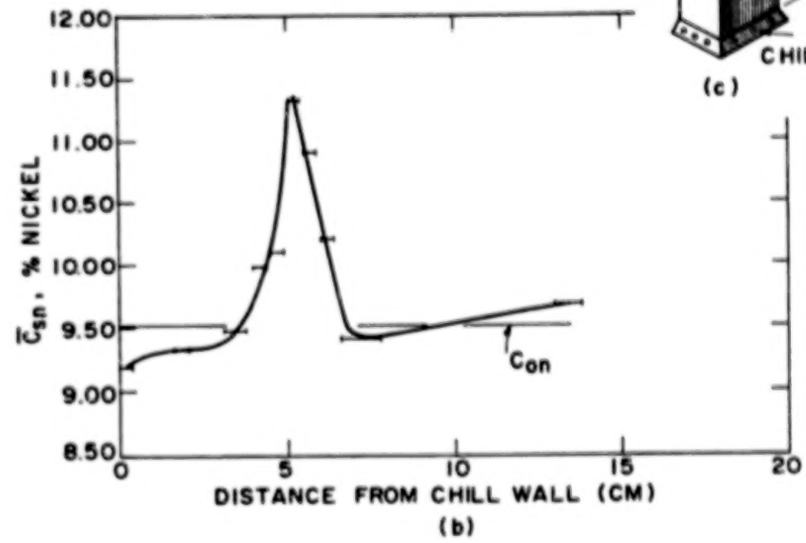

Macrosegregation in unidirectional ingot, cross-section reduced 9 to 1. Al 4.70 pct Cu 9.51 pct Ni; (a) measured composition of copper, $\bar{C}_{sm}$, vs distance from chill (at $y_o z_o$); (b) measured composition of nickel, $\bar{C}_{sn}$, vs distance from chill (at $y_o z_o$); (c) sketch of ingot.

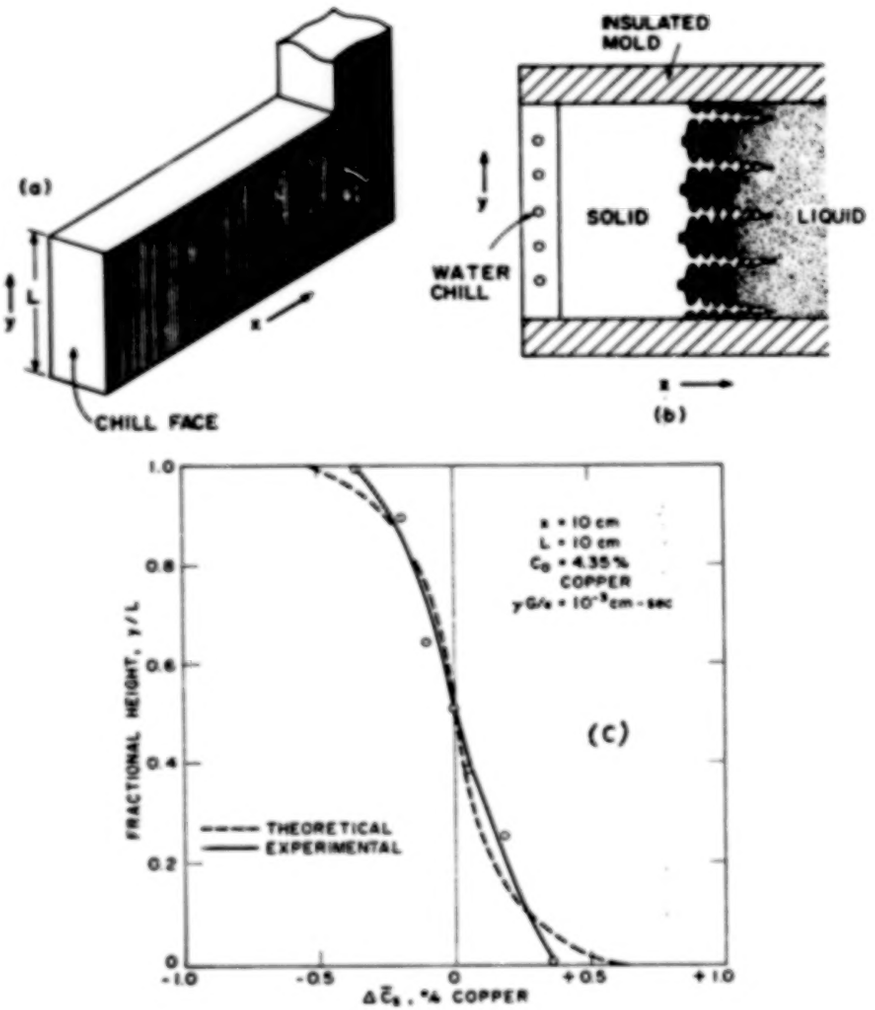

Macrosegregation in a horizontal unidirectional ingot of Al-4.35%Cu alloy, uniform cross-section; (a) sketch of ingot, (b) sketch of "mushy" zone, (c) experimental and calculated final local average copper composition variation, $\Delta \bar{C}_s = C_0 - \bar{C}_s$, along the y axis.

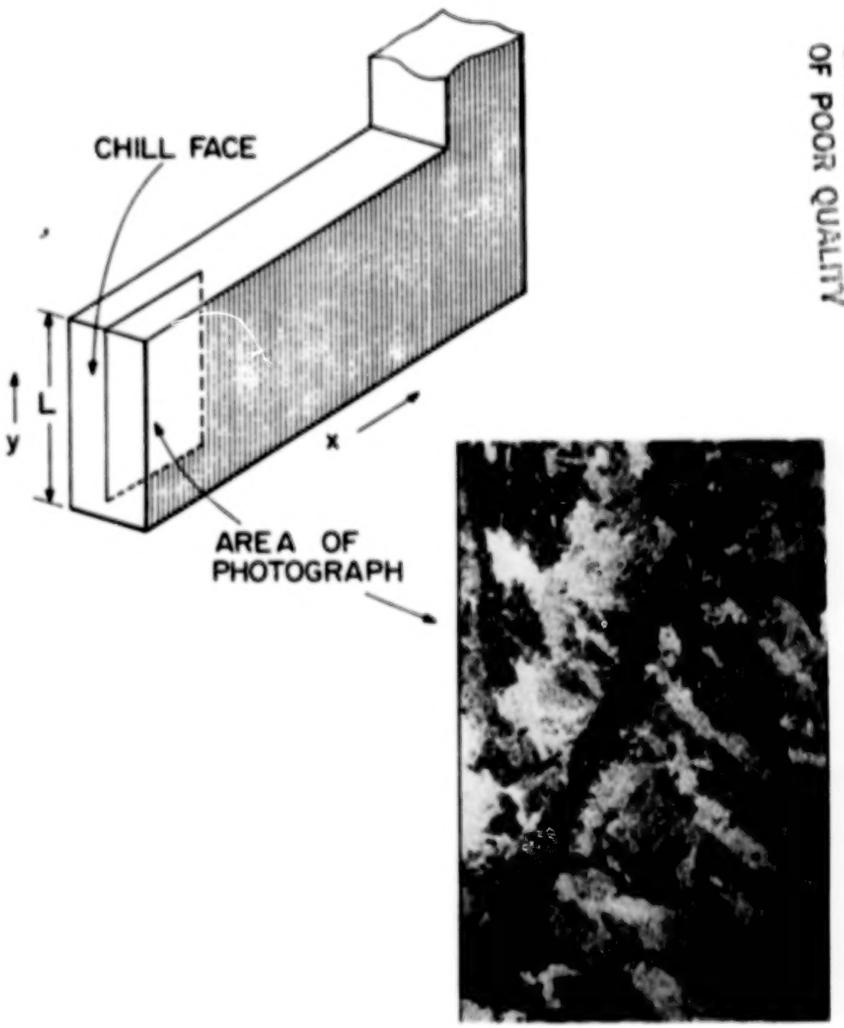

Channel segregate formed in a horizontal unidirectional ingot of Al-20%Cu alloy cast at low solidification rate.

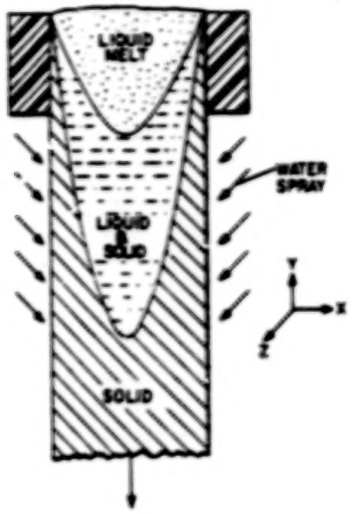

Schematic illustration of solidification in continuous casting.

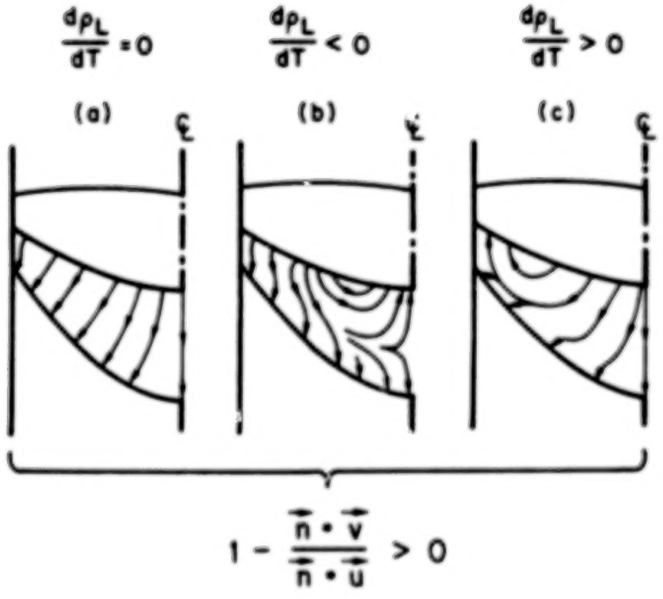

Schematic illustration of possible interdendritic fluid flow in axi-symmetric ingots. (a) Flow resulting in negative segregation at ingot center line, (b) flow resulting in positive segregation, (c) flow resulting in enhanced negative segregation.

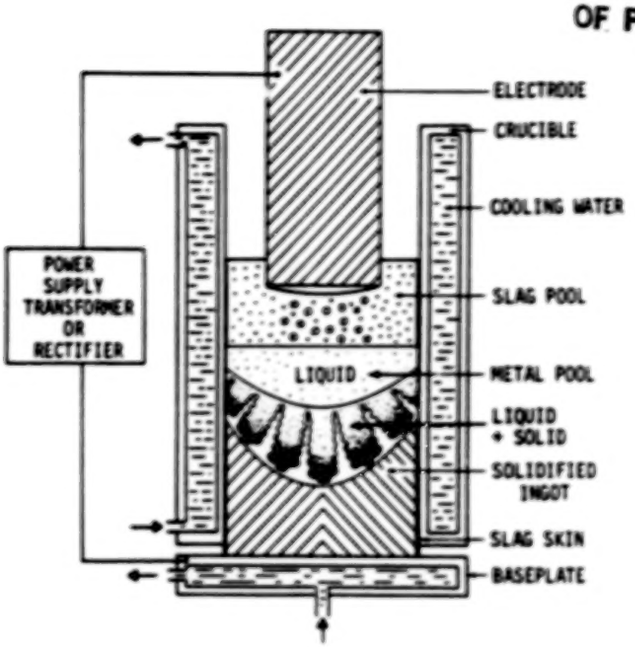

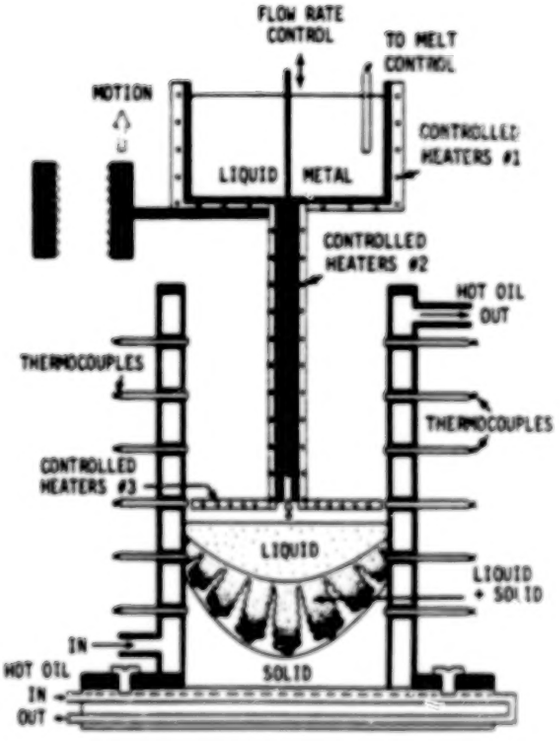

Schematic illustration of the laboratory apparatus for simulation of macrosegregation.

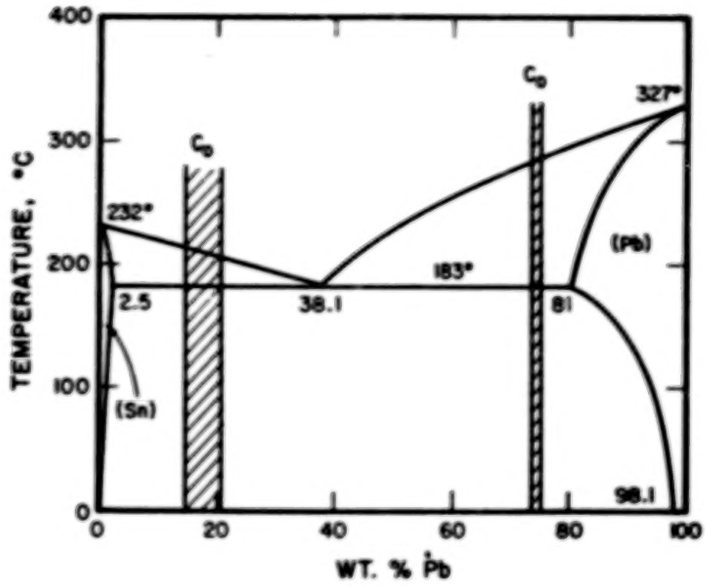

Phase diagram of the Sn-Pb system. Shaded areas represent alloys studies in this work.

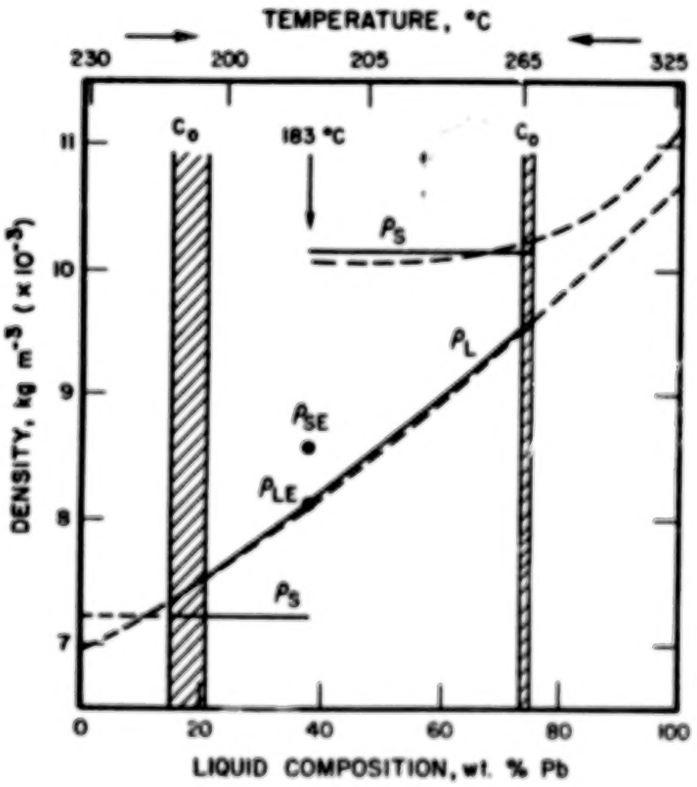

Liquid and solid densities of Sn-Pb alloys on both sides of eutectic versus composition and temperature of the liquid. ρ_S, ρ_L, ρ_{SE} and ρ_{LE} designate the densities of the solid, liquid, eutectic solid and eutectic liquid, respectively. Solid lines were used in calculations, dashed lines are from references [18] and [19] and shaded areas are alloys studied in this work.

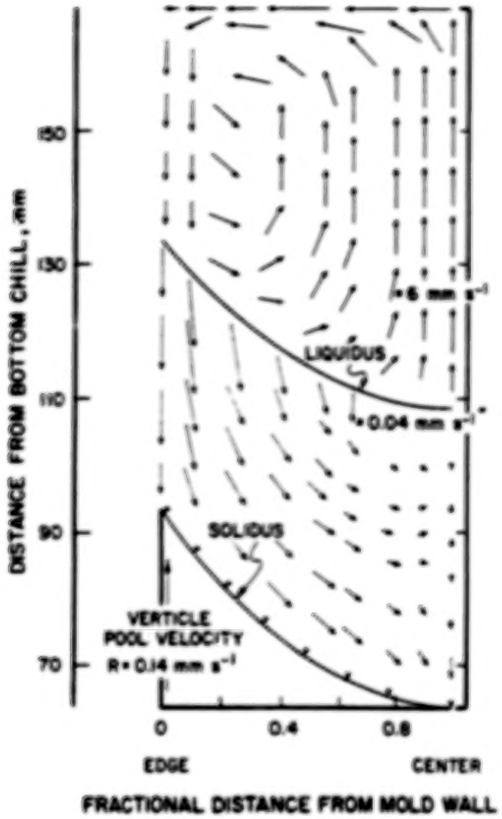

Calculated flow velocities in the Sn-16% Pb ingot. The resulting segregation profile is shown on page 18.

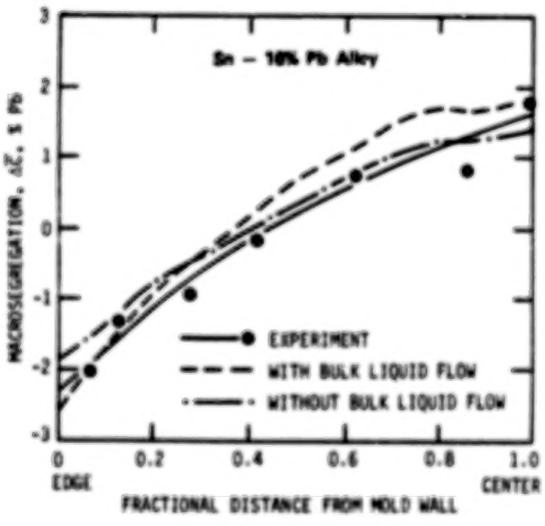

Comparison of experimental and theoretical segregation profiles in the Sn-16% Pb ingot. Calculated flow velocity distribution for this ingot is shown on page 17.

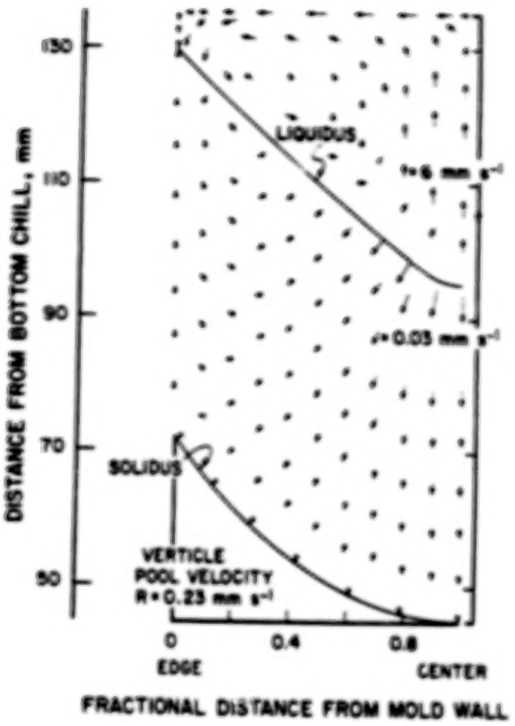

Calculated isotherms and flow velocities in the Pb-26.5% Sn ingot. The resulting segregation profile is shown on page 20.

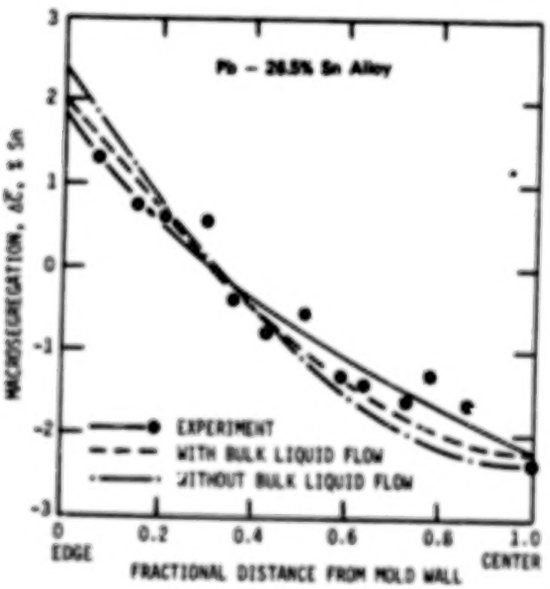

Comparison of experimental and theoretical segregation profiles in the Pb-26.5% Sn ingot. Calculated flow velocity distributions for this ingot are shown on page 19.

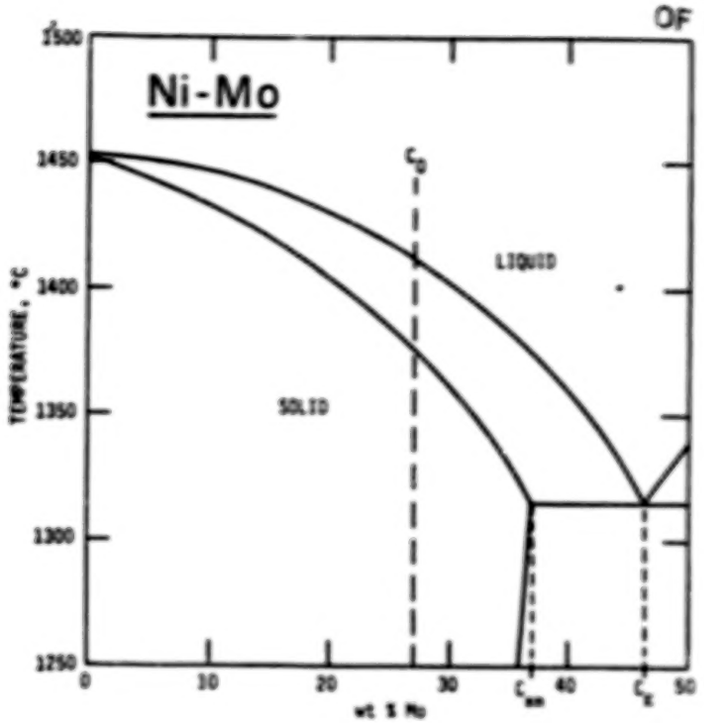

Nickel-rich corner of the Ni-Mo phase diagram.

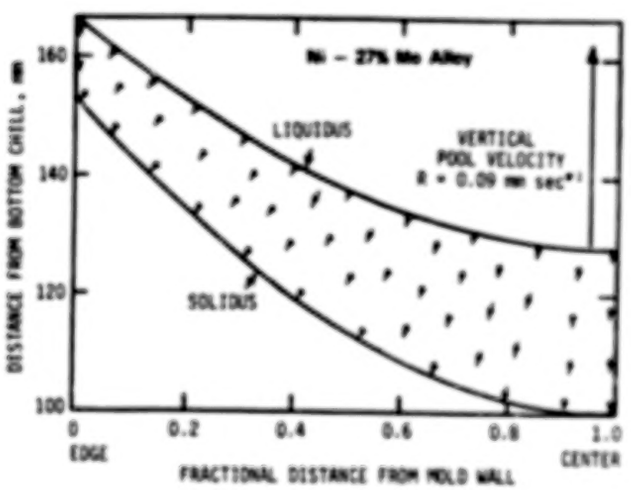

Calculated flow velocities in a 200 mm dian Ni-27 pct Mo ESR ingot. The arrows designate the direction of interdendritic fluid flow. The length of each arrow denotes its magnitude. Note that flow is consistently from the hotter to the cooler regime.

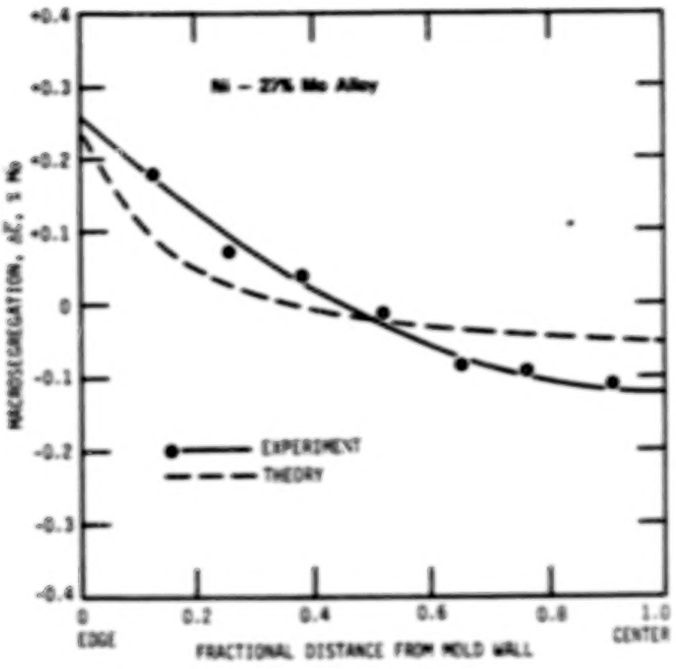

Comparison of experimental and theoretical segregation profiles in the Ni-27 pct Mo alloy. 200 mm diam, ESR ingot. The value of $\gamma = 1.5 \times 10^{-5}$ mm² was used for the computer calculations. Cross sectional area analyzed was 100 mm from the bottom of the ingot.

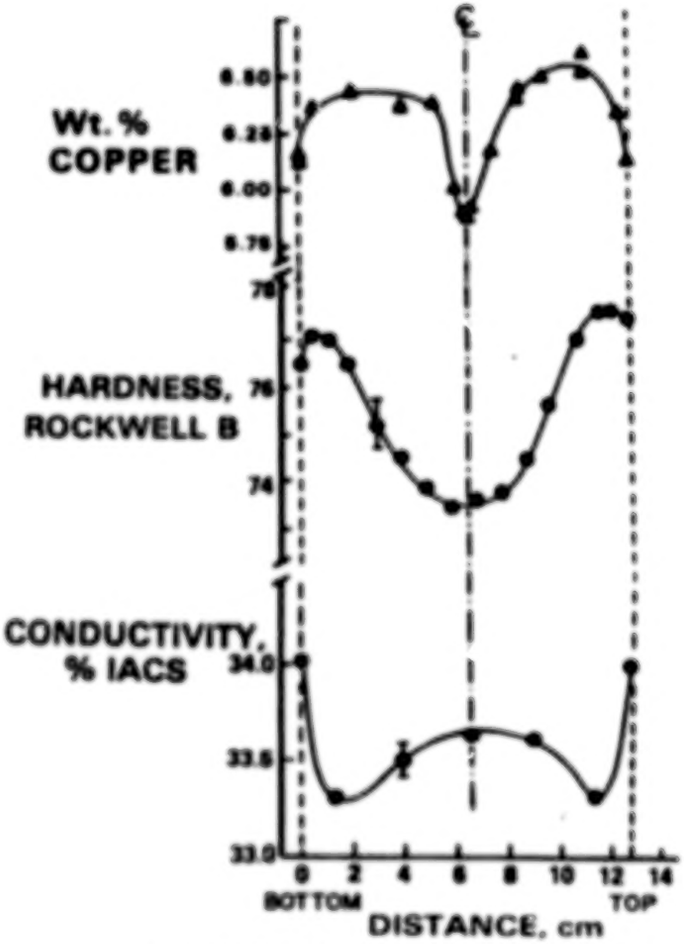

Measured average composition (wt.% copper) hardness (HRB) and conductivity (%IACS) versus distance through (bottom to top) an as-received 12.7 cm (5 inches) thick plate of 2219-T851 aluminum alloy (Reynolds Lot No. 7950777-01). The dotted lines indicate location of top and bottom.

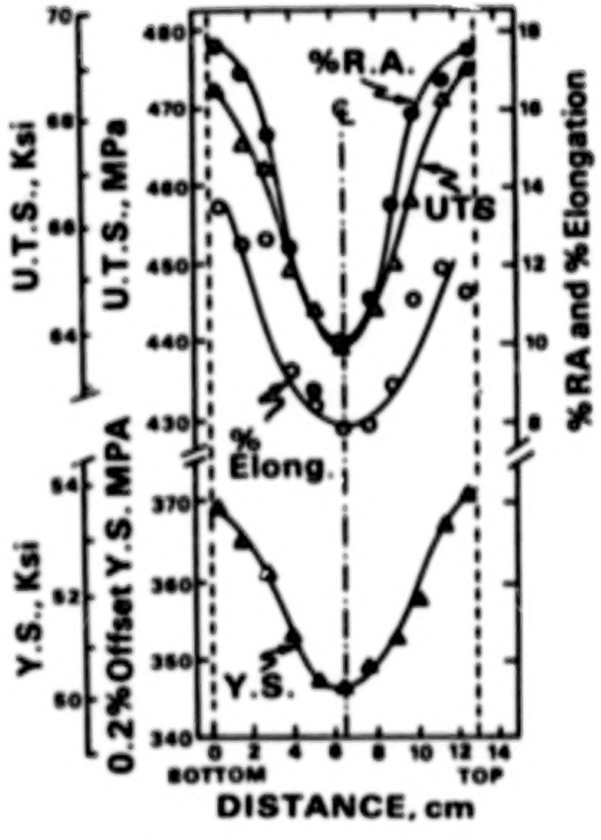

Measured yield stress, ultimate tensile stress, percent elongation and reduction in area versus distance through (bottom to top) an as-received 12.7 cm (5 inches) thick plate of 2219-T851 aluminum alloy (Reynolds Lot No. 7950777-01).

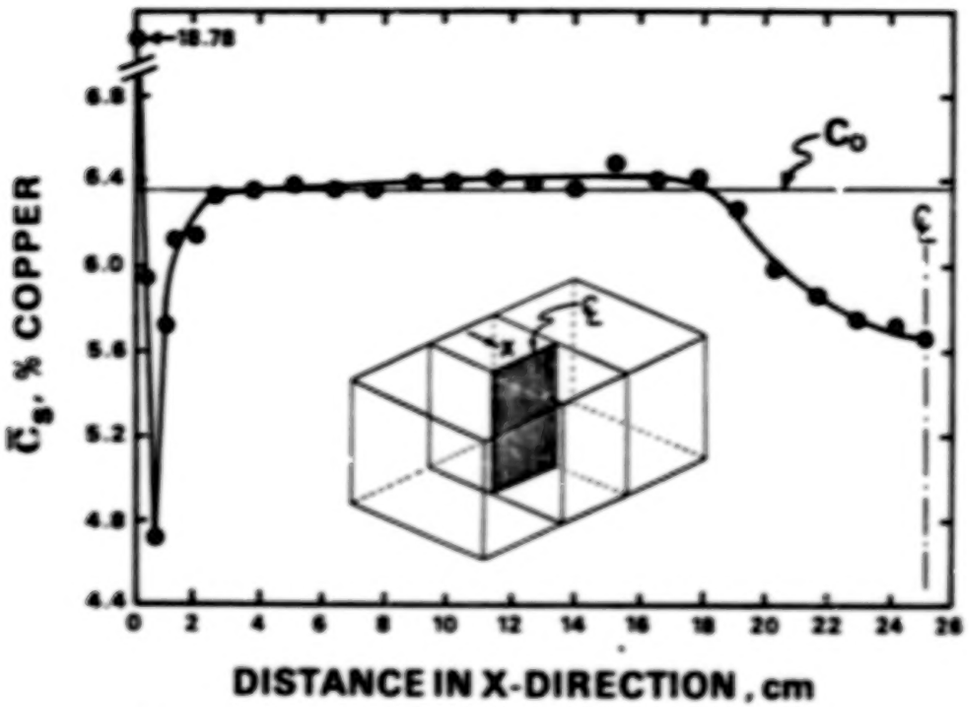

Macrosegregation profile, average copper content versus distance from the chill face, across the short transverse direction of a semi-continuous DC cast ingot of 2219 aluminum alloy. Ingot is from the Reynolds McCook plant. It is identified as 2219-13402-80.

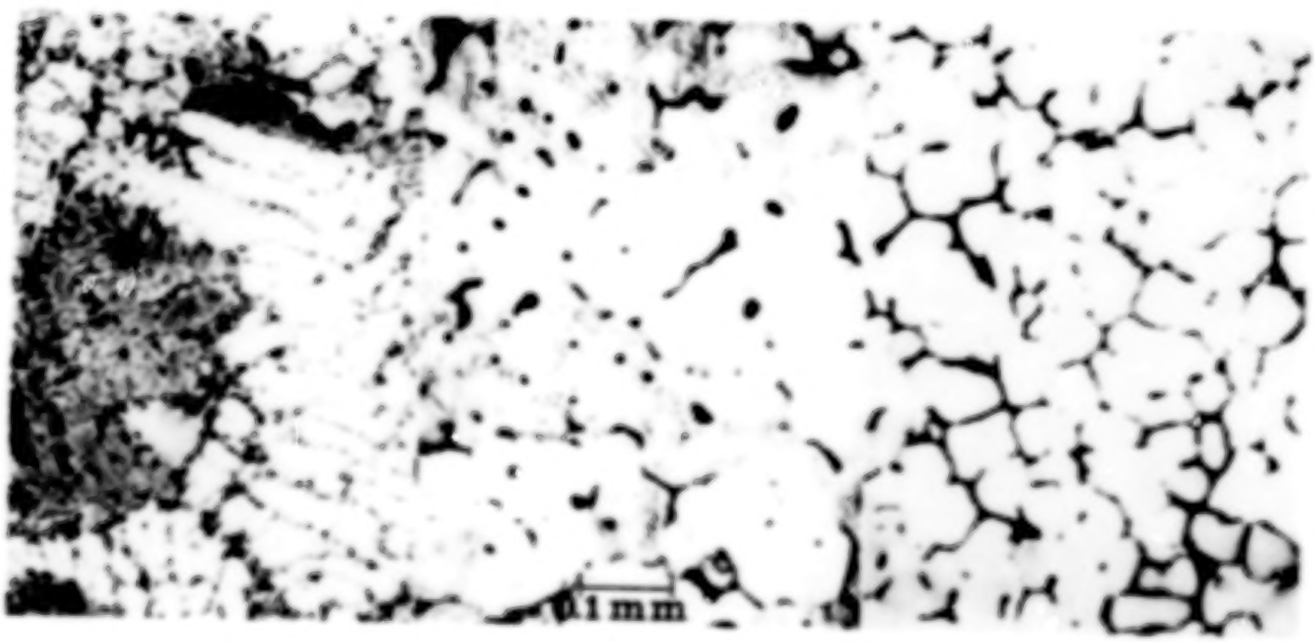

Optical micrographs of DC cast ingot at different distances from the chill surface: (a) chill face (on left), (b) 0.5 cm from chill face (c) 1.7 cm from the chill face.

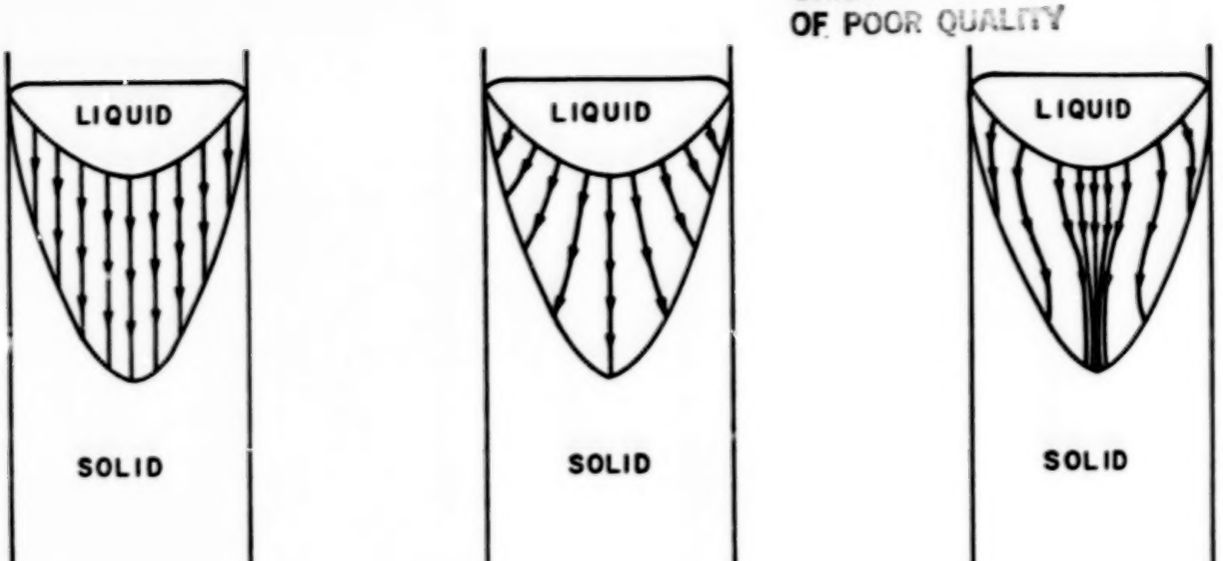

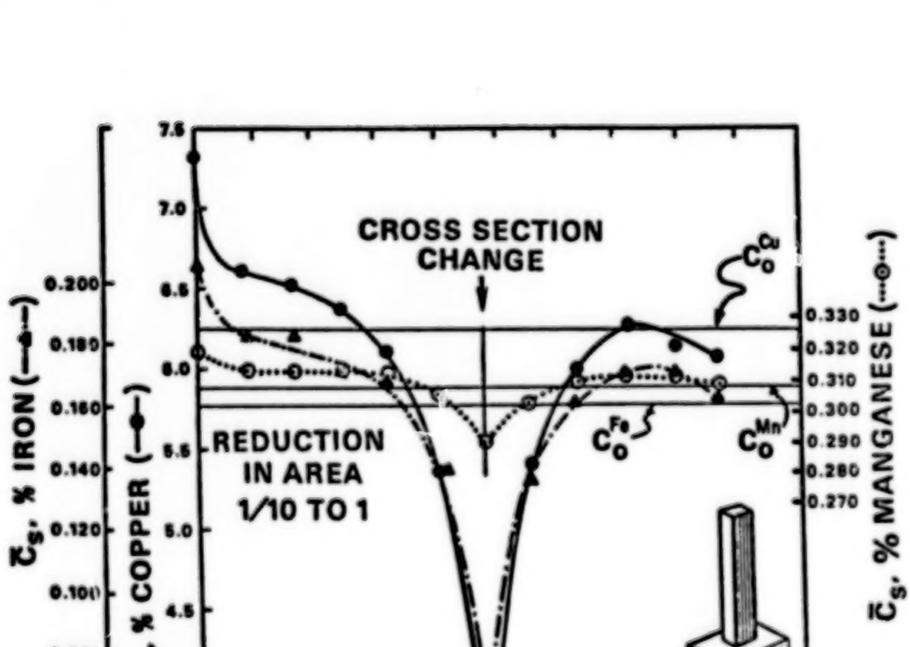

Macrosegregation profile, average copper, iron and manganese content versus distance from the bottom chill, in a unidirectionally solidified reduced cross section laboratory ingot of 2219 aluminum alloy. C_o's denote the average content of each element.

C-3

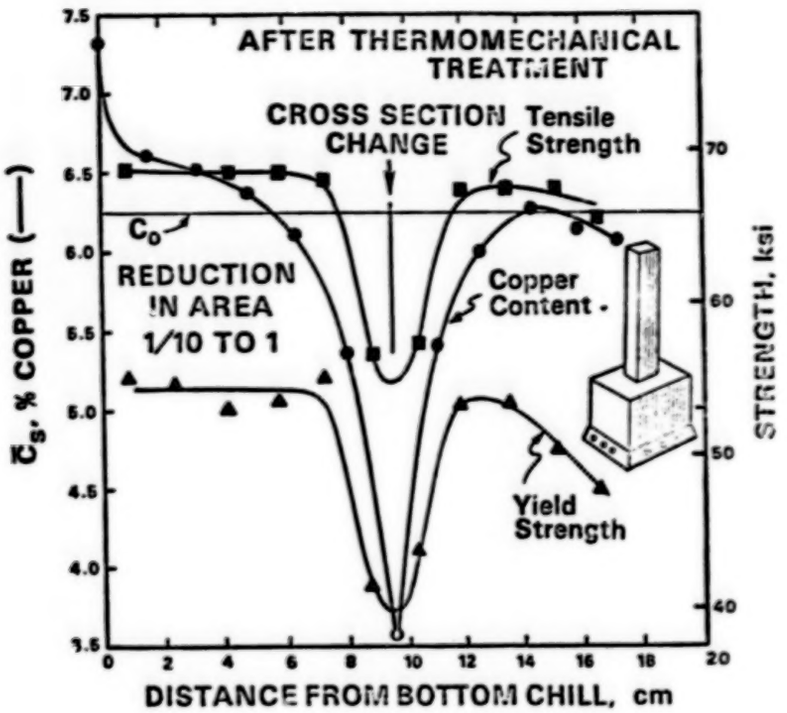

Tensile and yield strength after thermomechanical treatment to T87* condition and copper content versus distance from the bottom chill in a unidirectionally solidified reduced cross section laboratory ingot of 2219 aluminum alloy.

END

DATE

FILMED

DEC 18 1984